河南省职业教育教学成果奖
附件材料

成 果 名 称	双碳战略背景下“风光储充放”五位一体新型电力技术人才培养模式创新与实践
第一完成单位	郑州电力职业技术学院
主 要 完 成 人	华红艳、马银安、张红丽、李响、张之枫、王文豪、王春红、范莉、孙爱芬、魏继红、李杰虎、马锐
推 荐 序 号	□□□□

附件目录：

三、国家级和省级科研项目

三、国家级和省级科研项目

（一）省级科研项目

序号	年份	项目名称	负责人	部门	页码
1	2025	河南省新型电力系统智能状态监测与故障诊断工程技术研究中心	省级	河南省科学技术厅	1
2	2024	河南省绿色低碳电力系统稳定控制与数字化运维工程研究中心	省级	河南省发改委	2
3	2026	基于多矢量无权重因子的永磁同步电机模型预测控制策略研究	刘建萍	河南省教育厅	3
4	2024	基于系统灵活性的高比例可再生能源电力规划	华红艳	河南省教育厅	4
5	2024	基于共享通道的双向无线电能和信息同时传输系统特性研究	张红丽	河南省教育厅	5
6	2023	发电厂直流系统故障主动监测与隔离技术研究及装置开发	周永闯	河南省教育厅	6
7	2023	电动汽车与智能电网、分布式发电融合技术研究	李响	河南省科学技术厅	7
8	2021	规模化电动汽车与电网智能互动协调控制策略研究	李响	河南省科学技术厅	8
9	2020	大数据背景下的智能配电网全寿命周期评价体系研究	李响	河南省科学技术厅	9

（二）专利、软著、团标

序号	年份	项目名称	负责人	部门	页码
1	2023	一种智慧变电站及变电站的监控系统	李响	国家知识产权局	10
2	2021	一种多功能电力设备散热装置	李响	国家知识产权局	11
3	2023	区域终端集成供能系统长期负荷混合预测方法	王文豪	国家知识产权局	12
4	2022	一种智能家用能源信息综合简化处理方法	王文豪	国家知识产权局	13
5	2025	一种电力应急维修装置	范莉	国家知识产权局	14
6	2024	一种挂靠式无线电监控主机装置	范莉	国家知识产权局	15
7	2024	一种电力设备安装用提升装置	魏继红	国家知识产权局	16
8	2023	一种新型新能源发电用风能发电装置	马银安	国家知识产权局	17

9	2023	一种家用屋顶型光伏发电管理控制终端	王春红	国家知识产权局	18
10	2023	一种电力电缆维修用卷绕设备	王春红	国家知识产权局	19
11	2023	一种用于屋顶的光伏板固定结构	王春红	国家知识产权局	20
12	2022	一种新能源电力监测装置	马银安	国家知识产权局	21
13	2022	一种变电站电气安装充气式防尘棚	王文豪	国家知识产权局	22
14	2022	一种多功能鱼塘高压线防触电报警装置	王文豪	国家知识产权局	23
15	2021	一种发电厂直流故障监测装置	马银安	国家知识产权局	24
16	2021	一种发电厂直流故障监测装置	马银安	国家知识产权局	25
17	2020	一种可移动的防尘散热型电力配电柜	马银安	国家知识产权局	26
18	2025	基于系统灵活性的高比例可再生能源电力线路规划设计信息化软件 V1.0	华红艳	国家版权局	27
19	2023	穿管作业机器人远程智能操控系统 V1.0	魏继红	国家版权局	28
20	2023	基于人工智能、大数据运算一体化的配电设备故障处理平台 V1.0	魏继红	国家版权局	29
21	2021	基于共享通道的双向无线电能能耗分析管控系统 V1.0	范莉	国家版权局	30
22	2020	电力系统设备可靠性评估监测管理软件 V1.0	李响	国家版权局	31
23	2025	光伏发电工程施工现场安全防护与应急技术规范	华红艳	西安市质量与标准化协会	32

（三）科研论文

序号	论文题目	期刊名称	期刊等级	发表时间	对象（填写主持人/成员）	作者位次	页码
1	Evaluation of the Development Level and Key Measures of.New.Power System.in.Ecological Protection Cities	第 37 届中国控制与决策会议	EI	2025.05.16	主持人	1	34
2	Research Status and Method of Aviation Sensor Performance	ICCSIE 2020 Joumal of Physics	EI	2020.10.01	主持人	1	43
3	全面定位的薄板精密磨削方法分析	中国机械	普刊	2026.01.10	主持人	2	45
4	无线电能与信息同时传输的研究与分析	电力技术研究	普刊	2023.10.25	成员（3）	1	53

5	基于共享通道的双向无线电能和信息同时传输系统特性研究	流体测量与控制	普刊	2024.04.25	成员（3）	1	57
6	基于重复控制的通风机变频调速系统死区补偿方法研究	煤矿机械	中文核心	2020.03.01	成员（2）	1	67
7	双碳目标下源-网-荷多层评价体系研究	中国电机工程学报	EI	2021.08.31	成员（4）	1	68
8	考虑大规模新能源接入的电网性能评价指标体系	电力系统保护与控制	中文核心	2024.08.1	成员（4）	1	77
9	基于电力大数据和供电网格的电网发展评价方法	郑州航空工业管理学院学报	普刊	2025.04.01	成员（4）	1	91
10	A Modified Method for Calculating the Uplift Capacity ofMicropiles Considering the Correction of the CriticalEmbedment Depth	BUILDINGS	SCI	2025.04.27	成员（6）	5	101
11	Characteristics Investigation on Bearing Performance of aNovel Assembled Micropile Foundation in OverheadTransmission Lines	ADVANCES IN CIVIL ENGINEERING	SCI	2025.05.08	成员（6）	6	119
12	中小容量家用屋顶型光伏发电并网关键技术应用研究	电气技术与经济	普刊	2024.10.20	成员（7）	1	141
13	基于改进的高斯过程回归的SOC估计算法	储能科学与技术	中文核心	2022.01.05	成员（9）	1	149

（一）省级科研项目

1.河南省新型电力系统智能状态监测与故障诊断工程技术研究中心

河南省科学技术厅文件

豫科实〔2025〕1号

关于认定建设2024年度河南省工程技术研究中心的通知

各省辖市科学技术局，济源示范区、郑州航空港经济综合实验区管委会科技主管部门，各县（市）科技管理部门，各国家高新区、国家郑州经济技术开发区管委会，省直有关部门，各有关单位：

根据《河南省工程技术研究中心建设运行管理办法（暂行）》《关于组织申报2024年河南省工程技术研究中心的通知》要求，经主管部门推荐、专家评审、研究、公示等程序，认定建设2024年度河南省工程技术研究中心318家，现予公布（名单见附件）。

请各主管部门和依托单位加强对省工程技术研究中心的指导、管理和服务保障，各省工程技术研究中心充分发挥示范带头

— 1 —

序号	工程技术研究中心名称	依托单位	共建单位	主管部门
163	河南省智能增量配电网工程技术研究中心	郑州航空港兴港电力有限公司		郑州航空港经济综合实验区
164	河南省轨道交通装备智能制造工程技术研究中心	郑州铁路职业技术学院	郑州畅想高科股份有限公司	河南省教育厅
165	河南省新型电力系统智能状态监测与故障诊断工程技术研究中心	郑州电力职业技术学院	郑州万特电气股份有限公司	中牟县科学技术局
166	河南省固态电池电解质工程技术研究中心	新乡华锐锂电新能源股份有限公司		新乡市科学技术局
167	河南省配电设备类型试验检测工程技术研究中心	漯河汇力实业（集团）有限公司		漯河市科学技术局
168	河南省智慧城轨工程技术研究中心	河南辉煌城轨科技有限公司		郑州高新技术产业开发区
169	河南省智能电网设备工程技术研究中心	河南华盛隆源电气有限公司		长葛市科学技术局
170	河南省新型电力系统继电保护及自动化控制工程技术研究中心	河南许继继保电气自动化有限公司		许昌市科学技术局
171	河南省汽车用高强韧铁基粉末冶金制品工程技术研究中心	南阳南粉复合材料有限公司		淅川县科学技术局
172	河南省智慧输配电及数字化服务工程技术研究中心	国源电力集团有限公司		郑州市科学技术局
173	河南省新型风力发电装备与智能控制工程技术研究中心	河南国网自控电气有限公司		洛阳市科学技术局

— 18 —

2.河南省绿色低碳电力系统稳定控制与数字化运维工程研究中心

河南省发展和改革委员会文件

豫发改高技〔2024〕260号

河南省发展和改革委员会
关于河南省电动载运先进动力与能源工程研究中心等140个省工程研究中心的批复

各省辖市、济源示范区、航空港区发展改革部门，省有关单位：

报来河南省工程研究中心申请报告收悉，经委托第三方机构评估和社会公示，现批复如下。

一、原则同意河南省电动载运先进动力与能源工程研究中心等140个省工程研究中心（名单见附件）申请报告，建设过程中的项目管理、资金使用等事项，严格按照国家和省有关规定执行。

二、请按照《河南省工程研究中心管理办法》，抓紧推进相关工程研究中心建设，切实加强跟踪管理和协调服务，重大

— 1 —

问题及时向我委报告。

三、省工程研究中心每2年开展一次运行评价。届时请按照有关要求，组织工程研究中心报送运行情况材料。我委将统一开展运行评价，对不合格的，将撤销省工程研究中心资格。

附件：2024年河南省工程研究中心名单

河南省发展和改革委员会

2024年5月23日

— 2 —

附 件

2024年河南省工程研究中心名单

序号	研究中心名称	牵头建设单位	主要任务和建设内容	主管单位
1	河南省电动载运先进动力与能源工程研究中心	哈工大郑州研究院	开展先进电驱动系统、无线供电、电磁装备以及超级铜线、高速轴承等系统和部件开发、脉冲电源以及大功率电磁推进等关键技术研究，建设新能源载运装备创新等研发平台。	郑州市发展改革委
2	河南省空天信息智能处理与集成应用工程研究中心	河南省科学院空天信息研究所	开展空天平台与新体制载荷研制、空天信息智能处理与应用服务等关键技术攻关研究，建设通导遥卫星集成应用、空天地一体化大数据集成等研发平台。	河南省科学院
19	河南省超大功率连续波发射技术工程研究中心	中国电子科技集团公司第二十七研究所	开展超大功率连续波功率源、超大功率微波网络、高压大功率直流输出μs级快速切断等关键技术攻关研究，建设深空探测超大功率连续波发射实验室等研发平台。	郑州市发展改革委
20	河南省绿色低碳电力系统稳定控制与数字化运维工程研究中心	郑州电力职业技术学院	开展分布式电力系统稳定控制与保护、交直混联电力系统稳定与控制、基于数字孪生的数字化电力设备智能运维等关键技术攻关研究，建设新型电力系统稳定控制及数字化运维的先进技术、装备试验、成果转化等研究平台。	河南省教育厅
21	河南省儿童睡眠呼吸疾病早期筛查与精准诊疗工程研究中心	河南省儿童医院（郑州儿童医院）	开展儿童睡眠呼吸疾病早期筛查、智能化睡眠监测、远程监测与互联网医疗的多学科综合治疗等关键技术攻关研究，建设儿童睡眠呼吸疾病流行病学与科普教育、人工智能与互联网医疗、儿童睡眠呼吸疾病的多学科综合救治等研发平台。	郑州市发展改革委
22	河南省新能源领域用线缆工程研究中心	河南通达电缆股份有限公司	开展光伏电缆、变频器专用电力电缆、绝缘防火电缆、新能源汽车用车载高压电缆、耐高温防火新能源汽车用充电电缆等关键技术攻关研究，建设电气性能、机械性能、环境适应性、电磁兼容、生产工艺等研发平台。	洛阳市发展改革委

— 6 —

3.基于多矢量无权重因子的永磁同步电机模型预测控制策略研究

河南省高等学校重点科研项目结项证书

豫教科技【2026】0319号

该项目提交的研究资料完整，结项报告系统详实，经审查符合结项要求，准予结项。

河南省教育厅

2026年02月04日

项目名称：基于多矢量无权重因子的永磁同步电机模型预测控制策略研究
立项时间：2023年10月28日
项目编号：24B470008
承担单位：郑州电力职业技术学院
项目负责人：刘建萍
项目参加者（共11名）：

排序	姓名	性别	单位
2	范莉	女	郑州电力职业技术学院
3	李悦功	男	郑州宇通集团有限公司
4	马艳丽	女	郑州电力职业技术学院
5	孟翠霞	女	郑州电力职业技术学院
6	马小莉	女	郑州电力职业技术学院
7	孙爱芬	女	郑州电力职业技术学院
8	李雪霞	女	郑州经贸学院
9	张瑞南	女	郑州电力职业技术学院
10	李晓平	女	郑州电力职业技术学院
11	郑一达	男	郑州电力职业技术学院

结项等级：合格

4.基于系统灵活性的高比例可再生能源电力规划

河 南 省 教 育 厅

教科技〔2024〕315 号

河 南 省 教 育 厅
关于公布 2025 年度河南省高等学校重点科研项目计划立项的通知

各高等学校：

为增强高等学校科技创新能力，引导和鼓励高校科技工作者加强基础研究、开展原始性创新与前沿探索，培养科研学术骨干，推动学科建设和发展，根据《河南省高等学校重点科研项目管理办法（修订）》（教科技〔2019〕234 号）精神，按照《河南省教育厅办公室关于申报 2025 年度河南省高等学校重点科研项目计划的通知》（教办科技〔2024〕193 号）要求，经过学校推荐、专家评审、公示等环节，省教育厅研究确定了 2025 年度河南省高等学校重点科研项目计划（下称“重点项目”），现将立项名单予以

25B430043	含 Cu 抗菌不锈钢材料及其产业化研究	郑州电力职业技术学院	郭慧
25B460027	基于车路云多源信息融合的智能网联汽车协作决策调度控制系统研究	郑州电力职业技术学院	冯培源
25B460040	盾构机可扩展限流阀模块化设计及其多学科优化研究	郑州电力职业技术学院	王姗姗
25B470013	基于系统灵活性的高比例可再生能源电力规划	郑州电力职业技术学院	华红艳
25B470017	风光储充一体化智能充电桩设计研究	郑州电力职业技术学院	马艳丽
25B520049	面向恶劣成像环境的鲁棒视觉智能感知关键技术研究	郑州电力职业技术学院	王云亮
25B880025	元宇宙对教与学理论的重构与应用技术设计及实现	郑州电子信息职业技术学院	张敏

5.基于共享通道的双向无线电能和信息同时传输系统特性研究

河　南　省　教　育　厅

河南省高等学校重点科研项目计划
立 项 通 知

郑州电力职业技术学院：

你单位申报的下列研究课题，经专家评审、省教育厅审核，已列为河南省高等学校重点科研项目计划，并以 教科技〔2021〕383号 文件批准下达。现通知如下：

项目编号：22B480006

项目名称：基于共享通道的双向无线电能和信息同时传输系统特性研究

项目负责人：张红丽

项目研究期限：2022年01月01日--2023年12月31日

项目组成员：

排序	姓名	性别	单位
2	刘建萍	女	郑州电力职业技术学院
3	李悦功	男	河南省省直能源实业有限公司
4	范莉	女	郑州电力职业技术学院
5	王春红	女	郑州电力职业技术学院
6	黄宏伟	男	河南中电投华新电力工程有限公司
7	张之枫	男	郑州电力职业技术学院
8	高芳庭	男	郑州电力职业技术学院
-	-	-	-
-	-	-	-
-	-	-	-

（项目组共 8 人）

2021年10月22日

河南省教育厅 科研管理专用章

河南省高等学校重点科研项目结项证书

豫教科技【2024】0007号

该项目提交的研究资料完整，结项报告系统详实，经审查符合结项要求，准予结项。

河南省教育厅

2024年01月02日

河南省教育厅 科研管理专用章

项目名称：基于共享通道的双向无线电能和信息同时传输系统特性研究

立项时间：2021年10月27日

项目编号：22B480006

承担单位：郑州电力职业技术学院

项目负责人：张红丽

项目参加者（共9名）：

排序	姓名	性别	单位
2	刘建萍	女	郑州电力职业技术学院
3	李悦功	男	河南省省直能源实业有限公司
4	范莉	女	郑州电力职业技术学院
5	王春红	女	郑州电力职业技术学院
6	周永闯	男	郑州电力职业技术学院
7	张之枫	男	郑州电力职业技术学院
8	孙爱芬	女	郑州电力职业技术学院
9	郑一达	男	郑州电力职业技术学院
-	-	-	-
-	-	-	-

结项等级：合格

6.发电厂直流系统故障主动监测与隔离技术研究及装置开发

河南省高等学校重点科研项目结项证书

豫教科技【2023】0319号

该项目提交的研究资料完整，结项报告系统详实，经审查符合结项要求，准予结项。

河南省教育厅

2023年04月03日

项目名称：发电厂直流系统故障主动监测与隔离技术研究及装置开发
立项时间：2020年09月04日
项目编号：21B470012
承担单位：郑州电力职业技术学院
项目负责人：周永闯
项目参加者（共16名）：

排序	姓名	性别	单位
2	刘小彩		郑州电力职业技术学院
3	周俊玲		郑州电力职业技术学院
4	周晓利		郑州电力职业技术学院
5	张红丽		郑州电力职业技术学院
6	魏继红		郑州电力职业技术学院
7	马锐		郑州电力职业技术学院
8	张小龙		郑州电力职业技术学院
9	李超		郑州电力职业技术学院
10	孙爱芬		郑州电力职业技术学院
11	马艳丽		郑州电力职业技术学院
12	杨春暖		郑州电力职业技术学院
13	马银安		郑州电力职业技术学院
14	任万英		郑州电力职业技术学院
15	张之枫		郑州电力职业技术学院
16	何玉婷		郑州电力职业技术学院

结项等级：合格

7.电动汽车与智能电网、分布式发电融合技术研究

河南省科技攻关计划项目
结项证书

该项目提交的研究资料完整，总结报告系统详实，经审查符合结项要求，准予结项。

河南省科学技术厅
科技计划专用章
2023 年 7 月 3 日

项目名称：电动汽车与智能电网、分布式发电融合技术研究

立项年度：2022 年

项目编号：222102240117

承担单位：郑州航空工业管理学院

项目负责人：李响

项目参加人（共 7 名）：

王龙、张丹、李福恩、孙方涛、吴鹏、黄文力、王威立

8.规模化电动汽车与电网智能互动协调控制策略研究

河南省高新技术领域科技攻关项目
结项证书

豫科高（2021）448号

该项目提交的研究资料完整，总结报告系统详实，经审查，符合结项要求，准予结项。

河南省科学技术厅
高新技术发展及产业化处
2021年11月1日

项目名称： 规模化电动汽车与电网智能互动协调控制策略研究

立项时间： 2021年1月

项目编号： 212102210254

承担单位： 郑州航空工业管理学院

项目负责人： 李响

项目参加者（共柒名）：

王娜娜　王　龙　黄文力　胡天彤
刘顺新　张　丹　常绪成

结项形式：论文论著 研究报告 其他

9.大数据背景下的智能配电网全寿命周期评价体系研究

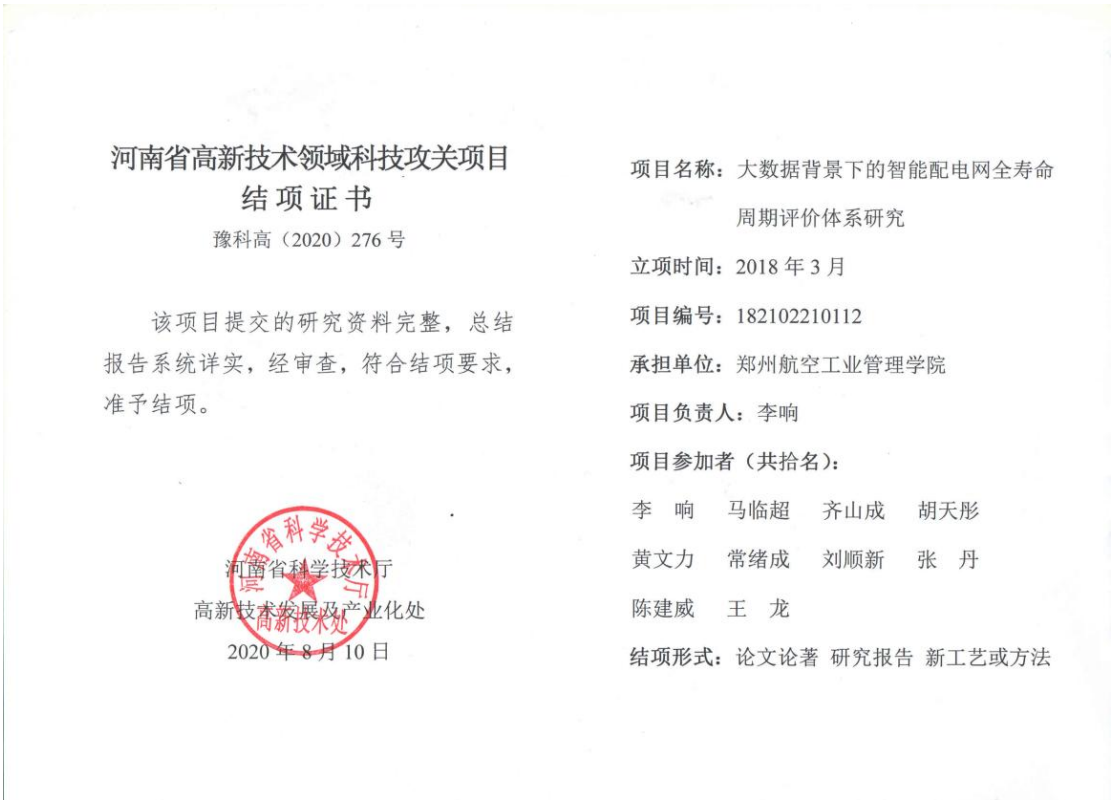

河南省高新技术领域科技攻关项目
结项证书

豫科高（2020）276号

该项目提交的研究资料完整，总结报告系统详实，经审查，符合结项要求，准予结项。

河南省科学技术厅
高新技术发展及产业化处
2020年8月10日

项目名称：大数据背景下的智能配电网全寿命周期评价体系研究

立项时间：2018年3月

项目编号：182102210112

承担单位：郑州航空工业管理学院

项目负责人：李响

项目参加者（共拾名）：

李　响　　马临超　　齐山成　　胡天彤

黄文力　　常绪成　　刘顺新　　张　丹

陈建威　　王　龙

结项形式：论文论著 研究报告 新工艺或方法

（二）专利、软著、团标

1.一种智慧变电站及变电站的监控系统

证书号第6225768号

发明专利证书

发明名称：一种智慧变电站及变电站的监控系统

发　明　人：李响;王娜娜;王咸立;黄文力;常绪成;胡天彤;王龙张丹;刘顺新

专　利　号：ZL 2021 1 1103714.1

专利申请日：2021年09月22日

专利权人：郑州航空工业管理学院;郑州信息科技职业学院

地　　址：450000 河南省郑州市二七区大学中路2号

授权公告日：2023年08月11日　　授权公告号：CN 113759794 B

国家知识产权局依照中华人民共和国专利法进行审查，决定授予专利权，颁发发明专利证书并在专利登记簿上予以登记。专利权自授权公告之日起生效。专利权期限为二十年，自申请日起算。

专利证书记载专利权登记时的法律状况。专利权的转移、质押、无效、终止、恢复和专利权人的姓名或名称、国籍、地址变更等事项记载在专利登记簿上。

局长
申长雨

国家知识产权局
2023年08月11日

第1页(共2页)

其他事项参见续页

2.一种多功能电力设备散热装置

证书号第4498668号

发明专利证书

发明名称：一种多功能电力设备散热装置

发明人：李响；马临超；齐山成；黄文力；白首华；胡天彤；郭广颂；王龙；常绪成；张丹；刘顺新

专利号：ZL 2020 1 0205879.9

专利申请日：2020年03月23日

专利权人：郑州航空工业管理学院

地址：450046 河南省郑州市郑东新区文苑西路15号

授权公告日：2021年06月22日　　授权公告号：CN 111244801 B

国家知识产权局依照中华人民共和国专利法进行审查，决定授予专利权，颁发发明专利证书并在专利登记簿上予以登记。专利权自授权公告之日起生效。专利权期限为二十年，自申请日起算。

专利证书记载专利权登记时的法律状况。专利权的转移、质押、无效、终止、恢复和专利权人的姓名或名称、国籍、地址变更等事项记载在专利登记簿上。

局长
申长雨

国家知识产权局

2021年06月22日

第1页(共2页)

其他事项参见续页

3.区域终端集成供能系统长期负荷混合预测方法

证书号第5705204号

发明专利证书

发明名称：区域终端集成供能系统长期负荷混合预测方法

发明人：耿翠英;黄泽华;郭建宇;娄北;王文豪;林烽;刘洋;张龙

专利号：ZL 2020 1 0571419.8

专利申请日：2020年06月19日

专利权人：国网河南省电力公司经济技术研究院;国家电网有限公司

地址：450000 河南省郑州市二七区嵩山南路87号院办公区C楼1-10层

授权公告日：2023年01月20日　　授权公告号：CN 111754037 B

国家知识产权局依照中华人民共和国专利法进行审查，决定授予专利权，颁发发明专利证书并在专利登记簿上予以登记。专利权自授权公告之日起生效，专利权期限为二十年，自申请日起算。

专利证书记载专利权登记时的法律状况。专利权的转移、质押、无效、终止、恢复和专利权人的姓名或名称、国籍、地址变更等事项记载在专利登记簿上。

局长
申长雨

国家知识产权局
2023年01月20日

第 1 页 (共 2 页)

其他事项参见续页

4.一种智能家用能源信息综合简化处理方法

证书号第4956171号

发明专利证书

发明名称：一种智能家用能源信息综合简化处理方法

发明人：郑征;王棨;吴军波;姬正骁;王松;许长清;张海宁;张琳娟
张平;周楠;邱超;郭璞;卢丹;李锰;余晓鹏;田春等;毛玉宾

专利号：ZL 2019 1 0435423.9

专利申请日：2019年05月23日

专利权人：国网河南省电力公司经济技术研究院;国家电网有限公司

地址：450000 河南省郑州市二七区嵩山南路87号院办公区C楼1-10层

授权公告日：2022年02月22日　　授权公告号：CN 110011867 B

国家知识产权局依照中华人民共和国专利法进行审查，决定授予专利权，颁发发明专利证书并在专利登记簿上予以登记。专利权自授权公告之日起生效。专利权期限为二十年，自申请日起算。

专利证书记载专利权登记时的法律状况。专利权的转移、质押、无效、终止、恢复和专利权人的姓名或名称、国籍、地址变更等事项记载在专利登记簿上。

局长
申长雨

国家知识产权局
2022年02月22日

第1页(共3页)

其他事项参见续页

5.一种电力应急维修装置

证书号第23174386号

专利公告信息

实用新型专利证书

实用新型名称：一种电力应急维修装置

专 利 权 人：郑州电力职业技术学院;郑州德凯工程技术有限公司

地　　址：451450 河南省郑州市中牟县商都大街东段1933号

发 明 人：范莉;刘建萍;张红丽;赵明;任磊磊

专　利　号：ZL 2024 2 2413377.1　　授权公告号：CN 223194294 U

专利申请日：2024年10月08日　　授权公告日：2025年08月05日

申请日时申请人：郑州电力职业技术学院;郑州德凯工程技术有限公司

申请日时发明人：范莉;刘建萍;张红丽;赵明;任磊磊

国家知识产权局依照中华人民共和国专利法进行审查，决定授予专利权，并予以公告。

专利权自授权公告之日起生效。专利权有效性及专利权人变更等法律信息以专利登记簿记载为准。

局长
申长雨

国家知识产权局
2025年08月05日

第1页(共1页)

6.一种挂靠式无线电监控主机装置

证书号第21230720号

专利公告信息

实用新型专利证书

实用新型名称：一种挂靠式无线电监控主机

专 利 权 人：郑州德凯工程技术有限公司;郑州电力职业技术学院

地　　址：450000 河南省郑州市金水区宝瑞路115号河南省信息安全产业示范基地6号楼7层703号

发 明 人：刘建萍;李寿山;张红丽;张莉宾;张之枫;范莉;李悦功

专　利　号：ZL 2023 2 2229167.2　　授权公告号：CN 221258455 U

专利申请日：2023年08月18日　　授权公告日：2024年07月02日

申请日时申请人：郑州德凯工程技术有限公司;郑州电力职业技术学院

申请日时发明人：刘建萍;李寿山;张红丽;张莉宾;张之枫;范莉;李悦功

国家知识产权局依照中华人民共和国专利法进行审查，决定授予专利权，并予以公告。

专利权自授权公告之日起生效。专利权有效性及专利权人变更等法律信息以专利登记簿记载为准。

局长
申长雨

国家知识产权局
2024年07月02日

第1页(共1页)

7.一种电力设备安装用提升装置

证书号第20793252号

实用新型专利证书

实用新型名称：一种电力设备安装用提升装置

发　明　人：魏继红;赵言赫

专　利　号：ZL 2023 2 2254395.5

专利申请日：2023年08月22日

专　利　权　人：郑州电力职业技术学院

地　　址：450000 河南省郑州市中牟县商都大道东段1933号

授权公告日：2024年04月19日　　授权公告号：CN 220811746 U

国家知识产权局依照中华人民共和国专利法经过初步审查，决定授予专利权，颁发实用新型专利证书并在专利登记簿上予以登记。专利权自授权公告之日起生效。专利权期限为十年，自申请日起算。

专利证书记载专利权登记时的法律状况。专利权的转移、质押、无效、终止、恢复和专利权人的姓名或名称、国籍、地址变更等事项记载在专利登记簿上。

局长
申长雨

国家知识产权局
2024年04月19日

第1页（共2页）

其他事项参见续页

8.一种新型新能源发电用风能发电装置

证书号第18379530号

实用新型专利证书

实用新型名称：一种新型新能源发电用风能发电装置

发　明　人：校香云;梁卫玲;马银安;魏继征

专　利　号：ZL 2022 2 2774377.5

专利申请日：2022年10月22日

专利权人：郑州电力职业技术学院

地　　址：450000 河南省郑州市中牟县商都大街东段

授权公告日：2023年01月31日　　授权公告号：CN 218407672 U

国家知识产权局依照中华人民共和国专利法经过初步审查，决定授予专利权，颁发实用新型专利证书并在专利登记簿上予以登记。专利权自授权公告之日起生效。专利权期限为十年，自申请日起算。

专利证书记载专利权登记时的法律状况。专利权的转移、质押、无效、终止、恢复和专利权人的姓名或名称、国籍、地址变更等事项记载在专利登记簿上。

局长
申长雨

国家知识产权局

2023年01月31日

第 1 页 (共 2 页)

其他事项参见续页

9.一种家用屋顶型光伏发电管理控制终端

证书号第19921577号

实用新型专利证书

实用新型名称：一种家用屋顶型光伏发电管理控制终端

发　明　人：王春红;任万英;马锐;翁玉娟;陈锋;马艳丽;魏勇
王建民

专　利　号：ZL 2023 2 1586708.0

专利申请日：2023年06月21日

专　利　权　人：郑州电力职业技术学院;许昌中意电气科技有限公司

地　　址：451450 河南省郑州市中牟县商都大街东段1933号

授权公告日：2023年10月31日　　授权公告号：CN 219937761 U

国家知识产权局依照中华人民共和国专利法经过初步审查，决定授予专利权，颁发实用新型专利证书并在专利登记簿上予以登记。专利权自授权公告之日起生效。专利权期限为十年，自申请日起算。

专利证书记载专利权登记时的法律状况。专利权的转移、质押、无效、终止、恢复和专利权人的姓名或名称、国籍、地址变更等事项记载在专利登记簿上。

局长
申长雨

国家知识产权局
2023年10月31日

第1页（共2页）

其他事项参见续页

10.一种电力电缆维修用卷绕设备

证书号第19216074号

实用新型专利证书

实用新型名称：一种电力电缆维修用卷绕设备

发　明　人：马艳丽;王丹;王春红;翁玉娟;常文晓

专　利　号：ZL 2023 2 0115427.0

专利申请日：2023年02月06日

专利权人：郑州电力职业技术学院

地　　址：451450 河南省郑州市中牟县新区商都大街东段1933号

授权公告日：2023年06月23日　　授权公告号：CN 219238847 U

国家知识产权局依照中华人民共和国专利法经过初步审查，决定授予专利权，颁发实用新型专利证书并在专利登记簿上予以登记。专利权自授权公告之日起生效。专利权期限为十年，自申请日起算。

专利证书记载专利权登记时的法律状况。专利权的转移、质押、无效、终止、恢复和专利权人的姓名或名称、国籍、地址变更等事项记载在专利登记簿上。

局长
申长雨

国家知识产权局
2023年06月23日

第1页 (共2页)

其他事项参见续页

11.一种用于屋顶的光伏板固定结构

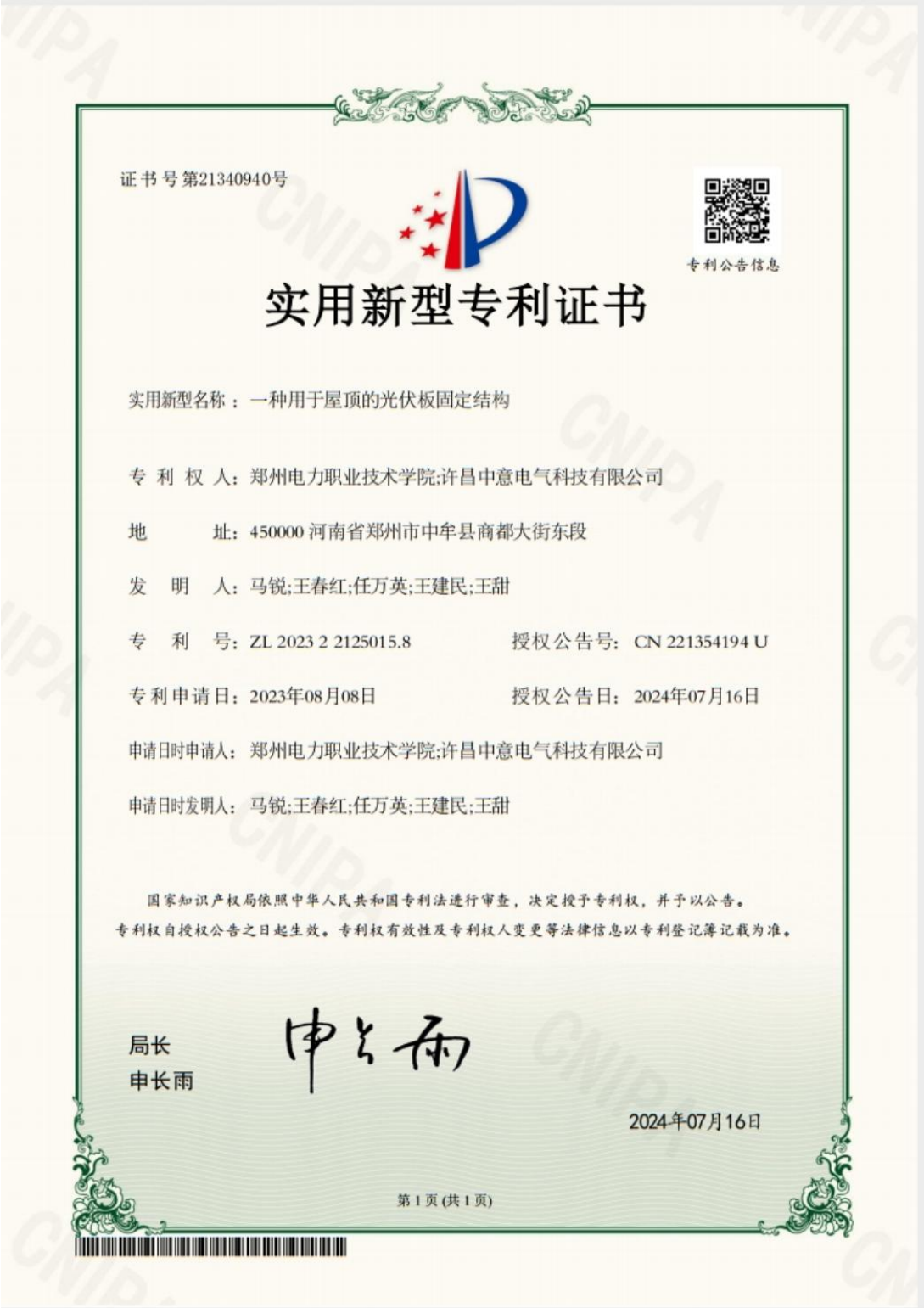

证书号第21340940号

专利公告信息

实用新型专利证书

实用新型名称：一种用于屋顶的光伏板固定结构

专 利 权 人：郑州电力职业技术学院;许昌中意电气科技有限公司

地　　址：450000 河南省郑州市中牟县商都大街东段

发 明 人：马锐;王春红;任万英;王建民;王甜

专　利　号：ZL 2023 2 2125015.8　　授权公告号：CN 221354194 U

专利申请日：2023年08月08日　　授权公告日：2024年07月16日

申请日时申请人：郑州电力职业技术学院;许昌中意电气科技有限公司

申请日时发明人：马锐;王春红;任万英;王建民;王甜

国家知识产权局依照中华人民共和国专利法进行审查，决定授予专利权，并予以公告。

专利权自授权公告之日起生效。专利权有效性及专利权人变更等法律信息以专利登记簿记载为准。

局长
申长雨

2024年07月16日

第 1 页 (共 1 页)

12.一种新能源电力监测装置

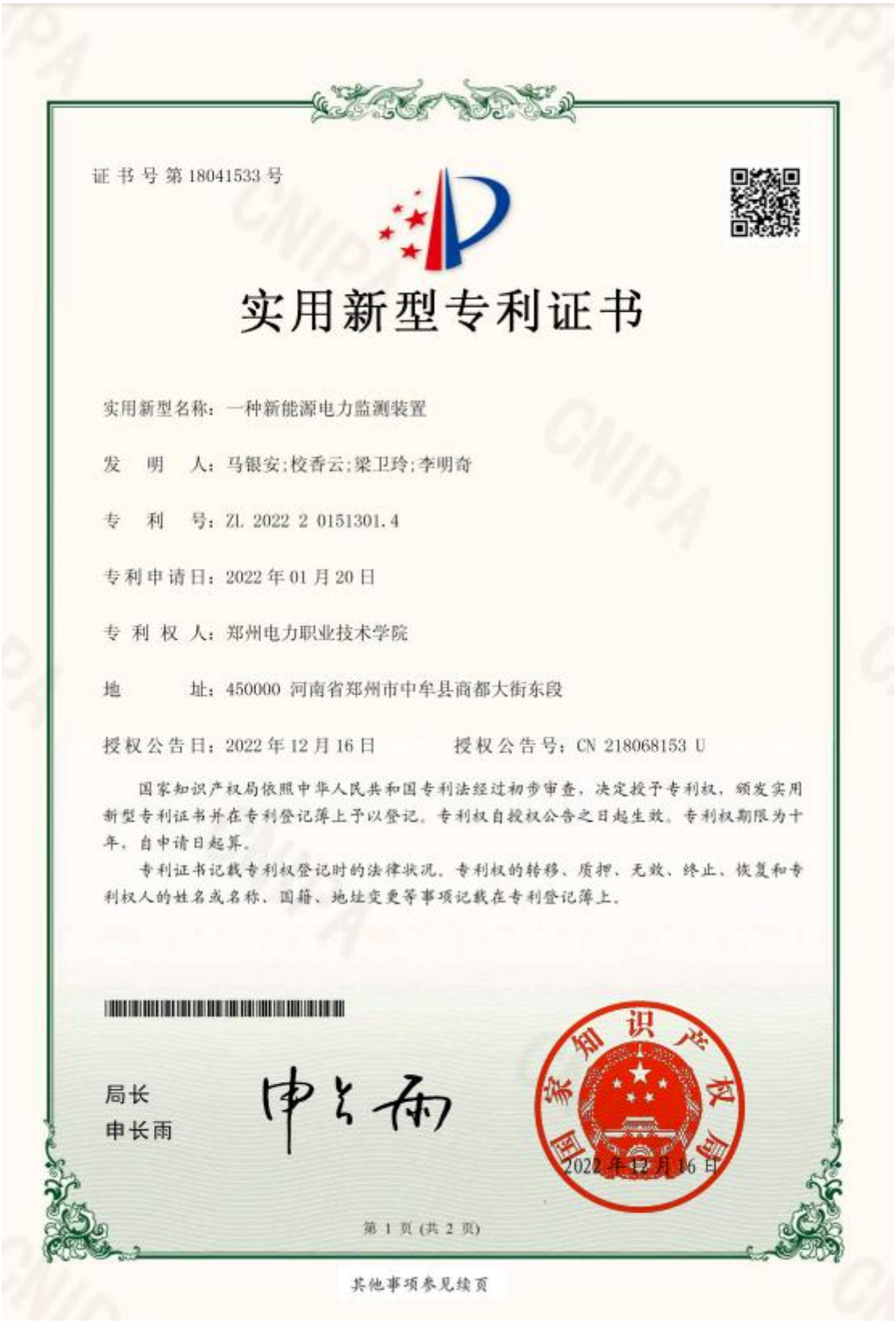

证书号第18041533号

实用新型专利证书

实用新型名称：一种新能源电力监测装置

发　明　人：马银安;校香云;梁卫玲;李明奇

专　利　号：ZL 2022 2 0151301.4

专利申请日：2022年01月20日

专利权人：郑州电力职业技术学院

地　　址：450000 河南省郑州市中牟县商都大街东段

授权公告日：2022年12月16日　　授权公告号：CN 218068153 U

国家知识产权局依照中华人民共和国专利法经过初步审查，决定授予专利权，颁发实用新型专利证书并在专利登记簿上予以登记。专利权自授权公告之日起生效。专利权期限为十年，自申请日起算。

专利证书记载专利权登记时的法律状况。专利权的转移、质押、无效、终止、恢复和专利权人的姓名或名称、国籍、地址变更等事项记载在专利登记簿上。

局长
申长雨

国家知识产权局
2022年12月16日

第 1 页 (共 2 页)

其他事项参见续页

13.一种变电站电气安装充气式防尘棚

证书号第15579407号

实用新型专利证书

实用新型名称：一种变电站电气安装充气式防尘棚

发　明　人：耿翠英;郭建宇;李晓蕾;陈上吉;王文豪;李宗;李锰;张龙林烽;刘洋;娄北

专　利　号：ZL 2021 2 1707467.1

专利申请日：2021年07月26日

专利权人：国网河南省电力公司经济技术研究院
国网河南省电力公司;国家电网有限公司

地　　址：450099 河南省郑州市二七区嵩山南路87号院办公区C楼1-10层

授权公告日：2022年01月21日　　授权公告号：CN 215595117 U

国家知识产权局依照中华人民共和国专利法经过初步审查，决定授予专利权，颁发实用新型专利证书并在专利登记簿上予以登记。专利权自授权公告之日起生效。专利权期限为十年，自申请日起算。

专利证书记载专利权登记时的法律状况。专利权的转移、质押、无效、终止、恢复和专利权人的姓名或名称、国籍、地址变更等事项记载在专利登记簿上。

局长
申长雨

国家知识产权局
2022年01月21日

第1页(共2页)

其他事项参见续页

14.一种多功能鱼塘高压线防触电报警装置

证书号第15583563号

实用新型专利证书

实用新型名称：一种多功能鱼塘高压线防触电报警装置

发　明　人：郭建宇;耿翠英;李晓蕾;陈上吉;王文豪;杨莹;李锰;张龙林烽;刘洋;娄北

专　利　号：ZL 2021 2 1706602.0

专利申请日：2021年07月26日

专 利 权 人：国网河南省电力公司经济技术研究院
国网河南省电力公司;国家电网有限公司

地　　址：450099 河南省郑州市二七区嵩山南路87号院办公区C楼1-10层

授权公告日：2022年01月21日　　授权公告号：CN 215599790 U

国家知识产权局依照中华人民共和国专利法经过初步审查，决定授予专利权，颁发实用新型专利证书并在专利登记簿上予以登记。专利权自授权公告之日起生效。专利权期限为十年，自申请日起算。

专利证书记载专利权登记时的法律状况。专利权的转移、质押、无效、终止、恢复和专利权人的姓名或名称、国籍、地址变更等事项记载在专利登记簿上。

局长
申长雨

国家知识产权局
2022年01月21日

第1页(共2页)

其他事项参见续页

15.一种发电厂直流接地故障分析装置

证书号第14413099号

实用新型专利证书

实用新型名称：一种发电厂直流接地故障分析装置

发　明　人：马银安;梁卫玲;王建华

专　利　号：ZL 2021 2 0475466.2

专利申请日：2021年03月05日

专利权人：郑州电力职业技术学院

地　　址：450000 河南省郑州市中牟县商都大街东段

授权公告日：2021年10月19日　　授权公告号：CN 214427587 U

国家知识产权局依照中华人民共和国专利法经过初步审查，决定授予专利权，颁发实用新型专利证书并在专利登记簿上予以登记。专利权自授权公告之日起生效。专利权期限为十年，自申请日起算。

专利证书记载专利权登记时的法律状况。专利权的转移、质押、无效、终止、恢复和专利权人的姓名或名称、国籍、地址变更等事项记载在专利登记簿上。

局长
申长雨

国家知识产权局

2021年10月19日

第1页(共2页)

其他事项参见续页

16.一种发电厂直流故障监测装置

证书号第14147409号

实用新型专利证书

实用新型名称：一种发电厂直流故障监测装置

发　明　人：梁卫玲;马银安;徐志文

专　利　号：ZL 2021 2 0196643.3

专利申请日：2021年01月26日

专利权人：郑州电力职业技术学院

地　　址：450000 河南省郑州市中牟县商都大街东段

授权公告日：2021年09月10日　　授权公告号：CN 214174536 U

国家知识产权局依照中华人民共和国专利法经过初步审查，决定授予专利权，颁发实用新型专利证书并在专利登记簿上予以登记。专利权自授权公告之日起生效。专利权期限为十年，自申请日起算。

专利证书记载专利权登记时的法律状况。专利权的转移、质押、无效、终止、恢复和专利权人的姓名或名称、国籍、地址变更等事项记载在专利登记簿上。

局长
申长雨

国家知识产权局

2021年09月10日

第1页(共2页)

其他事项参见续页

17.一种可移动的防尘散热型电力配电柜

证书号第11742496号

实用新型专利证书

实用新型名称：一种可移动的防尘散热型电力配电柜

发　明　人：马银安;周迎迎

专　利　号：ZL 2020 2 0884437.7

专利申请日：2020年05月22日

专利权人：郑州电力职业技术学院

地　　址：451450 河南省郑州市中牟县商都大街东段1933号

授权公告日：2020年10月27日　　授权公告号：CN 211790152 U

国家知识产权局依照中华人民共和国专利法经过初步审查，决定授予专利权，颁发实用新型专利证书并在专利登记簿上予以登记。专利权自授权公告之日起生效。专利权期限为十年，自申请日起算。

专利证书记载专利权登记时的法律状况。专利权的转移、质押、无效、终止、恢复和专利权人的姓名或名称、国籍、地址变更等事项记载在专利登记簿上。

局长
申长雨

国家知识产权局
2020年10月27日

第1页(共2页)

其他事项参见续页

18.基于系统灵活性的高比例可再生能源电力线路规划设计信息化软件 V1.0

中华人民共和国国家版权局
计算机软件著作权登记证书

证书号： 软著登字第16147665号

软 件 名 称： 基于系统灵活性的高比例可再生能源电力线路规划设计信息化软件
V1.0

著 作 权 人： 华红艳;李科乐;李帅贤;李家乐

权利取得方式： 原始取得

权 利 范 围： 全部权利

登 记 号： 2025SR1491467

根据《计算机软件保护条例》和《计算机软件著作权登记办法》的规定，经中国版权保护中心审核，对以上事项予以登记。

中华人民共和国国家版权局
计算机软件著作权登记专用章

2025年08月08日

19.基于共享通道的双向无线电能能耗分析管控系统 V1.0

中华人民共和国国家版权局

计算机软件著作权登记证书

证书号：软著登字第8425641号

软件名称：基于共享通道的双向无线电能能耗分析管控系统V1.0

著作权人：郑州电力职业技术学院;刘建萍;范莉

开发完成日期：2021年09月16日

首次发表日期：未发表

权利取得方式：原始取得

权利范围：全部权利

登记号：2021SR1703015

根据《计算机软件保护条例》和《计算机软件著作权登记办法》的规定，经中国版权保护中心审核，对以上事项予以登记。

中华人民共和国国家版权局 计算机软件著作权登记专用章

No. 09273960

2021年11月11日

20.穿管作业机器人远程智能操控系统 V1.0

中华人民共和国国家版权局

计算机软件著作权登记证书

证书号：软著登字第12312010号

软件名称：穿管作业机器人远程智能操控系统 V1.0

著作权人：赵言赫;魏继红

开发完成日期：2023年07月06日

首次发表日期：2023年08月08日

权利取得方式：原始取得

权利范围：全部权利

登记号：2023SR1724837

根据《计算机软件保护条例》和《计算机软件著作权登记办法》的规定，经中国版权保护中心审核，对以上事项予以登记。

中华人民共和国国家版权局 计算机软件著作权登记专用章

2023年12月22日

21.基于人工智能、大数据运算一体化的配电设备故障处理平台 V1.0

中华人民共和国国家版权局

计算机软件著作权登记证书

证书号：软著登字第11592425号

软件名称：基于人工智能、大数据运算一体化的配电设备故障处理平台
V1.0

著作权人：赵言赫;魏继红

开发完成日期：2023年03月01日

首次发表日期：2023年03月08日

权利取得方式：原始取得

权利范围：全部权利

登记号：2023SR1005252

根据《计算机软件保护条例》和《计算机软件著作权登记办法》的规定，经中国版权保护中心审核，对以上事项予以登记。

中华人民共和国国家版权局
计算机软件著作权登记专用章

2023年09月04日

22.电力系统设备可靠性评估监测管理软件 V1.0

38

中华人民共和国国家版权局

计算机软件著作权登记证书

证书号：软著登字第5433383号

软件名称：电力系统设备可靠性评估监测管理软件 V1.0

著作权人：郑州航空工业管理学院;李响

开发完成日期：2020年04月03日

首次发表日期：未发表

权利取得方式：原始取得

权利范围：全部权利

登记号：2020SR0554687

根据《计算机软件保护条例》和《计算机软件著作权登记办法》的规定，经中国版权保护中心审核，对以上事项予以登记。

中华人民共和国国家版权局 计算机软件著作权登记专用章

No. 05787433

2020年06月02日

23.光伏发电工程施工现场安全防护与应急技术规范

ICS 27.160
CCS D4416

T/XZBX

西安市质量与标准化协会团体标准

T/XZBX 0056—2025

光伏发电工程施工现场安全防护与应急技术规范

Technical specification for on-site safety protection and emergency response in photovoltaic power generation projects

2025－08－15 发布　　2025－09－01 实施

西安市质量与标准化协会　　发 布

前　言

本文件按照GB/T 1.1—2020《标准化工作导则　第1部分：标准化文件的结构和起草规则》的规定起草。

请注意本文件的某些内容可能涉及专利。本文件的发布机构不承担识别专利的责任。

本文件由西安市质量与标准化协会提出并归口。

本文件起草单位：中建二局第一建筑工程有限公司、盐城新源电力建设监理有限公司、华能陇东能源有限责任公司、西安源能初心信息科技有限公司、衡丰发电有限责任公司、中国能源建设集团西北电力建设工程有限公司、郑州电力职业技术学院、中电建湖北电力建设有限公司、中国石油天然气股份有限公司辽河油田分公司欢喜岭采油厂、衡水市建设工程安全监督站、华宝人力资源有限公司、中通服网盈科技有限公司、中远融通工程咨询有限公司、郑州枫伙电力科技有限公司、广州发展新能源集团股份有限公司华北分公司。

本文件主要起草人：李岩、吉中良、王大鹏、董彦军、穆伟、华红艳、胡启宪、李秀全、王继伟、焦建国、张军、库杰、乔新颖、郭瑞玲、王亚莉、张永昌、苗丁丁、李晓燕、苏颖斐、周敬阳、葛攀攀、闫灵敏、谢政华、赵淑娅、赵家豪、杨金金。

（三）科研论文

1.Evaluation of the Development Level and Key Measures of.New.Power System.in.Ecological Protection Cities

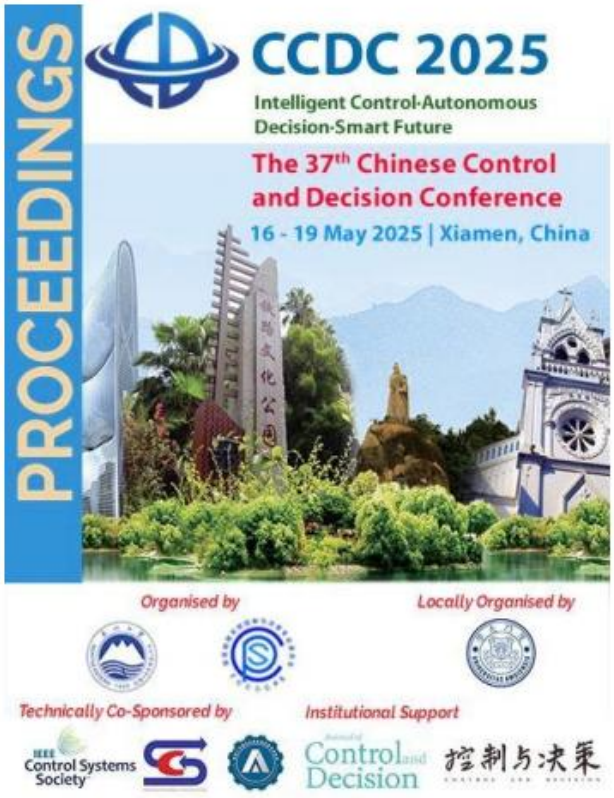

出版物封面

Sunday, 18 May 2025

SunA01	IntelliSense and advanced sensing, detection technology (1) (Special Session)
SunA02	AI enabled smart grid and energy internet (1) (Special Session)
SunA03	Educational reform and innovation on intelligent control disciplines (Special Session)
SunA04	AI-driven operational optimization and control of metallurgical process (1) (Special Session)
SunA05	Control and management on smart city (Building) (1) (Special Session)
SunA06	Swarm perception and cooperation control of marine unmanned systems (1) (Special Session)
SunA07	Data-driven adaptive learning systems and applications (1) (Special Session)
SunA08	Intelligent perception, control, and decision-making for unmanned systems in complex environments (1) (Special Session)
SunA09	Fault diagnosis, prognosis and prediction maintenance (2)
SunA10	Industrial big data and industrial artificial intelligence (2)
SunA11	Intelligent perception, synergic decision-making, and security for robots and unmanned systems (2)
SunA5	Interactive Session
SunB01	IntelliSense and advanced sensing, detection technology (2) (Special Session)
SunB02	AI enabled smart grid and energy internet (2) (Special Session)
SunB03	New energy control and smart energy (Special Session)
SunB04	AI-driven operational optimization and control of metallurgical process (2) (Special Session)
SunB05	Control and management on smart city (Building) (2) (Special Session)
SunB06	Swarm perception and cooperation control of marine unmanned systems (2) (Special Session)
SunB07	Data-driven adaptive learning systems and applications (2) (Special Session)
SunB08	Intelligent perception, control, and decision-making for unmanned systems in complex environments (2) (Special Session)
SunB09	Energy big data and energy system digitalization
SunB10	Distributed intelligent algorithms and applications (Special Session)
SunB11	Intelligent perception, synergic decision-making, and security for robots and unmanned systems (3)
SunB5	Interactive Session
SunC01	IntelliSense and advanced sensing, detection technology (3) (Special Session)
SunC02	Research and empowering application of AI algorithm in municipal solid waste (1) (Invited Session)
SunC03	Cooperative safety control of swarm intelligent unmanned system (Invited Session)
SunC04	Intelligent guidance and control of aerospace vehicles (Invited Session)

目录

Evaluation of the Development Level and Key Measures of New Power System in Ecological Protection Cities

Hongyan Hua[1], Huachen Feng[2,3], Xiang Li[2,3], Mingwei Dong[2,3], Zhuo Chen[4], Ke Zhao[2,3]
[1]School of Automation, Zhengzhou University of Aeronautics, Zhengzhou Electric Power Technology College, Zhengzhou, China
[2]School of Electrical Engineering, Zhengzhou Electric Power Technology College, Zhengzhou, China
[3]School of automation Zhengzhou university of aeronautics, Zhengzhou, China
[4]Engineering Department Sucheng Xinyu Testing and Research Institute Co. Ltd, Zhengzhou, China

ABSTRACT

Ecological protection cities prioritize environmental conservation as the foundation for social development. The construction of a new power system in such cities adheres to the dual carbon goals and selects an indicator system across five dimensions: clean and low-carbon, safe and controllable, flexible and efficient, intelligent and friendly, and open and interactive. Using the analytic hierarchy process (AHP) and expert methods, weights are determined through pairwise comparisons of indicators at each hierarchical level based on international and domestic advanced power system standards. Evaluation functions are established to construct a comprehensive assessment model tailored for ecological protection cities. Development goals and implementation plans are formulated, and this model is tested/fully or validated through a case study in an ecological protection city.

Keywords: Dual-carbon target, New power system, Safe and controllable, Flexible and efficient, Intelligent and friendly

Evaluation of the Development Level and Key Measures of New Power System in Ecological Protection Cities

1st *Hongyan Hua
School of Automation
Zhengzhou University of Aeronautics
Zhengzhou Electric Power Technology College
Zhengzhou, China
hhyhuahongyan@163.com

2nd Huachen Feng
School of Electrical Engineering
Zhengzhou Electric Power Technology College
Zhengzhou, China
m19503833685@163.com

3rd Xiang Li
School of Automation
Zhengzhou University of Aeronautics
Zhengzhou, China
Lixiang@zua.edu.cn

4th Mingwei Dong
School of Electrical Engineering
Zhengzhou Electric Power Technology College
Zhengzhou, China
2809962671@qq.com

5th Zhuo Chen
Engineering Department
Xuchang Kaipu Testing and Research Institute Co.,Ltd
Zhengzhou, China
smfengkeming@163.com

6th Ke Zhao
School of Automation
Zhengzhou University of Aeronautics
Zhengzhou, China
1723886898@qq.com

***Abstract*—Ecological protection cities prioritize environmental conservation as the foundation for social development. The construction of a new power system in such cities adheres to the dual carbon goals and selects an indicator system across five dimensions: clean and low-carbon, safe and controllable, flexible and efficient, intelligent and friendly, and open and interactive. Using the analytic hierarchy process (AHP) and expert methods, weights are determined through pairwise comparisons of indicators at each hierarchical level. Based on international and domestic advanced power system standards, evaluation functions are established to construct a comprehensive assessment model tailored for ecological protection cities. Development goals and implementation plans are formulated, and the model's feasibility is validated through a case study in an ecological protection city.**

***Index Terms*—Dual-carbon target; New power system; Safe and controllable; Flexible and efficient; Intelligent and friendly**

Introduction

Under the green and low-carbon goals, the transformation of traditional power systems to new power systems is an inevitable trend [1] [2] [3]. Ecological protection cities often have a good ecological environment, with abundant natural ecology represented by mountains and waters, and relatively concentrated rare and endangered wild animals and plants. Protecting the ecological environment is the premise of economic and social development, and energy development is often subject to rigid constraints [4] [5]. On the grid side, the load level is often not high, but the safety standard requirements are high [6] [7], and the pressure for high-quality power supply services is great [8] [9].

Given these unique constraints, this paper proposes an evaluation framework and targeted measures for new power systems in ecological protection cities, focusing on environmental preservation and sustainable energy development.

Comprehensive Evaluation Model for the Development Level of the New Power System

A. Indicator System

Based on the basic characteristics of the new power system, 26 indicators are carefully selected from five dimensions: clean and low-carbon, safe and controllable, flexible and efficient, intelligent and friendly, and open and interactive to evaluate the new power system in ecological protection cities. The evaluation indicator system for the development level of the new power system in ecological protection cities is shown in the following table:

TABLE I. EVALUATION INDICATOR SYSTEM FOR THE DEVELOPMENT LEVEL OF THE NEW POWER SYSTEM IN ECOLOGICAL PROTECTION CITIES

Primary Indicator	Secondary Indicator	Tertiary Indicator	Unit
Evaluation Indicator System for the Development Level of the New Power System in Ecological Protection Cities	Clean and Low-carbon	Proportion of Clean Energy Installed Capacity	%
		Proportion of Clean Energy Power Generation	%
		New Energy Accommodation Rate	%
		Proportion of New Energy Curtailment	%
		Overall Line Loss Rate	%
		Proportion of High-loss Distribution Transformers	%
	Safe and Controllable	110 - 35 kV Main Transformer N-1 Pass Rate	%
		110 - 10 kV Line N-1 Pass Rate	%
		Proportion of 110 - 10 kV High-fault Transformers	%
		Proportion of 110 - 10 kV High-fault Lines	%
		Proportion of New Energy Dispatchable Capacity	%
		New Energy Connection Margin	%
		Number of Power Limitation Occurrences	%
		Proportion of Controllable Load to the Maximum Power Load	%

Fund projects: 1. Henan Province Higher Education Key Scientific Research Project(25B470013) 2. Ministry of Education Industry-University Cooperation Project (231104309141 85, 231104309095554, 202101203017); 3. Henan Province Higher Education Teaching Reform Key Project (2024SJGLX0694); 4. Zhengzhou University of Aeronautics Teaching Project (zhjy23-63)

979-8-3315-1056-5/25/$31.00©2025 IEEE

Primary Indicator	Secondary Indicator	Tertiary Indicator	Unit
	Flexible and Efficient	Proportion of Flexible Regulation Power Source Capacity	%
		Probability of Insufficient Up-regulation Flexibility	%
		Probability of Insufficient Down-regulation Flexibility	%
		Proportion of 110 - 10 kV Light-load Main Transformers	%
		Proportion of 110 - 10 kV Light-load Lines	%
		Proportion of 110 - 10 kV Heavy-load Main Transformers	%
		Proportion of 110 - 10 kV Heavy-load Lines	%
	Intelligent and Friendly	Proportion of Intelligent Substations	%
		Effective Coverage Rate of Distribution Automation	%
		Installation Rate of Smart Meters	%
		Proportion of Predictable New Energy Power Stations	%
		Proportion of New Energy Power Stations with Energy Storage	%
		Proportion of Users with Time-of-use Electricity Price	%
	Open and Interactive	Proportion of Electric Energy in Terminal Energy Consumption	%
		Completion Rate of Electric Vehicle Charging Station Planning	%
		Proportion of Electric Vehicle-to-Grid (V2G) Technology	%
		Number of Users of Multi-energy Complementary Microgrids	Household

In the clean and low-carbon aspect, there are 6 indicators, focusing on evaluating the clean and low-carbon level of the power source side and the grid side. In the safe and controllable aspect, there are 8 indicators, focusing on evaluating the grid structure, equipment failure situation, new energy and load control situation, etc. In the flexible and efficient aspect, there are 7 indicators, focusing on evaluating the dispatch flexibility and equipment operation efficiency and benefit situation. In the intelligent and friendly aspect, there are 6 indicators, focusing on evaluating the application situation of intelligent substation technology, the effective coverage situation of distribution automation, and the coordination situation of source-grid-load-storage. In the open and interactive aspect, there are 4 indicators, focusing on evaluating the access situation of new technologies such as electric vehicles and multi-energy complementary microgrids and diversified loads.

B. Evaluation Method

1) Weight Setting

The weight setting adopts the analytic hierarchy process.Firstly, the problem is decomposed into different levels according to the overall goal to construct a multi-level analysis model. Then, the importance of the indicators in the level is compared pairwise according to a certain scale to determine the importance (i.e., weight value) of each indicator in each level relative to the indicator in the upper level. The flow chart for determining weights by the analytic hierarchy process is as follows:

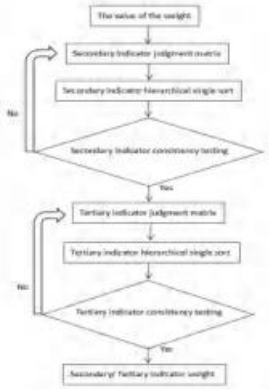

Fig. 1. Flow Chart for Weight Setting by Analytic Hierarchy Process

The evaluation system for the new power system in ecological protection cities mainly has three levels. Firstly, taking the overall goal as the first-level indicator and as a reference, on the basis of constructing the judgment matrix of the second-level indicators, calculate the importance (i.e., weight) of each second-level indicator and sort them. Conduct consistency verification. If the verification is unsuccessful, return to modify the judgment matrix of the second-level indicators. If the verification is successful, construct the judgment matrix of the third-level indicators, calculate the importance of each third-level indicator and sort them. Conduct consistency verification. If the verification is unsuccessful, return to modify the judgment matrix of the third-level indicators. If the verification is successful, obtain the weights of the third-level indicators. In addition, if the evaluation system has multiple layers, the weights of each indicator can still be determined layer by layer according to the upper and lower level order.

2) Scoring Function

The scoring function is evaluated according to the leading power system indicator at home and abroad, the required values of the guidelines and standards, and the average level within the region. Generally,three evaluation function models are adopted:

1.For indicators where the smaller the target value,the better,the evaluation function is as follows:

$$u(x)=\begin{cases}100 & x\le a_1\\ 100(x-a_2)/(a_1-a_2) & a_1\le x\le a_2\\ 0 & x>a_2\end{cases} \quad (1)$$

Or

$$u(x)=\begin{cases}100 & x\le a_1\\ ax^2+bx+c & a_1\le x\le a_2\\ 0 & x>a_2\end{cases} \quad (2)$$

2.For indicators where the larger the target value,the better,the evaluation function is as follows:

$$u(x)=\begin{cases}0 & x\le a_2\\ 100(x-a_2)/(a_1-a_2) & a_2\le x\le a_1\\ 100 & x>a_1\end{cases} \quad (3)$$

Or

$$u(x)=\begin{cases}0 & x\le a_2\\ ax^2+bx+c & a_2\le x\le a_1\\ 100 & x>a_1\end{cases} \quad (4)$$

3. For indicators where the target value is within a certain interval,the evaluation function is as follows:

$$u(x)=\begin{cases}100 & a_{11}\le x\le a_{12}\\ 100(x-a_{11})/(a_{11}-a_{21}) & a_{21}\le x\le a_{11}\\ 100(x-a_{22})/(a_{12}-a_{22}) & a_{12}\le x\le a_{22}\\ 0 & x<a_{21}\ or\ x>a_{22}\end{cases} \quad (5)$$

Overall Goals and Development Directions

A. Overall Goals

The development strategy of the new power system is formulated according to the idea of "overall planning and step-by-step implementation". The development process of the new power system experiences three stages: the initial stage, the development stage, and the completion stage.

In the initial stage, vigorously support the connection of new energy mainly based on photovoltaics, promote the construction of the integrated energy network with the distribution network as the core, actively serve the transformation of energy consumption patterns, and build a development pattern of the new power system with regional characteristic differences and user attribute differences.

In the development stage, promote the dominant position of new energy installed capacity, initially form a new power system with new energy as the main body, deeply transform the grid form, power consumption form, etc., accelerate the implementation progress of intelligent distribution networks and active distribution networks, and basically build a strong and intelligent distribution network.

In the completion stage, the source-grid-load-storage system and market mechanism tend to be perfect, the resilient, elastic, and active distribution networks are fully built, and the new power system is basically completed, with the ability to supply power safely and stably and the ability to defend against the risk of large-scale power outages.

B. Development Directions of Each Stage

The development directions and tasks of each stage are clearly defined as follows:

1) Initial stage

Firstly, construct the architecture of the development pattern of the new power system in ecological protection cities. Start to build an intelligent interactive, open sharing, and collaborative efficient modern power network platform, and construct the architecture of the development pattern of the new power system with regional characteristic differences and user attribute differences.

Secondly, promote the characteristic utilization of new energy in multiple scenarios and carry out demonstration projects. Leverage the "Guang ' e Bao" (State Grid PV Cloud Network) platform to facilitate local new energy development, promote the clean production of rural energy, and carry out distributed photovoltaic projects on a large scale, build a project for the benefit of the people, send "sunshine income" to the people, create a typical case of comprehensive rural revitalization, and promote the characteristic utilization of new energy in multiple scenarios.

Thirdly, formulate power supply safety standards under the requirement of high-quality development of the distribution network. Strengthen the construction of the high-voltage distribution network grid, build a large-scale and high-efficiency clean energy allocation platform, and increase the N-1 pass rate of main transformers and lines to 100%. The 10kV distribution network should mainly be a cable network, supplemented by an overhead network. While improving the grid, accelerate the construction of distribution automation and strive to make the effective coverage rate of distribution automation reach 100%.

Fourthly, carry out key technology construction projects for the new power system. Combined with digital construction, relying on power big data, blockchain and other technologies, continuously improve the holographic perception and intelligent level of the power system. Encourage the "new energy + energy storage/hydropower packaging" model to improve the stability of new energy generation and prevent the intermittence and randomness of new energy generation. Strengthen the research and application of key technologies such as virtual power plants and digital twin grids.

Fifthly, formulate a management improvement plan. In terms of concept innovation, initially form a new governance model; formulate a management model suitable for the development of the new power system.

2) Development stage

Firstly, comprehensively improve the technical level and equipment level of the distribution network. Strengthen the construction of the distribution network grid structure and equipment selection, thus promoting the high-quality development of the distribution network and improving the elasticity and resilience of the urban distribution network.

Secondly, comprehensively promote the implementation of key technologies for strong and intelligent power grids. Optimize and improve the network architecture, improve the safety level and acceptance ability of the power grid, and build a clean, efficient, safe and reliable clean energy allocation.

Thirdly, carry out large-scale application actions of energy storage, and innovate application scenarios and business models. On the power generation side, have functions such as frequency modulation and voltage support. Reasonably plan energy storage on the grid side, increase system regulation ability, provide standby power for the grid, and provide frequency modulation auxiliary services. On the user side, reduce transformer capacity fees, improve power quality, facilitate demand side management and user time-of-use electricity price management.

Fourthly, comprehensively promote an efficient and lean management mode. Implement reliability management through six measures such as project quota management, implementation of condition-based maintenance, transfer power supply management, power outage event merging management, live-line work, and major power outage management.

Fifthly, strictly implement power supply safety standards.

Fig. 2. Application and Functions of Energy Storage in Each Link of the Power System

3) Completion stage

Firstly, solidify power technology and normalize management: further improve the power generation, distribution and power consumption technologies and management levels. After reaching various technical goals, finally implement solidification and normalization of management. Secondly, widely apply and build intelligent communities and intelligent power consumption equipment, and comprehensively promote two-way interactive services; distributed energy systems and various terminal power consumption devices with power generation and power consumption functions achieve "plug-and-play". Thirdly, fully build a new power system: the distribution network has a strong bearing capacity for accepting new energy and diversified loads, promotes the priority local and nearby development and utilization of new energy, and has good flexibility.

Key Measures and Critical Technologies

A. Clean and Low-carbon Measures

Firstly, large-scale development of distributed photovoltaics. In line with the principle of "government organization and market operation", promote the integrated development of photovoltaic new energy economy and modern rural industries to achieve regional renewable energy coverage. Conduct an analysis of the access capacity of distributed power sources, and formulate typical grid-connected models for distributed photovoltaics. Secondly, expansion and renovation of hydropower stations. Thirdly, strengthen the construction of new energy grid- connected infrastructure. Fourthly, rational application of microgrid technology. Fifthly, promote energy substitution projects.

B. Safe and Controllable Measures

Firstly, attach importance to power grid safety assessment. In accordance with technical guidelines such as the "Regulations on Emergency Handling and Investigation and Handling of Power Safety Accidents" (Order 599) and the "Guide for Power System Security and Stability", carefully sort out power grid risks, establish three lines of defense for the power grid, and prevent the risks of the power grid itself and those brought about by the large-scale access of new energy.

Secondly, strengthen the high-voltage grid. With the 220kV substation as the center, the 110kV power grid realizes the chain and ring network power supply mode. Clearly define the 110kV tie lines, ensure that the tie lines have sufficient standby capacity, and ensure that the load can be transferred in case of accidents. Generally, the 110kV substation should preferably meet the "dual power supply requirements", and the power sources should come from two independent power points as much as possible. If it is difficult to achieve, they can come from the same high-voltage power point.

Thirdly, optimize the medium-voltage grid. In the central urban area, the overhead lines should preferably adopt the multi-section two-tie connection, and the cables should adopt the double-ring network structure; in towns or suburbs, the overhead lines should preferably adopt the multi-section two-tie connection, and the cables should adopt the single-ring network structure; in rural areas, the overhead single-tie connection should be adopted.

Fourthly, optimize the layout of energy storage on the power grid side. Develop electrochemical energy storage according to local conditions and configure energy storage at key nodes to improve the safety and stability level of the power grid.

Fifthly, strengthen the safety management of the distribution network. Establish the idea of safety first, be familiar with the grid structure, and strengthen equipment maintenance.

Sixthly, promote new technologies for distribution network safety. Such as automation transformation technology, equipment insulation technology, personal and equipment safety protection technology, etc.

C. Flexible and Efficient Measures

Firstly, increase the proportion of flexible regulation power sources on the supply side and rationally layout energy storage on the source-grid side. On the one hand, carry out renovation projects of pumped storage power stations according to local conditions and consider the transformation of pumped storage power stations with conditions into hybrid pumped storage power stations. On the other hand, actively respond to the rapid growth of new energy and rationally layout electrochemical energy storage on the power source side and the power grid side.

Secondly, strengthen the power demand response. Deeply tap flexible regulation resources such as elastic loads and virtual power plants. In the development stage of the new power system, the scale of demand response users should reach about 5% of the maximum power load.

Thirdly, scientifically promote the cross-regional transmission of new energy and improve the level of power grid interconnection and mutual assistance. Based on the smart grid, promote the construction of transmission lines to realize the cross-regional and long-distance transmission of energy, strengthen energy exchanges and cooperation with surrounding areas, and optimize the external energy supply environment and cross-regional energy security mechanism.

Fourthly, use market means to encourage the construction of flexibility resources. On the power source side, promote the implementation of the "new energy + energy storage" incentive mechanism and develop pumped storage power stations according to local conditions to ensure the diversity and adequacy of flexible power supply. On the power grid side, actively carry out demand response capabilities and use market means such as peak-valley electricity prices and interruptible load electricity prices to improve the enthusiasm of users to participate in power

system regulation. In terms of carbon trading, explore the carbon trading market mechanism, combine it with the power market, couple carbon prices with power generation costs, and stimulate enterprises to invest in low-carbon technologies and energy.

D. Intelligent and Friendly Measures

Firstly, apply intelligent substation technology. Applicable to the new intelligent substations of 110kV - 220kV or the intelligent transformation projects of in-service substations. With safety and reliability as the premise, focus on applying relatively mature and cost-effective technologies and equipment.

Secondly, accelerate the construction of distribution automation. Improve the technical level of distribution automation. The construction of distribution automation should be compatible with the primary grid and equipment of the distribution network. The distribution automation system should be synchronously coordinated and planned with information systems such as PMS and power grid GIS platforms to meet the information interaction requirements and provide technical support for the whole process management of the distribution network.

E. Open and Interactive Measures

Firstly, deeply carry out the application of energy digital technology and comprehensive energy services. Utilize energy big data technology to strengthen the analysis of power consumption data, characterize user behaviors and portraits, and provide comprehensive energy services such as energy efficiency management.

Secondly, promote the establishment of load resource utilization technology. Open up the data and control channels between load equipment, acquisition terminals, virtual power plants, power grid dispatching systems and trading systems to achieve closed-loop intensive management of load resources that are observable, measurable, controllable and adjustable.

Application and Development Measures of the Evaluation System

The system is applied to an ecological protection city in central China. The development goal of this city is mainly ecological protection. Combined with the power system development situation of this place, the scores of various indicators are shown in the following table:

TABLE II. COMPREHENSIVE EVALUATION OF AN ECOLOGICAL PROTECTION CITY

Primary Indicator	Secondary Indicator	Tertiary Indicator	Secondary	Tertiary	Score
Evaluation Indicator System for the Development Level of the New Power System in Ecological Protection Cities	Clean and Low-carbon	Proportion of Clean Energy	0.25	0.17	4.17
		Proportion of Clean Energy	0.25	0.17	4.17
		New Energy Accommodation Rate	0.25	0.17	4.17
		Proportion of New Energy Curtailment	0.25	0.17	4.17
		Overall Line Loss Rate	0.25	0.17	2.30
		Proportion of High-loss Distribution	0.25	0.17	4.17
	Safe and Controllable	110-35 kV Main Transformer N-1 Pass Rate	0.25	0.13	1.92
		110 - 10 kV Line N-1 Pass Rate	0.25	0.13	2.90
		Proportion of 110-10 kV High-	0.25	0.13	2.60
		Proportion of 110-10 kV High-fault Lines	0.25	0.13	2.50
		Proportion of New Energy Dispatchable	0.25	0.13	1.78
		New Energy Connection	0.25	0.13	3.13
		Number of Power Limitation Occurrences	0.25	0.13	3.13
		Proportion of Controllable Load to the	0.25	0.13	3.13
	Flexible and Efficient	Proportion of Flexible Regulation Power Source	0.2	0.14	0.00
		Probability of Insufficient Up-regulation	0.2	0.14	2.86
		Probability of Insufficient Down-regulation Flexibility	0.2	0.14	2.86
		Proportion of 110-10 kV Light-load Main	0.2	0.14	2.42
		Proportion of 110-10 kV Light-load Lines	0.2	0.14	1.43
		Proportion of 110 - 10 kV Heavy-load Main Transformers	0.2	0.14	1.67
		Proportion of 110 - 10 kV Heavy-load	0.2	0.14	1.90
	Intelligent and Friendly	Proportion of Intelligent	0.15	0.14	0.56
		Effective Coverage Rate of Distribution	0.15	0.17	1.18
		Installation Rate of Smart Meters	0.15	0.17	2.50
		Proportion of Predictable New Energy Power	0.15	0.17	2.50
		Proportion of New Energy Power Stations	0.15	0.17	0.00
		Proportion of Users with Time-of-use Electricity	0.15	0.17	2.50
	Open and Interactive	Proportion of Electric Energy in Terminal	0.15	0.25	3.75
		Completion Rate of Electric Vehicle Charging Station Planning	0.15	0.25	3.75
		Proportion of Electric Vehicle-to-Grid (V2G) Technology	0.15	0.25	0.00

Primary Indicator	Secondary Indicator	Tertiary Indicator	Seco nda	Terti ary	Score
		Number of Users of Multi-energy Complementary Microgrids	0.15	0.25	0.00
Comprehensive Score					74.09

Since the construction of the new power system in this city is in its initial stage, the comprehensive score is not high, which is 74.09 points. The scores, analyses and suggestions for each sub-item are as follows:

In the clean and low-carbon aspect, the score is 23.14 with a score rate of 92.55%. Since the city mainly has hydropower and photovoltaics, the clean level on the power supply side of the grid is relatively high. However, due to the long power supply distance of substations, the network loss is relatively high.

In the safe and controllable aspect, the score is 21.08 with a score rate of 84.33%. The grid structure of the high-voltage distribution network in this city is mainly ring and chain, which is generally strong, and high-fault equipment can be solved or replaced in a timely manner. However, on the power source side, there are many small hydropower stations in this city with poor controllability, which need to be rectified or standardized. On the grid side, due to many mountainous areas in this city, there are quite a number of single-radiation lines in the medium-voltage distribution network, and the grid structure needs to be further strengthened. On the load side, considering that controllable loads have a positive effect on the safety and stability of the power grid, the scope of controllable loads can be considered to be expanded.

In the flexible and efficient aspect, the score is 13.13 with a score rate of 65.66%. At present, there is not much photovoltaic access, and there is no problem of insufficient up/down regulation flexibility in dispatching. With the rapid development of photovoltaics, the randomness and intermittence on the power source side will increase, which will inevitably put forward higher requirements for the flexibility of the system. In terms of operation efficiency and benefits,there are some inefficient and heavy-load equipment.

In the intelligent and friendly aspect, the score is 9.24 with a score rate of 61.6%. At present, most of the substations in this city are not intelligent substations, and the coverage rate of distribution automation is relatively low, so the intelligence of the power grid needs to be further strengthened. At the same time, considering that "new energy + energy storage" is the future development direction of energy, it should be encouraged.

In the open and interactive aspect, the score is 7.5 with a score rate of 50%. With the rapid development of new energy, the access of electric vehicles and microgrid users puts forward higher requirements for the open and interactive nature of the distribution network. It is necessary to explore practical paths in aspects such as extensive interconnection, digital transformation and comprehensive energy systems.

When formulating the development goals and development measures of this city, reference can be made to the "Overall Goals and Development Directions" and "Key Measures and Key Technologies" sections.

CONCLUSIONS

This paper starts from the basic characteristics of the power system, combines the regional characteristics and development strategies of ecological protection cities, and formulates specific, feasible and clear-targeted development goals and key measures for the new power system. The main achievements are summarized as follows:

(1) An evaluation indicator system for the development of the source-grid-load-storage new power system is constructed, starting from the basic characteristics of the new power system. This system includes multiple dimensions such as clean and low-carbon, safe and controllable, flexible and efficient, intelligent and friendly, and open and interactive, with a total of 26 indicators. At the same time, the analytic hierarchy process and expert method are used to determine the indicator weights and construct three evaluation functions, thus establishing a comprehensive evaluation for the new power system suitable for ecological protection cities.

(2) Propose short-, medium- and long-term development measures in aspects such as clean and low-carbon, safe and controllable, flexible and efficient, intelligent and friendly, and open and interactive, respectively. Clearly define the improvement degree of core indicators in different stages and construct an economically effective technical route to achieve the goals of the new power system.

(3) The constructed source-grid-load-storage new power system development evaluation system is applied to the power system of a central city, clarifying the shortcomings and goals of the new power system construction in this city and verifying the feasibility and applicability of the system.

REFERENCES

[1]Kang Chongqing, Yao Liangzhong.Key scientific issues and theoretical research framework for power systems with a high proportion of renewable energy [J] .Power system automation, 2017, 41 (9) : 1-11.

[2]Xing Haijun, Cheng Haozhong, Zhang Shenxi, etc . A review of research on active distribution network planning [J] .Power Grid Technology, 2015, 39 (10) : 2705-2711.

[3]Karimyan P, Gharehpetian G B, Abedi M, et al. Long term scheduling for optimal allocation and sizing of DG unit considering load variations and DG type[J] International Journal of Electrical Power & Energy Systems, 2014, 54: 277-287.

[4]DONG L, JIA L I, TIANJIAO P U, et al. Distributionally robust optimization model of active distribution network considering uncertainties of source and load[J]. Journal of Modern Power Systems and Clean Energy, 2019, 7 (6) :1-11.

[5]Ye Bin, Wang Xuli, Ma Jing, etc. Research on the benefit evaluation of distribution network considering microgrid and multiple load under the new power reform[J].Power Engineering Technology, 2019, 38(3) : 108-114.

[6]Zhao Bo, Xu Zhicheng, Xu Chen, et al. Network partitionbased zonal voltage control for distribution networks with distributed PV systems[J]. IEEE Trans on Smart Grid, 2018, 9 (5) : 4087-4098.

[7]Liu Bo, Ke De Ping, Li Peng,etc.Method for identifying the power of distributed photovoltaic power generation in the area of low-voltage distribution station[J].Power system automation, 2019, 43(19) : 111-116, 123.

[8]Gao Hui,Xu Qing, Ouyang Zengkai,etc.Analysis of source-grid-load coordination and optimization control strategy with multiple types of distributed generators[J].Power Engineering Technology, 2018, 37 (4) : 21-26.

[9]Gao Guoliang.Research on the loss reduction and planning of the distribution network after the access of distributed generators[D].Jinan: Shandong University, 2019.

2.Research Status and Method of Aviation Sensor Performance

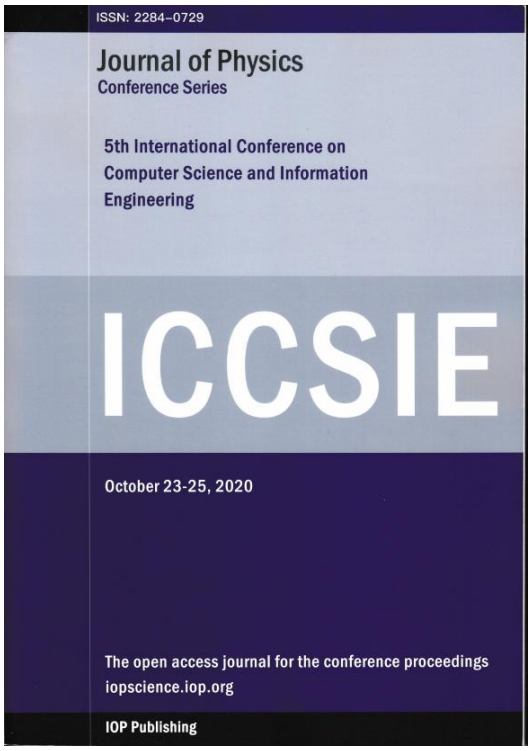

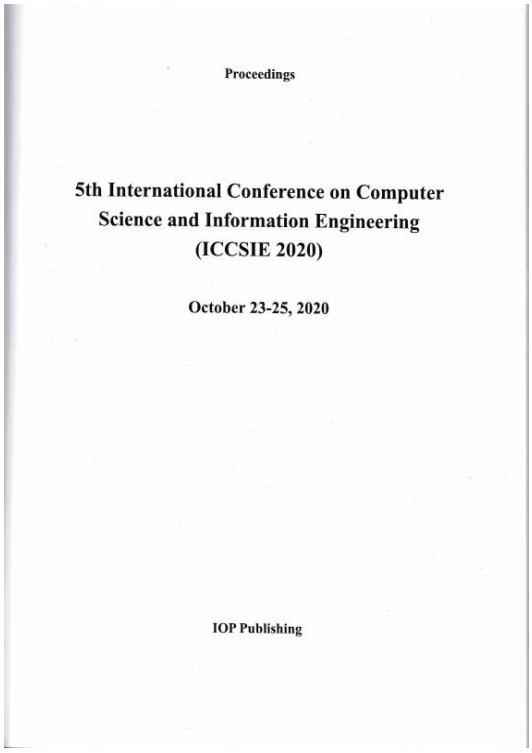

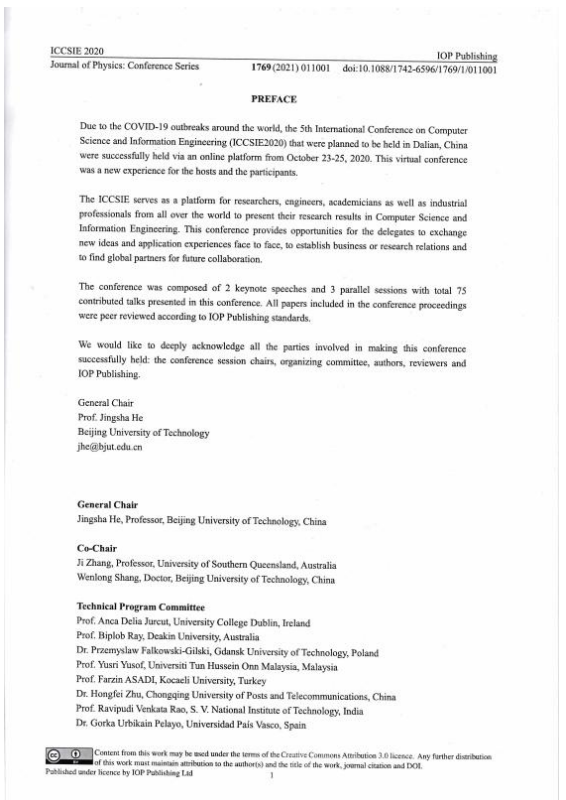

ICCSIE 2020 IOP Publishing
Journal of Physics: Conference Series **1769** (2021) 011001 doi:10.1088/1742-6596/1769/1/011001

PREFACE

Due to the COVID-19 outbreaks around the world, the 5th International Conference on Computer Science and Information Engineering (ICCSIE2020) that were planned to be held in Dalian, China were successfully held via an online platform from October 23-25, 2020. This virtual conference was a new experience for the hosts and the participants.

The ICCSIE serves as a platform for researchers, engineers, academicians as well as industrial professionals from all over the world to present their research results in Computer Science and Information Engineering. This conference provides opportunities for the delegates to exchange new ideas and application experiences face to face, to establish business or research relations and to find global partners for future collaboration.

The conference was composed of 2 keynote speeches and 3 parallel sessions with total 75 contributed talks presented in this conference. All papers included in the conference proceedings were peer reviewed according to IOP Publishing standards.

We would like to deeply acknowledge all the parties involved in making this conference successfully held: the conference session chairs, organizing committee, authors, reviewers and IOP Publishing.

General Chair
Prof. Jingsha He
Beijing University of Technology
jhe@bjut.edu.cn

General Chair
Jingsha He, Professor, Beijing University of Technology, China

Co-Chair
Ji Zhang, Professor, University of Southern Queensland, Australia
Wenlong Shang, Doctor, Beijing University of Technology, China

Technical Program Committee
Prof. Anca Delia Jurcut, University College Dublin, Ireland
Prof. Biplob Ray, Deakin University, Australia
Dr. Przemyslaw Falkowski-Gilski, Gdansk University of Technology, Poland
Prof. Yusri Yusof, Universiti Tun Hussein Onn Malaysia, Malaysia
Prof. Farzin ASADI, Kocaeli University, Turkey
Dr. Hongfei Zhu, Chongqing University of Posts and Telecommunications, China
Prof. Ravipudi Venkata Rao, S. V. National Institute of Technology, India
Dr. Gorka Urbikain Pelayo, Universidad Pais Vasco, Spain

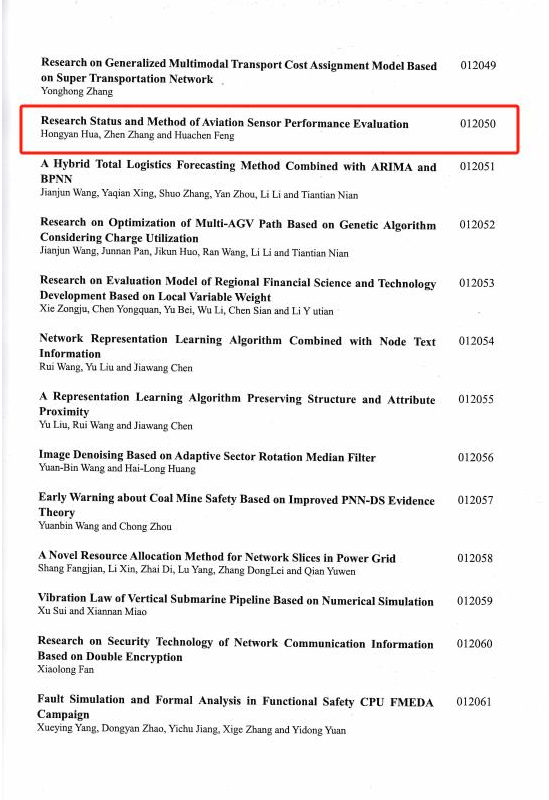

Research Status and Method of Aviation Sensor Performance Evaluation

Hongyan Hua[1], Zhen Zhang[1,*], Huachen Feng[2]

[1]School of Intelligent Engineering, Zhengzhou University of Aeronautics, Zhengzhou, China
[2]College of Art and Design, Shaanxi University of Science & Technology, Xi'an, China

Corresponding author's e-mail: deepwhitezorro@163.com

Abstract. Aviation sensor is an important guarantee for aircraft safety flight, ground test and flight test accuracy and reliability. In this paper, through the analysis of the problems existing in the actual working environment of aviation sensors, the necessity of evaluating the performance of aviation sensors in the actual working environment is clarified. Combined with the comparison of the research status of the performance evaluation methods of aviation sensors at home and abroad, the development direction of the performance evaluation research of aviation sensors in the actual working environment in the future is proposed.

Keywords. Aviation sensor, research scheme, working environment, performance evaluation

1. Introduction

In the field of aviation, in order to ensure the correct and safe flight of aircraft and complete various complex tasks, it is necessary to install corresponding sensors in the key parts of the aircraft and different airborne equipment systems. The number of various sensors installed on a modern aircraft is as many as hundreds or even thousands. Sensors are not only directly installed on the aircraft to ensure safe flight, but also widely used in various ground tests and flight tests, such as aircraft structural strength test, wind tunnel test, engine test, etc., to complete the measurement of some special parameters of aircraft. These sensors are collectively referred to as aviation sensors [1].

Although the development history of China's aviation sensor is short, the domestic aviation sensor industry has developed rapidly in recent years, and the gap with foreign countries is gradually narrowing. With the wide application of new materials, new processes and new technologies in the aviation field, the development trend of aviation sensors is micro miniaturization, integration, intelligence and networking [2]. As a variable conversion unit in the five basic units of aviation test system, aviation sensor is used to measure the pressure, temperature, acceleration, speed, displacement and other important parameters of aircraft, various auxiliary devices and mission equipment. Its performance will directly affect the service life and flight safety of aircraft, the accuracy and reliability of aviation product ground test and flight test . Due to the variety of aviation sensors and high technical requirements, a large number of aviation sensors often work in the harsh environment of high temperature, high altitude and severe vibration. Therefore, it is necessary to use effective methods to

evaluate the performance of aviation sensors to ensure the accuracy of measurement data of sensors in the working environment.

In this paper, based on the problems existing in the actual working environment of aviation sensors, the status quo of performance evaluation methods of aviation sensors at home and abroad is compared, and a possible development direction is proposed for the performance evaluation methods of aviation sensors in the actual working environment in the future.

2. Current problems

With the continuous breakthrough of aviation technology, aircraft is gradually entering a new development stage of high temperature, high altitude and high speed. Many aerial sensors need to work in extremely harsh actual working environment such as severe vibration, high temperature, high pressure and corrosivity, which brings huge problems and challenges to the use of sensors. For example, the pressure sensor in the aircraft engine often needs to work in the unstable air flow environment with the temperature range of 600 ~ 800 ℃, and the ambient temperature in the combustion chamber of pulse detonation engine is more than 1000 ℃. Since the air flow contacts the combustion chamber, the pressure sensor plays an important role in controlling the gas and fuel mixture by detecting the air pressure. Once the test data of the pressure sensor is not accurate, the risk of aircraft out of control will be greatly increased [3].

The structure of modern aero-engine is more and more complex, and the aerodynamic performance of the engine is easy to be unstable in the working process. In order to maintain the normal operation of the engine, the anti-surge system is equipped on the aircraft. As a key component of anti-surge system, the surge differential pressure sensor can comprehensively judge the working state of the engine by measuring the difference between the total pressure and static pressure at the compressor outlet, combined with other relevant parameters. Therefore, the accuracy of the surge differential pressure sensor measurement data is directly related to whether the engine can work normally. Once there is a problem, it may cause serious consequences. Because surge differential pressure sensor is installed on the engine shell, its actual working conditions are often in the extremely harsh environment such as high temperature and violent vibration. At present, the performance calibration of surge sensor can only be carried out under the laboratory standard conditions. There is a lack of accurate evaluation method and measurement results analysis of surge differential pressure sensor under actual working conditions, so it is difficult to judge the performance of surge sensor in actual working environment.

In foreign aviation flight, there have been tragic accidents due to inaccurate sensor measurement data. In the Ethiopian Airlines crash in early 2019, the black box data of the crashed flight showed that the angle of attack sensor on the Boeing 737max mistakenly activated the automatic system on board, which led to the crash. Relevant research also shows that if there is water around the angle of attack sensor, when the aircraft flies to a certain height, the performance of the sensor may be affected or even malfunction due to the freezing of the high altitude cold environment. When the aircraft encounters bird impact, the sensor also has data error [4]. It can be seen that the performance of airborne sensors may change or even fail in complex actual working environment, and the performance evaluation method of sensors in laboratory conditions can not meet the requirements of actual conditions.

3. Domestic research status

In China, the research on the performance evaluation method of aviation sensor in the actual working environment is still in its infancy, most of which focus on the development of calibration device simulating the actual working environment and the use of certain technology to compensate the sensor's sensitive environmental stress, and there is no complete sensor performance evaluation system.

3.1. Development of calibration device simulating actual working environment

报告编号：**L24N2021-0552**

检 索 报 告

一、检索要求

1. 委 托 人：张琳(Zhang, Zhen)
2. 委托单位：郑州航空工业管理学院
3. 检索目的：论文被 EI 收录情况

二、检索范围

Engineering Village （Database: Compendex）	1969-present	网络版

三、检索结果

委托人提供的**1**篇论文被EI收录，论文收录情况见附件一。
特此证明！

东北师范大学科技查新咨询中心
教育部科技查新工作站（L24）
（盖 章）

检索报告人：曹宇

2021 年 **5** 月 **17** 日

附件一：EI收录情况

第 1 条，共 1 条
Accession number:20211110081419
Title:Research Status and Method of Aviation Sensor Performance Evaluation (Open Access)
Authors:Hua, Hongyan (1); Zhang, Zhen (1); Feng, Huachen (2)
Author affiliation:(1) School of Intelligent Engineering, Zhengzhou University of Aeronautics, Zhengzhou, China; (2) College of Art and Design, Shaanxi University of Science and Technology, Xi'an, China
Corresponding author:Zhang, Zhen(deepwhitezorro@163.com)
Source title:Journal of Physics: Conference Series
Abbreviated source title:J. Phys. Conf. Ser.
Volume:1769
Part number:1 of 1
Issue:1
Issue title:5th International Conference on Computer Science and Information Engineering, ICCSIE 2020
Issue date:February 23, 2021
Publication year:2021
Article number:012050
Language:English
ISSN:17426588
E-ISSN:17426596
Document type:Conference article (CA)
Conference name:5th International Conference on Computer Science and Information Engineering, ICCSIE 2020
Conference date:October 23, 2020 - October 25, 2020
Conference location:Dalian, Virtual, China
Conference code:167544
Publisher:IOP Publishing Ltd
Abstract:Aviation sensor is an important guarantee for aircraft safety flight, ground test and flight test accuracy and reliability. In this paper, through the analysis of the problems existing in the actual working environment of aviation sensors, the necessity of evaluating the performance of aviation sensors in the actual working environment is clarified. Combined with the comparison of the research status of the performance evaluation methods of aviation sensors at home and abroad, the development direction of the performance evaluation research of aviation sensors in the actual working environment in the future is proposed.
 © 2021 Published under licence by IOP Publishing Ltd.
Number of references:0
Main heading:Physics
Uncontrolled terms:Aircraft safety - Development directions - Evaluation methods - Evaluation research - Ground tests - Research status - Sensor performance - Working environment
DOI:10.1088/1742-6596/1769/1/012050

Database:Compendex
Compilation and indexing terms, Copyright 2021 Elsevier Inc.

The End

3.全面定位的薄板精密磨削方法分析

MACHINE CHINA

中国机械（旬刊）

机械工业与智能制造产学研用协同创新平台

2026年1月 上旬刊 第01期 总第697期（1982年创刊）

主管单位：中国工业经济联合会
主办单位：中国工业报社
出版发行：《中国机械》杂志社
地　　址：北京市石景山区翔鹰大厦15层1502（100043）

社　　长：徐金宝
总 编 辑：郭俐君
编　　审：陈永光
执行总编辑：聂立芳
副总编辑：孙　静　霍　悦
编辑部主任：孙　静（兼）
编辑部主任助理：揭　旗
编　　辑：孙正坤　姚　媛　赵　昕　高彦楠
美术编辑：赵可心
行　　政：金勇军　王嘉宝

国内统一连续出版物号：CN 11-5417/TH
国际标准连续出版物号：ISSN 1003-0085
国内邮发代号：28-165
海外发行代号：C8179
广告经营许可证：京西工商广登字第20170109号

官方网站：http://www.MachineChina1982.cn
电子邮箱：jxzzs@cinn.cn
投稿咨询：010-67410636

印　　刷：廊坊市鸿煊印刷有限公司
定　　价：36.00元

目 次

全面定位的薄板精密磨削方法分析

冯克明[1,2,3] 华红艳[4]

（1. 郑州三磨超硬材料有限公司 河南 郑州 450001）

（2. 郑州磨料磨具磨削研究所有限公司 河南 郑州 450001）

（3. 国机金刚石（河南）有限公司 河南 郑州 450016）

（4. 郑州电力职业技术学院 河南 郑州 451450）

摘 要：本文基于薄板零件在磨削加工中易形变的难点进行分析研究。深度剖析影响加工形变的因素，分析薄件形变成因，包括残余应力、定位与夹持、磨削力与磨削热等相关技术问题。针对薄件形态多样、定位接触不均匀、三点定面不适用、直接夹持不科学、磨削应力极其复杂等问题，提出基于全面定位的平面磨削新方法，并制订了薄件磨前校平、全面定位、锋利磨削、对称去量四个平坦化磨削规则，旨在实现薄件的精密加工。

关键词：超薄零件；精密磨削；全面定位；锋利磨削；接触刚度

Analysis of Precision Grinding Method for Thin Plates with Comprehensive Positioning

Feng Keming[1,2,3] Hua Hongyan[4]

（1.Zhengzhou Sanmo Superhard Materials Co., Ltd., Zhengzhou 450001, China）

（2.Zhengzhou Research Institute for Abrasives & Grinding Co., Ltd., Zhengzhou 450001, China）

（3.Sinomach Diamond (Henan) Co., Ltd., Zhengzhou 450016, China）

（4.Zhengzhou Electric Power Technology College, Zhengzhou 451450, China）

Abstract: This paper conducts an analysis and research based on the difficult problem of easy deformation of thin-plate parts during grinding. It deeply dissects the factors affecting machining deformation and analyzes the causes of deformation of thin-plate parts, including residual stress, positioning and clamping, grinding force, grinding heat and other related technical issues. Aiming at the problems of thin-plate parts such as diverse shapes, uneven positioning contact, inapplicability of three-point plane positioning, unscientific direct clamping and extremely complex grinding stress, a new surface grinding method based on full-plane positioning is proposed, and four flattening grinding rules are formulated, namely leveling before grinding of thin parts, full-plane positioning, sharp-state grinding and symmetrical allowance removal, which are intended to realize the precision machining of thin-plate parts.

Keywords: ultra-thin parts; precision grinding; full positioning; sharp grinding; contact stiffness

0 引言

薄板类零件（简称薄件）通常指长厚比（最大轮廓尺寸 / 厚度）＞ 20 的零件[1]，具有厚度薄、精度高、能耗低、性能优的特征。这些薄件在制造过程中对力热极其敏感、易产生形变，导致尺寸精度、面形精度超差，严重制约了薄件的生产和使用。

为了消除或改善薄件加工形变，国内外学者进行了大量的研究及技术工作。如岳彩旭等[2]归纳了引起薄件加工变形的因素；易茜等[3]建立了薄件加工变形预测模型，对加工精度、可靠性进行了分析；潘博等[4]提出了翻面加工策略，并取得了一定效果；顾鹏等[5]建立了薄件磨削形变预测模型，得出了可抑制形变的磨削参数；丁腾威等[6]研究发现

砂轮磨损状态是影响工件变形的主要因素；Cao Le 等[7]对薄件加工误差进行了在线监测；Pan Bo 等[8]提出了采用双面研磨工艺可防止薄件发生变形；Hao Qinglong 等[9]设计了一种自适应夹具，实现了叶片无应力装夹；杨威等[10]通过大量试验和改进，得出了较为合理的切削参数；牛俊凯等[11]分析了磨削参数对蓝宝石磨削质量的影响；刘绪弟等[12]改进了工艺、工装及路径，实现了薄件的高精度加工；苟慎龙等[13]总结了有效避免加工形变的工艺方法；温俊等[14]研究了磨削温度阈值对残余应力形成的影响；朱传敏等[15]建立了薄件有限元模型，进行了温度场与应力场仿真，探讨了薄件磨削变形机理；赵炳尧[16]使用黏弹性垫，使薄件表面质量得到提升；周炼等[17]基于在位检测和补偿技术，实现了薄件的稳定磨削；王腾达等[18]发现了导致零件变形的主要原因等。本文基于薄件易变形、对力热敏感等特性，梳理了磨削加工全流程影响因素，剖析了主要因子及内在逻辑，提出了薄件精密磨削新方法。

1 薄件形变因素分析

磨削加工通过砂轮工作表面众多磨粒在零件表面的高速切削而实现多余材料的去除。其具有磨粒小、磨屑薄、纹理致密、加工精度高、表面质量好等优点。但是，砂轮呈多元、多刃、多孔、疏松、硬脆、非均质结构，磨粒形状、姿态、位置、磨刃前角、钝圆半径、出露高度等多维因素不确定，以及磨削接触区大、冷却液难进入、力热耦合严重等特征，使得磨削加工极其复杂。

针对薄件磨削形变问题，基于长期的工程实践，归纳磨削加工全流程影响因素如表 1 所示，包括磨床引起的形变，磨削加工产生的形变，薄件磨削前已存在的形变，薄件定位、装夹而导致的形变，工作环境、人为操作引起的形变。

磨床精度低会造成薄件形变，可通过工作台修复、磨床精化使磨削精度得到提升；薄件厚度薄、刚度低，定位、夹持不合理易产生形变；磨削过程中，磨削区受到磨削力及磨削热的影响会产生形变；薄件磨削前已经历多种工序，可能已存在原始形变；对于现场温度、湿度、洁净度等环境因素，便于控制、影响有限；对于人为因素，可通过职业培训、操作规程及加工工艺等来管控，影响不大。由此可见，

表 1 薄件磨削加工全流程形变分析

影响因素	过程分析		影响程度
磨床	磨削加工中	几何精度、运动精度、稳定性、重复精度等	小
定位、夹持		定位、夹持、受力因素	大
磨削		磨削力、磨削热影响	大
原始形态	非磨削因素	磨削前薄件已存在形变，如材料、工艺、物流	大
环境因素		温度、湿度、清洁度等	小
人为操作		人的素质、技能、状态等	小

薄件磨削形变主要来源于薄件磨削加工前可能已存在的形变、薄件的定位夹持引起的形变以及磨削过程中产生的新形变。

2 薄件形变成因分析

2.1 薄件初始形态

零件经过各种加工及处理后，必然有部分作用与影响残留在零件内部而产生内应力。磨削加工常见于机械零件的最后加工工序，说明零件在磨削加工前已经过多个工艺影响与作用，零件内已积聚了一定的内应力。

残余应力是指零件在去除外因作用后，零件内部为保持其平衡而产生的内应力，其影响因素主要是力与温度[19]。当外因去除后，内部不均匀的应力会在零件刚度高的地方继续潜伏、在刚度低的地方得到释放而产生形变、在应力集中且大于材料断裂强度的位置产生裂纹。因此，残余应力可使零件原有精度及表面质量改变，进而影响零件的尺寸、性能和服役寿命等。

残余应力本质由弹性应变产生，是一种不稳定的内应力，有强烈地恢复到没有应力的趋势[20]。为了加快零件残余应力释放，工程中常采用自然时效、热时效、振动时效等技术来消除。对于磨削加工，由于磨粒小、切入深度浅，磨削残余应力通常仅存在于零件表层微纳级深度区域[21,22]，最大不超过 1mm，且随着时间的延长而逐渐衰减，直至完全消失。

对于低刚度薄件，残余应力释放期短，且厚度越薄释放越快，甚至瞬间即获得释放。对于厚度≤2mm、长厚比≤100 的超薄件，因为其厚度超薄、长

厚比超大、刚度超低、散热条件超差，残余应力释放更快。可见，超薄件形变主要由残余应力引起；对于直径≤1000mm 圆形薄件，形变往往贯穿整体，不存在局部形变、局部平整现象。因此，可以认为超薄件在磨削加工前，其残余应力已完全消失，留下的主要是形变。以圆形超薄件为例，其常见形态主要有平整形（微形变）、瓦片形、中凸形、扭曲形等（图 1），很少有面形精度为零、绝对的理想平面。薄件具体形态主要与材料及其组织均匀性，残余应力状态、大小及其分布有关。

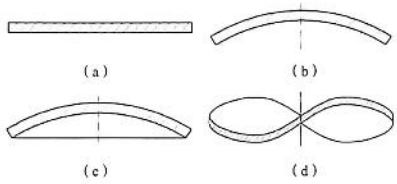

图 1 常见的圆形薄件形态

（a）平整形；（b）瓦片形；（c）中凸形；（d）扭曲形

基于残余应力特征及其释放机理，可以确定常态下薄件之凸面是原压应力（ – ）、凹面是原拉应力（ + ）释放的结果，如图 2 所示。

图 2 薄件内应力及其释放过程

2.2 薄件定位与夹持

定位与夹持是零件进行机械加工的重要工艺过程。零件平面定位首推三点定面经典法则，即通过三个不共线的点确定一个平面。但是，大量工程实践发现：三点定面理论不适用于薄件定位与加工。因为薄件厚度薄、残余应力释放快，薄件多呈现形变状态。若将薄件直接放置于标准基台上，薄件往往仅有极少点位与平台接触，绝大部分仍处于悬空状态（图 3）；并且，由于薄件抗弯刚度低而导致其全平面内各点接触刚度存在差异、分布极不均匀。

假设在外力（如电磁力）作用下使薄件全平面被吸附到平台上，则薄件原凸面受挤压产生压应力、原凹面受拉伸引发拉应力（图 4），相当于薄件又恢复到原内应力状态，其内部产生了相应的非均匀

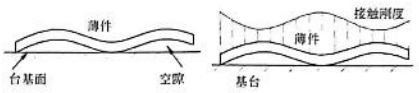

图 3 薄件形态与接触刚度

弹性形变和应力场。由于薄件的非均匀形态存在，在夹持时其夹持力（电磁力 + 形变力）也不均匀；待加工完毕撤去外力约束后，薄件会立即释放应力并重新恢复到原有形态。可见，在薄件存在初始形变状态下，即使精密加工也难以获得高的面形精度。

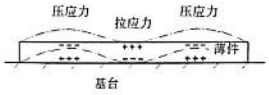

图 4 外力作用下薄件形态分析

2.3 磨削加工影响

基于经典的切削加工理论，砂轮表面有效磨粒对零件的磨削过程可分为滑擦、耕犁、切削三个阶段。相对于刀刃锐利（钝圆半径小）、角度规范的刀具，砂轮的特殊结构使其与零件的接触更加复杂。砂轮表面磨粒无数、分布无序，磨刃均呈负前角、较大钝圆半径状态，致使其挤压、摩擦作用显著；再加上砂轮高速旋转、磨粒高频撞击，使磨削力和磨削热波动大，法向磨削力、磨削温度、力比（法向力 / 切向力）、比磨削能等远高于刀具切削。磨削过程中有效磨粒主要处于滑擦、耕犁状态，有效磨粒及工件表面经历高速、高压、高频、高温、高摩擦、高应变的弹塑性形变过程，致使磨削加工表面产生了非常复杂的内应力及变质层。

磨削加工后零件表层残余应力主要由以下三种内应力构成[23]：

（1）机械挤压应力。基于砂轮表面众多磨粒的高频撞击、挤压作用，零件表层塑性形变大，里层基体形变小，仅处于弹性形变状态。当磨削结束后，零件里层弹性趋向恢复，但受到表层塑性形变的限制恢复不到原状，使零件表层产生压应力。

（2）温度梯度应力。由于磨削产生高温（500 – 1500℃），再加上砂轮导热性差、磨屑小储能有限，磨削产生的热量绝大部分传入零件，使零件与砂轮接触面承受磨削热作用；同时由于磨削区的移动及

冷却液的介入，零件受到冷热冲击作用，在深度方向形成较大的温度梯度，导致不均匀膨缩产生热应力。当磨削结束时，零件表面温度下降快，又受到零件里层的限制，使表层产生拉应力，甚至裂纹。

（3）组织相变应力。当磨削温度达到材料临界相变温度时，材料组织会发生相变。不同的组织具有不同的密度，不均匀的组织即产生相变应力。组织密度变小时体积膨胀，受周围组织限制产生压应力；反之，产生拉应力。

磨削应力是以上三种不均匀应力共同作用的结果，应力状态较为复杂（图 5）。若零件已存在初始内应力，随着磨削的持续进行，零件当下应力是已有的内应力与新的磨削应力不断叠加、演化、重构的新的平衡[24]。一般认为，当磨削以低温、塑性挤压为主去除材料时，零件表面多呈现压应力，如研磨、珩磨、抛光等；砂轮磨削中，热应力往往占据主导地位。因此，磨削加工表面大概率呈拉应力状态。

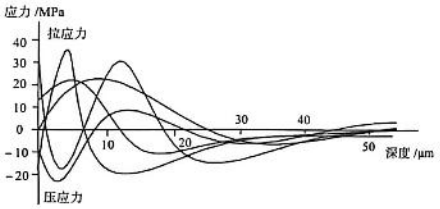

图 5　磨削残余应力例示

3　薄件精密磨削

对于薄件精密磨削，由于其刚度低、散热差，磨削力和磨削热会进一步放大其不均匀形变。因此，薄件精密磨削不能沿用传统的加工思路，其平坦化加工应遵守以下原则。

3.1　磨前校平

基于上述分析，薄件不仅会发生弯曲等简单二维变形，还会产生扭曲、翘曲等三维复杂变形。为了实现薄件的精密加工，其应具有一个高面形精度的基准平面。为此，最实用、最有效的方法就是在薄件磨削加工前增加校平工序，采用合理的处理方法，消除薄件不平整形态，提高其面形精度。

3.2　全面定位

根据前面分析，三点定面法则不适用于薄件定位与夹持。对于薄件加工，本文特提出全面定位（全平面定位）新工艺。具体是指薄件定位面应与标准台面自然接触、全面贴紧，这样薄件全平面接触刚度均匀分布，可均匀承受外力作用。若薄件面形复杂、难以实现全面接触，应采用易于去除的材料对其凹部进行填充，使其获得理想的平面（图 6）；或将薄件复杂形面离散为尽可能多的接触点，提高其全平面接触刚度均匀性。因此，全面定位也可称为随形定位，随薄件具体形态而给予尽可能多地接触与支撑，避免不均匀受力。

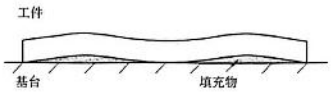

图 6　薄件全面定位示意图

目前，在薄件加工领域已出现许多便利实用技术，如柔性定位、浮动支撑、垫纸消隙、松香填充、石蜡填充、黏弹性垫等[25-28]。这些具体实例都可用全面定位来释义，即通过合适材料填充薄件之凹部，使薄件与基台达到近全面、微形变、微应力定位夹持状态，从而改善薄件接触刚度均匀性，便于后续受力与加工。

3.3　锋利磨削

锋利磨削是指通过砂轮优选、磨削参数优化、环境有效管控等，使砂轮持续锋利，达到磨削力小、磨削温度低的目的。如选用锐利的磨粒，钝圆半径小，有利于减小磨削力和磨削热；选用微晶、多晶磨粒，自锐性好，砂轮可持续锐利；选择组织疏松、硬度低的砂轮，磨粒易脱落、磨屑难黏附，砂轮可持续磨削；为避免砂轮过度磨损，应及时甚至提前修整砂轮；减小磨削区面积，便于磨削液注入，实现低温磨削；采用高压、有效射流，增强热交换，有利于减小磨削力和磨削热等[29]。

3.4　对称去量

对称去量是指在材料加工过程中，尽量做到工件双面对称去除多余材料。对于薄件磨削，最好能双面同时、等量、同条件下进行加工，如通过双端面磨削或双面研磨，达到受力对称、去量对称的目的。若没有相关装备，可采用普通磨床进行翻面磨削，通过互为基准、多次翻面，均化薄件双面加工余量、等量去除材料，改善磨削应力，提高薄件面形精度。

4 结语

基于薄件的加工难点，本文剖析了影响加工形变的因素，提出了磨前校平、全面定位、锋利磨削、对称去量的创新方案，解决了工程中长期存在的薄件平面磨削难题。

（1）薄件形变影响因素多。排除磨床、人为、环境因素外，薄件形变主要有磨削过程中由于磨削力和磨削热作用引起的磨削形变、薄件磨削前残余应力产生的原始形变，以及由薄件初始形态不确定引起的不均匀定位夹紧形变。

（2）薄件厚度薄、刚度低，传统三点定面经典法则不适用于薄件定位与加工。为此，本文提出全平面定位理念。全面定位下薄件可获得全面、无形变、无应力定位与夹持，接触刚度分布均匀。

（3）为了获得理想的薄件面形精度，要设法消除或减小各种不均匀因素的影响。增加校平处理工序，可提高薄件初始面形精度；通过全面定位夹持，可提高薄件接触刚度均匀性；保持锋利磨削、对称去量，可减小磨削力、磨削热、磨削应力的影响。

参考文献

[1] 吴清雨，殷耀君，姚素娴，等．薄板齿轮加工工艺研究与改进 [J]. 机械传动，2023,47(4):171-176.

[2] 岳彩旭，张俊涛，刘献礼，等．薄壁件铣削过程加工变形研究进展 [J]. 航空学报，2022,43(4):99-124.

[3] 易茜，李聪波，谣建，等．薄板类零件加工精度可靠性分析及工艺参数优化 [J]. 中国机械工程，2022,33(11):1269-1277.

[4] 潘博，康仁科，贺增旭，等．弱刚性构件磁流变抛光变形机理与抑制技术研究 [J]. 中国机械工程，2022,33(18):2190-2196.

[5] 上海交通大学．一种薄板类零件精密磨削表面翘曲表征及抑制方法 :202310923021.X[P].2023-11-14.

[6] 丁鹏威，冯硕，李娜，等 .GCr15 轴承钢磨削变形研究 [J/OL]. 机械科学与技术，1-8[2025-03-30].https://doi.org/10.13433/j.cnki.1003-8728.20250022.

[7] Cao Le,Zhang Xiaoming,Huang Tao,et al.Online monitoring machining errors of thin-walled workpiece:a knowledge embedded sparse bayesian regression approach[J].IEEE/ASME Transactions on Mechatronics,2019,24(3):1259-1270.

[8] Pan Bo,Kang Renke,Guo Jiang,et al.Precision fabrication of thin copper substrate by double-sided Lapping and chemical mechanical polishing[J].Journal of Manufacturing Processes,2019,44:47-54.

[9] Hao Qinglong,Yang Qian.A self-adaptive auxiliary fixture for deformation control in blade machining[J].The International Journal of Advanced Manufacturing Technology,2020,111(5/6):1415-1423.

[10] 杨威，施军良，程会民，等．大型薄板类零件数控铣削加工及质量控制 [J]. 金属加工 (冷加工),2023(6):64-68.

[11] 牛俊凯，张毅，韩欣，等．蓝宝石衬底片背面减薄磨削加工试验分析 [J]. 机械制造，2021,59(7):68-72.

[12] 刘绪弟，张桂珍，张永红．大型薄板零件加工变形控制工艺 [J]. 金属加工 (冷加工),2023(3):36-39.

[13] 苟慎龙，邱吕强，徐刚，等．金属薄板平面铣削形变分析与控制 [J]. 机械制造与自动化，2020,49(1):65-67.

[14] 温俊，唐进元，郑金超．平面磨削条件下温度阈值对残余应力形成的影响 [J]. 中南大学学报 (自然科学版),2019,50(3):530-539.

[15] 朱传敏，胡骁．薄板零件磨削变形有限元仿真 [J]. 物联网技术，2019,9(3):91-93+96.

[16] 赵炳圣．低刚度薄板件的平面磨削加工工艺研究 [D]. 大连：大连理工大学，2018.

[17] 成都精密光学工程研究中心．光学元件磨削加工面形误差和平行度误差的控制方法 :201610903213.4[P].2019-04-23.

[18] 王腾达，张红伟，刘红文．提高不锈钢薄板类零件几何精度的工艺探讨 [J]. 安阳工学院学报，2024,23(4):30-34.

[19] 付天章，李媛，陈明，等．平面磨削 GT35 残余应力形成机理与可控工艺方案 [J]. 制造技术与机床，2024(1):151-157.

[20] 顾巨骏，陶祥泽，赵颖涛．基于弹性理论的残余应力反演和变形计算 [J]. 固体力学学报，2024,45(2):188-200.

[21] 熊正权，窦哲雯，陈颖，等．面向超薄硅晶圆精密磨削工艺的内部残余应力分析 [J]. 表面技术，2025,54(2):161-172.

[22] 宗傲，王科荣，彭凯，等．熔石英磨削的残余应力层深度预测研究 [J]. 表面技术，2023,52(12):74-82.

[23] 丁子珊，滕益康，郭鑫现，等．考虑微观影响的磨削残余应力解析模型研究 [J]. 机械工程学报，2023,59(23):372-390.

[24] Mali R A,Gupta T V K,Ramkumar J.A comprehensive review of free-form surface milling-Advances over a decade[J].Journal of Manufacturing Processes,2021,62:132-167.

[25] 孙岩．多点定位式柔性夹持工装设计与研究 [J]. 内燃机与配件，2021(4):101-102.

[26] 崔亚超．点定位装夹在薄板类零件批量加工中的应用 [J]. 制造技术与机床，2021(4):106-110.

（下转第 70 页）

4.无线电能与信息同时传输的研究与分析

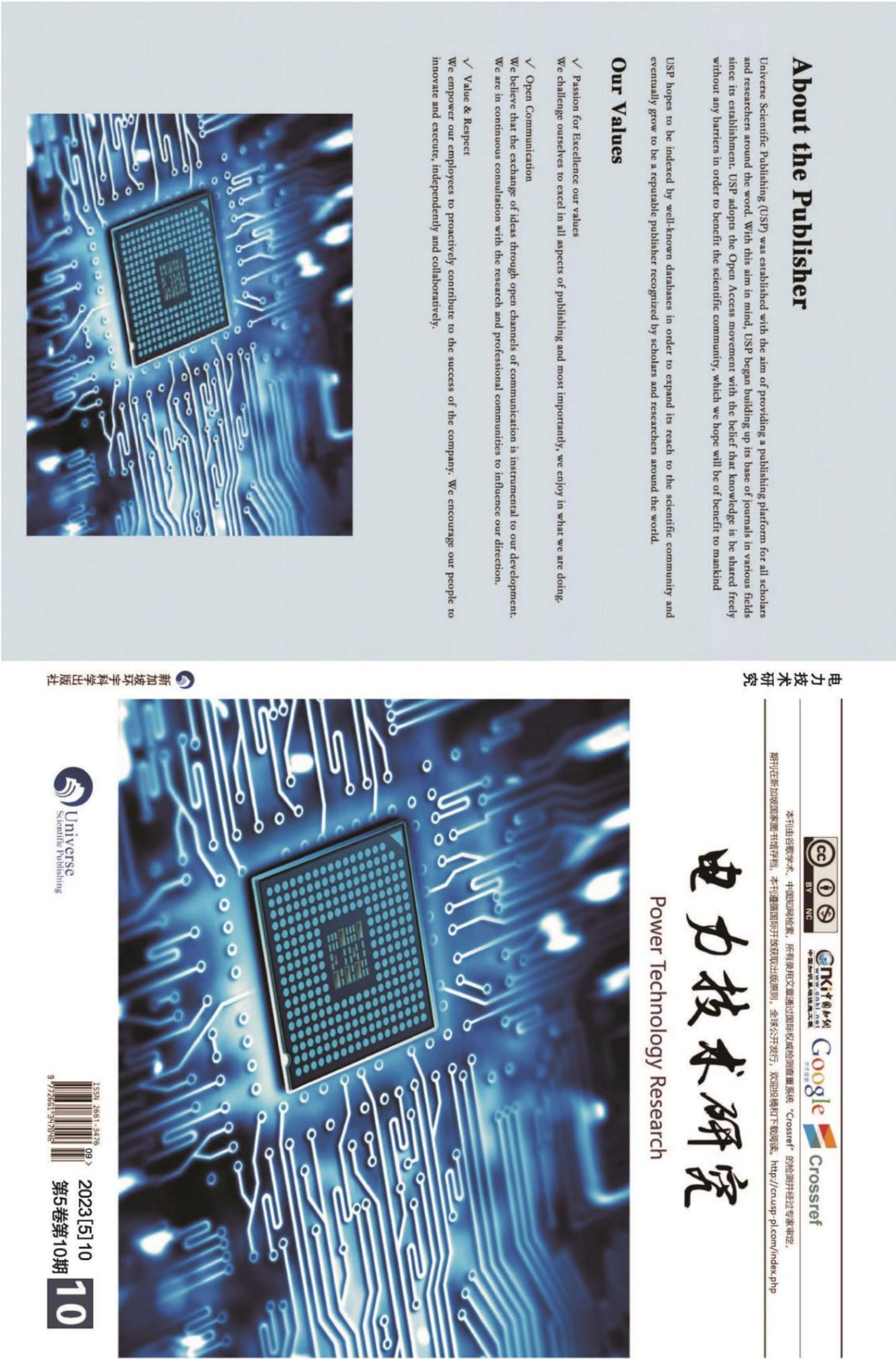

电力技术研究

2023 年 10 期
主　　管：新加坡电力技术研究出版社
主办单位：新加坡电力技术研究出版社
主　　编：杨林
执行主编：杨林
特邀编委：陆原

网　　址：http://cn.usp-pl.com/indcx.php/yxyj
电　　话：010-60845571
邮　　箱：dljsyjzzs@126.com
国际刊号：2661-3476
刊　　期：月刊
出版日期：每月 25 号
定　　价：20

出版单位
73 upper Paya Lebar road #07-02B-03 centro bianco Singapore(534818)

目　录

信息科学

技术理论

无线电能与信息同时传输的研究与分析

张红丽 刘建萍

（郑州电力职业技术学院 河南省郑州市 450000）

摘要：随着科技的飞速发展，无线电能传输（Wireless Power Transfer, WPT）与无线信息传输（Wireless Information Transfer, WIT）已成为当下研究的热点。本文将对无线电能与信息同时传输（Simultaneous Wireless Power and Information Transfer, SWIPT）技术的研究与分析进行深入探讨，阐述其基本原理、关键技术、应用场景与挑战等方面。

关键词：无线电能传输；信息；场景

一、引言

在现代社会，移动设备、物联网设备和智能家居等已经成为人们日常生活的重要组成部分。这些设备的普及和应用，离不开电能和信息的传输。然而，传统的有线连接方式在这些领域中的使用存在许多限制。比如，传输距离短，布线繁琐，不仅影响了设备的美观和便携性，还限制了设备的使用范围和灵活性。此外，有线连接还可能导致设备间的互相干扰，降低了系统的稳定性和可靠性。因此，无线传输技术成为了当前研究的热点。无线传输技术可以消除有线连接的种种限制，提供更方便、更灵活的解决方案。特别是无线电能与信息同时传输（SWIPT）技术，它能在同一传输介质中同时传递电能和信息，大大提高了传输效率，也极大地方便了设备的使用。

二、SWIPT 技术原理

SWIPT 技术是一种先进的无线传输技术，它基于电磁场耦合原理来实现电能和信息的同步传输。电磁场耦合是指两个或多个电路之间通过电磁场相互作用实现能量和信息的传输。在 SWIPT 技术中，电磁场耦合被用来在发送端和接收端之间建立高效的能量和信息传输通道。为了实现电能和信息的同步传输，SWIPT 技术采用了特殊的调制和解调方法。首先，发送端将电能和信息进行调制，将它们叠加在同一个传输信号中。这个叠加的信号通过电磁场耦合的方式传输到接收端。在接收端，信号经过解调处理，将电能和信息分离出来，然后分别供给给相应的设备使用。整个 SWIPT 系统中，能量与信息接收是核心部分。接收端需要设计高效的能量接收装置和信息解码装置，确保能够同时、准确地接收并处理电能和信息。这里的挑战在于如何在同一传输介质中高效地区分和处理这两种不同的信号，避免相互干扰，并确保传输的稳定性和可靠性。SWIPT 技术基于电磁场耦合原理，通过巧妙的信号调制与解调技术，以及高效的能量与信息接收装置，实现了在同一传输介质中同时传递电能和信息，为无线传输领域带来了创新和突破。

三、关键技术分析

（一）电磁场耦合技术

电磁场耦合技术是 SWIPT 的基石。电磁场耦合涉及到发送端和接收端之间的磁场或电场相互作用。目前，磁耦合由于其适中的传输距离、高效率及低成本，被广大应用所采纳。磁耦合的方式采用磁场作为传输介质，当发送端产生变化的磁场时，这个变化的磁场会在接收端引发感应电流，从而实现电能的无线传输。

为了增强磁耦合效果，多数 SWIPT 系统采用线圈结构。线圈的结构、大小、匝数等都会影响到磁场的强度和传输效率。因此，对线圈的优化设计是实现高效磁耦合的关键。

（二）信号调制与解调技术

为了实现电能与信息的同步传输，信号调制与解调技术是不可或缺的。调制是将原始信息嵌入到电能传输的信号中的过程，而解调则是从接收到的复合信号中提取出原始信息的过程。

在调制过程中，常用的方法有幅度调制、频率调制和相位调制。幅度调制是改变信号的幅度来代表不同的信息，频率调制是改变信号的频率，而相位调制则是改变信号的相位。选择哪种调制方法取决于应用的需求和传输介质的特性。解调过程需要准确地还原出原始信号，确保信息的完整性和准确性。各种干扰和噪声可能会影响到解调的效果，因此，采用合适的信号处理和误差校正技术是关键。

（三）能量与信息接收技术

接收端是 SWIPT 系统的关键部分，它需要同时接收并处理电能和信息。为了实现这一功能，接收端通常采用分离式结构，包括电能接收模块和信息接收模块。

电能接收模块负责将接收到的电磁能转换为可以直接供给负载使用的直流电。这一过程中涉及到整流、滤波等步骤，确保提供给负载的电能稳定可靠。

信息接收模块则从接收到的复合信号中提取出原始信息。这通常涉及到放大、解调、解码等操作，每一个步骤都需要精心设计，确保信息的准确提取。

为了确保两个模块互不干扰、稳定运行，还需要在接收端采取一系列的隔离和防护措施。电磁场耦合技术、信号调制与解调技术和能量与信息接收技术是 SWIPT 的三大关键技术。这三者紧密相连，缺一不可，它们共同构建了 SWIPT 技术的完整框架，为无线电能与信息的同时传输提供了坚实的技术支撑。随着科技的不断进步和创新，相信这些关键技术会进一步完善，推动 SWIPT 技

术走向更广泛的应用领域。

四、应用场景与挑战

（一）应用场景

1.移动设备充电

传统的有线充电方式，虽然成熟稳定，但存在诸多不便。想象一下，当你在开会、吃饭或是旅行时，因为电量不足，不得不寻找充电插座，这样的场景无疑限制了设备的使用范围。更糟糕的是，频繁的插拔充电线可能会对设备的充电接口造成磨损。

SWIPT 技术为移动设备充电带来了革新。有了它，只要设备处于发射端的覆盖范围内，就能实现无线充电。这样，无论是在家里的沙发上、咖啡馆的桌子旁，还是办公室的会议室里，只要放下手机，电能就会自动传输到设备中，为其充电。这样的充电方式不仅大大增加了设备的使用范围，还避免了频繁插拔线缆带来的接口磨损问题，极大地提升了用户体验。

2.物联网设备供电

物联网技术的崛起意味着我们周围充斥着大量的传感器、摄像头等物联网设备。这些设备多数时候需要持续、稳定的电能供应。传统的解决方案是通过线缆连接电源，但这样做不仅布线成本高，而且在一些特殊环境，如森林、河流等，布线难度极大甚至不可能实现。

SWIPT 技术为物联网设备的供电提供了新的思路。由于 SWIPT 技术可以实现一定距离内的无线电能传输，这意味着无论物联网设备被部署在哪里，只要在其传输范围内，都可以获得稳定的电能供应。这对于那些布线困难或是成本高昂的场景来说，无疑是一个巨大的优势。

3.智能家居

家居环境的智能化是现代家居行业的一个重要趋势。想象一下，当你走进家门，灯光自动亮起，音响播放你喜欢的音乐，空调调至舒适的温度...这一切都通过智能家居系统实现。但如果这些设备之间都是通过线缆连接的，那么家居环境的整洁度和美观度都会大打折扣。

利用 SWIPT 技术，这些设备可以实现无线互联。这意味着灯具、音响、空调等设备不再需要线缆连接，家居环境看起来更加整洁、美观。同时，无线的连接方式也为用户带来了更加便捷的控制体验。

（二）面临的挑战

1.传输效率与距离

尽管 SWIPT 技术在传输效率上已经取得了显著的进步，但在实际应用中，我们仍面临着许多挑战。特别是在为那些远离发射端的设备充电时，当前的传输效率与距离尚不能满足所有需求。想象一下，如果家里的智能家居设备或户外的物联网设备距离充电发射端过远，那么无线充电就可能变得效率低下或者根本无法实现。为了满足更多样化的场景需求，我们必须持续优化 SWIPT 技术，提高其传输效率并增大传输距离。

2.电磁辐射与干扰

每当谈及无线传输，电磁辐射都是一个不可回避的话题。电磁辐射不仅可能对人体健康产生影响，还可能干扰其他电子设备的正常运行。因此，如何确保 SWIPT 技术在传输过程中的电磁辐射维持在安全范围内，以及如何最大限度地避免与其他设备产生干扰，都是科研人员必须面对的问题。这需要我们在技术设计上更加精巧，也要在设备部署上进行合理规划。

3.成本与系统兼容性

对于任何新技术来说，要想从实验室走向大众市场，降低成本和提高系统兼容性都是必经之路。只有当 SWIPT 技术的成本与传统方式相当时，它才可能获得大规模的应用。这需要我们在材料选择、生产工艺等方面进行持续的创新和优化。同时，考虑到当前市场上存在众多品牌和型号的设备，如何确保各个厂商、各种设备都能适配同一套 SWIPT 标准，也是推动其广泛应用的关键。

SWIPT 技术虽然前景光明，但要真正实现广泛应用，仍需跨越多个难关。这不仅仅是学术界的研究任务，更需要产业界的共同努力。只有学术界与产业界紧密合作，将研究成果快速转化为实际产品，我们才能确保 SWIPT 技术持续、稳定地发展，并最终为人们的生活带来真正的便利和革命性的变化。希望在不久的将来，我们能够充分利用 SWIPT 技术，为这个世界创造更多的可能和奇迹。

五、结论与展望

本文从无线电能与信息同时传输技术的研究与分析出发，介绍了其基本原理、关键技术、应用场景与挑战等方面。SWIPT 技术作为未来无线传输领域的重要发展方向，将为我们的生活带来更多便捷与可能性。然而，要实现 SWIPT 技术的广泛应用，仍需解决诸多挑战。我们相信随着科技的不断进步与创新，这些问题将逐渐得到解决，推动 SWIPT 技术走向成熟与普及。

参考文献：

[1]闫孝如;王尚宇;陈伟华.心脏起搏器无线供能线圈偏移效率优化研究[J]. 传感器与微系统,2022(11)

[2]刘旭;宋翔昱;原熙博;夏晨阳;伍小杰.一种利用可切换补偿电容的三线圈无线电能传输系统互感识别及效率优化方法[J]. 中国电机工程学报,2022(22)

[3]徐伟;肖新宇;董定昊;唐一融;胡冬;刘毅.直线感应电机效率优化控制技术综述[J]. 电工技术学报,2021(05)

[4]廖莎;宋城.供电服务体系的效率优化策略分析[J]. 集成电路应用,2021(10)

基金项目：河南省高等学校重点科研项目，项目名称:《基于共享通道的双向无线电能和信息同时传输系统特性研究》，项目文件：河南省教育厅教科技〔2021〕383号文件，项目编号:22B480006

作者简介:张红丽 出生年月:1981年11月 性别:女 民族:汉 籍贯:郑州市 学历:硕士 职称:副教授 研究方向:电子与通信工程

5.基于共享通道的双向无线电能和信息同时传输系统特性研究

流体测量与控制
Fluid Measurement & Control

（双月刊 2020 年创刊）
2024 年第 2 期　　总第 21 期
2024 年 4 月 25 日

主　　管　上海电气控股集团有限公司
主　　办　上海自动化仪表有限公司

编 辑 出 版　《流体测量与控制》编辑部
地　　址　上海市山连路 377 号 5 号楼
邮　　编　200444
编　辑　部　(021)36129977-2052
广　告　部　(021)66987870
传　　真　(021)62801680
电 子 信 箱　liuticeliang@saic.sh.cn

发 行 范 围　国内外公开发行
印　　刷　上海铁路印刷有限公司
国 内 总 发 行　上海市报刊发行局
订　阅　处　全国各地邮政局(代号 4-967)
国 外 总 发 行　中国国际图书贸易集团有限公司
国 外 代 号　BM1874
定　　价　10 元
中 国 标 准　ISSN 2096-9023
连续出版物号　CN 31-2179/TH

目　次

期刊基本参数：CN 31-2179/TH * 2020 * b * A4 * 100 * zh * P * ￥10.00 * 2000 * 23 * 2024-04

No.2, 2024 (Serial No. 21)
Apr. 25, 2024 (Bimonthly)

Fluid Measurement & Control

CONTENTS

Competent Authority:
Shanghai Electric Holdings Group Co., Ltd.
Sponsor:
Shanghai Automation Instrumentation Co., Ltd.

Publisher:
Editorial Office of Fluid Measurement & Control
Address: No.5 Building, 377, Shanlian Road, Shanghai 200444, China
Editorial Department:
86-21-36129977-2052
Advertising Department:
86-21-66987870
Fax: 86-21-62801680
E-mail: liuticeliang@saic.sh.cn

Director of Editorial Department:
ZHANG Min

Editor in Chief:
ZENG Wenbin
Deputy Editor in Chief:
CHEN Yan
Editor in Charge:
SHI Zhefeng

Publication Code:
ISSN 2096-9023
CN 31-2179/TH

Abroad Distributor:
China International Book Trade Group Co., Ltd.

Code No: BM1874

Serial parameters: CN 31-2179/TH * 2020 * b * A4 * 100 * zh * P * ¥10.00 * 2000 * 23 * 2024-04

主办单位：上海自动化仪表有限公司
编辑出版：《流体测量与控制》编辑部
中国标准连续出版物号：ISSN 2096-9023 CN 31-2179/TH
报刊代号：4-967

地址：上海市山连路377号5号楼
邮编：200444
电话：(021) 36129977-2052
定价：10元

ISSN 2096-9023

基于共享通道的双向无线电能和信息同时传输系统特性研究

Research on Characteristics of Bidirectional Radio Energy and Information Simultaneous Transmission System Based on Shared Channel

张红丽[1]， 刘建萍[1]， 范 莉[1]， 张来宾[1]， 李志英[2]
(1.郑州电力职业技术学院，河南 郑州 451450；
2.郑州祥龙电力股份有限公司，河南 郑州 450000)
ZHANG Hongli[1]， LIU Jianping[1]， FAN Li[1]， ZHANG Laibin[1]， LI Zhiying[2]
(1.Zhengzhou Electric Power Technology College，Zhengzhou 451450，Henan，China；
2.Zhengzhou Xianglong Power Co.，Ltd.，Zhengzhou 450000，Henan，China)

摘 要： 随着电力电子技术、控制技术及开关电源相关技术的发展，电能和信号传输逐渐从以电缆为传输媒介的传统传输方式逐渐向无线传输方向发展。对于需要在水介质中长时间工作的电气设备而言，能量供应是维持其正常工作的关键因素，但由于电缆进行物理连接的传统传输方式在水介质中运用较为不便，并且存在较大的安全隐患，因此需要构建一个基于共享通道的双向无线电能和信息同时传输的系统。

关键词： 双向无线技术；共享通道；电能和信息同时传输；系统特性

Abstract: With the development of power electronics technology, control technology and related technologies of switching power supply, power and signal transmission has gradually developed from the traditional transmission mode with cable as transmission medium to wireless transmission. For electrical equipment that needs to work in the water medium for a long time, energy supply is the key factor to maintain its normal work, but the traditional transmission mode of physical connection by cable is more inconvenient to use in the water medium, and there are greater security risks, so it is necessary to build a two-way radio energy and information transmission system based on shared channels.

Key words: two-way wireless technology; shared channel; simultaneous transmission of electrical energy and information; system characteristic

中图分类号： TN913 **文献标志码：** A **文章编号：** 2096-9023(2024)02-0085-05

1 前言

随着计算机技术的高速发展，高清影像、局域物联、智能城市、自助行车等新型服务正在进行大规模普及与应用。无线通信发展将出现质的飞越，移动信息速率也会出现指数级增加，这种增加正在促进无线电系统的发展。无线化与宽频化是当今通信业乃至全部资讯业中的热门话题，如果将两者融合，将具有极大的发展潜力。光纤无线电技术可将无线电信息传送至远程天线单元之间的光缆线路上，在当前的无线电技术中，数字信息被普遍采用，但输出数据的应用对增加无线电数据的传输能力以及改善无线电单元的结构有着巨大的作用。

2 双向无线电通信的原理

双方无线电对讲机主要是用来发出和接受语音信号。每台双方无线电对讲机都包括1台发送机和1台接收机、1台话筒和1台扬声器、1根天线和1台供电。手提式双方无线通信的电源采用电池，而车载式无线电信号则由车辆供电。人对着麦克风讲话，声音信息便转变为电子信息。此信息再经发射机处理后放大成无线电信息，并传输至天线上，由天线将无线电信息传播至高空中。受信者的通信设备收到无线电信息后，将此信息送往接收机。由接收器将此无线电信息转换成原始的声音，并从无线电对讲机的扬声器播放，此时便能听到最原始的声音信息[1]。

基金项目： 河南省高等学校重点科研项目(22B480006)

2.1 简单的双向无线电系统

2个以上的无线电对讲机在互相"对话"后，需要同时运行。对于一个频率的单工用户，每个无线电用户都能够在一个频率上发出或收到消息。它和通话系统有所不同，电话是双工技术，能够同时发言与收听。使用者在讲话时，应该关心无线电电子计量学技术的信道有没有开放[2]。

2.2 高效率双向无线电通信步骤

假设每个无线电使用者都符合了下列规定，就能实现最高效率的双向无线电通信。

(1)不打断其他客户的话语，及时关注频道中的电话状态。大部分的双向无线电对讲机上都会有个监听按键，按下该按键即可看到频道中的通信状态，但发出的频道应该是一片空白的。

(2)将对讲机保持在垂直高度，扩音器/话筒则维持在嘴巴正前方10 cm左右。

(3)发言时，对着话筒清晰、缓慢陈述，不可长期占用语音频道。

2.3 噪声抑制

噪声控制是为了减少、控制或减少无用的无线电信号或噪声，使其无法通过扩声机发出。无线电对讲机所产生的背景噪声通常是未通过噪声控制的结果。因此，大部分无线电对讲机上均设有调节噪声控制模式和声音控制水准的选择开关以及指示灯。

2.4 载波抑制和编码抑制

载波控制在不发射时也会防止噪声从频率放大器传播出来，因而是安静的备用工作。编码控制使无线电的编码方式可以只听到用户所需要的内容。因此，当它过滤掉了转至特定无线电系统以外的任何其他信息，并且只有在对相同的无线电电子计量学或对讲机的解码模式时，才能看到所发的信息。编码控制主要包括专用线路(private line，PL)的单音编码抑制和数字化专用线路(digital private line，DPL)的数字化编码控制2类。

大部分无线广播对讲机均设有一种监听按键，令用户解除噪声控制，解除编码控制模式。按下该按键后，扩音机将发出信道上的全部声音通信。在同样的频段内而使用截然不同的抑制编码电话时，在发话时就应该首先听并确认频段内有没有其他的语音通话[3]，同时发话将干扰已经在进行着的谈话。

2.5 PL和DPL编码噪声抑制系统

单字调编码系统主要采用次音频技术，可采用42种不同的单字调编码。数字化编码系统的作用与单字调编码系统一样，可采用84种不同的数字编码，并通过音频技术来开启高功率放大。虽然这种技术被称为专用线路，但并无保密作用。

2.6 频率和频道

频率与频道范围是在无线电通信中常用的概念。每一个双向无线电企业的规范中，均会明确地列明其工作频段。同样，在主管机构所下发的应用许可证上，也列明了其工作的某些频段。无线电应用增多、频段日益拥堵之际，对频段的利用与管理也愈发重要。频段即无线电发出和接收消息的频段。频段承载通常是指一个频段内所规定的用户数量。在无线电应用较密集的地方，频段承载可以更合理地限定了可利用的频段数量，以及客户的通话能力[4]。

对无线电对讲机的数条通道，一条一道地进行检查，找出可能通过的空白通道[5]。当可访问的频道更多时，用户群的管理将更加简单。如无线广播对讲机具备PL/DPL的解码噪声控制能力，若同一用户群组中也拥有同样的PL/DPL编码能力，则应进行合并，以便于在同一频段上工作。除非他们需要切换信道，或转换至其他频段，才能固定在其通话小组的频段上。

3 基于共享通道的双向无线电能和信息同时传输系统

3.1 系统模型

融合网络一般是建立光载无线(radio-over-fiber，RoF)网络之上，整个框架都是在原RoF网络的基本上加以完善的，后来又增加了PWoF网络，使其能对远部的天线系统单元供电。本实验使用了OptiSystem的软件系统对其加以模拟，并获取了相应数值。试验框架如图1所示。

由图1所见，融合系统主要由两部分构成：上半部分信息的传输，以及下半部分融合系统信息双向传输特性的检验。

首先，在CO端由一对激光器生成光学输出信号，再通过加入不同的调节信号对光信号加以调节，调节后的信息在经由掺铒光纤放大(erbium-doped fiber amplifier，EDFA)电路扩大后，又经由过滤器过滤处理。

由2个高功率激光器(high power laser，HPLD)生成的光学仿真信息和馈电光与先前被加工的信息结合，经由循环器(circulator，CIR)流入光纤，而

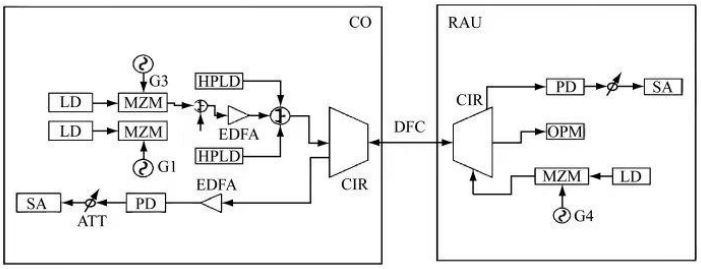

图1 融合系统框架图

后再送到RAU端口。在RAU端,先对信道实施光输出功率的检测,通过在线观测信道光输出功率(optical power meter,OPM)测算出该网络系统的光电量传输效果。信息由电光二极管(photodiode,PD)将之转化为电信号。电信号由信号分析仪(signal analyzer,SA)等设备加以检测,以获取有关的实验数据。与此同时,还从RAU中输入光信息并传送至CO,在CO端加以放大,再通过电光二极管转换为电信号等过程。此外,还需要通过检测光信息品质,评价该信息系统的双向传播特性[1-7]。在试验中,加入循环器的最主要目的就是使整个系统能够实现信息双向传送,区分各个方位的信息。

3.2 仿真结果分析

在仿真中,将仿真分成信息单一传送和混合发送2个阶段。首先完成光信息的传送仿真,然后实现光信号和电信号的信息混合传送,再进行双向传送,逐步提高模拟的难度,最后进行模拟。光传感的模拟结果如图2所示。

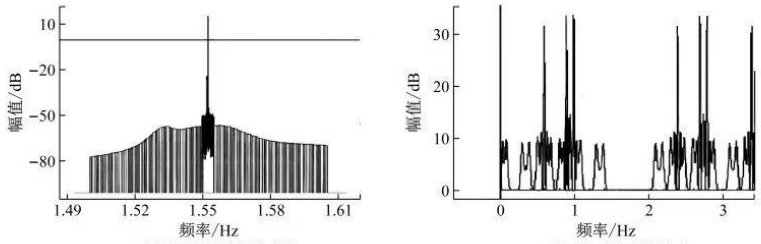

(a) 光调制信号的频谱变化 (b) 显示信号的频谱变化

图2 光信号传输对比图

加入的光脉冲信号经EDFA增强后的频率变化如图2(a)所示,恢复后如图2(b)所示。对比图2(a)与图2(b),显示信号的频谱变化和光调制信号的频谱变化一致。2个数据可以结合接收信息的误码率(bit error rate,BER)特征,但由于OptiSystem的软件环境的影响,采用了双面光纤,从而计算了整个系统的双向传输特征。通过利用BER特性研究结果可以看出,模拟数据在系统内的传递效果很好。因此,整个系统的双向传输特性试验也采用了上述实验结果。为达到这一效果,在光缆两端增加了环回器。环回器的主要功能是把各个信号的输入信号区分隔开,并在RAU一端输入激光信号,这些激光信号被以正弦信号调节,将调节后的信息经由光缆传送至CO一端,再对CO端进行放大或光电变换等,以此保证系统的双向传送特点。

4 基于共享通道的双向无线电能和信息同时传输系统案例

该系统是海下无线电能和信号共享通道传输系统,如图3所示。系统主要包括无线电能传输线路和无线信号传输线路,通过利用共同的磁场谐振式线圈及耦合线圈进行无线电能和信号的传输。海下无线电能和信号共享通道传输系统,无线电能传输线路具体结构包括依次连接的电源、高频逆变电路、能量谐振补偿电路、耦合线圈、高频整流电路、电压调理电路及负载。无线信号传输线路具体结构为高频载波电路、模拟开关、调制信号电路、耦合线圈、信号提取电路、信号解调电路、数字信号,其中模拟开关还接入数字信号。无线电能传输线路和无线信号传输线共用同1个耦合线圈。

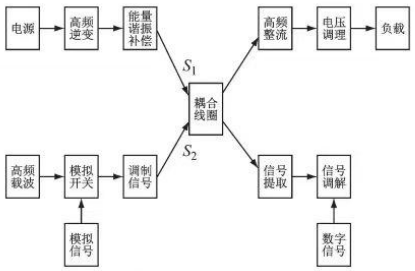

图3 共享通道的双向无线电能和信息同时传输系统

海下无线电能和信号共享通道传输系统由电源及包含4个NPN(type triode)增强型的MOSFET开关管Q_1、Q_2、Q_3、Q_4的全桥逆变电路构成。MOSFET开关管Q_1和MOSFET开关管Q_3之间还连接有电容C_p的一端。电容C_p的另一端依次连接电感L_p、开关S_1、电阻R_p后与耦合线圈连接的原边连接。耦合线圈的副边一端依次连接电阻R_s、二极管D_5、电阻R、二极管D_7后再次接入二极管D_5。所述二极管D_5和二极管D_7的两端还并联有二极管D_6和二极管D_8,二极管D_6和二极管D_8之间又连接至耦合线圈的副边的另一端。

所述电阻R两端还并联有电容C_0。所述电阻R_s与二极管D_5之间还连接有二极管D_9的正极,二极管D_9的负极依次连接二极管D_{10}、电阻R_4、A/D模块后接入耦合线圈的副边的另一端,A/D模块同时还与负载连接。所述电阻R_s与二极管D_9之间连接有电阻R_1的一端,二极管D_9与二极管D_{10}之间连接有电阻R_2的一端,二极管D_{10}与电阻R_4之间连接有电容C_1的一端以及电阻R_3的一端,电阻R_4和A/D模块之间连接有电容C_2的一端。所述电阻R_1的一端、电阻R_2的另一端、电容C_1的另一端、电阻R_3的另一端以及电容C_2的另一端均连接至耦合线圈的副边的另一端。

海下无线电能和信号共享通道传输系统中海下无线电能和信号共享通道传输方法,按照以下步骤实施:

(1)原边全桥逆变网络交流直流电转化。

(2)原副边补偿网络SN,即原边串联补偿,副边不补偿。

(3)基于2FSK的信号调制和信号的解调。

(4)基于磁耦合谐振无线电能传输的电能和信号切换。

海下无线电能和信号共享通道传输方法,所述步骤1具体按照以下步骤实施:

(1)当MOSFET开关管Q_1、MOSFET开关管Q_4闭合,MOSFET开关管Q_2、MOSFET开关管Q断开时,电流流经MOSFET开关管Q_1,MOSFET开关管Q_4形成回路。

(2)当MOSFET开关管Q_2、MOSFET开关管Q_3闭合,MOSFET开关管Q_1、MOSFET开关管Q_4断开时,MOSFET开关管Q_2、MOSFET开关管Q_3不能立即闭合,且在这一瞬间电感电流的方向不能突变,此时电流流经MOSFET开关管Q_2、MOSFET开关管Q_3开关的反并联二极管D_2、二极管D_3续流。

(3)电感电流过零后,MOSFET开关管Q_2、MOSFET开关管Q_3闭合,电感电流反向流过MOSFET开关管Q_2、MOSFET开关管Q_3。

(4)当MOSFET开关管Q_2、MOSFET开关管Q_3断开,MOSFET开关管QMOSFET开关管Q_4再次闭合时,同理MOSFET开关管Q_1、MOSFET开关管Q_4不能立即闭合,电流流经MOSFET开关管Q_1、MOSFET开关管Q_4的反并联二极管D_1、二极管D_4续流,之后的周期重复上述过程。

海下无线电能和信号共享通道传输方法,系统的原副边回路有以下关系:当ICPT系统工作在一个固定的负载范围时,负载阻值的变化范围在规定的区间,且系统工作在一个高频的状态,此时$R_s+R_{eq}/j\omega$忽略不计,则系统副边电流表示为SN拓扑网络的初次级电流之间没有相位差。当初级电感电流处于过零点时,次级电感电流也处于过零点,则磁耦合谐振无线电能、信号传输系统处于零能量储存状态。此时便可以将系统进行能量和信号传输的功能切换。

海下无线电能和信号共享通道传输方法中,所述步骤3具体可以按照以下步骤进行实施:

用载波f_1对二进制信号的1码进行传输,用载波f_2对其0码进行传输,振幅和初相位不变,控制是由2个不同频率的高频载波信号、数字信号、1个反向器、2个乘法器和1个加法器构成,数字信号直接与载波信号f_1相乘。当数字信号为1时,输出频率为f_1的载波;当数字信号为0时,输出为0。数字信号经过1个反向器后与载波信号f_2相乘,当数字信号为1时,输出为0;当信号为1时,输出频率为f_2的载波。将两部分用加法器相加后就输出频率不一样的高频信号2FSK,即实现用高频信号f_1表征数字信号1,高频信号f_2表征数字信号0。信号的解调过程就是将互感线圈传送的信号进行半波整流、包络

检测、低通滤波和比较输出环节，得到系统需要传输的信号。

海下无线电能和信号共享通道传输方法的特征在于，所述步骤4具体按照以下步骤进行实施：

电能经过全桥逆变后将能量传输到耦合线圈前端的功能切换开关S_1、S_2处。当开关S_1导通时，系统SN拓扑网络处于电能传输状态；当开关S_1关断时，耦合线圈与电能传输回路完全断开不再受电能传输的影响。系统的信号与能量的传输在时间上是互补的，能量和信号传输控制开关的切换周期是全桥逆变开关周期的整数倍，使得系统切换在电感电流过零点处。因此，信号的功能切换类似于能量功能切换回路。

5 结束语

通过使用RoF系统进行仿真实验，对双向无线电能和信息的同步传播进行研究，并以海下无线电能和信号共享通道传输系统为案例，对基于共享通道的双向无线电能和信息同时传输系统特性研究进行概述，可为无线技术的发展提供参考。

参考文献：

[1] 王宇，龚国庆．双向无线电能传输系统恒输出控制分析[J]．北京信息科技大学学报(自然科学版)，2022，37(1)：34-39.
[2] 赵仕桥．双向无线电能传输系统同步控制方法研究[D]．成都：西南交通大学，2021.
[3] 孙照帅．双向无线电能传输系统移相控制策略研究[D]．武汉：武汉理工大学，2020.
[4] 王波．ROF系统的信道编码技术和负载资源分配方案研究[D]．北京：北京邮电大学，2019.
[5] 严翔羽，叶全意，田锦，等．RoF技术在未来大都市网络中的应用[J]．广东通信技术，2018，38(6)：53-55.
[6] 赵志浩．无线电能传输网传能机制与优化问题研究[D]．重庆：重庆大学，2016.
[7] 安辉，王宾，邸净宇，等．电磁兼容检测分析及优化整改思路[J]．流体测量与控制，2022，3(6)：43-45.

(上接第84页)

6 结语

本文选择了目前主流的CORBA北向接口技术方案，以实现对电力通信网络管理的全面管理。AJAX技术也应用在这套电力通信控制系统中。若新增站点或光缆区段，系统会进行局部刷新，只对需要更新的部分进行更新，从而避免整页重装。这样的设计能够提高用户体验，节省系统资源。此外，相较于传统的Web同步通信模式，AJAX异步通信模式能够更快地响应用户的交互需求，使用户能够更加高效地操作和浏览系统。通过本文提出的促进不同厂商、平台之间的信息整合，实现对电力通信网络管理的全面管理和优化，提高系统灵活性和扩展性的电力通信管控系统。基于CORBA的电力通信管控系统，不仅可以帮助电力通信部门统一管理、优化业务流程、提高工作效率，还可以为电力部门提供丰富的数据分析，为该行业发展提供决策依据。

参考文献：

[1] 温柏坚，刘晔，蒋道环，等．电力行业智能化综合管控系统设计[J]．自动化与仪器仪表，2022(6)：149-153.
[2] 章飞．上海电力基建管控系统网络支撑应用分析[J]．大众标准化，2022(12)：31-33.
[3] 陈晓盈．计算机信息系统在电力通信工程管理中的应用研究[J]．电脑知识与技术，2022，18(16)：24-26.
[4] 金海，刘晴，蔡健挺．电力通信运行管控系统设计与开发[J]．信息通信，2013(1)：209.
[5] 张建华．电力智能通信网全程管控系统地区级系统运行模块方案设计[J]．华东电力，2011，39(10)：1691-1693.
[6] 黄德松．电力通信管控系统的研究与设计[D]．南宁：广西大学，2020.
[7] 殷文杰．小议光传输设备在电力系统通信中的应用[J]．流体测量与控制，2022，3(6)：6-10.

流体测量与控制 . 2024(02) 查看该刊数据库收录来源

记笔记

基于共享通道的双向无线电能和信息同时传输系统特性研究

张红丽[1] 刘建萍[1] 范莉[1] 张来宾[1] 李志英[2]
1.郑州电力职业技术学院 2.郑州祥龙电力股份有限公司

摘要： 随着电力电子技术、控制技术及开关电源相关技术的发展，电能和信号传输逐渐从以电缆为传输媒介的传统传输方式逐渐向无线传输方向发展。对于需要在水介质中长时间工作的电气设备而言，能量供应是维持其正常工作的关键因素，但由于电缆进行物理连接的传统传输方式在水介质中运用较为不便，并且存在较大的安全隐患，因此需要构建一个基于共享通道的双向无线电能和信息同时传输的系统。

关键词： 双向无线技术；共享通道；电能和信息同时传输；系统特性；

基金资助： 河南省高等学校重点科研项目（22B480006）；

专辑： 工程科技Ⅱ辑

专题： 电力工业

分类号： TM724

6.基于重复控制的通风机变频调速系统死区补偿方法研究

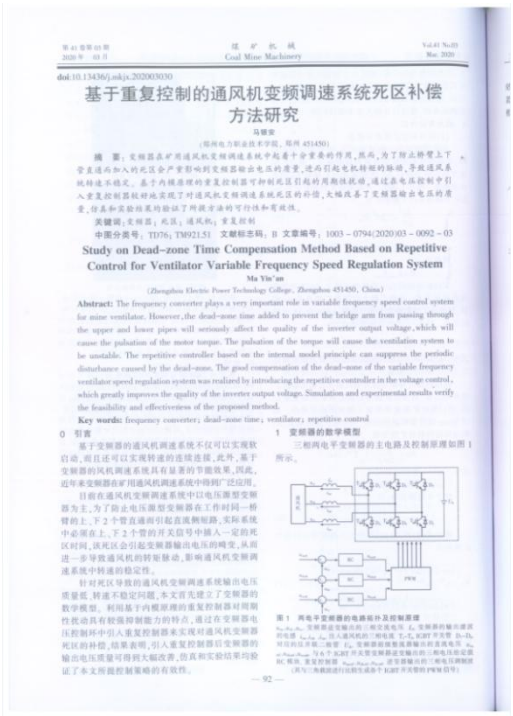

7.双碳目标下源-网-荷多层评价体系研究

报告编号：**L24N2023-0081**

检　索　报　告

一、检索要求

1. 委 托 人：李响(Li, Xiang)
2. 委托单位：郑州航空工业管理学院
3. 检索目的：论文被 EI 收录情况

二、检索范围

Engineering Village (Database: Compendex)	1969-present	网络版

三、检索结果

委托人提供的**1**篇论文被EI收录，论文收录情况见附件一。

特此证明！

检索报告人：曾宇

东北师范大学科技查新咨询中心

教育部科技查新工作站(L24)

2023 年 1 月 5 日

附件一： EI收录情况

第 1 条，共 1 条

Accession number:20214811247280
Title:Study on Multi-layer Evaluation System of Source-grid-load Under Carbon-neutral Goal
Title of translation:双碳目标下源-网-荷多层评价体系研究
Authors:Li, Xiang (1); Niu, Sai (2)
Author affiliation:(1) Zhengzhou Institute of Aeronautical Industry Management, Zhengzhou; 450015, China; (2) State Grid Nanyang Electric Power Company, Nanyang; 473000, China
Source title:Zhongguo Dianji Gongcheng Xuebao/Proceedings of the Chinese Society of Electrical Engineering
Abbreviated source title:Zhongguo Dianji Gongcheng Xuebao
Volume:41
Issue date:August 31, 2021
Publication year:2021
Pages:178-184
Language:Chinese
ISSN:02588013
CODEN:ZDGXER
Document type:Journal article (JA)
Publisher:Chinese Society for Electrical Engineering
Abstract: Under carbon-neutral goal, in order to promote energy upgrading, energy saving and emission reduction in the power industry, it is necessary to comprehensively analyze the low-carbon development level of power source, power grid and power consumption links, and establish a multi-layer assessment system of source-grid-load. Firstly, a multi-layer key index system of source-grid-load was established. On the source side, the upgrading and transformation of existing thermal power and the development and utilization of new energy were mainly considered; on the grid side, the equipment level and operation level were mainly considered; and on the load side, the substitution and promotion of electric energy were mainly considered. Secondly, on the premise of minimum square sum of subjective and objective weight deviation, AHP-entropy weight method was used to determine the comprehensive weight of indicators. The AHP method is based on expert experience, and the entropy weight method is based on historical data and carbon-neutral goal value. Then, the index membership function was constructed by combining the carbon-neutral goal and the average level of the index. Finally, the model was applied to the central urban power system to verify the effectiveness of the model.
 © 2021 Chin. Soc. for Elec. Eng.
Number of references:23
Main heading:Membership functions
Controlled terms:Energy conservation - Carbon - Emission control - Electric power transmission networks - Entropy - Hierarchical systems
Uncontrolled terms:Assessment system - Carbon neutrals - Energy - Energy-saving and emission reductions - Entropy weight method - Low carbon - Multi-layers - Power industry - Source-grid-load - Weight
Classification code:451.2 Air Pollution Control - 525.2 Energy Conservation - 641.1 Thermodynamics - 706.1.1 Electric Power Transmission - 804 Chemical Products Generally - 921 Mathematics - 961 Systems Science
DOI:10.13334/j.0258-8013.pcsee.211576
Funding details: Number: 212102210254, Acronym: -, Sponsor: -;
Funding text:基金项目：河南省科技攻关项目(212102210254) Project Supported by Scientific and Technological Projects of Henan Province (212102210254).

—The End—

DOI：10.13334/j.0258-8013.pcsee.211576　文章编号：0258-8013 (2021) S-0178-07　中图分类号：TM 715　文献标识码：A

双碳目标下源–网–荷多层评价体系研究

李响[1]，牛赛[2]

(1．郑州航空工业管理学院，河南省 郑州市 450015；2．南阳供电公司，河南省 南阳市 473000)

Study on Multi-layer Evaluation System of Source-grid-load Under Carbon-neutral Goal

LI Xiang[1], NIU Sai[2]

(1. Zhengzhou Institute of Aeronautical Industry Management, Zhengzhou 450015, Henan Province, China;

2. State Grid Nanyang Electric Power Company, Nanyang 473000, Henan Province, China)

ABSTRACT: Under carbon-neutral goal, in order to promote energy upgrading, energy saving and emission reduction in the power industry, it is necessary to comprehensively analyze the low-carbon development level of power source, power grid and power consumption links, and establish a multi-layer assessment system of source-grid-load. Firstly, a multi-layer key index system of source-grid-load was established. On the source side, the upgrading and transformation of existing thermal power and the development and utilization of new energy were mainly considered; on the grid side, the equipment level and operation level were mainly considered; and on the load side, the substitution and promotion of electric energy were mainly considered. Secondly, on the premise of minimum square sum of subjective and objective weight deviation, AHP-entropy weight method was used to determine the comprehensive weight of indicators. The AHP method is based on expert experience, and the entropy weight method is based on historical data and carbon-neutral goal value. Then, the index membership function was constructed by combining the carbon-neutral goal and the average level of the index. Finally, the model was applied to the central urban power system to verify the effectiveness of the model.

KEY WORDS: low-carbon; source-grid-load; assessment system; entropy weight method; weight

摘要：双碳目标下，为促进电力行业能源升级、节能减排，需对电源、电网、用电环节低碳化发展水平进行综合分析，建立源–网–荷多层评价体系。首先，建立源–网–荷多层关键指标体系，电源侧主要考虑现有火电升级改造及新能源发展利用情况，电网侧主要考虑装备水平及运行水平，负荷侧主要考虑电能替代推广情况。其次，以主客观权重偏差平方和最小为前提，利用层次分析(analytic hierarchy process，AHP)–熵权法确定指标综合权重，AHP 法基于专家经验，熵权法基于历史数据和双碳目标值。然后，结合双碳目标及指标平均水平，构造指标隶属度函数。最后，应用于中部城市电力系统，验证该模型的有效性。

关键词：低碳；源–网–荷；评价体系；熵权法；权重

0　引言

“碳达峰、碳中和”是党中央作出的重大战略决策，如何实现双碳目标也是当前研究热点与重点[1-2]。电力行业是我国碳排放的主要来源，推动能源动力转型、构建以新能源主体的电力系统是电力企业的内在使命，也是新形势下的外在需求[3-4]。因此，双碳目标对于我国电力系统来讲，是挑战也是机遇[5-6]。

国内外学者对电力的低碳、清洁展开了一系列研究，并应用于实际中，取得了较为丰硕的成果。文献[7-9]利用并优化碳捕集技术，降低火电的排放量，提高电厂的低碳性和经济性。文献[10]分析了碳交易机制对发电企业的影响，并为发电企业提供了具体的减排方案与技术。文献[11]以火电企业为研究对象，利用 DPSIR-5C 组合模型建立反映火电企业低碳水平的评价指标，结合 BTS-熵权法确定权重，从而对火电企业的低碳水平做出评价。文献[12]根据工程全寿命周期过程，选取能够反映电网低碳的核心指标，对国内部分城市的电网进行了评价分析。文献[13-14]从电网侧，结合智能算法，建立配电网的低碳评价模型，用于指导配电网低碳化工作。文献[15]考虑电网的区域、电压等级、设备类型的差异，根据输变电设备损耗率进行排序，对电网低碳性进行评价，为电网发展规划指明方向。文献[16-17]在综合考虑电能替代和能源结构，对能源结构进行评估或者对电能替代的效益进行评

基金项目：河南省科技攻关项目(212102210254)

Project Supported by Scientific and Technological Projects of Henan Province (212102210254).

估，以达到综合优化电源及用户侧的能效。文献[18]从社会经济、能源消费结构、环保约束等 5 个方面，结合云计算和熵权法，评估区域电能替代潜力，从而提出负荷侧低碳策略。

以上研究分别从电厂、电网、用户方面考虑了低碳措施及评价方法，侧重于单一环节的节能减排。双碳目标下，为促进电力行业能源升级、节能减排，本文在已有的研究成果基础上，综合考虑源–网–荷层面，分别电源侧、电网侧、负荷侧提出关键指标。电源侧不仅考虑现有火电的升级改造，而且考虑下新能源的装机容量、发电量和利用情况；电网侧注重考虑电网装备水平及运行水平；负荷侧着重考虑电能替代开展情况。为合理确定指标重要程度，利用层次分析(analytic hierarchy process，AHP)–熵权法进行赋权；依据节能减排目标和指标平均水平，建立指标隶属度函数。通过对中部某市的电力系统进行评价，验证评价模型的有效性，以期为电力企业发展提供决策参考。

1　实现双碳目标的关键评价指标选取

1.1　电源侧关键评价指标选取

为改变电能供应的能源结构，一方面在于改变火电的发展状态，另一方面大力促进和保障新能源的发展。火电及新能源发展方面的指标如图 1 所示。

我国以火电为主，但效率低、性能差的热电联产小火电和亚临界机组占比较大(50%左右)。因此，要改变能源结构，必须首先关停效率低、煤耗高的小火电，其次是对亚临界机组进行升级改造，提高机组的额定负荷参数及排放达标时的最低稳燃参数。

我国风光水资源丰富，近年来发展虽迅速，但基数小、能源利用效率不高，必须提高新能源占比及发电量，实施经济调度，优先安排新能源机组发电，防止弃光、弃风、弃水现象发生。

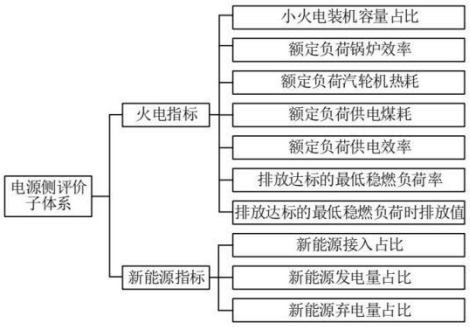

图 1　电源侧评价子体系指标

Fig. 1　Source side evaluation sub-system indexes

1.2　电网侧关键评价指标选取

电网是连接电源与用户的桥梁与纽带，在能源结构从高碳到低碳、化石到清洁能源转变的条件下，需要考虑电网设备的节能性和电网运行的高效、低碳性。电网侧评价子体系指标如图 2 所示。

在装备选型方面，需要选择低碳设备，使输电线路和变压器在运行时的损耗尽可能的低，同时考虑应用新型导线材料和节能性变压器，从设备源头降低电网运行损耗。

在电网运行方面，网损率直接反映电网损耗水平，因此将网损率作为电网低碳运行的主要考核指标之一。由于改善电网和设备的负荷特性，能够提高电网设备的运行效率，因此，将峰谷差、输变电设备的利用效率也作为主要考虑指标。同时考虑到安排发电计划的合理性，需要考虑节能调度执行情况。

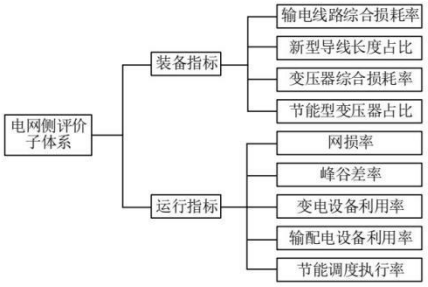

图 2　电网侧评价子体系指标

Fig. 2　Grid side evaluation sub-system indexes

1.3　负荷侧关键评价指标选取

电能替代是在负荷侧推动能源消费革命、实现双碳目标的重要途径。负荷侧的电能替代有 3 种：以电代煤、以电代油、以电代气。电能替代 3 个方面的指标如图 3 所示。

2　基于 AHP-熵权法的评价指标权重确定

2.1　指标权重流程图

双碳目标下源–网–荷多层评价体系的权重取值方法是 AHP-熵权法，取值流程如图 4 所示。

指标权重的求取，首先分别求取 AHP 主观权重和熵权客观权重，然后同等对待主、客观权重，并以偏差最小为目标求取综合权重。

2.2　基于 AHP 的评价指标主观权重赋值

AHP 法可将问题层次化，构建一个多层次的分

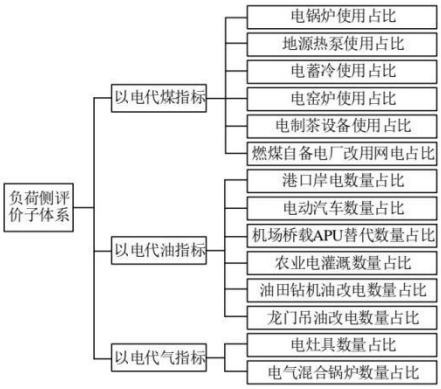

图 3 负荷侧评价子体系指标

Fig. 3 Load side evaluation sub-system indexes

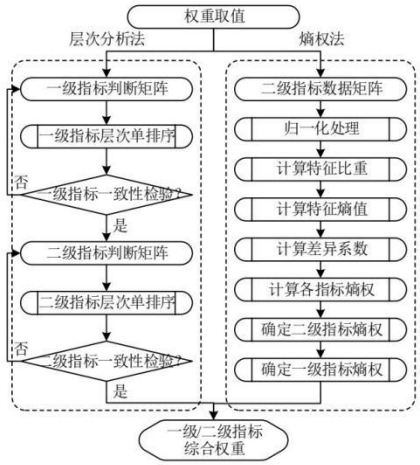

图 4 AHP-熵权法权重取值流程图

Fig. 4 Flow chart of AHP-entropy weight method

析模型结构，并相对于上级目标的重要性进行排序，由于该部分成果较为丰富[19-20]，所以在此不再赘述。

需要说明的是：由于 AHP 法依赖于专家经验，为了避免单个专家经验带来的缺陷，通过两种途径来使主观权重更加合理：途径 1 是每个专家形成单独的判断矩阵、权重计算、一致性检验，然后取权重的平均值；途径 2 是每个专家形成判断矩阵后，对判断矩阵的各元素进行平均，然后进行权重计算、一致性检验。

2.3 基于熵权法的评价指标客观权重赋值

为了获取指标的客观权重，需基于历史数据和双碳目标值构建权值。在构建二级指标的数据矩阵时，信息熵不仅计及该指标的建设成效，而且计及该指标与双碳目标值的差距，因此，需将指标历史值(至少两年数据)和双碳目标值作为数据矩阵的元素，计算二级指标熵权，自下而上通过累加的方法，求取一级指标熵权。具体步骤如下[21-23]：

1）形成评价对象原始数据矩阵。

设评价对象 i 有 m 个，评价指标 j 有 n 个，第 i 个评价对象的第 j 个指标的值记为 $X_{ij}(i=1,2,\cdots,m;\ j=1,2,\cdots,n)$，则形成的评价对象原始数据矩阵为

$$\boldsymbol{X}=\begin{bmatrix} X_{11} & X_{12} & \cdots & X_{1n} \\ X_{21} & X_{31} & \cdots & X_{2n} \\ \vdots & \vdots & \vdots & \vdots \\ X_{m1} & X_{m2} & \cdots & X_{mn} \end{bmatrix} \tag{1}$$

2）对评价对象原始数据矩阵归一化：

$$V_{ij}=\begin{cases} \dfrac{X_{ij}-\min(X_j)}{\max(X_j)-\min(X_j)}, & \text{越大越优的指标} \\ \dfrac{\max(X_j)-X_{ij}}{\max(X_j)-\min(X_j)}, & \text{越小越优的指标} \end{cases} \tag{2}$$

3）计算特征比重。

评价对象 i 的第 j 项指标下特征比重 P_{ij} 为

$$P_{ij}=\frac{V_{ij}}{\sum_{i=1}^{m}V_{ij}} \tag{3}$$

4）计算指标熵值：

$$E_j=-\ln\left(\frac{1}{m}\right)\sum_{i=1}^{m}P_{ij}\ln P_{ij} \tag{4}$$

5）计算差异系数 d_j：

$$d_j=1-e_j \tag{5}$$

d_j 越大，该指标提供的信息量越大，越应给予较大的指标权重。

6）确定各指标的熵权：

$$w_j=\frac{d_j}{\sum_{i=1}^{n}d_j} \tag{6}$$

2.4 基于 AHP-熵权法的综合权重赋值

为综合考虑主客观赋权法，假设：ω_i 为 AHP 法和熵权法组合后第 i 个指标的综合权重，将 $\omega_i^{(A)}$ 和 $\omega_i^{(H)}$的线性组合，则：

$$w_i=\alpha w_i^{(A)}+(1-\alpha)w_i^{(E)} \tag{7}$$

式中：$w_i^{(A)}$表示第 i 个指标的 AHP 权重；α 表示主

观偏好系数，$\alpha\in[0,1]$；$w_i^{(E)}$表示第 i 个指标的熵权权重；$1-\alpha$表示客观偏好系数。

以综合权重与主、客观权重的偏差平方和最小为目标，建立目标函数：

$$O=\sum_{i=1}^{m}[(\omega_i-\omega_i^{(A)})^2+(\omega_i-\omega_i^{(E)})^2] \tag{8}$$

要是 O 的最小值为 0，对上式求导，可得$\alpha=0.5$，即主、客观权重同等重要，式(7)转化为

$$w_i=0.5w_i^{(A)}+0.5w_i^{(E)} \tag{9}$$

最终求得各个指标的综合权重为

$$\boldsymbol{\omega}=\begin{bmatrix}\omega_1\\ \omega_2\\ \vdots\\ \omega_m\end{bmatrix}$$

3　隶属函数模型

统计各项指标的发展规律，本文采用的 3 种隶属函数模型。

1）越小越好的指标可采用模型 1：

$$u(x)=\begin{cases}100, & x\le a_1\\ \dfrac{100(x-a_2)}{a_1-a_2}, & a_1\le x\le a_2\\ 0. & x>a_2\end{cases} \tag{10}$$

或为

$$u(x)=\begin{cases}100, & x\le a_1\\ ax^2+bx+c, & a_1\le x\le a_2\\ 0, & x>a_2\end{cases} \tag{11}$$

2）越大越好的指标可采用模型 2：

$$u(x)=\begin{cases}0, & x\le a_2\\ \dfrac{100(x-a_2)}{a_1-a_2}, & a_2\le x\le a_1\\ 100, & x>a_1\end{cases} \tag{12}$$

或为

$$u(x)=\begin{cases}0, & x\le a_2\\ ax^2+bx+c, & a_2\le x\le a_1\\ 100, & x>a_1\end{cases} \tag{13}$$

3）在某一区间的指标可采用模型 3：

$$u(x)=\begin{cases}100, & a_{11}\le x\le a_{12}\\ \dfrac{100(x-a_{11})}{a_{11}-a_{21}}, & a_{21}\le x<a_{11}\\ \dfrac{100(x-a_{22})}{a_{12}-a_{22}}, & a_{12}<x\le a_{22}\\ 0, & x<a_{21}\ \text{or}\ x>a_{22}\end{cases} \tag{14}$$

4　算例分析

基于前述的双碳目标下源–网–荷多层评价模型，如表 1 所示，以我国中部某城市电力系统为例，在收集 2018—2020 年各项指标情况的基础上，结合指标要求，对该城市的电源侧、电网侧、负荷侧进行评价。

表 1　中部某城市源–网–荷多层评价算例

Table 1　An example of source-grid-load multi-layer evaluation of a city in central China

子体系	一级指标	二级指标	隶属度函数	评分	综合权重	得分
电源侧评价子体系	火电指标	小火电装机容量占比/%	当 $0\le x\le 100\%$ 时，$u(x)\equiv 100(1-x)$	75.35	0.0294	2.22
		额定负荷锅炉效率/%	当 $0\le x\le 100\%$ 时，$u(x)\equiv 100x$	80.31	0.0384	3.09
		额定负荷汽轮机热耗/(kJ/(kW·h))	$u(x)\equiv 0.00006x^2-1.1034x+4681.1$	75.25	0.0365	2.74
		额定负荷供电煤耗/(g/(kW·h))	$u(x)\equiv 0.0061x^2+2.0098x-19.485$	90.00	0.0285	2.57
		排放达标的最低稳燃负荷率/%	$u(x)\equiv 0.1782x^2-14.503x+295$	57.32	0.0419	2.40
		排放达标的最低稳燃负荷时排放值/(mg/m³)	粉尘：0.95；SO_2：3.3；氮氧化合物：28.61	3.62	0.0268	0.10
		火电指标得分	—	**381.85**	**0.2016**	**13.12**
	新能源指标	新能源接入占比/%	当 $0\le x\le 100\%$ 时，$u(x)\equiv 100x$	56.30	0.0505	2.84
		新能源发电量占比/%	当 $0\le x\le 100\%$ 时，$u(x)\equiv 100x$	23.68	0.0471	1.11
		新能源弃电量占比/%	当 $0\le x\le 100\%$ 时，$u(x)\equiv 100(1-x)$	100.00	0.0260	2.60
		新能源指标得分	—	**179.98**	**0.1236**	**6.56**
电网侧评价子体系	装备指标	输电线路综合损耗率/%	当 $x>4.5\%$ 时，$u(x)\equiv 0$ 当 $0\le x\le 4.5\%$ 时，$u(x)\equiv(900-20000x)/9$	100.00	0.0290	2.90
		新型导线长度占比/%	当 $0\le x\le 100\%$ 时，$u(x)\equiv 100x$	80.36	0.0277	2.22
		变压器综合损耗率/%	当 $x>5.2\%$ 时，$u(x)\equiv 0$ 当 $0\le x\le 5.2\%$ 时，$u(x)\equiv(1300-25000x)/13$	100.00	0.0304	3.04
		节能型变压器占比/%	当 $0\le x\le 100\%$ 时，$u(x)\equiv 100x$	100.00	0.0279	2.79
		装备指标得分	—	**380.36**	**0.1150**	**10.96**

续表

子体系	一级指标	二级指标	隶属度函数	评分	综合权重	得分
电网侧评价子体系		网损率/%	当 $x<3\%$ 时，$u(x)\equiv100$ 当 $3\%\le x\le10\%$ 时，$u(x)\equiv(10000x-300)/7$ 当 x 大于 10% 时，$u(x)\equiv0$	100.00	0.0345	3.45
	运行指标	峰谷差率/%	当 $0\le x\le100\%$ 时，$u(x)\equiv100(1-x)$	43.10	0.0313	1.35
		变电设备利用率/%	当 $x>75\%$ 时，$u(x)\equiv0$ 当 $x\le75\%$ 时，$u(x)\equiv400x/3$	85.30	0.0293	2.50
		输配电设备利用率/%	当 $x>80\%$ 时，$u(x)\equiv0$ 当 $x\le80\%$ 时，$u(x)\equiv1.25x$	83.50	0.0300	2.51
		节能调度执行率/%	当 $0\le x\le100\%$ 时，$u(x)\equiv100x$	100.00	0.0251	2.51
		运行指标得分	—	**411.90**	**0.1502**	**12.31**
	以电代煤指标	电锅炉使用占比/%	当 $0\le x\le100\%$ 时，$u(x)\equiv100x$	82.10	0.0367	3.01
		地源热泵使用占比/%		65.10	0.0357	2.32
		电蓄冷使用占比/%		79.88	0.0386	3.08
		电制茶设备使用占比/%		71.39	0.0357	2.55
		燃煤自备电厂改用网电占比/%		10.00	0.0395	0.39
		以电代煤指标得分	—	**308.47**	**0.1861**	**11.36**
负荷侧评价子体系	以电代油指标	港口岸电数量占比/%	当 $0\le x\le100\%$ 时，$u(x)\equiv100x$	19.85	0.0295	0.59
		电动汽车数量占比/%		10.00	0.0289	0.29
		机场桥载 APU 替代数量占比/%		70.00	0.0309	2.16
		农业电灌溉数量占比/%		73.90	0.0274	2.03
		油田钻机油改电数量占比/%		24.71	0.0254	0.63
		龙门吊油改电数量占比/%		33.06	0.0260	0.86
		以电代油指标得分	—	**231.52**	**0.1681**	**6.55**
	以电代气指标	电灶具数量占比/%	当 $0\le x\le100\%$ 时，$u(x)\equiv100x$	64.73	0.0318	2.06
		油气混合锅炉数量占比/%		54.30	0.0237	1.29
		以电代气指标得分	—	**119.03**	**0.0554**	**3.34**
		综合得分	—	**1704.64**	**1.00**	**64.19**

根据综合得分，该城市的低碳水平有待进一步提升，其中装备和运行水平指标得分较高，得分率分别为 95.27%和 81.99%；以电代油和新能源指标较差，得分率分别为 38.97%和 53.06%。为明确下一步的发展方向，对各个指标灵敏度进行排序，限于篇幅，对灵敏度较高的 5 个指标排序如图 5 所示。

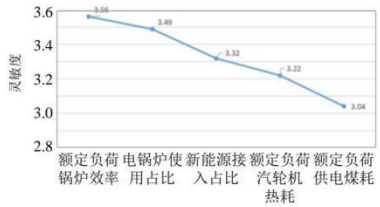

图 5 指标灵敏度排序

Fig. 5 Sensitivity sequencing of indicators

根据灵敏度排序，下一步需要做的额定如何锅炉效率、电锅炉使用占比、新能源接入占比、额定负荷汽轮机热耗及额定负荷供电煤耗。

5 结论

本文从电源侧、电网侧、负荷侧分别选取指标，结合 AHP-熵权法，建立源–网–荷多层评价模型，旨在对电力系统各环节进行更为全面合理的评价，通过理论研究和算例表明：

1）针对现有的研究成果主要体现在某一方面的碳排放改进或者评价，缺少对电力系统电源侧、电网侧、负荷侧的整体评价，本文建立了源–网–荷多层评价模型。

2）主、客观赋权法均存在取消，本文结合主客观赋权法，利用 AHP 法自上而下、熵权法自下而上，得到综合权重，这样可依据指标历史值变化以及现状情况，更加合理的衡量指标的重要性，以便在双碳目标下为电力企业决策提供理论支持。

3）建立隶属度函数时，为了合理评价各个指标的情况，需结合国际、国家、地方政府及电力企业在双碳目标下的要求，结合指标总体水平，形成指标散点值拟合曲线，可较为准确的衡量指标情况。

参考文献

[1] GASPARI M，LORENZONI A，FR ÍAS P，et al. Integrated Energy Services for the industrial sector：an innovative model for sustainable electricity supply[J]. Utilities

Policy，2017(45)：118-127.

[2] PERDAN S，AZAPAGIC A．Carbon trading：current schemes and future developments[J]．Energy Policy，2011，39(10)：6040-6054.

[3] 程耀华，张宁，康重庆，等．低碳多能源系统的研究框架及展望[J]．中国电机工程学报，2017，37(14)：4060-4069.
CHENG Yaohua，ZHANG Ning，KANG Chongqing，et al．Research framework and prospects of low-carbon multiple energy systems[J]．Proceedings of the CSEE，2017，37(14)：4060-4069(in Chinese).

[4] ZHANG N，HU Z，DAI D，et al．Unit commitment model in smart grid environment considering carbon emissions trading[J]．IEEE Transactions on Smart Grid，2016，7(1)：420-427.

[5] PAN Z，GUO Q，SUN H．Feasible region method based integrated heat and electricity dispatch considering building thermal inertia[J]．Applied Energy，2017，192：395-407.

[6] YANG Y，WU K，LONG H，et al．Integrated electricity and heating demand-side management for wind power integration in China[J]．Energy，2014，78：235-246.

[7] 崔扬，曾鹏，仲悟之，等．考虑富氧燃烧技术的电–气–热综合能源系统低碳经济调度[J]．中国电机工程学报，2021，41(2)：592-607.
CUI Yang，CENG Peng，ZHONG Wuzhi，et al．Low-carbon economic dispatch of electro-gas-thermal integrated energy system based on oxy-combustion technology[J]．Proceedings of the CSEE，2021，41(2)：592-607(in Chinese).

[8] 周任军，肖钧文，唐夏菲，等．电转气消纳新能源与碳捕集电厂碳利用的协调优化[J].电力自动化设备，2018，38(7)：61-67.
ZHOU Renjun，XIAO Junwen，TANG Xiafei，et al．Coordinated optimization of carbon utilization between power-to-gas renewable energy accommodation and carbon capture power plant[J]．Electric Power Automation Equipment，2018，38(7)：61-67(in Chinese).

[9] HE Liangce，LU Zhigang，ZHANG Jiangfeng，et al．Low-carbon economic dispatch for electricity and natural gas systems considering carbon capture systems and power-to-gas[J]．Applied Energy，2018，224：357-370.

[10] 檀勤良，丁毅宏，魏咏梅，等．碳交易及模糊预算下火电企业碳减排最优策略研究[J]．电网技术，2019，43(10)：3707-3714.
TAN Qinliang，DING Yihong，WEI Yongmei，et al．Research on optimal strategy of carbon emission reduction for thermal power enterprises under carbon trading and fuzzy budget[J]．Power System Technology，2019，43(10)：3707-3714(in Chinese).

[11] 段铭．基于改进 LSSVM 的火电企业低碳发展水平评价研究[D]．北京：华北电力大学，2019.
DUAN Ming．Research on evaluation of low carbon development level in thermal power enterprises based on improved LSSVM model[D]．Beijing：North China Electric Power University，2019(in Chinese).

[12] 孙彦龙，康重庆，陈宋宋，等．低碳电网评价指标体系与方法[J]．电力系统自动化，2014，38(17)：157-162.
SUN Yanlong，KANG Chongqing，CHEN Songsong，et al．Low-carbon power grid index system and evaluation method[J]．Automation of Electric Power Systems，2014，38(17)：157-162(in Chinese).

[13] 奇士杰．低碳经济下的配电网综合评估[D]．北京：华北电力大学，2019.
QI Shijie．Comprehensive evaluation of distribution network under low-carbon economy[D]．Beijing：North China Electric Power University，2019(in Chinese).

[14] 张汝佳．基于随机森林算法的智能电网低碳效益评价[D]．北京：华北电力大学，2019.
ZHANG Rujia．Evaluation of the low carbon effectiveness of smart grid base on random forest[D]．Beijing：North China Electric Power University，2019(in Chinese).

[15] 牛新生，田鑫，朱秀波等．山东电网低碳发展水平综合评价[J]．电力建设，2015，36(2)：141-148.
NIU Xinsheng，TIAN Xin，ZHU Xiubo，et al．Comprehensive evaluation of low-carbon development level of shandong power grid[J]．Electric Power Construction，2015，36(2)：141-148(in Chinese).

[16] 赵璞，周满，高建宇等．基于电能替代的园区综合能源规划评价方法[J]．中国电力，2021，54(4)：130-139.
ZHAO Pu，ZHOU Man，GAO Jianyu．et al．Evaluation method for park-level integrated energy system based on electric power substitution[J]．Electric Power，2021，54(4)：130-139(in Chinese).

[17] 张新鹤，宋阳，黄伟等．计及电源结构时空特性的电能替代评价[J]．中国电力，2019，52(3)：61-67.
ZHANG Xinhe，SONG Yang，HUANG Wei，et al．Evaluation of electric power replacement considering spatiotem-poral characteristics of power source structure[J]．Electric Power，2021，54(4)：130-139(in Chinese).

[18] 李艳梅，陈增．基于联系度优化 TOPSIS 法的区域电能替代潜力评估研究[J]．电网技术，2019，43(2)：687-693.
LI Yanmei，CHEN Zeng．Study on regional electric energy substitution potential evaluation based on TOPSIS Method of optimized connection degree[J]．Power System Technology，2019，43(2)：687-693(in Chinese).

[19] 刘万勋，于琳琳，张丽华，等．基于 AHP 和多级模糊

综合评判的电网发展水平评估[J]. 智慧电力，2020，48(5)：80-85.
LIU Wanxun，YU Linlin，ZHANG Lihua，et al. Evaluation of power grid development level based on AHP and multi-level fuzzy comprehensive evaluation[J]. Smart Power，2020，48(5)：80-85(in Chinese).

[20] 钱嘉欣，武家辉，姚磊等. 基于能值分析和多目标决策法的 CCHP-PV-Wind 系统综合性能评估研究[J]. 电力系统保护与控制，2021，49(2)：130-139.
QIAN Jiaxin，WU Jiahui，YAO Lei，et al. Comprehensive performance evaluation of a CCHP-PV-Wind system based on energy analysis and a multi-objective decision method[J]. Power System Protection and Control，2021，49(2)：130-139(in Chinese).

[21] 董福贵，张也，尚美美. 分布式能源系统多指标综合评价研究[J]. 中国电机工程学报，2016，36(12)：3214-3221.
DONG Fugui，ZHANG Ye，SHANG Meimei. Multi-criteria comprehensive evaluation of distributed energy system[J]. Proceedings of the CSEE，2016，36(12)：3214-3221(in Chinese).

[22] 南钰，宋瑞卿，陈鹏. 基于改进熵权-灰色关联法的配电网可靠性影响因素分析[J]. 电力系统保护与控制，2019，47(24)：101-107.
NAN Yu，SONG Ruiqing，CHEN Peng，et al. Study on the factors influencing the reliability analysis in distribution network based on improved entropy weight gray correlation analysis algorithm[J]. Power System Protection and Control，2019，47(24)：101-107(in Chinese).

[23] 邓红雷，戴栋，李述文. 基于层次分析–熵权组合法的架空输电线路综合运行风险评估[J]. 电力系统保护与控制，2017，45(1)：28-34.
DENG Honglei，DAI Dong，LI Shuwen. Comprehensive operation risk evaluation of overhead transmission line based on hierarchical analysis-entropy weight method[J]. Power System Protection and Control，2017，45(1)：28-34(in Chinese).

收稿日期：2021-05-08。

作者简介：

李响(1979)，男，工学硕士，副教授，主要从事电力系统分析与评估方面的研究工作，nomad0729@163.com。

李响

(**责任编辑** 吕鲜艳)

8.考虑大规模新能源接入的电网性能评价指标体系

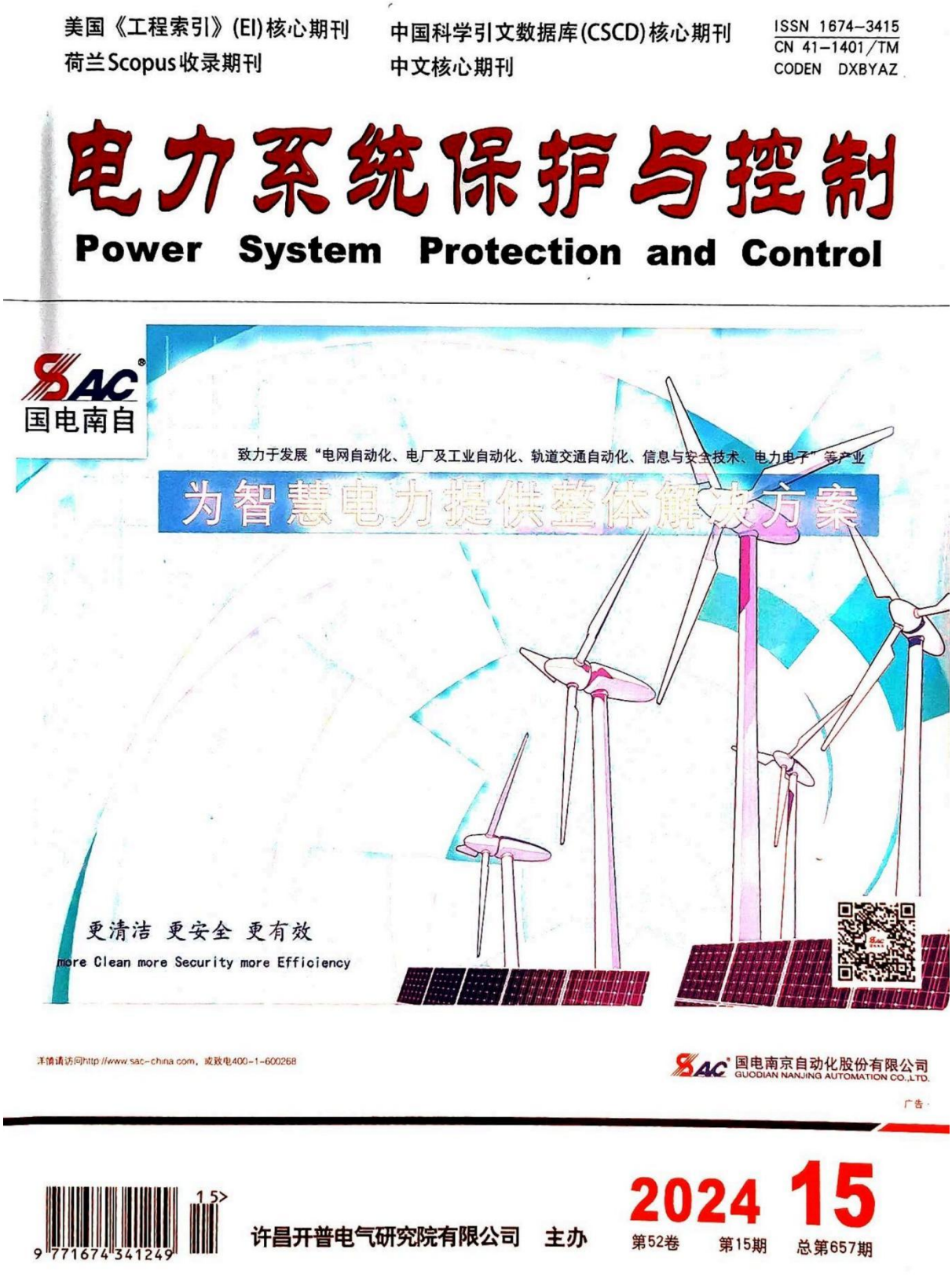

电力系统保护与控制

DIANLI XITONG BAOHU YU KONGZHI

第 52 卷第 15 期(总第 657 期) 2024 年 8 月 1 日出版

目 次

期刊基本参数：CN 41-1401/TM • 1973 • s • A4 • 192 • zh • P • ¥80.00 • • 16 • 2024-8

DOI: 10.19783/j.cnki.pspc.231246

考虑大规模新能源接入的电网性能评价指标体系

李 响[1]，武海潮[2]，王文雪[2]，安 全[2]

(1. 郑州航空工业管理学院，河南 郑州 450015；2. 河南聚研电力科技有限公司，河南 郑州 450000)

摘要：为了解决传统电网评价体系在评价大规模新能源和电网相互作用复杂机理时存在的不足，建立一套考虑大规模新能源接入的电网性能指标评价体系。首先，从新型电力系统的核心特征出发，贯穿“源网荷储”各个环节，构建包含接入水平、协调水平、适应水平以及承载水平 4 个维度的电网性能评价指标，显性表达各个指标的统计或计算方式。其次，采用 AHP-CRITIC 法进行主客观组合赋权，依据电网发展数据自身的客观属性，考虑数据离散程度以及皮尔逊相关系数，挖掘指标间的冲突性和变异性，以增强权重设置的科学性。最后，利用某城市新能源和电网数据对指标体系进行测算，通过对比分析说明所提指标体系与评价方法的有效性，并依据指标灵敏度大小对电网薄弱环节提出发展建议。

关键词：新能源；新型电力系统；指标体系；皮尔逊相关系数；权重

Performance evaluation index system of a power grid considering large-scale new energy

LI Xiang[1], WU Haichao[2], WANG Wenxue[2], AN Quan[2]

(1. Zhengzhou Institute of Aeronautical Industry Management, Zhengzhou 450015, China;
2. Henan Juyan Electric Power Technology Co., Ltd., Zhengzhou 450000, China)

Abstract: There are deficiencies in evaluating the complex mechanism of the mutual effects between large-scale new energy and the power grid by traditional power grid evaluation systems. Thus a performance evaluation index system is established considering large-scale new energy access. First, based on the key characteristics of the new power system and considering all parts of “power supply, grid, load and energy storage”, a power grid performance evaluation index containing connection, coordination, adaptation and carrying capacity levels can be set up. In addition, it explicitly expresses the statistical or calculation method for each index. Secondly, the AHP-CRITIC method is used to enable subjective and objective weights, and investigate the conflict and changeability among different indices based on the objective property of data from the power grid and computing standard deviation/Pearson correlation coefficient to highlight the scientific features on setting index weights. Finally, the index system for the data from new energy and the power grid in one city is surveyed and computed. The effectiveness of the proposed index system and evaluation method is shown through comparison and analysis. Some development proposals for weak parts of the power grid are proposed on the basis of the indicator’s sensitivity.

This work is supported by the Science and Technology Project of Henan Province (No. 222102240117).

Key words: new energy; new power system; index system; Pearson correlation coefficient; weight

0 引言

构建以新能源为主体的新型电力系统是我国电力发展的方向和目标[1-3]，“双碳”目标的不断落实，更加突出其重要性和紧迫性[4-5]。近年来，随着一系列利好政策的落实，以风电、光伏为代表的新能源发展迅速[6]。在大规模新能源接入电网时，一方面能够为电网提供绿色、环保的电能[7]，另一方面新能源的随机性、间歇性、波动性给电网的规划建设、运行调度带来了一定的影响[8-9]。

为了使新能源能够与电网协调发展、互相适应，研究人员对新能源和电网开展了大量的研究工作。文献[10]充分考虑分布式电源接入配电网后的环保效应，建立了包含设备运行状态、供电可靠性、

基金项目：河南省科技攻关项目资助(222102240117)

电能质量、经济性以及环保性能指标的配电网指标评估体系，适用于含高比例新能源接入的配电网评估。文献[11]针对高占比可再生能源的不确定性对电网带来的安全风险，从调度侧或新能源侧提出灵活性指标，对系统的灵活性进行评价。文献[12]以大规模风电为研究对象，从空间分布-电力潮流-指标类别 3 个维度，建立风电消纳全过程评价指标体系，为新能源消纳、规划打下基础。文献[13]从电源侧和电网侧提出适应水电站的评价指标体系，采用层次分析-熵权法对梯级水电接入电网的适应性进行评价。文献[14]从经济、安全、环境、技术 4 个方面选取 11 个指标，采用层次分析-熵权法对煤电和清洁能源的演化路径进行评价。文献[15]针对园区多能系统，将其能效分析分解为供能子系统和能源转换设备，建立评价体系对园区多能源系统综合能效进行评价。

在能源与电网融合大趋势下，针对大规模新能源与电网间相互作用的复杂机理[16-17]，本文基于新型电力系统的核心特征以及新能源接入对电网的要求，建立一套考虑大规模新能源接入的电网性能评价指标体系。该指标体系以促进新能源规模化发展为目标，贯穿源、网、荷、储各个环节，真实、全面地反映电网性能；显性表达各个指标的统计或计算方式，以量化大规模新能源接入时对电网接入水平、协调水平、适应水平及承载水平；采用层次分析法(analytic hierarchy process, AHP)和标准间冲突性相关性法(criteria importance through intercriteria correlation, CRITIC)，得到指标综合权重，从而实现大规模新能源并网时的多维度、多层级电网消纳能力综合评价。本文以某城市电网为研究对象，通过该城市新能源和电网数据对提出的指标体系进行测算，验证该指标体系的可行性和实用性。

1　评价指标体系的目标与准则

大规模新能源接入电网，在为电网提供绿色、环保能源的同时[18]，也对电网安全、电压质量、短路电流等方面带来了一定的影响[19-20]。因此，需要建立综合评价指标体系来评价新能源接入电网的适配程度，大规模新能源接入电网评价指标体系如图 1 所示，该指标体系以提高大规模新能源和电网之间的适配性为目的，从新型电力系统的核心特征及新能源接入对电网的要求出发，综合电网侧、电源侧、负荷侧、储能侧的要求，从接入水平、协调水平、适应水平和承载水平 4 个维度考量。

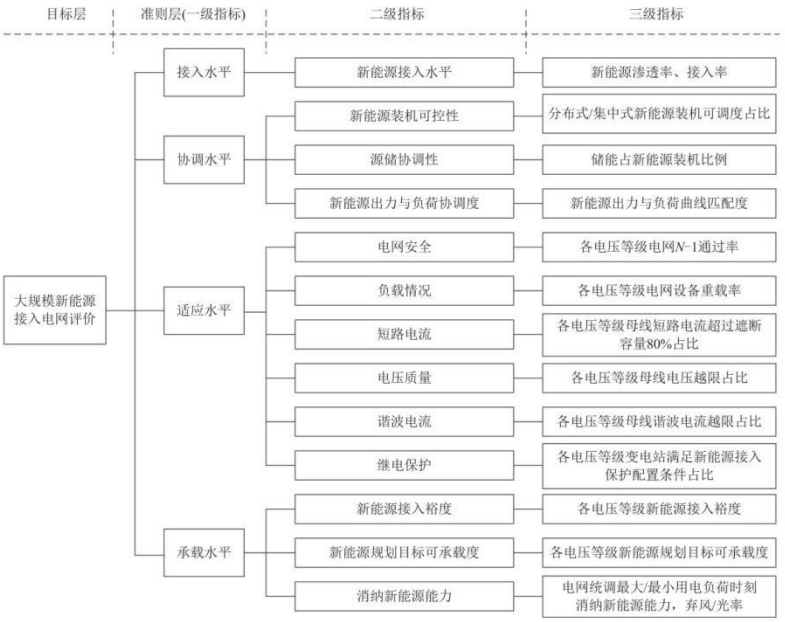

图 1 考虑大规模新能源接入电网的性能评价指标体系

Fig. 1 Performance evaluation index system of power grid considering the large-scale new energy integration

接入水平用来表征电网接入新能源的总体水平，其主要衡量并网新能源电站发电量、装机容量与用电量、总装机容量之间的比例关系，反映电网已接入新能源的基本情况。

协调水平用来表征新能源装机可控能力，以及与储能、负荷间的协调性。由于新能源存在一定的反调峰作用(发电高峰与用电高峰趋势相反)，新能源装机接入后，电网调度的灵活性可能会降低，发电、用电负荷的协调性可能会变差，将对电网调度安全带来较大影响。协调水平主要从源网荷储的协调性角度分析新能源接入对电网调度和安全的影响。

适应水平用来表征电网接入新能源的适应能力，即电网的坚强程度。新能源接入可能会导致设备 $N-1$ 不通过、重载设备增加、电压波动增大、谐波电流增加等方面的问题，从而对电网的安全稳定、供电能力、电压质量产生较大影响。电网越坚强，新能源接入后对这些方面的影响越小。

承载水平用来表征新能源消纳现状和接入裕度。新能源发电应尽可能以本地消纳为主，条件允许情况下才可通过主网外送，可通过典型负荷时刻新能源出力占比反映电网消纳能力。

2 评价指标

2.1 接入水平指标

接入水平指标主要反映电网新能源接入水平。三级指标包括新能源渗透率和接入率两个参数。

新能源渗透率 A_{11} 指新能源总发电量 ΣE_{NG} 占总发电量 ΣE_{G} 的比例，公式表示为

$$A_{11}=\frac{\Sigma E_{\mathrm{NG}}}{\Sigma E_{\mathrm{G}}}\times 100\% \tag{1}$$

新能源接入率 A_{12} 是指新能源装机总容量 ΣP_{NG} 占总装机容量 ΣP_{G} 的比例，如式(2)所示。

$$A_{12}=\frac{\Sigma P_{\mathrm{NG}}}{\Sigma P_{\mathrm{G}}}\times 100\% \tag{2}$$

2.2 协调水平指标

协调水平指标主要反映系统电源和负荷的协调性。二级指标有新能源装机可控性、源储协调性、新能源出力与负荷协调度。三级指标包括分布式/集中式新能源装机可调度占比、储能占新能源装机比例、新能源出力与负荷曲线匹配度。

1) 新能源装机可控性

集中式新能源装机可调度占比 B_{11} 是指可调度的集中式新能源装机容量 ΣP_{CCNG} 占新能源装机总容量的比例，如式(3)所示。

$$B_{11}=\frac{\Sigma P_{\mathrm{CCNG}}}{\Sigma P_{\mathrm{NG}}}\times 100\% \tag{3}$$

分布式新能源装机可调度占比 B_{12} 是指可调度的分布式新能源装机容量 ΣP_{CDNG} 占新能源装机总容量的比例，如式(4)所示。

$$B_{12}=\frac{\Sigma P_{\mathrm{CDNG}}}{\Sigma P_{\mathrm{NG}}}\times 100\% \tag{4}$$

2) 源储协调性

储能占新能源装机比例 B_{21} 是指储能装置装机容量 ΣP_{SPU} 占新能源装机总容量的比例，如式(5)所示。

$$B_{21}=\frac{\Sigma P_{\mathrm{SPU}}}{\Sigma P_{\mathrm{NG}}}\times 100\% \tag{5}$$

3) 新能源出力与负荷协调度

新能源出力与负荷协调度是指新能源出力曲线与负荷变化曲线的一致性，将出力曲线和负荷曲线标幺化后，进行匹配度计算，以此判断新能源出力与负荷之间的协调程度。有功功率标幺值 P_* 的计算公式为

$$P_*=\frac{P_t}{P_{\max}}\times 100\% \tag{6}$$

式中，P_t、$P_{\max}$ 分别为有功功率的实际值和最大值。

以新能源出力与年负荷曲线匹配度 B_{31} 为例，计算公式为

$$B_{31}=\left|\frac{\sum_{i=1}^{n}\left(P_{\mathrm{G},i}-\overline{P_{\mathrm{G}}}\right)\left(P_{\mathrm{L},i}-\overline{P_{\mathrm{L}}}\right)}{\sqrt{\sum_{i=1}^{n}\left(P_{\mathrm{G},i}-\overline{P_{\mathrm{G}}}\right)^2}\sqrt{\sum_{i=1}^{n}\left(P_{\mathrm{L},i}-\overline{P_{\mathrm{L}}}\right)^2}}\right| \tag{7}$$

式中：$P_{\mathrm{G},i}$、$\overline{P_{\mathrm{G}}}$ 分别为新能源年出力曲线的标幺值及平均值；$P_{\mathrm{L},i}$、$\overline{P_{\mathrm{L}}}$ 分别为年负荷曲线最大值的标幺值及平均值。

计算新能源出力与典型日负荷曲线匹配度 B_{32}，需要采用典型日的新能源出力数据和负荷数据。

2.3 适应水平指标

适应水平指标主要反映电网对大规模新能源接入的适应能力、坚强程度。二级指标有电网安全、负载情况、短路电流、电压质量、谐波电流和继电保护。三级指标包括各电压等级电网 $N-1$ 通过率、电网设备重载率、母线短路电流超过遮断容量 80% 占比、母线电压越限占比、母线谐波电流越限占比、变电站满足新能源接入保护配置条件占比。

某一电压等级电网的 $N-1$ 通过率是指该电压等级电网通过 $N-1$ 的设备数量占电网设备总量的比例。以 220 kV 电网的 $N-1$ 通过率 C_{11} 为例，如式(8)所示。

$$C_{11}=\frac{N_{\mathrm{P220}N-1}}{N_{220}}\times 100\% \tag{8}$$

式中，$N_{\mathrm{P220}N-1}$、N_{220}分别为通过$N-1$的220 kV设备数量及220 kV设备总量，电力设备一般指变压器和线路。

1) 重载情况

某一电压等级重载设备占比是指该电压等级电网中重载设备数量占设备总量比例。以220 kV重载设备占比C_{21}为例，如式(9)所示。

$$C_{21}=\frac{N_{220\mathrm{OQ}}}{N_{220}}\times 100\% \tag{9}$$

式中，$N_{220\mathrm{OQ}}$为220 kV重载设备数量。

2) 短路电流

某一电压等级的短路电流超过遮断容量80%占比指该电压等级电网中短路电流超过断路器遮断容量80%的母线占比。以220 kV短路电流超过遮断容量80%占比C_{31}为例，如式(10)所示。

$$C_{31}=\frac{N_{220\mathrm{BSO}}}{N_{220\mathrm{B}}}\times 100\% \tag{10}$$

式中，$N_{220\mathrm{BSO}}$、$N_{220\mathrm{B}}$分别为220 kV短路电流超过遮断容量80%的母线数量、母线总量。

3) 电压质量

某一电压等级的母线电压越限占比是指该电压等级电网中母线电压越限占比。以220 kV母线电压越限占比C_{41}为例，如式(11)所示。

$$C_{41}=\frac{N_{220\mathrm{BVO}}}{N_{220\mathrm{B}}}\times 100\% \tag{11}$$

式中，$N_{220\mathrm{BVO}}$为220 kV母线电压越限数量。

4) 谐波电流

某一电压等级的母线谐波电流越限占比是指该电压等级电网中母线谐波电流越限占比。以220 kV母线谐波电流越限占比C_{51}为例，如式(12)所示。

$$C_{51}=\frac{N_{220\mathrm{BHCO}}}{N_{220\mathrm{B}}}\times 100\% \tag{12}$$

式中，$N_{220\mathrm{BHCO}}$为220 kV母线谐波电流越限数量。

5) 继电保护

某一电压等级线路满足新能源接入保护配置条件占比是指该电压等级满足新能源接入保护配置条件线路占线路总条数的比例。以220 kV线路满足新能源接入保护配置条件占比C_{61}为例，如式(13)所示。

$$C_{61}=\frac{N_{220\mathrm{MRPL}}}{N_{220\mathrm{L}}}\times 100\% \tag{13}$$

式中，$N_{220\mathrm{MRPL}}$、$N_{220\mathrm{L}}$分别为220 kV满足新能源接入保护配置条件线路条数、220 kV线路总条数。

2.4 承载水平评价指标

承载水平指标主要反映电网接入新能源剩余容量、新能源规划目标可承载度以及电网消纳新能源的能力，二级指标有新能源接入裕度、新能源规划目标可承载度、消纳新能源能力。三级指标包括各电压等级新能源接入裕度、各电压等级新能源规划目标可承载度、电网统调最大/最小用电负荷时刻消纳新能源裕度、弃风/光率。

1) 新能源接入裕度

某一电压等级的新能源接入裕度是指该电压等级新能源装机剩余容量占最大允许新能源接入容量的比例。以220 kV及以下新能源接入裕度D_{11}为例，如式(14)所示。

$$D_{11}=\left(1-\frac{\Sigma P_{220\mathrm{NGM}}}{\Sigma P_{220\mathrm{NGD}}}\right)\times 100\% \tag{14}$$

式中，$\Sigma P_{220\mathrm{NGD}}$、$\Sigma P_{220\mathrm{NGM}}$分别为220 kV已接入的新能源装机容量、可接入的新能源最大装机容量。

2) 新能源规划目标可承载度

某一电压等级的新能源规划目标可承载度是指已规划新能源装机容量占最大允许新能源接入容量比例。以220 kV新能源规划目标可承载度D_{21}为例，如式(15)所示。

$$D_{21}=\frac{\Sigma P_{220\mathrm{NGM}}}{\Sigma P_{220\mathrm{NPGD}}}\times 100\% \tag{15}$$

式中，$\Sigma P_{220\mathrm{NGM}}$、$\Sigma P_{220\mathrm{NPGD}}$分别为220 kV新能源装机规划容量、新能源装机规划最大允许容量。

3) 消纳新能源能力

电网统调最大用电负荷时刻消纳新能源裕度D_{31}反映在最大用电负荷时刻负荷消纳新能源的能力。

$$D_{31}=\left(1-\frac{\Sigma P_{\mathrm{NGD.MAX}}}{\Sigma P_{\mathrm{L.MAX}}}\right)\times 100\% \tag{16}$$

式中，$\Sigma P_{\mathrm{NGD.MAX}}$、$\Sigma P_{\mathrm{L.MAX}}$分别为统调最大用电负荷时刻新能源出力及负荷之和。

电网统调最小用电负荷时刻消纳新能源裕度D_{32}反映在最小用电负荷时刻负荷消纳新能源的能力。

$$D_{32}=\left(1-\frac{\Sigma P_{\mathrm{NGD.MIN}}}{\Sigma P_{\mathrm{L.MIN}}}\right)\times 100\% \tag{17}$$

式中，$\Sigma P_{\mathrm{NGD.MIN}}$、$\Sigma P_{\mathrm{L.MIN}}$分别为统调最小用电负荷时刻新能源出力、负荷之和。

弃风/光率指由于电网接纳能力不足、风/光电场建设工期不匹配和风/光电不稳定等导致的风机/

光伏停止发电的现象。以弃风率 D_{33} 为例，如式(18)所示。

$$D_{33}=\frac{\Sigma P_{\mathrm{AWP}}}{\Sigma P_{\mathrm{AWPG}}+\Sigma P_{\mathrm{AWP}}}\times 100\% \tag{18}$$

式中，ΣP_{AWP}、ΣP_{AWPG} 分别为弃风电量、风电实际发电量。

3 基于 AHP-CRITIC 法组合赋权

主观赋权常采用 AHP 法，该方法能够结合专家经验对指标重要性进行判断，首先建立初始判断矩阵，求取判断矩阵的最大特征值，然后进行一致性判断，得到主观权重向量 $\boldsymbol{\alpha}$。

为克服主观赋权的随意性，采用 CRITIC 法进行客观赋权，通过计算指标的标准差和相关系数充分挖掘大规模新能源并网时电网性能指标的差异性和冲突性。假设有 m 个方案，每个方案有 n 个指标，则评价矩阵为

$$\boldsymbol{X}=\begin{bmatrix} x_{11} & x_{12} & \cdots & x_{1n} \\ x_{21} & x_{22} & \cdots & x_{2n} \\ \vdots & \vdots & & \vdots \\ x_{m1} & x_{m2} & \cdots & x_{mn} \end{bmatrix} \tag{19}$$

为消除量纲对评价结果的影响，对各个指标进行无量纲处理，形成无量纲的标准矩阵 $\boldsymbol{X}''$，使所有数据能用统一的标准去衡量。

对于正向指标，标准化后的对应元素如式(20)所示。

$$x_{ij}^{1'}=\frac{x_{ij}^{1}-\min(\boldsymbol{x}_j^{1})}{\max(\boldsymbol{x}_j^{1})-\min(\boldsymbol{x}_j^{1})} \tag{20}$$

式中：$\boldsymbol{x}_j^{1}$ 表示正向指标列向量；x_{ij}^{1} 表示正向指标列向量 $\boldsymbol{x}_j^{1}$ 中的各元素；$x_{ij}^{1'}$ 表示标准化后的正向指标。

对于逆向指标标准化后的对应元素如式(21)所示。

$$x_{ij}^{2'}=\frac{\max(\boldsymbol{x}_j^{2})-x_{ij}^{2}}{\max(\boldsymbol{x}_j^{2})-\min(\boldsymbol{x}_j^{2})} \tag{21}$$

式中：$\boldsymbol{x}_j^{2}$ 表示逆向指标列向量；x_{ij}^{2} 表示逆向指标列向量 $\boldsymbol{x}_j^{2}$ 中的各元素；$x_{ij}^{2'}$ 表示标准化后的逆向指标。

第 i 个指标的变异性 σ_i 如式(22)所示。

$$\sigma_i=\sqrt{\frac{1}{m}\sum_{j=1}^{m}(x_{ij}''-\overline{x_i''})^2} \tag{22}$$

式中：x_{ij}'' 表示标准矩阵 $\boldsymbol{X}''$ 第 i 行、第 j 列元素；$\overline{x''}_i$ 表示第 i 个指标的均值。

指标的冲突性 ρ_{ij} 为如式(23)所示。

$$\rho_{ij}=\mathrm{cov}(\boldsymbol{X}_i'',\boldsymbol{X}_j'')/(\sigma_i\sigma_j) \tag{23}$$

式中，$\mathrm{cov}(\boldsymbol{X}_i'',\boldsymbol{X}_j'')$ 表示标准矩阵 $\boldsymbol{X}''$ 第 i 行和第 j 行的协方差。

根据 CRITIC 方法计算每个指标所包含的信息 G_i，如式(24)所示。

$$G_i=\sigma_i\sum_{j=1}^{n}(1-\rho_{ij}) \tag{24}$$

客观权重 β_i 计算公式如式(25)所示。

$$\beta_i=\frac{G_i}{\sum_{j=1}^{n}G_i} \tag{25}$$

由主观权重向量 $\boldsymbol{\alpha}$ 和客观权重向量 $\boldsymbol{\beta}$ 可得到综合权重向量 $\boldsymbol{H}$，如式(26)所示。

$$\boldsymbol{H}=k\boldsymbol{\alpha}+(1-k)\boldsymbol{\beta} \tag{26}$$

式中，k 为偏好系数，取值区间为[0,1]，一般取 0.5。

4 应用实例

4.1 自然资源和电网基本情况

以中部某城市为例，该城市太阳能资源丰富，年日照时间达 1200~2400 h，是太阳能资源一类地区，适宜开发光伏发电；境内 600 m 以上高山 17 座，平均风速高于 5.5 m/s。同时，具有可利用荒山荒坡 2.34 万亩、屋顶 22 万 m^2。

截至2022年底，该城市新能源累计投资74亿元，装机达 117.46 万 kW，其中，风电装机 63.6 万 kW，光伏装机 52.6 万 kW，年发电能力近 15 亿 kWh。该城市电网有 220 kV 变电站 2 座，4 台主变总容量为 54 万 kVA；110 kV 变电站 6 座，9 台主变总容量为 38.45 万 kVA；110 kV 架空线路 16 条，总长度为 218.34 km；35 kV 变电站 11 座，19 台主变总容量为 13.53 万 kVA；35 kV 架空线路 23 条，总长度为 309.41 km；10 kV 变压器 2783 台，总容量为 46.98 万 kVA；10 kV 架空线路 112 条，总长度为 2158.36 km。

4.2 指标体系与评价方法

本文所建立的三级指标体系及不同权重设定方法对比如表 1 所示，一级、二级指标及相关计算结果如表 2 所示，与传统指标体系与评价方法相比，有以下特征。

1) 在指标体系方面，传统的评估体系一般侧重于新能源接入时对电网消纳能力、安全风险、电能质量等某一方面的评价[21-22]。以风光为代表的大规模新能源并网，改变了传统电力系统的结构和运行方式，传统的指标体系不再适用。本文所建立的电网性能指标体系以电网安全稳定运行和大规模新

能源消纳为前提，以合理调配资源、优化协同控制为目标，从接入水平、协调水平、适应水平和承载水平 4 个维度分层级、分电压等级评估“源网荷储”适配性，是传统评价指标体系所无法得出的，因此，本文所建立的评价指标体系更加全面、合理。

表 1 三级指标的相关计算数据

Table 1 Related calculation data of the third-level indicators

三级指标	指标值	指标评分	主观权重	客观权重		指标得分	
			(AHP 法)	CRITIC 法	熵权法	AHP-CRITIC 法	AHP-熵权法
新能源渗透率 A_{11}	21.82	81.81	0.057	0.019	0.019	3.10	3.11
新能源接入率 A_{12}	42.53	52.41	0.057	0.019	0.020	1.98	2.00
集中式新能源装机可调度占比 B_{11}	61.50	80.75	0.066	0.020	0.024	3.47	3.63
分布式新能源装机可调度占比 B_{12}	15.21	100	0.028	0.019	0.020	2.36	2.40
储能占新能源装机比例 B_{21}	10.49	61.96	0.050	0.019	0.019	2.13	2.14
新能源出力与年负荷曲线匹配度 B_{31}	50.34	60.45	0.015	0.019	0.020	1.02	1.04
新能源出力与典型日负荷曲线匹配度 B_{32}	73.21	90.95	0.015	0.020	0.024	1.59	1.76
220 kV 电网 $N-1$ 通过率 C_{11}	92.94	71.76	0.014	0.027	0.019	1.48	1.19
110 kV 电网 $N-1$ 通过率 C_{12}	86.09	92.17	0.008	0.024	0.042	1.44	2.29
35 kV 电网 $N-1$ 通过率 C_{13}	71.32	82.65	0.005	0.019	0.019	0.98	0.99
10 kV 线路 $N-1$ 通过率 C_{14}	64.92	79.89	0.004	0.019	0.019	0.90	0.92
220 kV 重载设备占比(变压器+线路)C_{21}	19.05	80.95	0.018	0.019	0.019	1.47	1.49
110 kV 重载设备占比(变压器+线路)C_{22}	12.17	71.3	0.010	0.028	0.018	1.34	0.97
35 kV 重载设备占比(变压器+线路)C_{23}	14.71	61.18	0.006	0.027	0.021	1.03	0.84
10 kV 重载设备占比(变压器+线路)C_{24}	5.14	84.31	0.004	0.027	0.019	1.33	1.00
220 kV 母线短路电流超过遮断容量 80%占比 C_{31}	1.23	75.4	0.030	0.027	0.019	2.14	1.85
110 kV 母线短路电流超过遮断容量 80%占比 C_{32}	0.00	100	0.016	0.029	0.018	2.26	1.68
35 kV 母线短路电流超过遮断容量 80%占比 C_{33}	0.00	100	0.011	0.029	0.018	1.99	1.41
10 kV 母线短路电流超过遮断容量 80%占比 C_{34}	1.78	64.4	0.008	0.028	0.025	1.16	1.04
220 kV 母线电压越限占比 C_{41}	2.18	70.93	0.022	0.030	0.018	1.83	1.41
110 kV 母线电压越限占比 C_{42}	1.21	83.87	0.012	0.030	0.018	1.74	1.24
35 kV 母线电压越限占比 C_{43}	1.43	80.93	0.008	0.023	0.048	1.27	2.24
10 kV 母线电压越限占比 C_{44}	2.88	61.6	0.006	0.023	0.048	0.90	1.64
220 kV 母线谐波电流越限占比 C_{51}	0.00	100	0.014	0.029	0.018	2.13	1.55
110 kV 母线谐波电流越限占比 C_{52}	0.69	90.8	0.007	0.027	0.019	1.56	1.19
35 kV 母线谐波电流越限占比 C_{53}	1.83	75.6	0.005	0.019	0.020	0.90	0.94
10 kV 母线谐波电流越限占比 C_{54}	2.56	65.87	0.003	0.019	0.019	0.73	0.74
220 kV 线路满足新能源接入保护配置条件占比 C_{61}	100	100	0.039	0.024	0.048	3.13	4.31
110 kV 线路满足新能源接入保护配置条件占比 C_{62}	90.34	90.34	0.021	0.019	0.020	1.80	1.86
35 kV 线路满足新能源接入保护配置条件占比 C_{63}	70.23	70.23	0.014	0.019	0.019	1.14	1.13
10 kV 线路满足新能源接入保护配置条件占比 C_{64}	40.84	60.56	0.010	0.019	0.019	0.87	0.88
220 kV 及以下新能源接入裕度 D_{11}	66.24	86.24	0.098	0.029	0.028	5.47	5.41
110 kV 及以下新能源接入裕度 D_{12}	95.86	97.93	0.053	0.023	0.042	3.72	4.65
35 kV 及以下新能源接入裕度 D_{13}	92.46	100	0.035	0.022	0.030	2.85	3.21
10 kV 及以下新能源接入裕度 D_{14}	92.45	100	0.025	0.023	0.020	2.37	2.27
220 kV 及以下新能源规划目标可承载度 D_{21}	83.77	83.77	0.059	0.020	0.018	3.27	3.19
110 kV 及以下新能源规划目标可承载度 D_{22}	47.66	47.66	0.032	0.020	0.025	1.24	1.35
35 kV 及以下新能源规划目标可承载度 D_{23}	67.00	67	0.021	0.019	0.018	1.33	1.31
10 kV 及以下新能源规划目标可承载度 D_{24}	81.56	90.78	0.015	0.019	0.020	1.54	1.59
电网统调最大用电负荷时刻消纳新能源能力 D_{31}	74.26	42.77	0.021	0.027	0.018	1.03	0.84
电网统调最小用电负荷时刻消纳新能源能力 D_{32}	−32.92	0	0.055	0.022	0.033	0.00	0.00
弃风率 D_{33}	0.00	100	0.004	0.029	0.018	1.67	1.09
弃光率 D_{34}	0.00	100	0.004	0.029	0.018	1.67	1.09

表 2 一级和二级指标的相关计算数据

Table 2 Related calculation data of the first-level and second-level indicators

一级指标	二级指标	指标权重		指标得分	
		一级	二级	一级	二级
接入水平 A	新能源接入水平 A_1	0.075	0.075	5.08	5.08
协调水平 B	新能源装机可控性 B_1	0.134	0.066	10.57	5.83
	源储协调性 B_2		0.034		2.13
	新能源出力与负荷协调度 B_3		0.034		2.61
适应水平 C	电网安全 C_1	0.438	0.059	35.52	4.80
	负载情况 C_2		0.070		5.17
	短路电流 C_3		0.091		7.55
	电压质量 C_4		0.077		5.74
	谐波电流 C_5		0.060		5.32
	继电保护 C_6		0.081		6.94
承载水平 D	新能源接入裕度 D_1	0.353	0.155	26.16	14.41
	新能源规划目标可承载度 D_2		0.101		7.38
	消纳新能源能力 D_3		0.097		4.37

2) 在权重设置方面，传统评价模型的客观权重设定方法一般是熵权法[23-24]，该方法的基本思路是根据指标所含信息有序程度的差异性来确定指标权重，其本身无法处理强相关性的指标，也不能考虑指标间的互动关系，因此不能充分体现指标的实际重要性。而 CRITIC 法不仅考虑了指标变异大小影响，而且考虑了指标间的冲突性；指标变异性以标准差体现，标准差越大，方案间的取值差距越大；指标冲突性以皮尔逊相关系数为基础，若两个指标有较强的正相关，两个指标冲突性较低，权重也越小。

如图 2 所示，以三级指标 A_{11} 和 C_{51} 为例，当新能源渗透率不高时，220 kV 母线谐波电流越限占比不受其影响；当渗透率达到一定水平时，220 kV 母线谐波电流越限占比将随之升高。当两者不相关时(相关系数为 0)，采用 CRITIC 法得到两个指标的客观权重分别为 0.0184 和 0.0271，采用熵权法得到两个指标的客观权重分别为 0.0192 和 0.0176。当两个指标相关系数增大时，采用 CRITIC 法时两个指标客观权重呈下降趋势，而采用熵权法时 C_{51} 指标权重明显升高。一般而言，当两个指标强相关时，应适当降低指标权重甚至去除某一指标。由于大规模新能源并网时作用机理较为复杂，新能源接入率、渗透率与各电压等级电网的重过载、$N-1$ 通过率、电能质量等指标间存在一定的关联性，因此，在设置

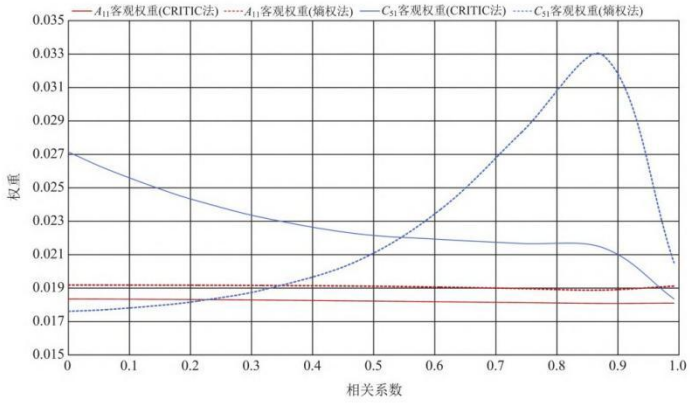

图 2 客观权重设置方法对比

Fig. 2 Comparison of objective weight setting methods

指标权重时需要充分考虑指标间的冲突性和变异性，故 AHP-CRITIC 法是一种更适合的主客观赋权法。

4.3 评价结果和发展重点

如表 2 所示，该城市大规模新能源接入时电网性能水平综合评分为 77.33，准则层的评价结果和发展重点如下。

1) 接入水平 A

接入水平得分 5.08，得分率偏低。主要原因是新能源装机容量偏高、电网统调最小用电负荷时刻消纳新能源能力不足，需要外送，导致三级指标中新能源接入率 A_{12} 评分为 52.41，偏低。若要提高接入水平，选取评分较低的指标并计算灵敏度，如图 3 所示，根据指标灵敏度高低确定发展重点顺序为：新能源渗透率 $A_{11}(0.0031)$ ＞新能源接入率 $A_{12}(0.0007)$，即优先考虑新能源就地消纳，提高新能源渗透率水平。

2) 协调水平 B

协调水平得分 10.57，二级指标中源储协调性 B_2、新能源出力与负荷协调度 B_3 得分分别为 2.13 和 2.61，得分率不高。三级指标中，储能占新能源装机比例 B_{21}、新能源出力与年负荷曲线匹配度 B_{31} 得分偏低。若要提高协调水平，根据灵敏度确定发展重点顺序为：新能源出力与年负荷曲线匹配度 $B_{31}(0.008)$ ＞储能占新能源装机比例 $B_{21}(0.003)$。即可通过增加可控负荷、提升储能配置等方式，改善负荷和新能源的出力曲线，增加源荷全年出力的匹配度。

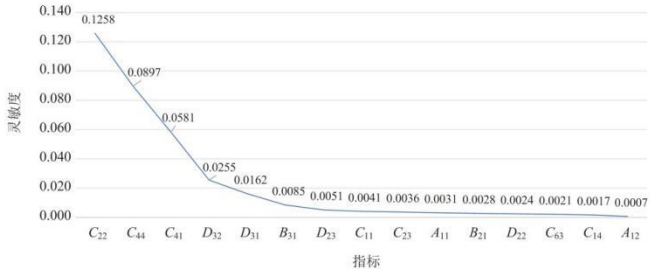

图 3 指标灵敏度排序

Fig. 3 Sensitivity ranking of indicators

3) 适应水平 C

适应水平得分 35.52，得分率较高。二级指标中负载情况 C_2、电压质量 C_4 得分别为 5.17、5.74，得分率不高。主要原因春腰、秋腰时刻，新能源大发、用电负荷较小，电能需要外送，导致 35~220 kV 线路和主变重过载情况较多，负载率得分较低；加上新能源发电具有波动性和间歇性，导致电网电压越限情况较多。根据灵敏度确定发展重点顺序为：110 kV 重载设备占比 $C_{22}(0.1258)$ ＞10 kV 母线电压越限占比 $C_{44}(0.0897)$ ＞220 kV 母线电压越限占比 $C_{41}(0.0581)$ ＞220 kV 电网 $N-1$ 通过率 $C_{11}(0.0041)$ ＞35 kV 重载设备占比 $C_{23}(0.0036)$ ＞35 kV 线路满足新能源接入保护配置条件占比 $C_{63}(0.0021)$ ＞10 kV 线路 N-1 通过率 $C_{14}(0.0017)$。即可通过合理分配负荷、优化 35~220 kV 网架结构、加强 10 kV 电网转供能力建设、提高 10 kV 和 220 kV 无功补偿等措施，提高电网对大规模新能源接入时的适应性。

4) 承载水平 D

承载水平得分 26.16，二级指标中消纳新能源能力 D_3、新能源规划目标可承载度 D_2 得分分别为 4.37、7.38，得分率不高。由于该城市风能、太阳能发电站较多，本地消纳有限，且未来 35~110 kV 电网对大规模新能源承载能力有限，根据灵敏度确定发展重点顺序为：电网统调最小用电负荷时刻消纳新能源能力 $D_{32}(0.0255)$ ＞电网统调最大用电负荷时刻消纳新能源能力 $D_{31}(0.0162)$ ＞35 kV 及以下新能源规划目标可承载度 $D_{23}(0.0051)$ ＞110 kV 及以下新能源规划目标可承载度 $D_{22}(0.0024)$。

5 结论

本文构建了大规模新能源接入的电网性能评价指标体系，通过实际电网验证，该指标体系具有较强的实用性和有效性，通过研究得到如下结论。

1) 大规模新能源接入电网的评价指标体系不仅考虑了新能源随机性和波动性对电网电能质量、安全稳定的影响，而且还考虑了新能源承载能力以及储能的积极作用，贯穿了源网荷储各个环节，能够更真实、全面地对电网消纳新能源能力进行评价。

2) 由于当前处于新型电力系统发展阶段，大规

模新能源以及储能、电动汽车充电桩等多元负荷接入电网时，作用机理较为复杂，电网安全、重过载、承载力等电网性能方面指标间存在冲突性和变异性，采用 AHP-CRITIC 法不仅能够兼顾专家经验，而且能够充分利用电网发展数据自身的客观属性，使各项指标权重取值更加合理。同时还能够根据资源禀赋不同改变指标的相对重要性，促进电网差异化发展。

3) 在大规模新能源接入时，电网性能评价是一个属性多样、关系复杂的决策问题，需要立足电网已接入新能源情况，对源网负荷/出力特性匹配程度、大规模新能源并网影响以及电网对新能源承载能力进行全面评估，利用电网规划、发展、运行等多源数据，显性表达各个指标的统计或计算方式，保证评价体系的实操性和评价结果的真实性。

参考文献

[1] 习近平. 中央财经委员会第九次会议[EB/OL]. [2021-03-25]. http://www.gov.cn/xinwen/2021-03/15/content_5593154.htm.
XI Jinping. The ninth meeting of the central financial leading group[EB/OL]. [2021-03-25]. http://www.gov.cn/xinwen/2021-03/15/content_5593154.htm.

[2] 周孝信, 陈树勇, 鲁宗相, 等. 能源转型中我国新一代电力系统的技术特征[J]. 中国电机工程学报, 2018, 38(7): 1893-1904.
ZHOU Xiaoxin, CHEN Shuyong, LU Zongxiang, et al. Technology features of the new generation power system in China[J]. Proceedings of the CSEE, 2018, 38(7): 1893-1904.

[3] 刘沅昆, 张维静, 张艳, 等. 面向新型电力系统的新能源与储能联合规划方法[J]. 智慧电力, 2022, 50(10): 1-8.
LIU Yuankun, ZHANG Weijing, ZHANG Yan, et al. Joint planning method of renewable energy and energy storage for new-type power system[J]. Smart Power, 2022, 50(10): 1-8.

[4] 郝文斌, 孟志高, 张勇, 等. 新型电力系统下多分布式电源接入配电网承载力评估方法研究[J]. 电力系统保护与控制, 2023, 51(14): 23-33.
HAO Wenbin, MENG Zhigao, ZHANG Yong, et al. Carrying capacity evaluation of multiple distributed power supply access to the distribution network with the background of a new power system[J]. Power System Protection and Control, 2023, 51(14): 23-33.

[5] 黎博, 陈民铀, 钟海旺, 等. 高比例可再生能源新型电力系统长期规划综述[J]. 中国电机工程学报, 2023, 43(2): 555-581.
LI Bo, CHEN Minyou, ZHONG Haiwang, et al. A review of long-term planning of new power systems with large share of renewable energy[J]. Proceedings of the CSEE, 2023, 43(2): 555-581.

[6] 郭剑波. 新型电力系统面临的挑战以及有关机制思考[J]. 中国电力企业管理, 2021(25): 8-11.
GUO Jianbo. Thinking about challenges and mechanisms faced by new power system[J]. China Power Enterprise Management, 2021(25): 8-11.

[7] 谢小荣, 贺静波, 毛航银, 等. “双高”电力系统稳定性的新问题及分类探讨[J]. 中国电机工程学报, 2021, 41(2): 461-475.
XIE Xiaorong, HE Jingbo, MAO Hangyin, et al. New issues and classification of power system stability with high shares of renewables and power electronics[J]. Proceedings of the CSEE, 2021, 41(2): 461-475.

[8] 张立辉, 戴谷禹, 聂青云, 等. 碳交易机制下计及用电行为的虚拟电厂经济调度模型[J]. 电力系统保护与控制, 2020, 48(24): 154-163.
ZHANG Lihui, DAI Guyu, NIE Qingyun, et al. Economic dispatch model of virtual power plant considering electricity consumption under a carbon trading mechanism[J]. Power System Protection and Control, 2020, 48(24): 154-163.

[9] SALVIA M, RECKIEN D, PIETRAPERTOSA F, et al. Will climate mitigation ambitions lead to carbon neutrality? An analysis of the local-level plans of 327 cities in the EU[J]. Renewable and Sustainable Energy Reviews, 2021, 135: 110253.

[10] 何璇, 高崇, 曹华珍, 等. 基于改进层次分析法的配电网指标评估[J]. 电测与仪表, 2022, 59(10): 93-99.
HE Xuan, GAO Chong, CAO Huazhen, et al. Index evaluation of distribution network based on improved analytic hierarchy process[J]. Electrical Measurement & Instrumentation, 2022, 59(10): 93-99.

[11] 白帆, 陈红坤, 陈磊, 等. 基于确定型评价指标的电力系统调度灵活性研究[J]. 电力系统保护与控制, 2020, 48(10): 52-60.
BAI Fan, CHEN Hongkun, CHEN Lei, et al. Research on dispatching flexibility of power system based on deterministic evaluation index[J]. Power System Protection and Control, 2020, 48(10): 52-60.

[12] 施贵荣, 孙荣富, 丁华杰, 等. 大规模风电并网的评估指标体系构建与应用[J]. 电网技术, 2021, 45(3): 841-848.
SHI Guirong, SUN Rongfu, DING Huajie, et al. Construction and application on evaluation index system of large-scale wind power integration[J]. Power System Technology, 2021, 45(3): 841-848.

[13] 杜明坤, 黄媛, 刘俊勇, 等. 考虑梯级电站开发规划接入的电网适应性综合评估[J]. 电力系统及其自动化学

报, 2021, 33(9): 1-8.
DU Mingkun, HUANG Yuan, LIU Junyong, et al. Comprehensive evaluation on grid adaptability considering the access of cascaded power stations under planning and development[J]. Proceedings of the CSU-EPSA, 2021, 33(9): 1-8.

[14] 王晓彬, 孟婧, 石访, 等. 煤电与清洁电源协同演进优化模型及综合评价体系研究[J]. 电力系统保护与控制, 2022, 50(13): 43-52.
WANG Xiaobin, MENG Jing, SHI Fang, et al. An optimization model and comprehensive evaluation system for the synergistic evolution of coal-fired power plants and clean power sources[J]. Power System Protection and Control, 2022, 50(13): 43-52.

[15] 刘洪, 赵越, 刘晓鸥, 等. 计及能源品位差异的园区多能源系统综合能效评估[J]. 电网技术, 2019, 43(8): 2835-2843.
LIU Hong, ZHAO Yue, LIU Xiaoou, et al. Comprehensive energy efficiency assessment of park-level multi-energy system considering difference of energy grade[J]. Power System Technology, 2019, 43(8): 2835-2843.

[16] 吴涵, 孙力文, 项晟, 等. 计及可再生能源与负荷高维时序相关性的主动配电网扩展规划[J]. 电力系统自动化, 2022, 46(16): 40-51.
WU Han, SUN Liwen, XIANG Sheng, et al. Expansion planning of active distribution network considering high-dimensional temporal correlation between renewable energy and load[J]. Automation of Electric Power Systems, 2022, 46(16): 40-51.

[17] 杨楠, 董邦天, 黄禹, 等. 考虑不确定性和多主体博弈的增量配电网源网荷协同规划方法[J]. 中国电机工程学报, 2019, 39(9): 2689-2701.
YANG Nan, DONG Bangtian, HUANG Yu, et al. Incremental distribution network source-load collaborative planning method considering uncertainty and multi-agent game[J]. Proceedings of the CSEE, 2019, 39(9): 2689-2701.

[18] 唐巍, 张志刚, 张璐, 等. 考虑微能网聚合整形和资产利用率提升的配电网规划[J]. 电力系统自动化, 2023, 47(8): 89-98.
TANG Wei, ZHANG Zhigang, ZHANG Lu, et al. Distribution network planning considering aggregated shaping for micro-energy grids and improvement of asset utilization rate[J]. Automation of Electric Power Systems, 2023, 47(8): 89-98.

[19] 张天翼, 王海风. 风电并入弱交流系统引发次同步振荡的研究方法综述[J]. 电力系统保护与控制, 2021, 49(16): 177-187.
ZHANG Tianyi, WANG Haifeng. Research methods for subsynchronous oscillation induced by wind power under weak AC system: a review[J]. Power System Protection and Control, 2021, 49(16): 177-187.

[20] 梁琛, 王维洲, 马喜平, 等. 基于随机潮流的高比例新能源接入配电网的极限线损分析[J]. 智慧电力, 2022, 50(12): 34-40, 78.
LIANG Chen, WANG Weizhou, MA Xiping, et al. Analysis on limit line loss in high proportion of renewable energy distribution network based on stochastic power flow[J]. Smart Power, 2022, 50(12): 34-40, 78.

[21] 杜丹, 新能源发电与电网协调发展综合评价研究[D]. 北京: 华北电力大学, 2022.
DU Dan. Research on comprehensive assessment of coordinated development between new energy generation and power grid[D]. Beijing: North China Electric Power University, 2022.

[22] 颜湘武, 梁白雪, 贾焦心, 等. 高渗透率光伏并网对系统暂态频率稳定性影响的量化评估[J]. 可再生能源, 2022, 40(9): 1232-1240.
YAN Xiangwu, LIANG Baixue, JIA Jiaoxin, et al. Quantitative evaluation of transient frequency stability of high permeability photovoltaic grid connected system[J]. Renewable Energy Sources, 2022, 40(9): 1232-1240.

[23] 戴国华, 戴睿, 张琪瑞, 等. 基于主客观赋权相结合的省级电网发展诊断分析方法与实证研究[J]. 电力系统保护与控制, 2022, 50(2): 110-118.
DAI Guohua, DAI Rui, ZHANG Qirui, et al. Empirical study and analysis of provincial power grid development diagnosis based on the combination of a subjective and objective weighting method[J]. Power System Protection and Control, 2022, 50(2): 110-118.

[24] 田春筝, 殷奕恒, 关朝杰, 等. 基于供电分区的中高压配电网综合评价策略[J]. 电力系统保护与控制, 2018, 46(21): 152-159.
TIAN Chunzheng, YIN Yiheng, GUAN Chaojie, et al. Comprehensive evaluation strategy of medium and high voltage distribution network based on power supply division[J]. Power System Protection and Control, 2018, 46(21): 152-159.

收稿日期：2023-09-21；　**修回日期：**2023-12-15

作者简介：

李　响(1979—)，男，硕士，副教授，主要研究方向为新能源发电与并网技术、配电网规划。E-mail: nomad0729@163.com

(编辑　周金梅)

报告编号：**L24N2024-1561**

检　索　报　告

一、检索要求

1. 委 托 人：李响(Li, Xiang)
2. 委托单位：郑州航空工业管理学院
3. 检索目的：论文被 EI 收录情况

二、检索范围

Engineering Village (Database: Compendex)	1969-present	网络版

三、检索结果

委托人提供的**1**篇论文被EI收录，论文收录情况见附件一。

特此证明！

检索报告人：　曹宇

东北师范大学科技查新咨询中心

教育部科技查新工作站(L24)

2024 年 8 月 22 日

附件一： EI收录情况

第 1 条，共 1 条

Accession number:20243316867300
Title:Performance evaluation index system of a power grid considering large-scale new energy
Title of translation:考虑大规模新能源接入的电网性能评价指标体系
Authors:Li, Xiang (1); Wu, Haichao (2); Wang, Wenxue (2); An, Quan (2)
Author affiliation:(1) Zhengzhou Institute of Aeronautical Industry Management, Zhengzhou; 450015, China; (2) Henan Juyan Electric Power Technology Co., Ltd., Zhengzhou; 450000, China
Source title:Dianli Xitong Baohu yu Kongzhi/Power System Protection and Control
Abbreviated source title:Dianli Xitong Baohu yu Kongzhi
Volume:52
Issue:15
Issue date:August 1, 2024
Publication year:2024
Pages:178-187
Language:Chinese
ISSN:16743415
Document type:Journal article (JA)
Publisher:Power System Protection and Control Press
Abstract: There are deficiencies in evaluating the complex mechanism of the mutual effects between large-scale new energy and the power grid by traditional power grid evaluation systems. Thus a performance evaluation index system is established considering large-scale new energy access. First, based on the key characteristics of the new power system and considering all parts of "power supply, grid, load and energy storage", a power grid performance evaluation index containing connection, coordination, adaptation and carrying capacity levels can be set up. In addition, it explicitly expresses the statistical or calculation method for each index. Secondly, the AHP-CRITIC method is used to enable subjective and objective weights, and investigate the conflict and changeability among different indices based on the objective property of data from the power grid and computing standard deviation/Pearson correlation coefficient to highlight the scientific features on setting index weights. Finally, the index system for the data from new energy and the power grid in one city is surveyed and computed. The effectiveness of the proposed index system and evaluation method is shown through comparison and analysis. Some development proposals for weak parts of the power grid are proposed on the basis of the indicator's sensitivity.
Number of references:24
Main heading:Digital storage
Controlled terms:Correlation methods - Electric power system protection
Uncontrolled terms:Complex mechanisms - Indices systems - Large-scales - New energies - New power system - Pearson correlation coefficients - Performance evaluation index systems - Power - Power grids - Weight
Classification code:706.1 Electric Power Systems - 722.1 Data Storage, Equipment and Techniques - 922.2 Mathematical Statistics
DOI:10.19783/j.cnki.pspc.231246
Funding details: Number: 222102240117, Acronym: -, Sponsor: Special Fund Project for Science and Technology Innovation Strategy of Guangdong Province;
Funding text:LI Xiang1, WU Haichao2, WANG Wenxue2, AN Quan2 (1. Zhengzhou Institute of Aeronautical Industry Management, Zhengzhou 450015, China; 2. Henan Juyan Electric Power Technology Co., Ltd., Zhengzhou 450000, China) Abstract: There are deficiencies in evaluating the complex mechanism of the mutual effects between large-scale new energy and the power grid by traditional power grid evaluation systems. Thus a performance evaluation index system is established considering large-scale new energy access. First, based on the key characteristics of the new power system and considering all parts of \u201Cpower supply, grid, load and energy storage\u201D, a power grid performance evaluation index containing connection, coordination, adaptation and carrying capacity levels can be set up. In addition, it explicitly expresses the statistical or calculation method for each index. Secondly, the AHP-CRITIC method is used to enable subjective and objective weights, and investigate the conflict and changeability among different indices based on the objective property of data from the power grid and computing standard deviation/Pearson correlation coefficient to highlight the scientific features on setting index weights. Finally, the index system for the data from new energy and the power grid in one city is surveyed and computed. The effectiveness of the proposed index system and evaluation method is shown through comparison and analysis. Some development proposals for weak parts of the power grid are proposed on the basis of the indicator\u2019s sensitivity. This work is supported by the Science and Technology Project of Henan Province (No. 222102240117). Key words: new energy; new power system; index system; Pearson correlation coefficient; weight

Database:Compendex

—The End—

9.基于电力大数据和供电网格的电网发展评价方法

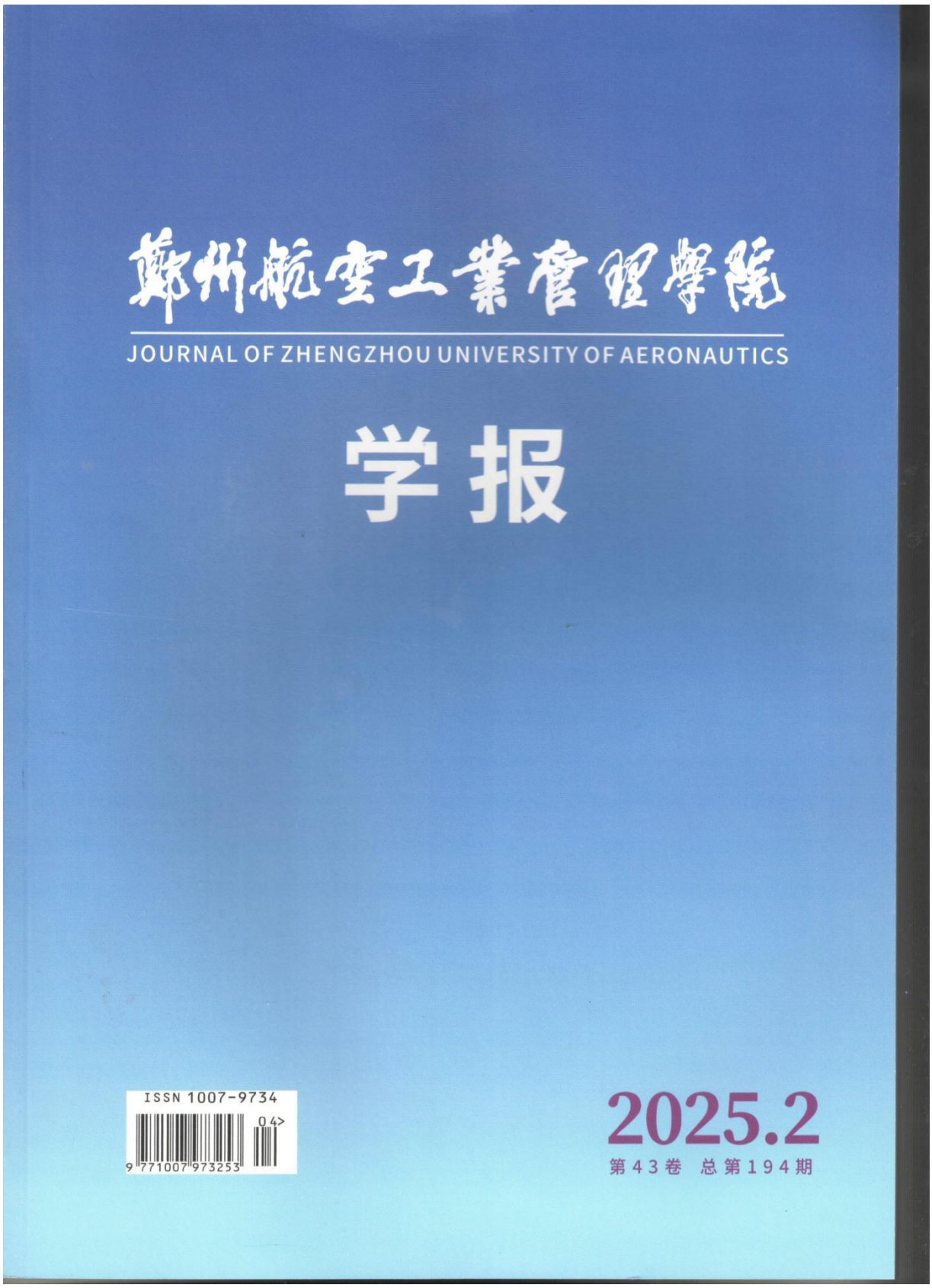

本期执行编辑:裴媛慧 英文编校:庄文辉

DOI:10.19327/j.cnki.zuaxb.1007-9734.2025.02.010

基于电力大数据和供电网格的电网发展评价方法

李 响[1],胡天彤[1],陈 卓[2],李秋燕[3],郭寅远[2],张 丹[1],华红艳[1]

(1.郑州航空工业管理学院,河南 郑州 450046;
2.许昌开普检测研究院股份有限公司,河南 许昌 461000;
3.国网河南省电力有限公司 经济技术研究院,河南 郑州 450000)

摘 要:为明确电网发展方向,提出一种基于电力大数据平台和供电网格的电网发展评价方法。首先,依据新型电力系统基本特征,从清洁低碳、安全可控、灵活高效、智能友好、开放互动五个维度构建指标体系;其次,融合电力大数据平台,挖掘海量数据信息,采用熵权法设置指标权重;然后,考虑变电站供区、电网结构、行政划分等因素,将电网划分为若干供电网格,逐级对电网进行精益化评估;最后,某城市配电网应用结果表明,该评价模型具有操作简单、评价合理、便于决策等优点。

关键词:电力大数据;供电网格;电网发展评价;指标体系;熵权法

中图分类号:TM73; TP311.13 **文献标识码**:A **文章编号**:1007-9734(2025)02-0077-08

0 引 言

构建以新能源为主的新型电力系统是我国电力系统发展的目标和必由之路[1-3]。电网作为电力系统中枢,承担着能源交互、用电安全、平稳运行的责任[4-6]。打造技术先进、安全可靠、绿色高效的世界一流电网,是我国电网的发展目标。开展电网发展评估能够发现电网薄弱环节和存在问题,有利于促进电网科学发展,提升电网管理水平和投资决策水平[7-8]。同时,电网数字化、信息化水平的不断提高[9-10],电力大数据呈快速增长态势,也更有利于电网发展评估工作的数据采集和信息挖掘[11]。

文献[12]在分析了未来电力系统发展重点和内涵特征的基础上,对我国电力系统在电力需求、电源电力流、电网发展、电力新技术重点攻关方向进行了研判,并对电力发展路径进行了中长期展望。文献[13-14]从电网性能不同角度建立了省级电网发展评价指标体系和评分函数,以便评价、识别省级电网的运行状态和薄弱环节,解决了省级电网发展评价指标选取和量化问题。文献[15-16]分别研究了物元分析法和模糊层次分析法在电网诊断分析工作的应用,解决了数据挖掘算法在电网发展诊断应用中的问题。文献[17-18]分别建立了电网安全风险评估模型,评估了电网运行安全性和可靠性,解决了电网安全风险及可靠性量化评估问题。文献[19]以配电网为核心,针对用户侧和配网侧提出评价指标,采用网络分析法—反熵权,对区域综合能源系统进行评价,解决了权重计算不准确导致指标之间交叉和相互影响的问题。

上述研究表明,电网发展评估需要以指标信息为基础[20],以数据挖掘为核心[21],以实际应用为导向。目前,有不少研究人员和学者都非常重视电网评价[22-23],为电网发展评价打下了良好的应用和研究基础。但随着电网的数字化、智慧化建设不断推进,跨专业、跨单位、跨层级的电力大数据平台不断贯通,电网的检测、监控数据也日益立体化、全景化,

收稿日期:2024-07-30

基金项目:河南省科技攻关项目(232102240102);河南省高等教育教学改革研究与实践重点项目(2024SJGLX0694);教育部供需对接就业育人项目(2023122891671)

作者简介:李 响,副教授,研究方向为新能源发电与并网技术、新型电力系统发展评估及规划。

电力企业扁平化管理、精益化投资需要电网发展评价多维化、精细化。同时，新能源渗透率不断提升，电动汽车、储能等新型主体不断接入，而现有的评价方法一般注重电网安全、可靠、经济性能评价，针对新能源、储能、电动汽车等新要素评价较少，难以体现新型电力系统源网荷储间的复杂作用机理。因此，电网评价需要更加充分利用和挖掘电力大数据，科学合理地定位电网发展阶段；供电部门需要一套体现新型电力系统特征的系统化、精细化评价方法进行指导。

本文利用电力大数据平台，在划分供电网格的基础上，依据新型电力系统基本特征，从清洁低碳、安全可控、灵活高效、智能友好、开放互动五个维度建立指标体系，充分挖掘指标数据信息，利用熵权法确定指标权重，建立电网发展评价模型。通过应用于某城市电网，验证评价模型的可行性和实用性。

1　电力大数据应用及评估模型架构

随着电网数字化、信息化、智能化建设水平的提高，越来越多的监测设备应用于发电、变电、输电、配电、用电等各个环节，电力数据呈现快速增长态势，电力企业和从业人员越来越重视电力大数据的挖掘与应用。目前，电力大数据广泛应用于电力检修、市场分析、调度等各个方面，电力部门也建立了数据采集及电力调控系统，如数据采集与监视控制系统（Supervisory Control And Data Acquisition，SCADA）、能量管理系统（Energy Management System，EMS）、生产管理系统（Ower Production Management System，PMS）、调度自动化系统、电力营销信息系统、网上电网等。电力大数据平台的数据来源如图1所示。

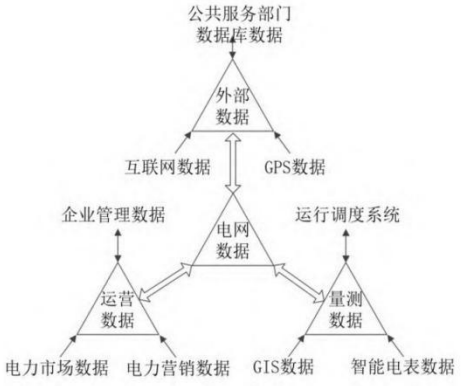

图1　电力大数据平台的数据来源

在电网的供给侧、需求侧以及公共服务的数据融合背景下，发电企业、电网企业以及用户在能源层面实现了一定程度的交互，但电力大数据的海量性、异构性也使大数据的挖掘与应用面临诸多问题。因此，利用SCADA系统、各种数据采集系统以及电网各部门的业务系统，设计和建立统一的融合型电网大数据平台是打破行业间壁垒，充分利用、挖掘电力大数据价值的关键，是实现电网数字化、智慧化的基础。

基于诸多系统的历史与实时数据，充分利用这些海量数据挖掘有效信息，推动形成电力数据驱动的创新模式和发展模式，促进电力运营、服务、管理全面发展，是电力大数据的发展方向。结合电力系统的转型升级、电网高质量发展对电网评价工作带来的挑战，以及电力大数据技术水平现状和应用需求，本文提出的电网发展评价模型结构如图2所示，由数据层、指标层和应用层组成。

图2　电网发展评价模型结构

数据层为评价模型的基础层，也是电网建设、运行的一部分，当前电力部门的智能化发展和信息化建设，结合大数据存储和处理技术，为电力工作者和研究人员提供了丰富的多源异构的数据资源，也为指标层中的各种指标以及评价工作中的数据分析提供了数据支撑。指标层主要结合新型电力系统特

征,从清洁低碳、安全可控、灵活高效、智能友好、开放互动五个维度建立指标体系。应用层根据指标数据,结合不同需求建立对应指标体系,采用电网发展评价模型对电网进行评价,发现电网发展短板,从而确定电网发展方向。

2　电网发展评价指标的构建

新型电力系统是以清洁低碳、安全可控、灵活高效、智能友好、开放互动为基本特征的,而电网是新型电力系统的重要组成部分,也是重要的交互平台,因此,新形势下,电网发展评价也需要围绕这五个基本特征展开(见表1)。

表1　电网发展评价指标体系

一级指标	二级指标	单位
清洁低碳	清洁能源装机容量占比	%
	清洁能源发电量占比	%
	清洁能源弃电量占比	%
	综合线损率	%
安全可控	变压器/线路N-1通过率	%
	高故障线路/变压器占比	%
	新能源可调度容量占比	%
	可控负荷占最高用电负荷比例	%
灵活高效	灵活调节电源容量占比(*)	%
	上调灵活性不足概率(*)	%
	下调灵活性不足概率(*)	%
	轻载变压器/线路占比	%
	重载变压器/线路占比	%
智能友好	智能变电站占比(*)	%
	配电自动化有效覆盖率	%
	智能电表安装率	%
	可预测新能源发电站占比	%
	配置储能的新能源发电站占比	%
开放互动	电能占终端能源消费比例	%
	电动汽车充电站规划目标完成率	%
	电动汽车与电网互动技术(V2G)占比	%

注:标注有*号的指标只适用于高压电网。

电网发展评价指标体系共有21个指标,其中清洁低碳方面共有4个指标,重在评价电源侧和电网侧的清洁低碳水平;安全可控方面共有4个指标,重在评价电网结构情况、设备故障情况、新能源及负荷控制情况等;灵活高效方面共有5个指标,重在评价调度灵活性、设备运行效率效益情况;智能友好方面共有5个指标,重在评价智能变电站技术应用情况、配电自动化有效覆盖情况以及源网荷储协同情况;开放互动方面共有3个指标,重在评价电动汽车等新要素接入情况、电能替代情况。

3　电网发展评价方法

3.1　评价方法

电网发展评价以提高电网性能水平为目标,依

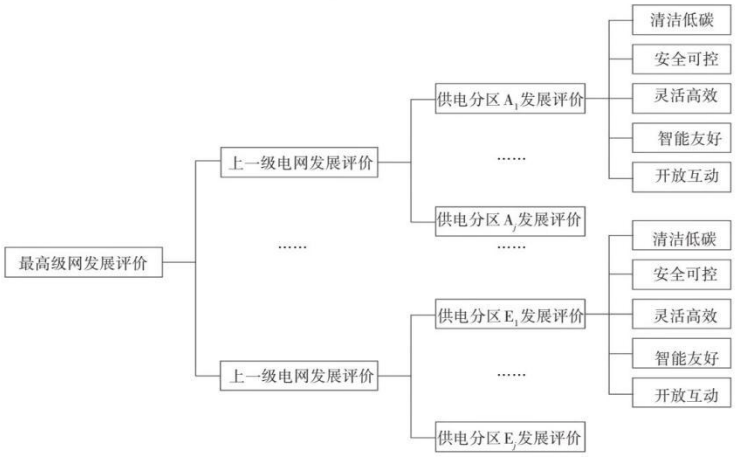

图3　电网发展评价方法

托电力大数据平台，逐级筛选电网发展中存在的问题，精准定位存在问题的设备或范围，绘制供电区域发展水平评估图，优化资源配置，明确投资方向。电网发展评价方法如图3所示。

首先，确定评价电网对象，按照电压等级和行政区域进行分层分区，一个城市电网划分为若干个供电网格电网，供电网格电网又由供电单元组成。供电单元的划分主要由向某一地块或用户供电的一条或者几条10 kV线路组成，在技术层面，供电单元是网架分析、建设方案的最小单元。供电网格的划分主要结合公路、河流等地理条件，考虑变电站供区、电网结构、行政划分等因素，在地理上划分为若干个供电网格，供电网格之间尽量独立或者电气联系不紧密。供电单元划分如图4所示。

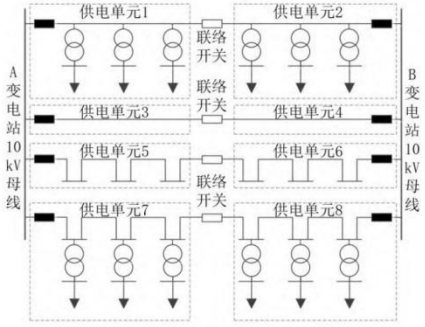

图4　供电单元的划分

然后，依托电力大数据平台，获得供电网格电网基础数据、运行数据，得到电网发展评价的指标参数，根据电网历史数据和实时数据，结合指标建设目标，计算评价指标信息熵，从而确定指标权重。

最后，在计算各个供电网格电网发展评价分数的基础上，逐级对上一级电网进行发展评价，直至最高级电网，从而完成对全区电网发展情况的分层分级评估。需要注意的是，电压等级不同，评价的指标也有所区别，比如，中压配电网一般接入的分布式电源容量小，可不考虑灵活性评价，而高压电网接入的新能源电站容量一般较大，则需要考虑灵活性评价。

3.2 评分函数

评分函数依据国内外先进的电力系统指标水平、导则标准要求值以及区域电网平均水平进行评价。为了避免量纲带来的不统一，各个指标均采用百分比为单位。指标集按照目标值越小越好和越大越好分类，一般采用两种评价函数模型：

适用于目标值越小越好的指标（负向指标），评价函数$u(x)$如公式(1)(2)所示：

$$u(x)=\begin{cases}100 & x\leqslant a_1\\ 100(x-a_2)/(a_1-a_2) & a_1<x<a_2\\ 0 & x\geqslant a_2\end{cases}\tag{1}$$

或为：

$$u(x)=\begin{cases}100 & x\leqslant a_1\\ ax^2+bx+c & a_1<x<a_2\\ 0 & x\geqslant a_2\end{cases}\tag{2}$$

式中，x表示指标值，a_1、a_2分别表示指标区间值下限和上限；a、b、c为常数，由曲线拟合得到。

适用于目标值越大越好的指标（正向指标），评价函数$u(x)$如公式(3)(4)所示：

$$u(x)=\begin{cases}0 & x\leqslant a_1\\ 100(x-a_1)/(a_2-a_1) & a_1<x<a_2\\ 100 & x\geqslant a_2\end{cases}\tag{3}$$

或为：

$$u(x)=\begin{cases}0 & x\leqslant a_1\\ ax^2+bx+c & a_1<x<a_2\\ 100 & x\geqslant a_2\end{cases}\tag{4}$$

3.3 权重取值

熵权法是一种基于信息熵的指标权重确定方法。当一个指标信息熵越大，发生变异的概率越小，那么权重也就越小；相反，当一个指标信息熵越小，发生变异的概率越大，那么权重越大。为了得到该指标的信息熵，可以统计同一地区电网的不同年份值，也可以统计不同地区电网的指标值。假设指标集合有m个指标，通过大数据平台，得到n年历史数据，为了衡量电网指标值与目标值的差距，可采用目标值作为一年数据，组成指标矩阵为：

$$\boldsymbol{X}=\begin{bmatrix}x_{11} & x_{12} & \cdots & x_{1n}\\ x_{21} & x_{22} & \cdots & x_{1n}\\ \vdots & \vdots & & \vdots\\ x_{m1} & x_{m2} & \cdots & x_{mn}\end{bmatrix}\tag{5}$$

为消除量纲的影响，需对指标矩阵进行归一化处理，归一时需分两种情况。

情况1：正向指标归一化

$$Y_{ij}=\frac{X_{ij}-\min(X_i)}{\max(X_i)-\min(X_i)}\tag{6}$$

式中，Y_{ij}表示归一后的指标，X_{ij}表示指标矩阵X的第i行第j列元素，X_i表示指标矩阵X第i行指标各元素。

情况2：负向指标归一化

$$Y_{ij}=\frac{\max(X_i)-X_{ij}}{\max(X_i)-\min(X_i)}\tag{7}$$

归一化考虑目标值的好处是不仅能够反映指标

建设情况权重，而且能够考虑指标当年值与目标差距，因此，能够更加合理设置指标权重。

求取各指标在不同历史年份的比值，也就是对应第i项指标在j个方案中所占比重p_{ij}为：

$$p_{ij}=\frac{Y_{ij}}{\sum_{j=1}^{m}Y_{ij}} \qquad i=1,2\cdots n;\ j=1,2\cdots m \tag{8}$$

各个指标信息熵E_j的公式为：

$$E_j=-\ln(n)^{-1}\sum_{i=1}^{n}p_{ij}\ln p_{ij} \tag{9}$$

通过信息熵得到第j个指标权重w_j为：

$$w_j=\frac{1-E_j}{m-\sum E_j} \qquad j=1,2\cdots m \tag{10}$$

4　算　例

4.1　电网基本情况

以某城市电网为例，该城市电网共有四个电压等级：220 kV、110 kV、35 kV 和 10 kV。城市内共有 220 kV 变电站 2 座，容量为 480 MVA；110 kV 变电站 7 座，容量为 286 MVA；35 kV 变电站 10 座，容量为 105.2 MVA。35 kV 及以上电压等级的变电站接线如图 5 所示。

该城市 10kV 配电网共有 152 条 10 kV 线路，10 kV 典型接线有单联络和单环网两种接线模式，根据该城市配电网电网特征、管理需求、地理条件，划分了 152 个供电单元、22 个供电网格。

4.2　电网发展评价

根据评价需求，评价 22 个供电网格的电网发展发展情况。限于篇幅，从大数据平台中选择近三年的电网发展数据，验证本文所提出的评价方法的可行性，并以供电网格 1 的二级指标得分及权重设置为例，如表 2 所示。

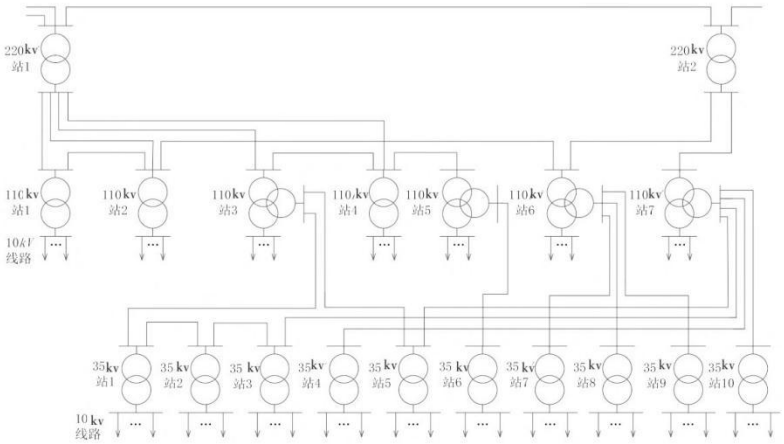

图 5　变电站接线示意图

表 2　二级指标得分及权重设置

二级指标	2020	2021	2022	目标值(%)	指标得分	权重设置		
						熵权法(考虑目标值)	熵权法(不考虑目标值)	标准离差法
清洁能源装机容量占比(%)	21.5	23.6	25.9	70	2.42	0.065	0.055	0.068
清洁能源发电量占比(%)	18.4	20.1	22.3	75	2.11	0.071	0.053	0.061
综合线损率(%)	6.5	6.3	6.2	5	3.98	0.045	0.051	0.005
线路N-1通过率(%)	67.1	70.3	73.2	100	3.62	0.049	0.056	0.095
高故障变压器占比(%)	1.2	1.1	0.9	0	3.86	0.047	0.064	0.005
高故障线路占比(%)	4.7	3.6	3.2	0	1.22	0.034	0.050	0.024
新能源可调度容量占比(%)	90.3	92.5	94.7	100	2.96	0.031	0.055	0.068

续表2 二级指标得分及权重设置

二级指标	2020	2021	2022	目标值(%)	指标得分	权重设置		
						熵权法(考虑目标值)	熵权法(不考虑目标值)	标准离差法
可控负荷占最高用电负荷比例(%)	3.5	4.7	5.1	30	1.18	0.069	0.072	0.026
轻载变压器占比(%)	25.3	23.7	21.1	0	2.59	0.055	0.061	0.066
轻载线路占比(%)	14.6	13.9	13.2	0	4.29	0.064	0.055	0.022
重载变压器占比(%)	2.5	2.3	2.1	0	4.20	0.053	0.055	0.006
重载线路占比(%)	3.2	2.9	2.8	0	3.94	0.055	0.050	0.006
配电自动化有效覆盖率(%)	70.5	73.8	76.4	100	3.60	0.047	0.058	0.092
可预测新能源发电站占比(%)	80.2	81.4	83.7	100	4.55	0.054	0.051	0.055
配置储能的新能源发电站占比(%)	10.2	11.5	13.6	100	1.09	0.080	0.052	0.053
电能占终端能源消费比例(%)	30.3	33.6	37.5	80	2.63	0.056	0.054	0.112
电动汽车充电站规划目标完成率(%)	50.6	55.1	60.8	100	2.96	0.049	0.053	0.159
电动汽车与电网互动技术(V2G)占比(%)	4.3	6.7	9.3	100	0.69	0.075	0.055	0.078

22个供电网格一级指标及综合得分如表3所示。

表3 一级指标得分及综合得分

供电网格	清洁低碳	安全可控	灵活高效	智能友好	开放互动	综合得分
1	8.50	12.84	15.01	9.23	6.29	51.88
2	6.29	13.89	14.04	8.00	9.29	51.51
3	8.83	21.85	15.67	13.65	16.75	76.75
4	6.34	14.54	16.90	14.63	8.88	61.29
5	7.12	15.43	20.71	8.51	14.54	66.31
6	13.61	20.77	17.19	16.37	14.61	82.55
7	15.07	10.98	14.31	17.72	14.96	73.04
8	12.18	18.43	18.33	14.89	17.00	80.83
9	11.97	18.70	17.38	12.85	9.05	69.95
10	7.48	19.70	14.41	9.15	13.59	64.33
11	13.77	12.32	17.45	15.21	16.67	75.42
12	12.10	22.91	14.78	14.06	9.22	73.07
13	11.69	18.70	13.51	8.15	12.82	64.87
14	11.48	10.76	14.44	17.09	6.73	60.50
15	14.14	18.92	21.70	13.32	9.37	77.45
16	7.52	10.37	14.14	13.44	9.33	54.80
17	14.14	14.07	21.80	11.94	7.24	69.19
18	8.06	16.35	12.40	9.72	6.01	52.54
19	6.91	20.58	15.01	17.83	8.93	69.26
20	6.68	15.18	15.43	10.94	12.45	60.68
21	9.45	17.26	19.22	17.72	8.46	72.11
22	17.18	15.84	12.93	8.39	15.01	69.35

从综合评分来看，电网发展情况较好的有网格6、网格8和网格15；电网发展存在明显短板的有网格1和网格2。统计各个网格评价指标得分，将各个网格的一级指标得分、二级指标得分以及综合得分分别排序上报，分析其存在的问题及电网短板，并进行有针对性的电网改造。通过表2可知，网格1在清洁能源接入、储能配置、电能替代、电动汽车与电网互动技术方面存在短板，说明该供电区域电网发展较为落后，需要推动能源生产和消费向清洁低碳转型，提高储能配置，加快新型电力系统转型发展。

4.3 评价方法对比

电网发展评价中，常规方法有层次分析法和标准离差法，层次分析法为主观赋权法，存在一定的主观随意性，一般需要与客观赋权法相结合。标准离差法虽为客观赋权法，但指标权重往往取决于指标的变异程度，且没有无量纲化处理过程，以表2数据为例，清洁能源装机容量占比、线路N-1通过率等指标变异大，权重明显偏大，而综合线损率、高故障变压器占比等指标变异小，权重明显偏小。常规的熵

权法虽然能够对指标数据矩阵进行无量纲化处理,并利用指标变化的信息熵确定指标权重,但如果不考虑目标值,指标权重也存在不合理之处,如新能源可调度容量占比,2020 ~ 2022年指标值均在90%以上,且目标值为100%,若不考虑目标值,则权重为0.055,但由于该指标已接近于目标值,电网发展空间小,因此,权重不宜偏大。采用目标值的熵权法,权重设定为0.031,有效地降低了指标权重,有利于明确电网发展方向,也说明本文权重设置的合理性和鲁棒性。

5　结　论

为了合理评价电网发展阶段和建设方向,制定具体可行、定位明确的新型电力系统发展目标及重点措施,本文依托电力大数据平台,提出一种基于电力大数据平台和供电网格的电网发展评价方法,主要成果总结如下:

(1)结合新型电力系统基本特征,从清洁低碳、安全可控、灵活高效、智能友好、开放互动五个维度出发,精选21个二级关键评价指标,构建了较为全面、系统的电网发展评价指标体系。

(2)由于电网是一个动态系统,每一年度的指标值均会产生变化,采用熵权法确定指标权重时,基于历史数据和实时数据,可以反映电网建设成效;同时需要引入指标目标,以便反映电网发展现状与电网发展目标的差距。权重设置也可结合主观赋权法,体现区域电网发展差异。

(3)通过将基于电力大数据平台和供电网格的电网发展评估模型应用于某城市电网,发现了该城市电网发展薄弱环节,明确了电网发展和投资方向,验证了该评估模型的可行性与实用性。

参考文献:

[1]郭剑波.新型电力系统面临的挑战以及有关机制思考[J].中国电力企业管理,2021(25):8-11.

[2]王灿,张雅欣.碳中和愿景的实现路径与政策体系[J].中国环境管理,2020(6):58-64.

[3]BREYER C,KHALILI S,BOGDANOV D,et al.On the history and future of 100% renewable energy systems research[J].IEEE Access,2022(10):78176-78218.

[4]李玲,黄晨翔,谭皓琳,等.基于自适应空间差分进化算法的节能优化研究[J].郑州航空工业管理学院学报,2024,42(5):105-112.

[5]黄鸣宇,张庆平,张沈习,等.高比例清洁能源接入下计及需求响应的配电网重构[J].电力系统保护与控制,2022,50(1):116-123.

[6]潘险险,余梦泽,隋宇,等.计及多关联因素的电力行业碳排放权分配方案[J].电力系统自动化,2020,44(1):35-42.

[7]白帆,陈红坤,陈磊,等.基于确定型评价指标的电力系统调度灵活性研究[J].电力系统保护与控制,2020,48(10):52-60.

[8]马杰,李秋燕,丁岩,等.含高渗透率可再生能源的配电网灵活性评价指标体系及计算方法[J].电力系统及其自动化学报,2020,32(9):99-104.

[9]曾治安,姚树友,郑晓玲,等.基于移动互联网技术的继电保护设备智能运维管理模式探讨[J].电力系统保护与控制,2019,47(16):80-86.

[10]PENG X S,YANG F,WANG G J,et al.A convolutional neural network-based deep learning methodology for recognition of partial discharge patterns from high-voltage cables[J].IEEE Transactions on Power Delivery,2019,34(4):1460-1469.

[11]彭小圣,邓迪元,程时杰,等.面向智能电网应用的电力大数据关键技术[J].中国电机工程学报,2015,35(3):503-511.

[12]李晖,刘栋,姚丹阳.面向碳达峰碳中和目标的我国电力系统发展研判[J].中国电机工程学报,2021,41(18):6245-6259.

[13]戴国华,戴睿,张琪瑞,等.基于主客观赋权相结合的省级电网发展诊断分析方法与实证研究[J].电力系统保护与控制,2022,50(2):110-118.

[14]王倩,王伟,陈上吉,等.省级智能电网发展程度评估体系与方法[J].电力系统及其自动化学报,2016,28(8):110-118.

[15]艾欣,赵璐,王智冬,等.物元分析法及其在电网发展诊断中的应用研究[J].华北电力大学学报,2020,47(3):10-18.

[16]龚贵宝.基于模糊层次分析法的区域电网发展诊断研究[D].北京:中国矿业大学,2019.

[17]彭云豪,董希建,周海强,等.电网安全稳定控制系统可靠性评估[J].电力系统保护与控制,2020,48(13):123-131.

[18]陈兴华,李峰,陈睿,等.计及安全稳定二、三道防线的电网运行风险评估[J].电力系统及其自动化学报,2020,48(4):159-166.

[19]陈柏森,廖清芬,刘涤尘,等.区域综合能源系统的综合评估指标与方法[J].电力系统自动化,2018,42(4):174-182.

[20]李佳莲.基于粗糙集与差异集成赋权的地市级电网诊断评价体系[D].北京:华北电力大学,2016.

[21]刘骏锋.基于实测数据的综合能源系统综合评价[D].北京:北京交通大学,2019.

[22]徐润萍.配电网综合评价指标体系及应用研究[D].北京:华北电力大学,2019.
[23]王正阳,詹智民,罗宾,等.基于网络层次分析法的电网发展诊断模型研究[J].郑州大学学报(工学版),2018,39(2):39-43.

责任编校:陈 强,裴媛慧

Evaluation Method for Power Grid Development Based on Electric Power Big Data and Power Supply

LI Xiang[1],HU Tiantong[1],CHEN Zhuo[1],LI Qiuyan[1],GUO Yinyuan[1],ZHANG Dan[1],HUA Hongyan[1]

(1.Zhengzhou University of Aeronautics,Zhengzhou 450046,China;
2.Xuchang Ketop Testing Research Institute Co., Ltd., Xuchang 461000,China;
3.Economic and Technological Research Institue,State Grid Henan Electric Power Co., Ltd., Zhengzhou 450000,China)

Abstract: To clarify the direction of the power grid development,a development evaluation method based on power big data platform and power supply grid is proposed in this paper.Firstly,based on the basic characteristics of the new power system,an index system is constructed from five dimensions:clean and low-carbon,safe and controllable,flexible and efficient,intelligent and friendly,and open interaction. Secondly,by leveraging the integrated power big data platform, massive amounts of data are mined, and the entropy weight method is employed to determine indicator weights. Then, considering factors such as the substation supply area, grid structure, and administrative divisions, the grid is divided into several power supply grids, and a hierarchical evaluation is conducted for refined assessment. Finally, the application results in a city distribution network show that the evaluation model has the advantages of simple operation, reasonable evaluation, and easy decision-making.

Key words: power big data; power supply grid; power grid development evaluation; index system; entropy weight method

10.A Modified Method for Calculating the Uplift Capacity ofMicropiles Considering the Correction of the CriticalEmbedment Depth

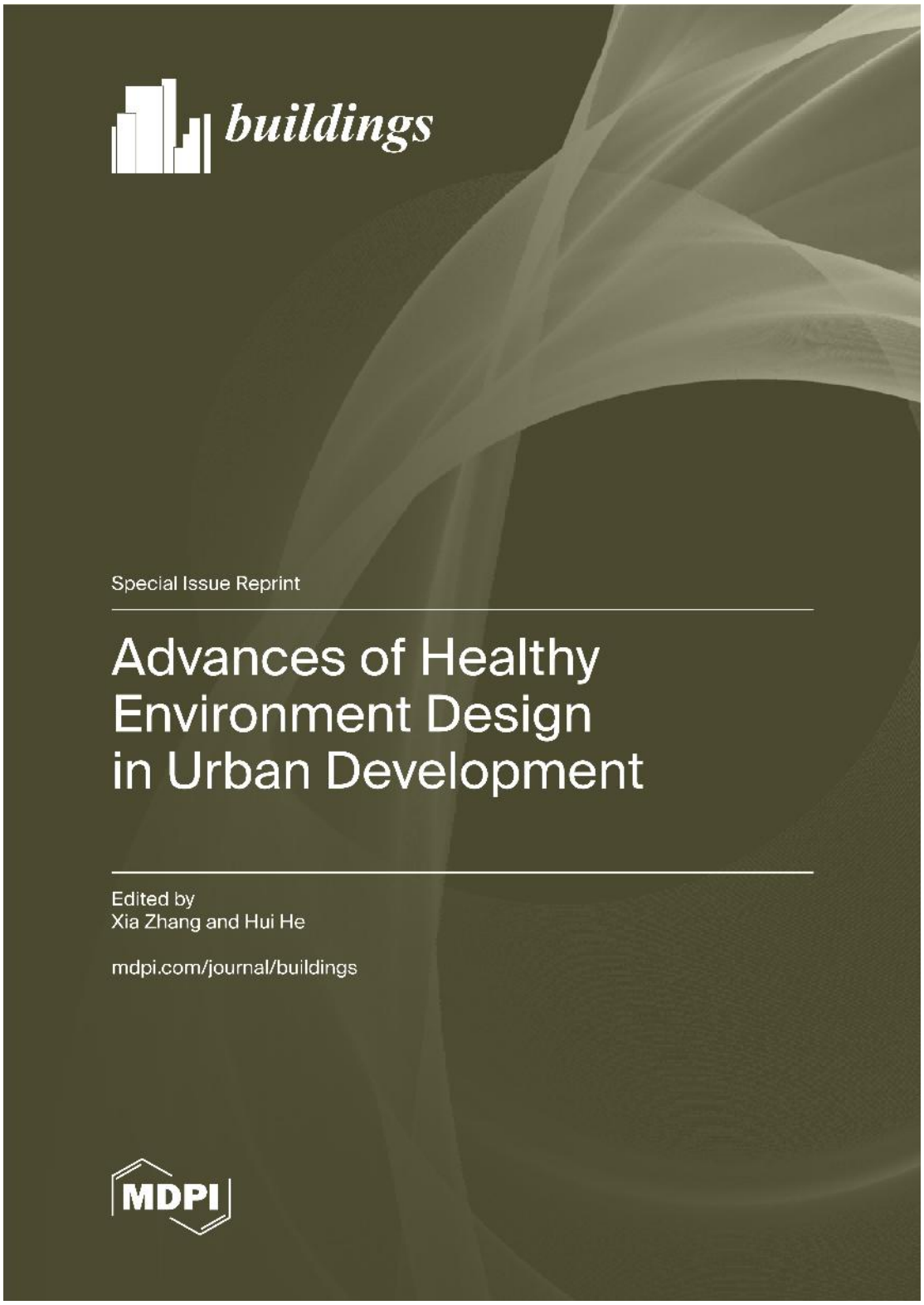

buildings

MDPI

Article

A Modified Method for Calculating the Uplift Capacity of Micropiles Considering the Correction of the Critical Embedment Depth

Linli Bao [1,2], Yuesong Zheng [1], Yi Zhou [1], Dongya Wu [2], Wenhao Wang [1], Zhaoxiang Guo [3] and Zhijun Xu [3,*]

[1] State Grid Henan Economic Research Institute, Zhengzhou 450052, China; 15736378667@163.com (L.B.); dljizwh@126.com (Y.Z.); 13592613015@163.com (Y.Z.); wangwenhao@126.com (W.W.)
[2] State Grid Henan Electric Power Company, Zhengzhou 450052, China; dongya426@163.com
[3] College of Civil Engineering and Architecture, Henan University of Technology, Zhengzhou 450001, China; guozhaoxiang@stu.haut.edu.cn
* Correspondence: xuzhijun@haut.edu.cn; Tel.: +86 18623718583

Abstract: As environmentally friendly pile foundations with small diameters and higher slenderness ratios, micropiles are widely used in fields such as transmission line engineering and building reinforcement. However, the available research has primarily focused on their bearing performance under compressive and horizontal loads, and there is insufficient research on predicting the uplift capacity of micropiles. This study investigated the load transfer mechanism and the behavior of the surrounding soil using model tests and finite element simulations. The ultimate uplift capacities and load distributions of micropiles with different slenderness ratios were analyzed. The results show that as the slenderness ratio increases, the ultimate uplift capacity of a pile gradually increases. However, this rate of increase diminishes gradually. Additionally, the restraining effect and range of the surrounding soil at the lower part of the pile are enhanced. The critical embedment depth of the micropiles shifts further away from the pile tip as the slenderness ratio increases. Finally, this study proposed a novel modification to Shanker's model of incorporating variations in the critical embedment depth based on the slenderness ratios. Subsequently, a modified model for the ultimate uplift capacity of micropiles was proposed and validated using a model test. The proposed model effectively predicts the uplift bearing capacity of micropiles with high slenderness ratios, which is practical for engineering applications.

Keywords: uplift capacity; critical embedment depth; load transfer mechanism; slenderness ratio; finite element analysis; micropiles

Academic Editor: Eugeniusz Koda

Received: 25 March 2025
Revised: 15 April 2025
Accepted: 24 April 2025
Published: 27 April 2025

Citation: Bao, L.; Zheng, Y.; Zhou, Y.; Wu, D.; Wang, W.; Guo, Z.; Xu, Z. A Modified Method for Calculating the Uplift Capacity of Micropiles Considering the Correction of the Critical Embedment Depth. *Buildings* **2025**, *15*, 1486. https://doi.org/10.3390/buildings15091486

1. Introduction

Against the background of rapid urbanization, the construction and reinforcement of infrastructure have imposed higher demands on the quality and time costs of ground improvements. As a new type of environmentally friendly foundation, the diameter of a micropile is usually less than 300 mm, and its slenderness ratio is greater than 30 [1–3]. Micropiles not only have the advantages of small pile diameters, lightweight construction equipment, short construction periods, and low impacts on the surrounding environment but can also be adapted to inaccessible and unfavorable site conditions, such as those located in hilly or mountainous areas. Consequently, micropiles have been widely applied in various fields, including transmission line projects [4–6] and civil engineering [7].

Numerous scholars have conducted research on the bearing performance of micropiles. As a load transfer structure for foundations, micropiles often bear compressive, uplift, and

lateral loads [2,8,9]. Borthakur et al. [10] established an empirical method for calculating the bearing capacity of micropile groups using experiments and data analyses, providing an important reference for engineering design. Li et al. [11] found that an uplift load created steep load–displacement curves, leading to risks of sudden damage, through field tests and numerical simulations of micropile groups in alpine mountains. Tsukada et al. [12] introduced a system effect index to quantitatively evaluate the enhancement effect of micropiles on foundations' bearing capacities. Jiang et al. [13] developed a three-dimensional numerical model based on field tests and centrifuge tests for analyzing the bearing capacity characteristics of waveform micropiles. Their numerical analysis revealed the load transfer mechanism of the waveform micropiles, and they proposed a new equation for bearing capacity predictions. Elsawwaf et al. [14] investigated the behavior of inclined micropile raft foundations under combined vertical and lateral loads using finite element models calibrated through field tests. Their results showed that increasing the vertical load continuously reduces the lateral bearing capacity of micropile raft foundations. Lee et al. [15] explored the reinforcement effect of micropiles and the bearing characteristics of micropile raft foundations by varying the cohesion of the upper soil and the pile stiffness. Their results indicated that the reinforcement effect of micropiles increases with soil cohesion but is more significant under low-cohesion conditions. Compared to the research on predicting the bearing performance and ultimate capacity under compressive and lateral loads, research on the prediction of the ultimate capacity under uplift loads is more limited. Therefore, it is necessary to conduct further research into the prediction of the ultimate uplift capacity of micropiles.

Research on the prediction of the ultimate uplift capacity of micropiles primarily includes empirical methods [16], limit equilibrium methods [17–20], and limit equilibrium methods that consider arching effects [21–23]. Empirical methods, typically based on historical data or field tests, are simple to operate and can quickly yield prediction results. However, the accuracy of these methods heavily relies on engineering experience, and their predictive performance may be unsatisfactory under new engineering conditions. Limit equilibrium methods that consider arching effects are mainly applicable to cohesionless soils [24], resulting in a relatively narrow scope of application. Considering the simplicity and applicability of these methods, limit equilibrium methods are more suitable for predicting the uplift capacity of piles. Nevertheless, the research on the uplift capacity of piles has predominantly focused on piles with slenderness ratios of less than 30 [18,19,25,26]. When the slenderness ratio exceeds 30, the critical embedment depth is simplified to 75% of the pile's length for calculation, ignoring the effect of the change in the critical embedment depth on the predicted results for cases with high slenderness ratios. Therefore, it is necessary to investigate the uplift bearing mechanism of micropiles further and evaluate the accuracy of the available prediction methods in assessing their ultimate uplift capacity.

Based on the aforementioned studies, the applicability of the existing prediction models for uplift capacity to micropiles with high slenderness ratios requires further evaluation. To address this, this paper investigates the load transfer mechanism of micropiles under uplift loads through model tests and finite element simulations and proposes a dynamically varying critical embedment depth dependent on the slenderness ratio. Subsequently, Shanker's model is improved by incorporating the critical embedment depth, resulting in a modified calculation method for predicting the ultimate uplift capacity of micropiles. This work provides a theoretical foundation for the application of micropiles in uplift-resistant engineering fields, such as transmission tower foundations and building reinforcement.

2. The Model Tests

2.1. The Model Piles

A large number of model tests under gravity can be carried out due to their low cost, which can ensure the reproducibility of the data and help us understand the significant characteristics of the uplift bearing capacity of miniature piles better [12]. For this reason, this study relies on engineering examples, and based on the similarity theory [27], the diameter of the model piles is designed to be 1/15 of that of the prototypes [28,29], with a diameter (d) of 20 mm and pile lengths (L) of 600 mm, 800 mm, and 1000 mm, respectively. Subsequently, for the model pile, the slenderness ratios (λ) are 30, 40, and 50, respectively, and the corresponding model piles are described as P30, P40, and P50, respectively. The model piles were made of solid aluminum alloy. Aluminum alloy was selected due to its high strength-to-weight ratio and ease of machining. To simulate the friction between the pile and the soil, the entire surface of the piles was polished, resulting in a pile–soil friction angle (δ) of 25.8°. Strain gauges were attached to one side of the model piles to monitor the changes in the axial force during the tests. The strain gauges used were the model 120-20 AA with a sensitivity of 2.0 mV/V, and they were evenly spaced at 100 mm intervals centered on the sensitive grid of the gauges. The dimensions of the model piles, the locations of the strain gauges, and the physical setup are shown in Figure 1.

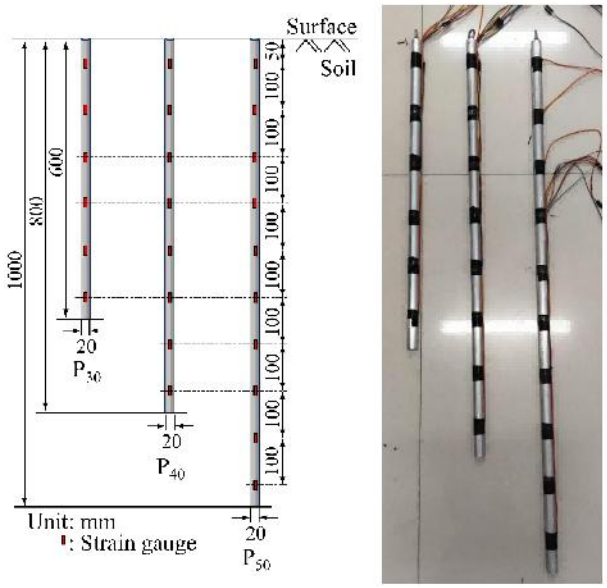

Figure 1. The model pile size, positions where the strain gauges were placed, and a physical map.

2.2. The Soil Sample

The soil sample consisted of a single sand layer with a density of 1.55 g/cm^3 and a relative density D_r of 0.501. The soil sample preparation procedure was as follows. Each 5 cm thick layer was compacted horizontally, and then the surface of each layer was scarified before adding the next layer to prevent stratification within the prepared soil sample. To ensure the accuracy of the tests, the prepared soil sample was left to settle for

24 h. After 24 h, the internal friction angle (φ) of the soil was determined to be 25° through direct shear tests (ASTM D3080-98 [30]). The results of the direct shear tests are shown in Figure 2.

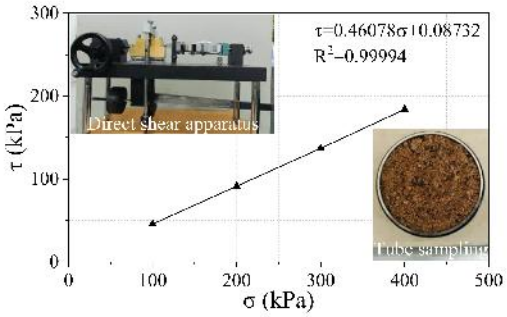

Figure 2. Results from direct shear tests.

2.3. The Loading System

The loading test system is shown in Figure 3. The system consists of a model box, an uplift loading device, displacement sensors, and a static strain acquisition system. The model box is made of tempered glass. The length, width, and height of the model box are 150 cm, 150 cm, and 120 cm, respectively, and the thickness of its walls is 10 mm. The uplift loading device consists of fixed pulleys, nylon ropes, and a weight container. Through the lever action of the two fixed pulleys, the gravity of the weights is transferred via the nylon ropes to apply an uplift load to the pile. The reaction frame of the uplift loading device is constructed using square steel tubes, with the fixed pulleys welded to the steel tubes to ensure reliable connections. The displacement sensors have a range of 0–20 mm and an error of −0.3%. The resolution and range of the static strain acquisition system (model JC-YBY-200) are 1 με and 0 ±30,000 με, respectively. The sampling rate is set to 2 times per second.

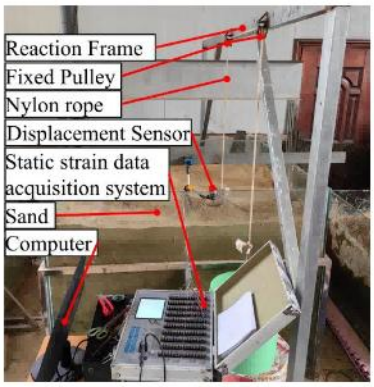

Figure 3. The loading test system.

3. Results and Discussions

3.1. The Bearing Capacity

The load–displacement curves of the uplifted micropiles under different slenderness ratios are shown in Figure 4. It can be observed that the load–displacement curves of the uplifted micropiles under different slenderness ratios exhibit similar trends from Figure 4. In the initial loading stage, the load–displacement curves develop linearly. The larger the slenderness ratio is, the greater the tangent slope of the curve in the linear stage is. As the load increases, the tangent slope of the curve gradually decreases, and the uplift displacement at the top of the pile increases nonlinearly and exponentially. Using the double-tangent method [20], the ultimate uplift capacity (UPC) of the pile was obtained. The ultimate uplift capacities of P_{30}, P_{40}, and P_{50} are 191 N, 375 N, and 491 N, respectively. The corresponding uplift displacements are 0.14 mm, 0.168 mm, and 0.18 mm, respectively. Compared to those of P_{30}, the UPC and its corresponding uplift displacement of P_{50} increased by 96% and 20%, respectively. Compared to those of P_{40}, the UPC and its corresponding uplift displacement of P_{50} increased by 31% and 7%, respectively. This indicates that as the slenderness ratio increases, the rate of the increase in the UPC and its corresponding uplift displacement in uplifted micropiles gradually decreases. This indicates that for micropiles under uplift loads with the same pile diameter, the improvement in the bearing capacity due to an increase in the pile length is limited.

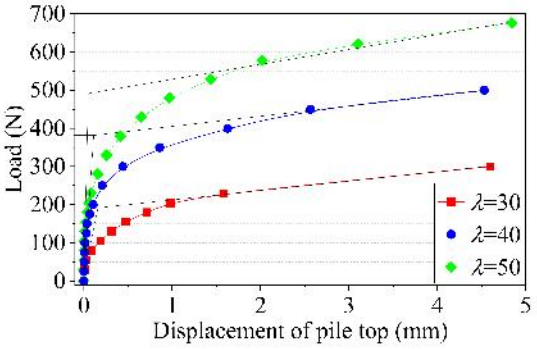

Figure 4. Load–displacement curves of micropiles with different slenderness ratios.

3.2. The Axial Force of the Piles

Equation (1) shows the formula for the axial forces along a pile shaft under different uplift loads [31], which can be used to obtain the axial forces of model piles under different loads, as shown in Figure 5. It can be observed that the axial forces along the pile shaft decrease gradually from the top to the bottom of the pile under different λ values from Figure 5. When λ is 30, the axial forces along the pile shaft exhibit an approximately linear distribution with the depth under all loads. As λ increases, the slope of the axial force curve gradually decreases under a large load. This indicates that for piles with large λ values, the transfer of the uplift load downward decreases as the buried depth increases. Therefore, the higher the slenderness ratio, the greater the extent of the embedment into the soil at the base of the micropile.

$$N_{ij} = E\varepsilon_{ij}A \tag{1}$$

where N_{ij} is the axial force of the pile at the i-th cross-section under the j-th load level; E is the elastic modulus of the pile; ε_{ij} is the strain of the pile; and A is the cross-sectional area of the pile.

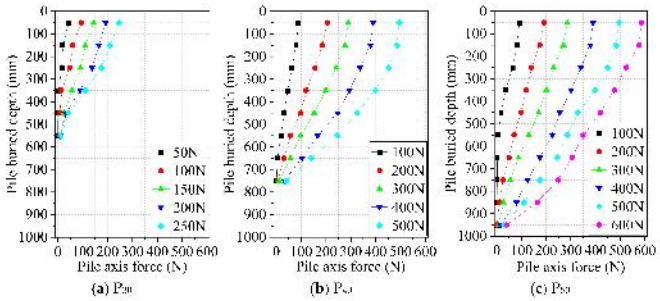

Figure 5. Axial forces of model piles under different loads.

3.3. The Side Friction Resistance

Figure 6 shows the average side resistance under different uplift loads calculated using Equation (2) [32]. It can be observed that the position of the maximum side friction resistance gradually shifts downward as the load increases. This indicates that in order to balance the uplift load, the pile's lateral frictional resistance gradually acts into deeper soil layers as the length-to-slenderness ratio increases. However, the distribution of the maximum side friction resistance varies with λ. For P_{30}, P_{40}, and P_{80}, the maximum side friction resistance occurs within buried depth ranges of 0.5–0.66 L, 0.625–0.875 L, and 0.7–0.9 L, respectively. This demonstrates that the larger λ is, the more significant the embedding effect of the soil around the lower part of the micropile. Therefore, it can be concluded that as the slenderness ratio increases, the point of the failure surface in the soil (that is, the critical embedding depth) moves further away from the bottom of the pile.

$$q_{si} = \frac{N_{ij} - N_{i+1,j}}{u_i l} \tag{2}$$

where q_{si} is the average side resistance of the pile segment between the i-th and $(i + 1)$-th cross-sections under the j-th load level; $N_{i+1, j}$ is the axial force at the $(i + 1)$-th cross-section under the j-th load level; ui is the perimeter of the pile; and l is the length of the pile segment between the i-th and $(i + 1)$-th cross-sections.

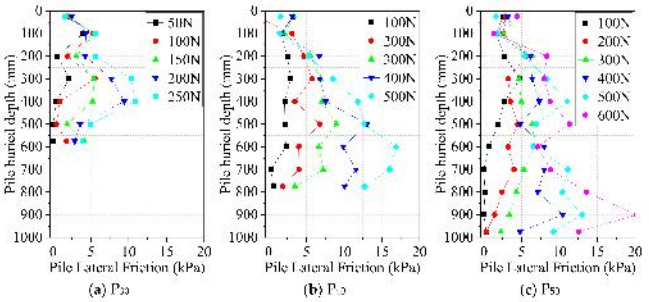

Figure 6. The distribution of the side friction resistance along the micropiles under different loads.

4. Prediction of the Ultimate Uplift Capacity

4.1. The Available Prediction Models and Improvements

(1) The standard model [33]

The standard model assumes that the failure surface occurs at the pile–soil interface, and the net ultimate uplift capacity of the pile can be estimated using Equation (3).

$$P_{nu} = \frac{\pi}{2} K_s d\gamma L^2 \tan\delta \tag{3}$$

where K_s is the lateral earth pressure coefficient; d is the diameter of the pile; γ is the unit weight of the soil; and L is the length of the pile.

(2) The truncated cone model

The truncated cone model assumes that the ultimate uplift capacity is equal to the self-weight within the failure surface, where the failure surface is a truncated inverted cone with the enveloping sides rising at $\varphi/2$ degrees from the vertical. This model is expressed using Equation (4).

$$P_{nu} = \frac{\pi}{3} L^3 \tan^2 \frac{\varphi}{2} \gamma \tag{4}$$

(3) Meyerhof's model [17]

Meyerhof's model neglects the weight of the pile and assumes that the soil failure mechanism under an uplift load follows a similar shape to that for a shallow anchor. The net ultimate uplift capacity of the pile can then be estimated using Equation (5).

$$P_{nu} = \frac{\pi}{2} K_u d\gamma L^2 \tan\delta \tag{5}$$

where, K_u is the uplift coefficient and can vary with in wide limits and depend not only on the soil properties, but also on the type of pile and method of installation.

(4) Das's model [18]

Based on experimental results, Das's model assumes that the friction resistance at the pile–soil interface increases linearly with depth until it reaches a critical embedment ratio. The critical embedment ratio depends on the relative density (D_r). The net ultimate uplift capacity of the pile can then be estimated using Equations (6) and (7).

$$P_{nu} = \frac{1}{2} p\gamma L^2 K_u \tan\delta \left[P_{nu} = If\ \lambda \le (\lambda)_{cr}\right] \tag{6}$$

$$P_{nu} \quad \frac{1}{2} p\gamma L_{cr}^2 K_u \tan\delta + p\gamma L_{cr} K_u \tan\delta (L - L_{cr}) \; P_{nu} \quad If\ \lambda > (\lambda)_{cr} \tag{7}$$

where

$$(\lambda)_{cr} = 0.156 D_r + 3.58 \ (\text{For } D_r < 70\%) \tag{8}$$

$$(\lambda)_{cr} = 14.5 \ (\text{For } D_r > 70\%) \tag{9}$$

where L_{cr} is the critical embedment depth, $(\lambda)_{cr} = L/L_{cr}$.

(5) Chattopadhyay's model [19]

Chattopadhyay's model assumes that the failure surface of the soil is curved. The net ultimate uplift capacity of the pile can then be estimated using Equation (10).

$$P_{nu} = A_1 \gamma \pi d L^2 \tag{10}$$

where A_1 is the net uplift capacity factor and depends on φ, δ, and λ.

(6) Shanker's model [20]

Shanker's model considers the angle between the soil failure surface and the horizontal, proposing a simplified method for predicting the net ultimate uplift capacity, as shown in Equation (11). Based on aforementioned studies on sliding failure surfaces [19], for piles with $\lambda \geq 20$, the failure surface is assumed to be tangent to the pile at a distance of $L/4$ from the pile tip. Therefore, Pu in this model is the sum of the values calculated using Equation (11) and the frictional resistance generated over the $L/4$ length.

$$P_{su} = \frac{C_1}{2}L^2 - \frac{C_2}{6}L^3 - \frac{\pi d^2}{4}L\gamma \tag{11}$$

where

$$C_1 = \pi d\gamma \left[\frac{1}{\tan\theta} - (\cos\theta - K_u \sin\theta)\tan\varphi \right] \tag{12}$$

$$C_2 = \frac{2\pi\gamma}{\tan\theta}\left[\frac{1}{\tan\theta} \quad (\cos\theta \quad K_u \sin\theta)\tan\varphi \right] \tag{13}$$

where θ is the angle of the failure surface to the horizontal.

Figure 7 compares the values calculated using these different prediction models with the experimental values. From Figure 7, it can be observed that as the slenderness ratio increases, the values predicted by the standard model and Meyerhof's model fall below the ideal line, with significant errors ranging from 71.8% to 73.8% and 50.3% to 54.9%, respectively. The truncated cone model provides predictions close to the ideal line for λ = 30 and 40, but the error reaches 65.5% for λ = 50. The values predicted by Das's and Chattopadhyay's models are relatively close, with the errors ranging from 12% to 39.5%. Shanker's model shows errors ranging from 8% to 40%. In summary, of these six models, Shanker's model demonstrates a better predictive capability for the ultimate uplift capacity of piles with high slenderness ratios. Additionally, Shanker's model is simple, involving neither complex analyses nor graphical methods, making it advantageous for engineers assessing the uplift capacity of foundation piles. Therefore, the following analysis and improvements are based on this prediction model.

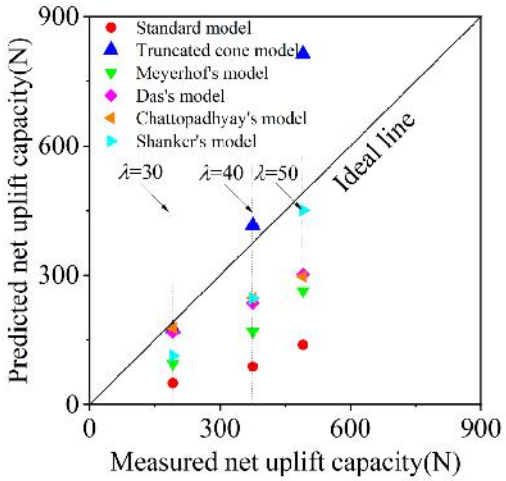

Figure 7. Comparison of the results using different prediction models and experimental results [17–20,33].

4.2. The Determination of L_{cr} for Micropiles with Different λ Values

4.2.1. The Finite Element Model

Based on the aforementioned experimental results, it is evident that the load distributions of different piles differ. Therefore, for micropiles with $\lambda \geq 30$, the critical embedment depth may differ. To investigate the variation in L_{cr} with different values for λ, a finite element analysis model was established using Abaqus software (2023) to simulate the deformation of the soil surrounding a micropile under an uplift load. The critical embedment depth was determined by analyzing the plastic strain of the surrounding soil. Figure 8 shows the finite element analysis model, where the side and bottom boundaries are constrained by roller and pinned supports, respectively. The dimensions of the calculation region in the soil are 75 d (length) × 90 d (width). Displacement loading was applied at the top of the pile, with a displacement of 5 mm. The cell type of the soil is CPE4R, and the cell type of the pile is CPS4R. The type of contact between the pile and soil is general contact, and the contact algorithm is an augmented Lagrange algorithm. The shear behavior at the pile–soil interface was defined based on Coulomb's friction law, where the tangential frictional stress is linearly proportional to the normal stress [34]. The pile–soil friction angle was set to 25.8°. The pile was modeled as a linear elastic material, while the soil was modeled using the Mohr–Coulomb model. The material parameters for the pile and soil are listed in Table 1. The pile diameter (d) is consistent with that in the model test. To enhance the generalizability of the results, additional cases with λ = 60 and λ = 70 were included.

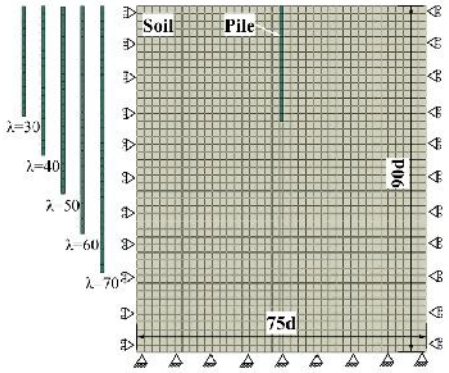

Figure 8. The finite element analysis model.

Table 1. Table of material parameters for pile and soil.

Unit	ρ (kg/m³)	E (MPa)	υ	φ (°)	Cohesion c (kPa)
Micropile	2.7	70,000	0.33	-	-
Soil mass	1.9	5.0	0.3	25	1

4.2.2. Validation of the Numerical Model

To validate the reliability of the numerical simulation model, the axial forces along the pile (at an uplift displacement of 5 mm at the top of the pile) and the load–displacement curves obtained from the model were compared with the experimental results. Figures 9 and 10 show comparisons of the axial forces along the pile and the load–displacement curves, respectively. It can be observed that the axial forces and the load–displacement curves calculated using the numerical model are in excellent agreement with the exper-

imental results from Figures 9 and 10. The maximum error in the axial forces is 3.5%. The ultimate uplift capacities calculated using the numerical model are 199 N (P_{30}), 390 N (P_{40}), and 511 N (P_{50}), with a maximum error of 4%. These results demonstrate that the established numerical model is highly reliable and can accurately predict the pile–soil interaction for micropiles under uplift loads. Based on the validated finite element model, the equivalent plastic strain contours of the surrounding soil for different micropiles at an uplift displacement of 5 mm were obtained, as shown in Figure 11.

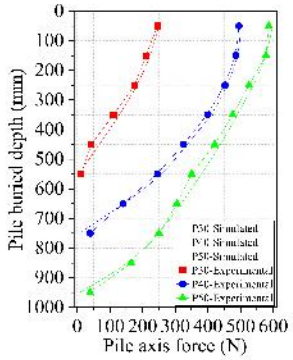

Figure 9. A comparison of the experimental and simulated axial forces along the piles.

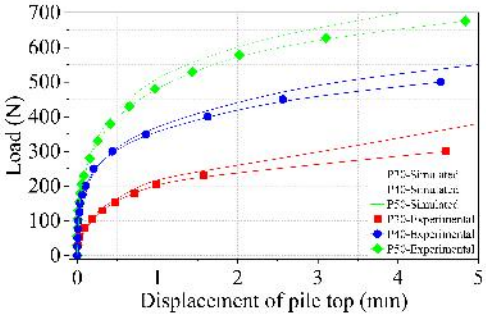

Figure 10. Comparison of experimental and simulated load–displacement.

From Figure 11, it can be observed that as λ increases, the extent of the failure surface in the surrounding soil expands, and the location of the failure surface, as well as the position of the maximum equivalent plastic strain, shifts deeper. The values of L_{cr}/L for the micropiles are 0.91, (λ = 30), 0.85 (λ = 40), 0.78 (λ = 50), 0.71 (λ = 60), and 0.62 (λ = 70). By performing linear fitting on L_{cr}/L for different values of λ, the relationship between L_{cr} and λ (Equation (14)) was obtained, as shown in Figure 12. Substituting $L = L_{cr}$ into Equation (11) yields Equation (15).

$$L_{cr} \quad (-0.0072\lambda + 1.134)L, \tag{14}$$

$$P_u = \frac{C_1}{2}L_{cr}^2 \; | \; \frac{C_2}{6}L_{cr}^3 \quad \frac{\pi}{2}K_s d\gamma(0.0072\lambda \quad 0.134)\tan\delta \quad \frac{\pi d^2}{4}L\gamma \tag{15}$$

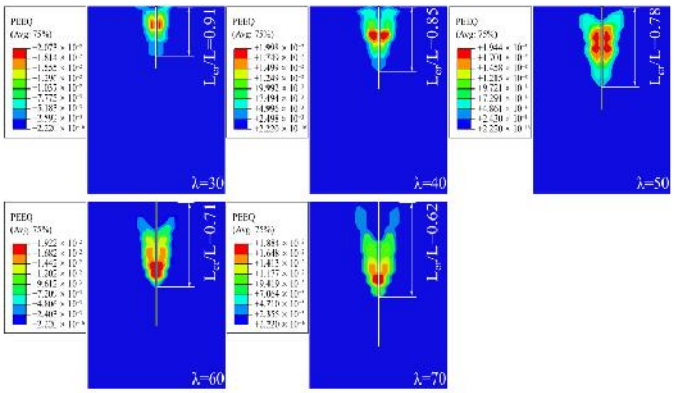

Figure 11. The contours of the equivalent plastic strain in the surrounding soil at an uplift displacement of 5 mm.

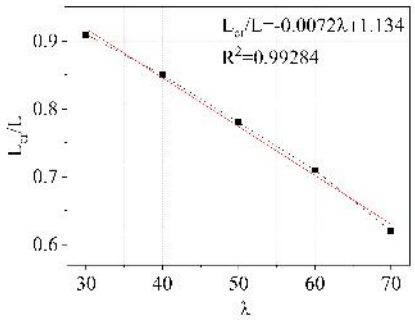

Figure 12. L_{cr} for different values of λ.

4.3. Validation of the Improved Model

Siddamal [35], Chattopadhyay [19], and Shanker [20] reported a series of model tests on piles with $\lambda \geq 30$ under uplift loads. Table 2 lists the test conditions, pile dimensions, theoretical predictions, and errors. The results show that the improved model has a very small error in the predictions for piles with high slenderness ratio compared to those of earlier models. Additionally, Figure 13 compares the results of the improved model with the measured values. The results show that the predicted values are in good agreement with the measured values, closely aligning with the ideal line, with the errors within 12%. This indicates that the improved model provides accurate predictions for the uplift capacity of micropiles.

Table 2. The results of the improved model are compared with the experimental results.

Data Sources	Expt. Parameters				λ	Expt. Results (N)	Model [illegible]		Truncated Cone Model		Model [17]		Model [18]		Model [19]		Model [20]		Improved Model	
	γ (kN/m³)	φ (°)	δ (°)	d (m)			(N)	Error (%)	(N)	Error (%)	(N)	Error (%)	(N)	Error (%)	(N)	Error (%)	(N)	Error (%)	(N)	Error (%)
[illegible] [illegible]	15.1	[illegible]	23	0.2	40	[illegible]	[illegible]	99.1	[illegible]	[illegible]	[illegible]	20.1	236.1	[illegible]	181.2	[illegible]	[illegible]	[illegible]	165.5	9.91
Chattopadhyay [14]	17.0	30	25	0.15	[illegible]	150	30.36	79.6	[illegible]	295.8	239	[illegible]	165	[illegible]	[illegible]	[illegible]	[illegible]	[illegible]	121.1	[illegible]
Shanker [5]	15.8	34	26	0.2	20	181.6	42.6	76.5	425.5	[illegible]	265.5	[illegible]	169	6.9	127.2	[illegible]	[illegible]	[illegible]	160.5	[illegible]
					40	363	77.8	79.1	[illegible]	[illegible]	468	28.9	239	34.2	163	[illegible]	[illegible]	7.71	404.5	11.4
	15.1	31	22	0.2	20	136.8	39.5	[illegible]	527.0	[illegible]	170	[illegible]	[illegible]	[illegible]	[illegible]	46.8	148.0	[illegible]	121.1	[illegible]
					40	242.4	[illegible]	71.0	771.5	218.3	287	[illegible]	68.3	71.8	80	[illegible]	[illegible]	[illegible]	214	[illegible]

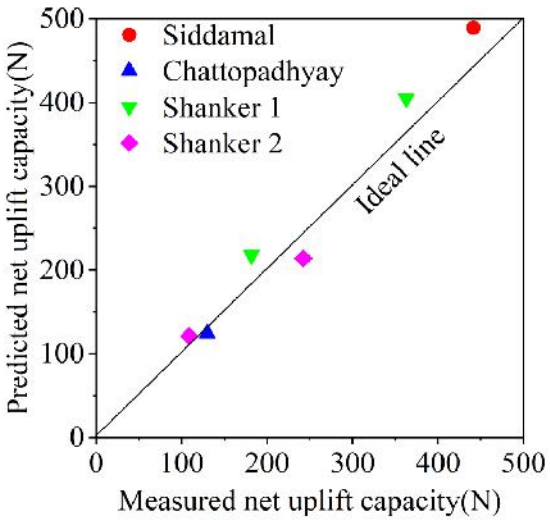

Figure 13. The results of the improved model are compared with the experimental results [19,20,35].

5. Conclusions

This study investigates the uplift bearing performance and the deformation of the surrounding soil for micropiles using model tests and finite element simulations. A modified model for the ultimate uplift capacity of micropiles is created based on Shanker's model. The following conclusions are obtained.

(1) As the slenderness ratio increases, the ultimate uplift capacity of a pile gradually increases, but the rate of increase decreases progressively. The load distribution of the micropiles varies with their slenderness ratios, showing that as the slenderness ratio increases, the embedment effect and range of the surrounding soil at the lower part of the pile become more significant, and the critical embedment depth of the micropile shifts further away from the tip of the pile.

(2) The improved model is suitable for predicting the uplift capacity of micropiles. Validation through case studies demonstrates that this method provides accurate predictions, with errors below 12%.

(3) The improved model is easy to use without a complex analysis and is suitable for the rapid design of micropiles in engineering. It is recommended in practical projects to first calculate L_{cr} using Equation (14) based on the preliminarily designed λ. Subsequently, P_{nu} should be calculated via Equation (15), compared with the design value, and an appropriate λ selected to optimize the design of the micropile size.

(4) The current model does not encompass specific soil conditions (e.g., expansive soil and collapsible loess). Future research will incorporate in situ testing and specialized soil analyses to expand the model's applicability.

Author Contributions: Conceptualization: L.B. and Y.Z. (Yuesong Zheng). Methodology: Z.G. Software: Y.Z. (Yi Zhou) Validation: D.W., W.W. and Z.G. Formal analysis: Z.X. Investigation: Y.Z. (Yuesong Zheng). Resources: Z.X. Data curation: Y.Z. (Yi Zhou). Writing—original draft preparation: W.W. Writing—review and editing: Z.G. Visualization: Z.G. Supervision: Z.X. Project

administration: Z.X. Funding acquisition: L.B. All authors have read and agreed to the published version of the manuscript.

Funding: The research was partially supported by a State Grid Henan Electric Power Company Science and Technology Project, named Research and Application of Key Technologies for Prefabricated Micro-Pile Foundations in Overhead Transmission Lines, under Grant No. 5217L024000Q.

Data Availability Statement: The data presented in this study can be made available on request to the corresponding author.

Acknowledgments: The authors sincerely thank the all respondents for their participation and the organizations for supporting this research.

Conflicts of Interest: Authors Linli Bao and Dongya Wu were employed by the company State Grid Henan Electric Power Company. The remaining authors declare that the research was conducted in the absence of any commercial or financial relationships that could be construed as a potential conflict of interest.

References

1. Bruce, D.A.; Dimillio, A.F.; Juran, I. *Introduction to Micropiles: An International Perspective*; Kentucky Geotechnical Special Publication, ASCE: Louisville, KY, USA, 1995; pp. 1–26.
2. Hwang, T.H.; Kim, K.H.; Shin, J.H. Experimental and numerical study on lateral resistance of micropile in sand. *KSCE J. Civ. Eng.* **2023**, *27*, 3740–3752. [CrossRef]
3. Kyung, D.; Lee, J. Uplift load-carrying capacity of single and group micropiles installed with inclined conditions. *J. Geotech. Geoenviron. Eng.* **2017**, *143*, 04017031. [CrossRef]
4. Wang, H.J. Research on micropile foundation of transmission tower on soft soil area. In Proceedings of the 2016 5th International Conference on Civil, Architectural and Hydraulic Engineering (ICCAHE 2016), Zhuhai, China, 30–31 July 2016; Beijing China Atlantis Press: Beijing, China, 2016; pp. 574–579.
5. Yu, X.; Wang, X. Research on the Design of Miniature Pile Foundation for Transmission Line. *E3S Web Conf. EDP Sci.* **2019**, *136*, 02022. [CrossRef]
6. Emirler, B.; Tolun, M.; Yildiz, A. Investigation on determining uplift capacity and failure mechanism of the pile groups in sand. *Ocean Eng.* **2020**, *218*, 108145. [CrossRef]
7. Elsawwaf, A.; El Sawwaf, M.; Farouk, A.; Aamer, I.; El Naggar, H. Restoration of tilted buildings via micropile underpinning: A case study of a multistory building supported by a raft foundation. *Buildings* **2023**, *13*, 422. [CrossRef]
8. Zhang, Y.; Zhang, L.; El Naggar, M.H.; Wu, W. Seismic response of pile group embedded in unsaturated soil considering the coupling of kinematic and inertia pile-pile interactions. *Comput. Geotech.* **2025**, *178*, 106937. [CrossRef]
9. Li, L.; Yan, N.; Liu, Z.; Wu, W.; Jiang, G.; Chen, L.; Liu, H. Investigation on the cyclic laterally-loaded response of pile-bucket foundation with grouted connection. *Mar. Struct.* **2025**, *103*, 103808. [CrossRef]
10. Borthakur, N.; Dey, A.K. Evaluation of group capacity of micro-pile in soft clayey soil from experimental analysis using SVM-based prediction model. *Int. J. Geomech.* **2020**, *20*, 04020008. [CrossRef]
11. Li, H.; Ren, G. Horizontal and uplift bearing characteristics of a cast-in-place micropile group foundation in a plateau mountainous area. *Sustainability* **2023**, *15*, 13354. [CrossRef]
12. Tsukada, Y.; Miura, K.; Tsubokawa, Y.; Otani, Y.; You, G.-L. Mechanism of bearing capacity of spread footings reinforced with micropiles. *Soils Found.* **2006**, *46*, 367–376. [CrossRef]
13. Jang, Y.E.; Kim, B.; Wang, C.; Han, J.-T. Prediction of vertical bearing capacity of waveform micropile. *Géotech. Lett.* **2019**, *9*, 198–204. [CrossRef]
14. Elsawwaf, A.; Nazir, A.; Azzam, W. The effect of combined loading on the behavior of micropiled rafts installed with inclined condition. *Environ. Sci. Pollut. Res.* **2022**, *29*, 81321–81336. [CrossRef] [PubMed]
15. Lee, K.I.L.; Kim, M.Y.; Hwang, T.H. Reinforcement effect of micropile and bearing characteristics of micropiled raft according to the cohesion of soil and stiffness of pile. *Geomech. Eng.* **2024**, *37*, 511–525.
16. Kishida, H. Stress distribution by model piles in sand. *Soils Found.* **1963**, *4*, 1–23. [CrossRef]
17. Meyerhof, G.G. Uplift resistance of inclined anchors and piles. In Proceedings of the 8th International Conference on Soil Mechanics and Foundation Engineering, Moscow, Russia, 6–11 August 1973; Volume 2, pp. 167–172.
18. Das, B.M. A procedure for estimation of uplift capacity of rough piles. *Soils Found.* **1983**, *23*, 122–126. [CrossRef]
19. Chattopadhyay, B.C.; Pise, P.J. Uplift capacity of piles in sand. *J. Geotech. Eng.* **1986**, *112*, 888–904. [CrossRef]

20. Shanker, K.; Basudhar, P.K.; Patra, N.R. Uplift capacity of single piles: Predictions and performance. *Geotech. Geol. Eng.* **2007**, *25*, 151–161. [CrossRef]
21. Shelke, A.; Patra, N.R. Effect of arching on uplift capacity of pile groups in sand. *Int. J. Geomech.* **2008**, *8*, 347–354. [CrossRef]
22. Zhang, Q.; Feng, R.; Liu, S.; Li, X. M. Estimation of uplift capacity of a single pile embedded in sand considering arching effect. *Int. J. Geomech.* **2018**, *18*, 06018021. [CrossRef]
23. Grindheim, B.; Trinh, N.; Li, C.C.; Høien, A.H. Investigating Load Arches and the Uplift Capacity of Rock Anchors: A Numerical Approach. *Rock Mech. Rock Eng.* **2024**, *57*, 7313–7342. [CrossRef]
24. Deshmukh, V.B.; Dewaikar, D.M.; Choudhury, D. Computations of uplift capacity of pile anchors in cohesionless soil. *Acta Geotech.* **2010**, *5*, 87–94. [CrossRef]
25. Chattopadyay, B.C. Uplift capacity of pile groups. In Proceedings of the 13thICSMFF, New Delhi, India, 5–10 January 1994; pp. 339–342.
26. Hong, W.P.; Chim, N. Prediction of uplift capacity of a micropile embedded in soil. *KSCE J. Civ. Eng.* **2015**, *19*, 116–126. [CrossRef]
27. Iai, S. Similitude for shaking table tests on soil-structure-fluid model in 1g gravitational field. *Soils Found.* **1989**, *29*, 105–118. [CrossRef]
28. FHWA. *Micropile Design and Construction Reference Manual for NHI Course 132078*; Federal Highway Administration, United States Department of Transportation: Washington, DC, USA, 2005.
29. Miura, K.; Tsukada, Y.; Tsubokawa, Y.; Ishito, M.; Nishimura, N.; Ohtani, Y.; You, G.L. Bearing capacity during the earthquake of the spread footing reinforced with micropiles. In Proceedings of the 12th World Conference on Earthquake Engineering, Auckland, New Zealand, Japan, 30 January–4 February 2000.
30. *ASTM D3080/D3080M-11*; Standard Test Method for Direct Shear Test of Soils Under Consolidated Drained Conditions. ASTM: West Conshohocken, PA, USA, 2014.
31. Da Silva, L.S.; Simões, R.; Gervásio, H. *Design of Steel Structures: Eurocode 3: Design of Steel Structures. Part 1-1: General Rules and Rules for Buildings*; John Wiley & Sons: Hoboken, NJ, USA, 2012.
32. American Petroleum Institute. *API RP 2GLO: Recommended Practice for Geotechnical and Foundation Design Considerations*, 2nd ed.; API Publishing Services: Washington, DC, USA, 2021.
33. Johnson, S.M.; Kavanagh, C.T. *The Design of Foundations for Buildings*; McGraw-Hill Book Company: New York, NY, USA, 1968.
34. Hong, Y.; He, B.; Wang, L.Z.; Wang, Z.; Ng, C.W.W.; Masín, D. Cyclic lateral response failure mechanisms of semi-rigid pile in soft clay: Centrifuge tests numerical modelling. *Can. Geotech. J.* **2017**, *54*, 806–824. [CrossRef]
35. Siddamal, U.V. Behavior of Pile Group Under Uplift Loads. Master's Thesis, Indian Institute of Technology, Chana City, India, 1989.

检 索 证 明

经检索《Science Citation Index Expanded》（SCI-EXPANDED）数据库和《中国科学院文献情报中心期刊分区表升级版》，以下1篇文献的收录简要信息、分区如下：

标题: A Modified Method for Calculating the Uplift Capacity of Micropiles Considering the Correction of the Critical Embedment Depth
作者: Bao, LL (Bao, Linli);Zheng, YS (Zheng, Yuesong);Zhou, Y (Zhou, Yi);Wu, DY (Wu, Dongya);Wang, WH (Wang, Wenhao);Guo, ZX (Guo, Zhaoxiang);Xu, ZJ (Xu, Zhijun)
来源出版物: BUILDINGS 卷:15 期:9 DOI:10.3390/buildings15091486 出版年:APR 27 2025
Web of Science 核心合集中的"被引频次"：0 次
期刊《**BUILDINGS**》**2023** 年影响因子为 **3.1**
2023 年 **JCR** 分区如下：

JCR® 类别	类别中的排序	JCR 分区
ENGINEERING, CIVIL	51/182	Q2
CONSTRUCTION & BUILDING TECHNOLOGY	28/92	Q2

经检索《中国科学院文献情报中心期刊分区表升级版》，**2025** 年分区如下：

刊名	Buildings		
年份	2025		
ISSN	2075-5309		
Review	否		
Open Access	是		
Web of Science	SCIE		
学科		分区	Top 期刊
大类	工程技术	3	否
小类:	CONSTRUCTION & BUILDING TECHNOLOGY 结构与建筑技术	3	-
小类:	ENGINEERING, CIVIL 工程：土木	3	-

特此证明
（详细内容见附件）

河南工业大学图书馆
检索人，李红艳
2025 年 05 月 20 日

地址：河南工业大学图书馆 10 楼 1004 室 电话：037167756359
检索邮箱：hgdcx@hautedu.cn 科技查新邮箱：hgdcxz@haut.edu.cn

第 1 条，共 1 条

标题: A Modified Method for Calculating the Uplift Capacity of Micropiles Considering the Correction of the Critical Embedment Depth

作者: Bao, LL (Bao, Linli);Zheng, YS (Zheng, Yuesong);Zhou, Y (Zhou, Yi);Wu, DY (Wu, Dongya);Wang, WH (Wang, Wenhao);Guo, ZX (Guo, Zhaoxiang);Xu, ZJ (Xu, Zhijun)

来源出版物: BUILDINGS 卷: 15 期:9 DOI: 10.3390/buildings15091486 出版年: APR 27 2025

Web of Science 核心合集中的 "被引频次": 0

被引频次合计: 0

使用次数 (最近 180 天): 0

使用次数 (2013 年至今): 0

引用的参考文献数: 35

摘要: As environmentally friendly pile foundations with small diameters and higher slenderness ratios, micropiles are widely used in fields such as transmission line engineering and building reinforcement. However, the available research has primarily focused on their bearing performance under compressive and horizontal loads, and there is insufficient research on predicting the uplift capacity of micropiles. This study investigated the load transfer mechanism and the behavior of the surrounding soil using model tests and finite element simulations. The ultimate uplift capacities and load distributions of micropiles with different slenderness ratios were analyzed. The results show that as the slenderness ratio increases, the ultimate uplift capacity of a pile gradually increases. However, this rate of increase diminishes gradually. Additionally, the restraining effect and range of the surrounding soil at the lower part of the pile are enhanced. The critical embedment depth of the micropiles shifts further away from the pile tip as the slenderness ratio increases. Finally, this study proposed a novel modification to Shanker's model of incorporating variations in the critical embedment depth based on the slenderness ratios. Subsequently, a modified model for the ultimate uplift capacity of micropiles was proposed and validated using a model test. The proposed model effectively predicts the uplift bearing capacity of micropiles with high slenderness ratios, which is practical for engineering applications.

入藏号: WOS:001486518200001

语言: English

文献类型: Article

作者关键词: uplift capacity;critical embedment depth;load transfer mechanism;slenderness ratio;finite element analysis;micropiles

KeyWords Plus: BEARING CAPACITY; PILE; PREDICTION

地址: [Bao, Linli; Zheng, Yuesong; Zhou, Yi; Wang, Wenhao] State Grid Henan Econ Res Inst, Zhengzhou 450052, Peoples R China;[Bao, Linli; Wu, Dongya] State Grid Henan Elect Power Co, Zhengzhou 450052, Peoples R China;[Guo, Zhaoxiang; Xu, Zhijun] Henan Univ Technol, Coll Civil Engn & Architecture, Zhengzhou 450001, Peoples R China

通讯作者地址: [Xu, Zhijun] (corresponding author), Henan Univ Technol, Coll Civil Engn & Architecture, Zhengzhou 450001, Peoples R China

电子邮件地址: 15738378667@163.com;dljizwh@126.com;13592613015@163.com;dongya426@163.com;wangwenhao@126.com,guozhaoxiang@stu.haut.edu.cn;xuzhijun@haut.edu.cn

出版商:MDPI

出版商地址: MDPI AG, Grosspeteranlage 5, CH-4052 BASEL, SWITZERLAND

Web of Science Index: 《Science Citation Index Expanded》 (SCI-EXPANDED)

Web of Science 类别:Construction & Building Technology;Engineering, Civil

研究方向:Construction & Building Technology;Engineering

IDS 号:2M2SL

eISSN: 2075-5309

来源出版物页码计数: 15

基金资助致谢:The research was partially supported by a State Grid Henan Electric Power Company Science and Technology Project, named Research and Application of Key Technologies for Prefabricated Micro-Pile Foundations in Overhead Transmission Lines, under Grant No. 5217L024000Q.

基金资助机构	授权号
State Grid Henan Electric Power Company Science and Technology Project	5217L024000Q
State Grid Henan Electric Power Company Science and Technology Project, named Research and Application of Key Technologies for Prefabricated Micro-Pile Foundations in Overhead Transmission Lines	

ESI 高被引论文: N

ESI 热点论文: N

输出日期: 2025 年 05 月 20 日

11.Characteristics Investigation on Bearing Performance of aNovel Assembled Micropile Foundation in OverheadTransmission Lines

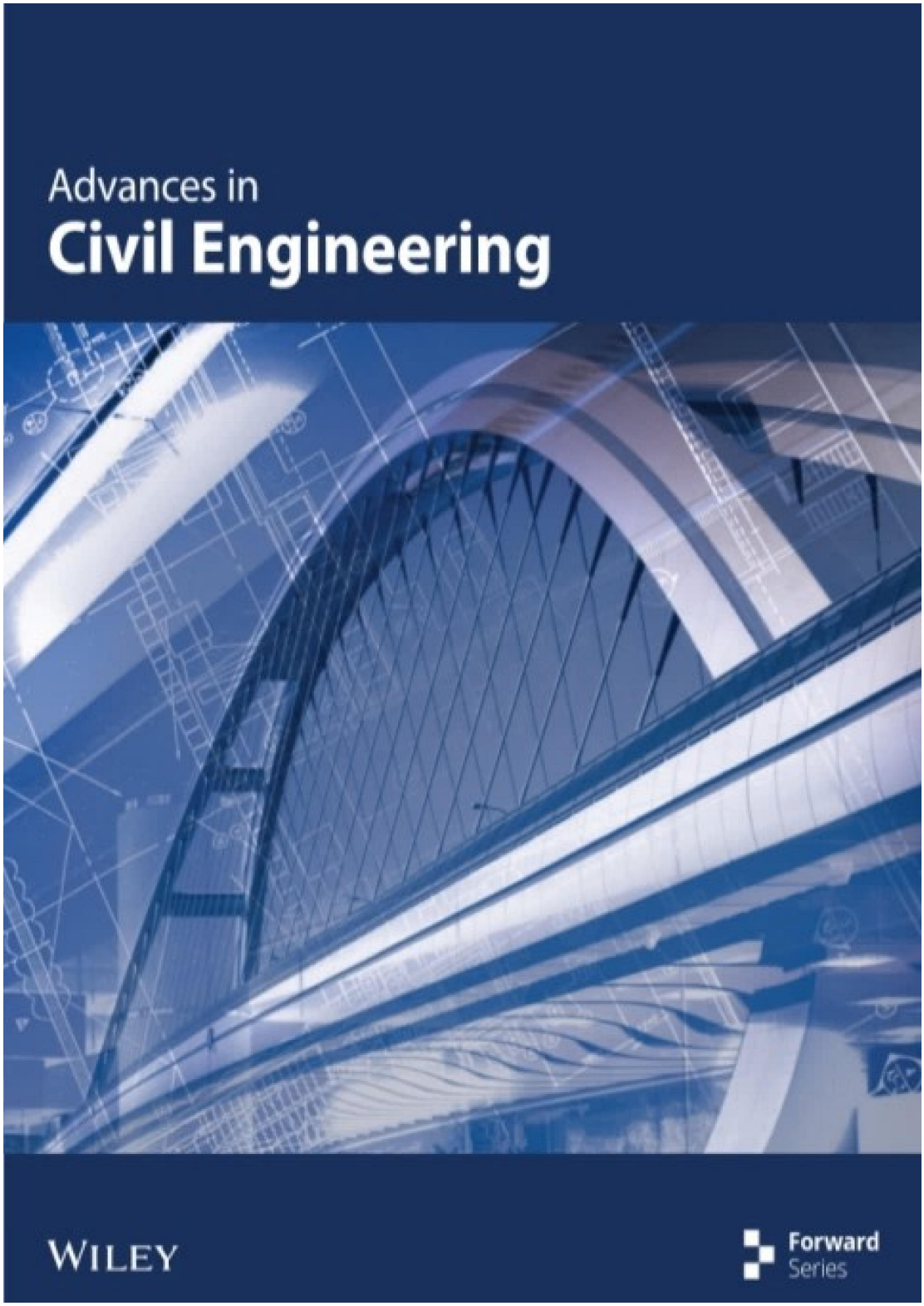

Wiley
Advances in Civil Engineering
Volume 2025, Article ID 3956237, 17 pages
https://doi.org/10.1155/adce/3956237

WILEY

Research Article

Characteristics Investigation on Bearing Performance of a Novel Assembled Micropile Foundation in Overhead Transmission Lines

Yuesong Zheng,[1] Linli Bao,[2] Zhaoxiang Guo,[3] Yi Zhou,[2] Dongya Wu,[2] Wenhao Wang,[2] Bo Xiao,[1] and Zhijun Xu[3]

[1]*State Grid Henan Economic Research Institute, Zhengzhou 450052, China*
[2]*State Grid Henan Electric Power Company, Zhengzhou 450000, China*
[3]*School of Civil Engineering, Henan University of Technology, Zhengzhou 450001, China*

Correspondence should be addressed to Zhijun Xu; xuzhijun@haut.edu.cn

Received 2 April 2025; Accepted 8 May 2025

Academic Editor: Guang Liang Feng

It is challenging to develop a widely accepted construction method of micropile foundation (MPF) for transmission line projects in complex terrains. A novel assembled MPF was proposed to address this challenge, and its characteristics of bearing performance were investigated assisted with model experiments and three-dimensional numerical simulations. Results show that the ultimate bearing capacity under vertical and horizontal loads maintained 95.0% and 92.6% of the performance for cast in situ foundations, respectively. Pronounced stress concentrations occur near prestressed tendons and connectors, creating visible load path indicators that enable real time structural health monitoring and targeted component replacement. Vertical loads are effectively transferred from prestressed tendons to shear keys, and then to connecting steel plates. Horizontal load resistance primarily relies on steel cylinder–pile interaction, demonstrating less than 3% directional displacement variation, comparable to cast-in-situ foundation integrity. The assembled connection system achieves consistent quality control through factory-manufactured components. The modular nature and standardized connections significantly advance the industrialization of power infrastructure construction.

Keywords: assembled micro pile; bearing performance; load transfer mechanism; overhead transmission lines; three dimensional numerical simulation

1. Introduction

As a cornerstone of technological advancement [1], the transmission of electrical energy is a crucial component of the overall functionality of power systems [2]. Overhead transmission lines (OTLs) emerge as the predominant solution for long-distance, high-capacity power delivery, particularly in expansive terrains with favorable geomorphological conditions [3]. Within this infrastructure system, tower foundations perform critical load-transfer functions, simultaneously resisting structural forces from aboveground components and geotechnical stresses from surrounding strata [4, 5]. Current construction challenges are magnified in mountainous grid projects, as exemplified by the Ningdian–Ruixiang corridor where mountainous terrain constitutes ~90% of the project area [6]. Conventional cast-in-situ pile foundations (CF) face threefold limitations under such complex topographical conditions: (1) restricted accessibility for heavy construction equipment, (2) safety hazards in manual excavation processes, and (3) quality inconsistencies in concrete placement. Therefore, to improve the construction efficiency and quality of transmission line projects, there is an urgent need for innovative foundation systems and construction techniques that support fully mechanized construction. In the context of global promotion of environmentally friendly materials and construction [7–9], green construction has become an industry consensus.

Micropile foundations (MPFs) present an environmentally conscious alternative demonstrating superior technical merits, which are compact cross-sections (typically 150–300 mm diameter), lightweight installation equipment (<5 t), reduced construction timelines (40%–60% faster than conventional methods), and enhanced adaptability to constrained sites [10, 11]. This technological shift addresses both operational safety concerns and sustainability requirements in modern power infrastructure development.

Researchers have conducted theoretical and experimental studies on the bearing capacity of single micropiles under vertical [12–14], inclined [15, 16], and horizontal [17, 18] loading conditions. The results show that single micropiles exhibit excellent bearing performance, and simplified calculation methods have been proposed as viable alternatives to conventional large-diameter piles. Cui et al. [19] proposed a novel analytical solution for horizontal vibration of floating piles in saturated soils, advancing the theoretical framework for micropile behavior under dynamic loading conditions. Regarding micropile group behavior, Sharma et al. [20] investigated 12 micropile configurations, identifying pile spacing, slenderness ratio, and soil compaction as critical parameters governing bearing performance. Complementary research by Hussain et al. [21] in granular soils (relative densities of 30%, 50%, and 80%) revealed enhanced group efficiency at 6D pile spacing under lateral loading. Kyung et al. [22] developed a field-test-based bearing capacity estimation method through model testing of inclined micropile groups under vertical loads, while Moradi Moghaddam et al. [23] demonstrated minimal construction method influence (drilling vs., driving) on performance via large-scale physical modeling. Hong et al. [24] and Zhang et al. [25] explored the failure modes and mechanisms under different geological conditions through system reliability analysis and bearing capacity analysis, respectively. Collectively, these studies confirm the superior bearing characteristics of micropile groups across diverse loading scenarios [26]. Xiong et al. [27] further investigated the compaction effects during pile group installation in saturated clay, revealing critical influences of pile spacing and length to diameter ratio on adjacent piles' deformation and bearing capacity. Notwithstanding these advantages, field implementation of cast-in-situ micropiles faces quality control challenges due to their reduced diameters. Assembled micropiles present a promising solution with enhanced quality assurance. To align with the mechanization trends in transmission line construction, systematic investigation of fully assembled MPFs (AF) becomes imperative.

Current assembled foundation systems encompass both spread and pile types. Experimental evaluations of assembled slab foundations by Wang et al. [28] revealed 90% flexural capacity retention compared to cast-in-situ foundations, accompanied by improved ductility. In pile foundation research, Yunsheng and Kai [29] developed wheel-type pile foundations for transmission lines, demonstrating simplified load transfer mechanisms. Zhou et al. [30] proposed a novel pipe pile system exhibiting superior self centering capability and ductility despite reduced bearing capacity relative to conventional piles. However, logistical constraints persist due to bulky components, necessitating the development of compact assembled pile systems.

Connection methodologies for assembled components primarily involve wet and dry techniques. Compared to wet connections, dry connections do not require on-site concrete pouring, making them more suitable for rapid construction and green emission reduction [31]. Jiang et al. [32] developed an innovative end-plate bolted connection between precast beams and composite columns, demonstrating exceptional seismic performance through cyclic loading tests. Bolted connections offer additional benefits including construction efficiency, cost effectiveness, and postdamage reparability [33, 34]. Jiang et al. [35] proposed a novel bolted connection for fully assembled shear walls, and quasi-static tests verified the integrity and seismic performance of the bolted precast shear walls. These advancements confirm the technical viability of prestressed and bolted connections for AFs.

Building upon a 110 kV transmission line micropile project, this study proposes an innovative modular AF system incorporating both prestressed tendon and bolted cap-pile connections (Figure 1). By modularizing the cap into three prefabricated units at the starting position (column base location) of the most unfavorable oblique section in the punching shear failure cone, the dimensions during transportation and installation phases are effectively reduced. Simultaneously, the connection between the cap and base piles adopts an integrated steel cylinder structure, forming standardized pile installation channels. This design significantly enhances installation convenience and resolves the persistent challenge of controlling positioning accuracy with traditional embedded bolts during prefabrication processes. Model tests [36, 37] and numerical simulation [38, 39] methods have been widely used in geotechnical engineering, and these methods can effectively study complex soil–structure interactions.Therefore, model tests and numerical simulation methods were used to assess the bearing behavior and settlement characteristics of the system under vertical and lateral loading. Comparative analyses with conventional cast-in-situ piles assessed load-bearing performance, stress distribution, and deformation patterns, ultimately validating the structural integrity and reliability of the proposed foundation system. These findings provide valuable insights for advancing assembled foundation design and mechanized construction in power transmission engineering.

2. The Proposed Assembled Micropile

This study investigates the application of micropiles in a 110 kV transmission line project. An AF design was developed through comprehensive analysis of geological conditions, load characteristics (as detailed in Table 1), and structural parameters including dimensions, material properties, and reinforcement configurations of conventional cast-in-situ concrete piles. The original foundation design employed reinforced cast-in-situ concrete piles with geometric specifications and reinforcement layouts illustrated in Figure 2. The structural components utilize differentiated concrete grades: C35 for the pile cap and higher-strength C60 for the micropiles. The designed micropiles feature a 6-m length with a 200-mm diameter, engineered

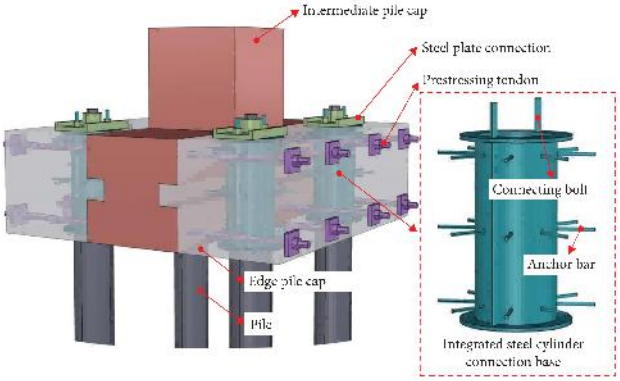

Figure 1: The proposed assembled micropile foundation.

Table 1: The loads.

Voltage level (kV)	Tower type	Number	Uplift (kN)			Compressive load (kN)		
			T_x	T_z	T_y	N_z	N_x	N_y
110	Straight-line tower	JQM-450	150	63	63	585	81.9	81.9

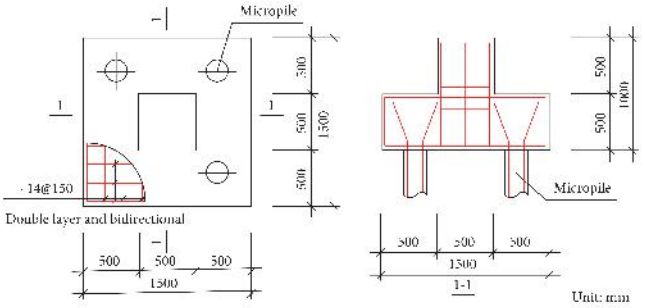

Figure 2: Dimensions and reinforcement layout of the cast-in-situ reinforced concrete pile foundation.

Table 2: Physical parameters of the soil.

Soil type	Layer thickness (m)	Physical parameters		
		Unit weight (kN/m^3)	Internal friction angle φ (°)	Cohesion c (kPa)
Cohesive soil	12	19	16	45

to interact with subsurface conditions characterized by the soil parameters presented in Table 2.

2.1. Assembled Cap. Figure 3 illustrates the modular division scheme of the assembled cap structure. The coordinate system is defined with the x-direction parallel to the splice seams and the y-direction perpendicular to these joints. To facilitate transportation and reduce the weight and size for on-site installation, the cap is divided into three smaller prefabricated units along the y-direction. During the installation phase, modified epoxy adhesive is employed for bonding and prestressed tendon connections. This modular configuration comprises three

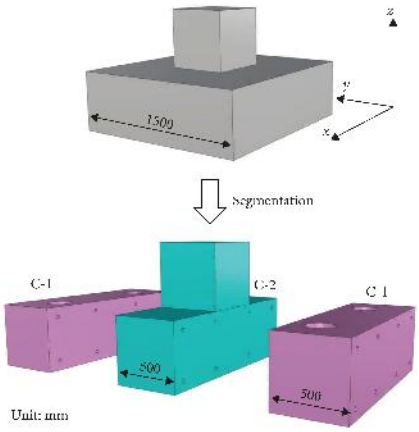

Figure 3: Dimensions of the assembled cap blocks.

Table 3: Parameters of assembled cap.

Component type	Concrete grade	Reinforcement	Volume (m^3)	Weight (t)	Quantity
C-1	C40	x-direction: C 10@200	0.344	0.86	2
C 2	C40	y direction: C 14@150	0.500	1.25	1

distinct components: two symmetrical end units designated as C-1 and a central unit labeled C-2. The technical specifications including physical parameters and reinforcement configurations for both C-1 and C-2 are systematically presented in Table 3, where C denotes HRB400-grade reinforcement.

2.2. Connection Design

2.2.1. Cap Connection Design. The cap connection system employs a composite mechanical joint comprising prestressed tendons and shear keys to address the dual loading conditions of transmission line foundations. Given that these foundations experience both uplift and compressive forces during service, the design incorporates prestressed tendons within the tensile zone of the cap to enhance bending resistance post-splicing. Concurrently, shear keys are strategically positioned at the cap's spliced interface to ensure effective shear load transfer.

2.2.1.1. Prestressed Tendon Configuration. The assembled cap design requires prestressed tendons to deliver tensile capacity and enhance structural integrity. To accommodate the combined compressive, uplift, and horizontal loads transmitted from the pile foundation, prestressed tendons are distributed across both the upper and lower regions of the cap cross section. During the tensioning phase, an initial one-sided prestressing operation induces eccentric loading (denoted as N_{pe}), generating nonuniform pressure distribution at the spliced contact surface. This eccentricity, illustrated in Figure 4, arises from the spatial offset between the tendon axis and the contact surface centroid. Figure 4 defines critical geometric parameters, where h represents the contact surface height and e_0 quantifies the prestress eccentricity.

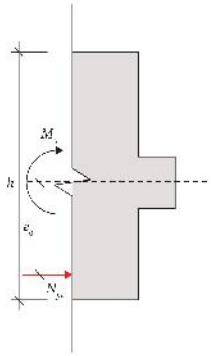

Figure 4: Stress at the splice contact surface during construction (tensioning on the bottom side of the cap).

The stress at the upper edge of the spliced foundation surface is

$$\sigma = -\frac{N_{pc}}{A} - \frac{N_{pc}e_0}{W}. \tag{1}$$

Substituting $A = bh$ and $W = \frac{bh^2}{6}$ into Equation (1) is

$$\sigma = \frac{6N_{pc}}{bh^2}\left(\frac{h}{6} - e_0\right). \tag{2}$$

where b is the width of the splice contact surface.

From Equation (2), the upper edge stress (σ) is larger than or equal to 0 when $e_0 < h/6$. To prevent excessive separation at the splice contact surface during prestressed tendon construction while maintaining cost-effectiveness in bending moment resistance, the eccentricity is specified as $e_0 = 110$ mm.

2.2.1.2. Prestressed Tendon Area and Tension Control Stress. The cross-sectional area of prestressed tendons and their tension control stress critically influence the bending moment capacity at the splice interface. The bending moment can be calculated using the following formula [40].

$$\begin{aligned} M_u = {} & \alpha_1 f_c b x\left(h_0 - \frac{x}{2}\right) + f_y' A_s'(h_0 - a_s') \\ & - \left(\sigma_{p0}' - f_{py}'\right) A_p'(h_0 - a_p') \end{aligned} \tag{3}$$

$$\alpha_1 f_c b x = f_y A_s - f_y' A_s' + f_{py} A_p + \left(\sigma_{p0}' - f_{py}'\right) A_p', \tag{4}$$

where M_u is the design value for the bending bearing capacity of the component splice contact surface; f_c is the design axial compressive strength of concrete; x is the height of concrete compression zone; b and h_0 are the width and effective height of splice contact surface, respectively; f_y/f_{py} and f_y'/f_{py}' are the design tensile and compressive strengths of ordinary reinforcement and prestressed tendons, respectively; A_p/A_p' is the cross-sectional area of the longitudinal prestressed tendons in the compression zone; A_s/A_s' is the cross-sectional area of the longitudinal ordinary reinforcement in the tension and compression zones; σ_{p0}' is the pre stress at the point where the normal concrete stress in the compression zone equals 0; a_s'/a_p' represents the distance from the resultant point of the longitudinal ordinary reinforcement/prestressed tendons to the compression edge of the cross-section.

As shown in Figure 3, the tensile edge stress at the splice interface can be determined using Equation (5).

$$\sigma = \frac{N_{pc}}{A} - \frac{M_u - N_{pc}e_0}{W} \geq 0. \tag{5}$$

Through comprehensive analysis of Equations (3), (4), and (6), the design incorporates four PSB930 prestressed threaded steel bars (25 mm diameter) on each side of the cap. The tension control stress is set at 790 MPa (0.85 fpyk), ensuring optimal performance.

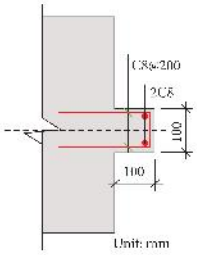

Figure 5: Shear key cross-section dimensions.

2.2.1.3. Shear Key Parameter Design. The shear resistance mechanism assumes complete shear transfer through shear keys, eliminating shear force in prestressed tendons. Equation (6) yields a minimum effective height requirement $h_0' \geq 86.3$ mm [41]. Accordingly, the shear keys are designed with 100 mm × 100 mm cross-sectional dimensions, featuring reinforcement details illustrated in Figure 5. This configuration ensures adequate shear resistance while maintaining structural efficiency.

$$V_u \quad 0.1 f_c b h_0' + 0.05 N_{pc} + 1.65 A_{sd}\sqrt{f_c f_y}. \tag{6}$$

where h_0' is the height of the shear key section; V_u is the shear bearing capacity; A_{sd} is the area of regular reinforcement.

2.2.2. Pile and Cap Connection Design. The innovative AF system incorporates an engineered steel cylinder connection base to enhance assembly efficiency and enable fully mechanized construction. This advanced configuration features preembedded anchor bolts precision-welded to a 8-mm thick steel cylinder, creating a unified connection interface for structural integration between pile elements and the cap. Field installation employs standardized connecting steel plates with bolted joints, ensuring rapid and precise alignment. The steel cylinder assembly is reinforced with 24HRB400-grade threaded steel bars (8-mm diameter × 100 mm length) circumferentially welded to its exterior surface. Critical connection components—including pile-top embedded bolts, interface plates, and the composite steel cylinder base are detailed in Figures 6 and 7, demonstrating the system's precision-engineered dimensional coordination.

The proposed foundation implements modular architecture, dividing the cap structure into three lightweight assembled units that optimize transportation logistics and installation efficiency. The multifunctional steel cylinder base serves dual purposes as both a precision alignment template during construction and a permanent bolted connection platform. When combined with the cap's prestressed tendon connection system, this design achieves complete dry assembly capability, eliminating traditional wet concrete joints and fulfilling stringent green construction requirements.

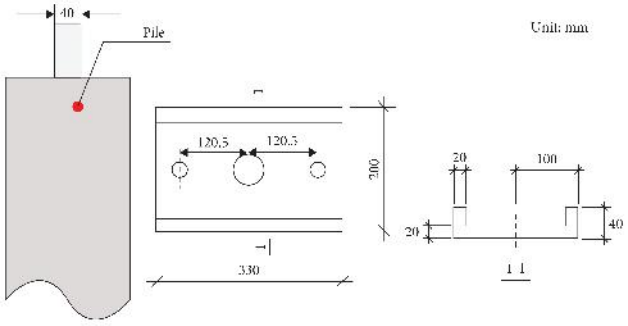

Figure 6: Dimensions of the connecting bolts and steel plates.

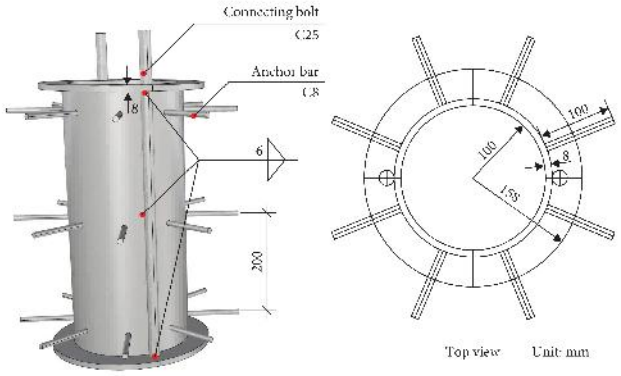

Figure 7: Integrated steel cylinder connection base.

3. Three-Dimensional Finite Element Model

To comprehensively evaluate the bearing performance and load transfer mechanisms of the novel assembled micropile, two distinct numerical models were developed: a static analysis model (SAM) for structural evaluation and a foundation soil interaction analysis model (FSAM) for geotechnical behavior assessment. Corresponding cast-in-situ pile models were established for comparative analysis. The FSAM primarily investigates the bearing characteristics of the innovative micropile under varying load conditions, while the SAM focuses on analyzing stress distribution and deformation patterns within the foundation system under operational loads.

3.1. Finite Element Model

3.1.1. Foundation–Soil Interaction Analysis Model. The micropile configuration features a total length (l_{-L}) of 6500 mm with an effective embedment depth of 6000 mm and a nominal diameter (D) of 200 mm. To minimize boundary effects, the soil domain was dimensioned as 22.5D × 22.5D in lateral extent with a vertical height of 35D [42]. Boundary constraints were implemented with roller supports along lateral surfaces and pinned constraints at the base. Loading was applied through displacement control at the pile head.

The model employs truss elements to simulate reinforcement bars and connection bolts within the steel cylinder, while C3D8R reduced integration hexahedral elements were adopted for other components. The pile–soil interface behavior was characterized using Coulomb's friction law, establishing a linear relationship between tangential friction stress and normal stress [43]. Figure 8 illustrates the developed interaction model between the assembled foundation system and surrounding soil matrix.

3.1.2. Static Analysis Model. The stress and deformation characteristics of the assembled cap and pile–cap connection structure were analyzed using a numerical model with the following specifications: The structural components were dimensioned

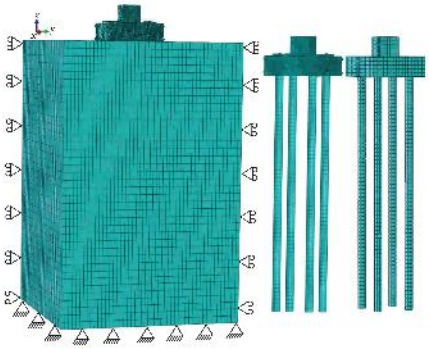

Figure 8: Assembled foundation and soil interaction analysis model.

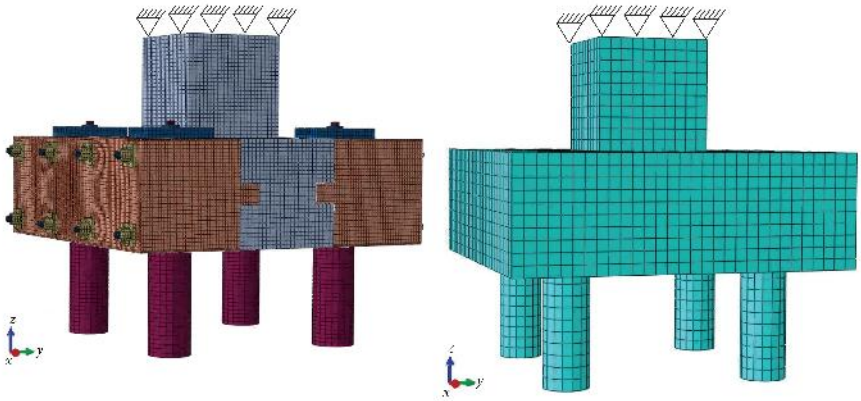

(a) (b)

Figure 9: Static analysis model: (a) assembled foundation model; (b) cast-in-situ pile foundation model.

with a total length (L_S) of 1000 mm and a diameter (D) of 200 mm. Three-dimensional fixed constraints were applied to the top surface of the C-2 model to simulate realistic boundary conditions. The loading configuration was implemented at the pile bottom, with the applied load corresponding to 1/4 of the foundation's design load capacity to ensure conservative structural evaluation.

The connecting bolts in the steel bar and the steel cylinder adopt the Truss element, and the rest of the element types are consistent with the FSAM. Reinforcement bars were fully embedded in the concrete matrix through constraint embedding, and a tie constraint formulation was implemented to ensure proper interaction between prestressed tendons and the cap structure. All remaining contact interfaces were simulated using hard contact formulations with surface to surface discretization to accurately replicate actual working conditions. The friction coefficients were specifically defined as 0.6 between critical interfaces: the connector–cap interface and the pile–steel cylinder interface, based on established experimental data [44]. The comprehensive SAM configuration is visually presented in Figure 9.

3.2. Material Parameters and Loading Scheme. The material parameters and constitutive models for FSAM and SAM are shown in Table 4.

The loading directions are set as compressive, uplift, and horizontal loads. The single horizontal load for SAM is divided into x and y directions. A staged loading process is used, with

Table 4: Material parameters and constitutive models.

Unit	Constitutive model	ρ (kg/m^3)	E (MPa)	v	φ (°)	c (kPa)
Concrete for the cap	Elastoplastic	2.5	31,500	0.2	—	—
Concrete for piles	Elastoplastic	2.5	36,800	0.2		
Reinforcement	Elastoplastic	7.85	200,000	0.3	—	—
Bolt	Elastoplastic	7.85	206,000	0.3	—	—
Prestressed tendon	Elastoplastic	7.85	195,000	0.3		
Soil	Mohr–Coulomb model	1.9	5.0	0.3	25	17.9

Table 5: SAM and FSAM loads.

Compressive load (kN)	Uplift load (kN)	Horizontal load (kN)	
		x	y
900	200	85	85

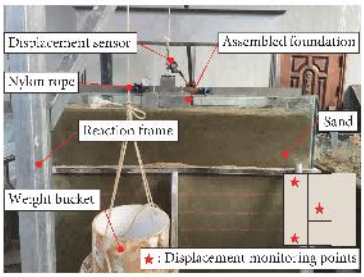

Figure 10: Experimental system.

each stage being 10% of the total design load [45]. The total load for SAM and FSAM is shown in Table 5.

3.3. Experimental Calibration. To validate the reliability of the numerical simulation model, a scale model experimental study was performed on the AF under uplift loading conditions. The test system comprised a scaled micropile, soil medium, test chamber, displacement measurement devices, and loading apparatus, as illustrated in Figure 10. The transparent test chamber, constructed from 10 mm thick tempered glass panels reinforced by a peripheral steel frame, measured 1.5 m (length) × 1.5 m (width) × 1.4 m (height), with a 1.4 m thick soil layer compacted to replicate field conditions. The soil preparation procedure is as follows. Each 5 cm thick soil layer is horizontally compacted, then the surface of each layer is rolled before adding the next layer of soil sample to prevent stratification in the prepared specimen. The same amount of soil is used for each layer to ensure uniform compaction density of the test soil. To ensure testing accuracy, the prepared soil must be left to stand for 24 h. High-precision displacement sensors with a 0–20 mm measurement range and 0.001 mm resolution were deployed to monitor deformation responses.

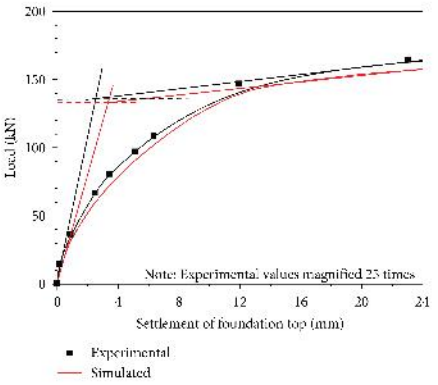

Figure 11: Comparison of experimental and simulated load–displacement curves under uplift load.

In accordance with similarity criteria [46], geometrical scaling of the micropile was implemented at a 1:5 ratio, resulting in prototype-equivalent dimensions of 1200 mm length (L) and 40 mm diameter (D), yielding an effective slenderness ratio (L/D) of 30. The pile tip was positioned 5D above the chamber base, while the lateral clearance between pile and chamber walls maintained a 17D distance to minimize boundary effects [47]. The scaled foundation utilized C60-grade concrete, while the soil medium consisted of river sand containing ≤5% clay content, classified as medium-dense coarse sand based on particle size distribution. Direct shear tests yielded an internal friction angle of 25° and a cohesion of 17.9 kPa for the soil. The loading protocol employed 10 incremental stages, each equivalent to 1/250 of the design uplift load specified in Table 5, culminating in a maximum applied load of 8 kN.

Figure 11 shows the comparison of the experimental and simulation results, which demonstrates strong correlation between experimental and numerical results. The finite element simulation accurately reproduces the experimental load–settlement behavior at the pile head, with measured and predicted ultimate uplift capacities of 136 and 132 kN, respectively. The marginal 2.9% discrepancy between these values confirms the numerical model's fidelity in capturing the system's mechanical response, thereby validating its reliability for engineering analyses.

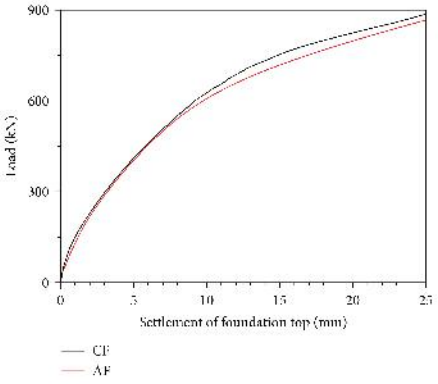

Figure 12: Load–settlement for AF and CF foundations under compressive load. AF, assembled micropile foundation; CF, cast in situ pile foundation.

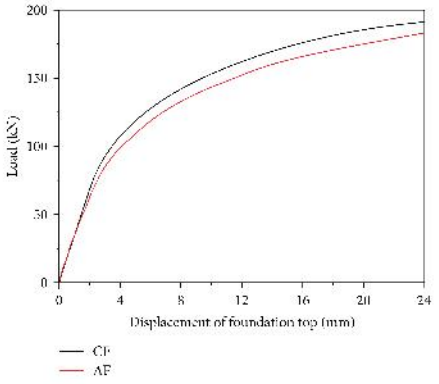

Figure 13: Load–displacement curves for AF and CF under uplift load. AF, assembled micropile foundation; CF, cast-in-situ pile foundation.

4. Results and Discussions

4.1. FSAM Analysis. Figure 12 illustrates the comparative load–displacement behavior of the AF and CF under compressive loading conditions, as derived from FSAM analysis. Both foundations exhibited comparable gradual softening behavior in their load–displacement curves, demonstrating similar post-peak response characteristics. Using the double-tangent method for failure criterion identification, the ultimate compressive bearing capacities of AF and CF are 565 kN and 594 kN, respectively. Compared with CF, the ultimate bearing capacity of AF has only been reduced 4.9%, which is satisfactory in engineering. Despite these differences, the fundamental load transfer mechanisms between the two foundation types showed remarkable consistency under compressive loading. This mechanistic similarity suggests that AFs can serve as viable alternatives to conventional cast-in-situ piles in compression-dominated applications, satisfying standard engineering performance requirements while offering potential advantages in construction efficiency and material optimization.

Figure 13 illustrates the load–displacement characteristics of AF and CF under uplift loading. Notably, the AF specimen demonstrates distinct behavioral differences compared to its cast-in-situ counterpart. Unlike CF's load–displacement curve which exhibits a conventional linear elastic phase, AF's response lacks a clearly defined linear development stage. This divergence arises from the soil-supported cap configuration of AF, which induces a marked displacement acceleration during the initial loading phase. Quantitative analysis reveals that the ultimate compressive bearing capacities of AF and CF are 153 kN and 161 kN, respectively. Compared with CF, the ultimate bearing capacity of AF only has been reduced 5.0%, which is satisfactory in engineering. The observed performance differences stem from fundamental structural distinctions: AF's assembled nature results in reduced structural integrity

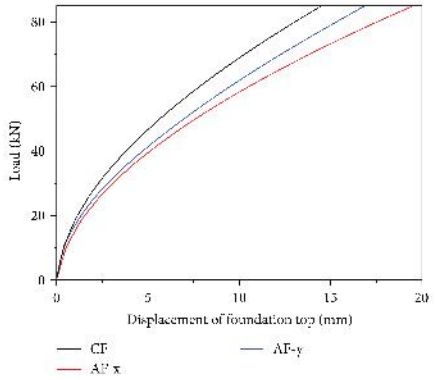

Figure 14: Load displacement curves for AF and CF under horizontal load. AF, assembled micropile foundation; CF, cast in situ pile foundation.

compared to CF's monolithic construction, precipitating earlier nonlinear response initiation under loading. Nevertheless, this assembled configuration demonstrates compensatory advantages through enhanced flexibility, as evidenced by the displacement characteristics during progressive loading stages.

Figure 14 illustrates the load–displacement characteristics of AF and CF under horizontal loading. Both configurations exhibit similar curve progression patterns under increasing horizontal loads. Following standard evaluation criteria [18], the ultimate horizontal bearing capacity was determined at 10 mm horizontal displacement. The analysis reveals that AF demonstrates ultimate bearing capacities of 63 and 64 kN in the x- and y-directions, respectively, showing 7.4% and

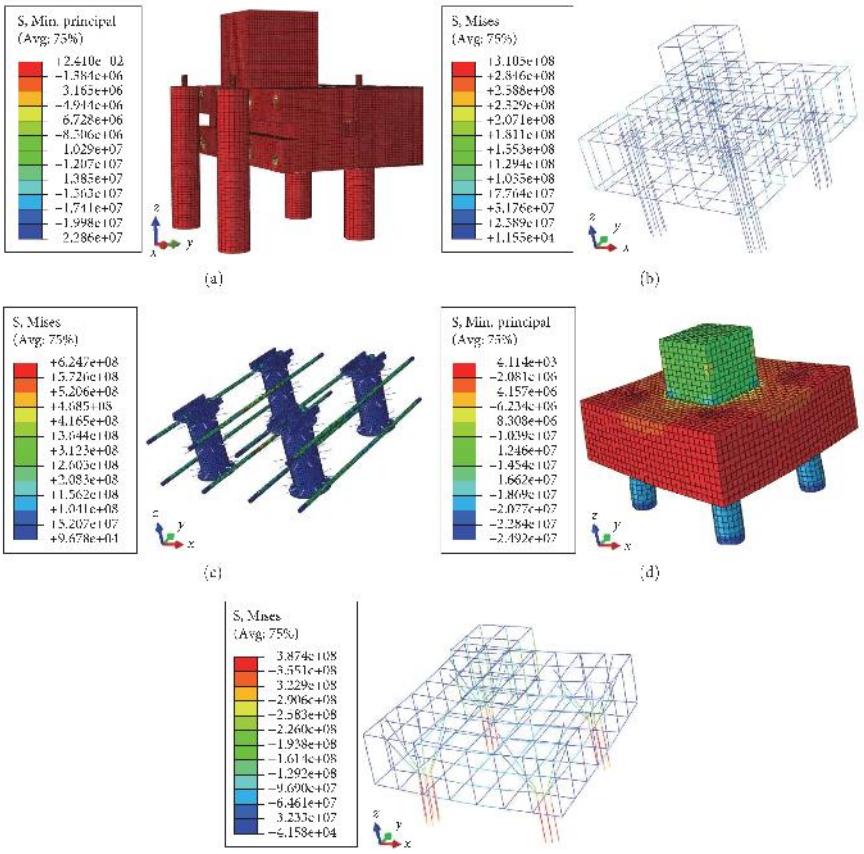

Figure 15: Stress distribution for AF and CF under compressive load. (a) Pressure distribution of concrete in AF. (b) Stress distribution of bars in AF. (c) Stress distribution of connection in AF. (d) Pressure distribution of concrete in CF. (e) Stress distribution of bars in CF. AF, assembled micropile foundation; CF, cast-in-situ pile foundation.

5.9% reductions compared to CF's uniform 68 kN capacity in both directions. This directional dependence in AF's performance indicates slightly superior resistance in the y-direction compared to the x direction.

Notably, despite these capacity variations, the AF maintains comparable bearing behavior to conventional cast in situ foundations under horizontal loading. The soil–structure interaction mechanisms for both foundation types show remarkable similarity, suggesting equivalent load transfer efficiency between the assembled system and traditional cast-in-situ construction. This performance equivalence highlights the technical viability of AFs as a competitive alternative to conventional cast-in-situ solutions.

4.2. SAM Analysis

4.2.1. Stress Distribution. Figure 15 illustrates the comparative stress distribution patterns between AF and CF under compressive loading conditions. A distinct stress redistribution phenomenon is observed in AF concrete compared to CF, with maximum concrete stresses concentrated adjacent to the prestressed tendons while maintaining lower stress levels at other locations. This contrasts with CF's stress pattern, where maximum reinforcement stresses occur at the base pile connection.

The reinforcement stress distribution reveals significant system differences: CF demonstrates higher stress

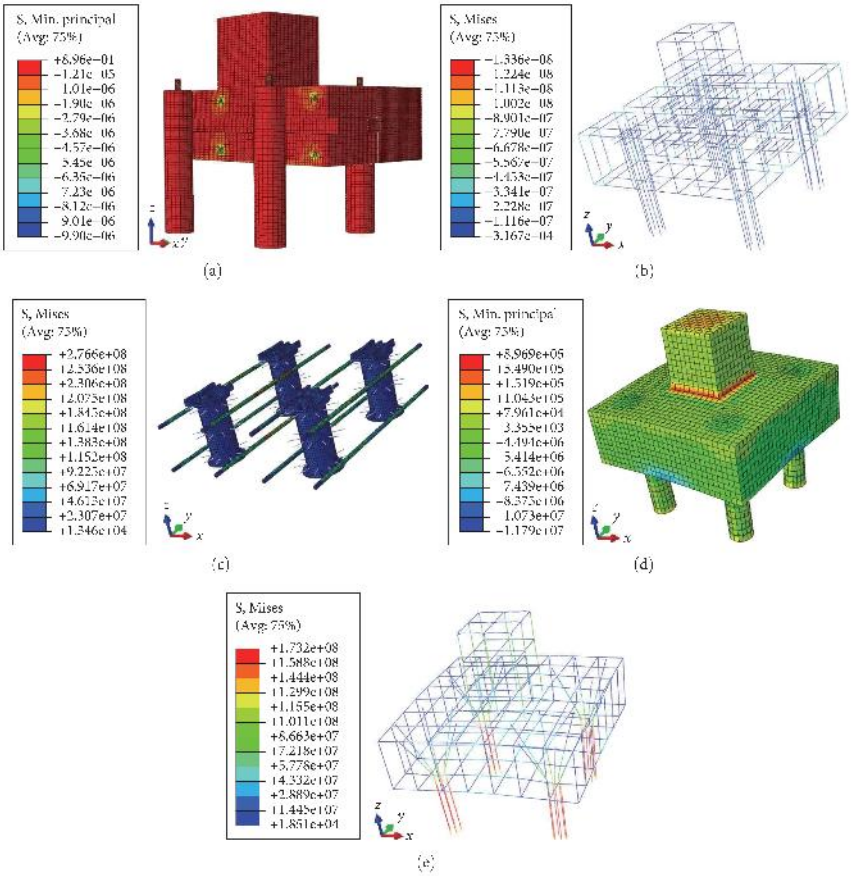

Figure 16: Stress distribution for AF and CF under uplift load. (a) Pressure distribution of concrete in AF. (b) Stress distribution of bars in AF. (c) Stress distribution of connection in AF. (d) Pressure distribution of concrete in CF. (e) Stress distribution of bars in CF. AF, assembled micropile foundation; CF, cast-in-situ pile foundation.

concentrations with a progressive decrease along the height, whereas AF exhibits a more uniform stress distribution across regular reinforcement members. Notably, the maximum reinforcement stress in AF (624.7 MPa at C-2 bottom reinforcement) remains well within the prestressed tendons' yield strength threshold.

The analytical results confirm AF's optimized load transfer mechanism, characterized by two distinct stress concentration zones: primary concentration at the lower prestressed tendons and secondary concentration at structural connectors. This strategic stress distribution offers dual advantages. It not only ensures efficient force transfer through the prestressing system but also localizes maximum stresses at accessible connector locations. Such design intentionality facilitates practical maintenance benefits, particularly enabling straightforward inspection and replacement of critical connection components during service life.

The observed stress patterns effectively demonstrate AF's superior force transfer mechanism compared to conventional systems, confirming its structural efficiency through controlled stress localization and systematic load distribution pathways.

Figure 16 illustrates the stress distribution patterns of AF and CF under uplift loading. Comparative analysis reveals that the stress distribution in both concrete components and conventional reinforcement of AF exhibits remarkable consistency with that observed under compressive loading. This uniform

stress response under vertical loading conditions not only demonstrates structural stability but also validates the reliability and design rationality of the AF system when subjected to uplift forces. Particularly noteworthy is the concentrated principal stress observed in the upper section of AF's prestressed tendons during uplift loading, which effectively demonstrates the structural efficiency of the dual-row prestressed tendon configuration. This targeted stress manifestation confirms the optimized load bearing mechanism achieved through the strategic placement of prestressed reinforcement elements.

Figure 17 illustrates the comparative stress distribution patterns of AF and CF under horizontal loading. For CF, the maximum compressive stress in concrete consistently manifests beneath the pile cap (Figure 17a, d, g). For AF, owing to higher prestressing loads, the maximum compressive stress under multidirectional horizontal loading remains concentrated near the prestressing tendons. While compressive stress at the pile base below the cap is negligible in AF, this region exhibits stress magnitudes comparable to CF. Reinforcement stress patterns near nonprestressed tendons in AF demonstrate remarkable consistency with CF counterparts, suggesting analogous stress distribution mechanisms between assembled and cast-in-situ systems under horizontal loading.

The proposed AF exhibits distinct load transfer characteristics. Vertical load is transmitted from the cap to the pile body primarily through the connecting steel plate interface. Horizontal load is transferred dominantly via frictional interaction between the connecting steel cylinder and pile surface, with secondary transmission (<10% based on stress distribution analysis) occurring through the steel plate connection. Notably, stress concentrations in the assembled system localize at connector interfaces, providing critical insights which are bearing capacity optimization through connector design, failure mode prediction under extreme loading conditions and performance validation of modular connection systems, respectively. This mechanistic divergence highlights the importance of connector design in assembled systems compared to monolithic cast-in-situ foundations while maintaining comparable overall stress distribution characteristics under service loads.

4.2.2. Displacement Distribution. Figure 18 illustrates the vertical displacement patterns at the center of the cap bottom for both AF and CF under compressive loading. The analysis reveals distinct deformation characteristics between the two structures. For CF, the cap center exhibits downward movement (maximum displacement: 0.1 mm) accompanied by upward displacement at the edges (minimum displacement: 0.054 mm), demonstrating a typical bending deformation pattern. AF presents more complex displacement behavior. In the x-direction, seven symmetrically distributed critical points emerge along the cap bottom, corresponding to specific structural features which are the cap center, splice seams, base piles, and midpoints between base piles and cap edges, respectively. Notably, the maximum x-direction displacement (−0.178 mm) occurs at splice seams, while the central displacement (−0.038 mm) remains 63% lower than CF's central displacement. The edge displacement of AF (0.146 mm) exceeds CF's by 46%, indicating enhanced edge deformation.

Y-direction analysis shows significant displacement variations at splice seams, with the vertical displacement at C-2 bottom reaching −0.042 mm (78% higher than CF). However, the cap edge displacement (0.14 mm) reduces to 40% of CF's corresponding value. Comparative analysis demonstrates that while AF exhibits increased overall deformation compared to CF, particularly with more pronounced edge uplift, the absolute deformation magnitudes remain minimal. The y-direction deformation performance surpasses x-direction behavior, suggesting anisotropic mechanical characteristics.

Subsequently, splice seams induce localized stress concentration, contributing to 178% greater displacement than CF at these positions. Base pile locations serve as secondary deformation control points. The symmetrical deformation pattern confirms structural integrity despite localized variations. Anisotropic deformation highlights the importance of directional considerations in structural design. These findings emphasize the significant influence of splice seams and base pile arrangements on AF's deformation characteristics, providing essential insights for composite structure optimization under compressive loads.

Figure 19 illustrates the vertical displacement patterns at the center–bottom position of both AF and CF caps under uplift loading conditions. The analysis reveals distinct deformation characteristics: the CF cap exhibits upward movement at its central region accompanied by downward displacement at the peripheral zones, creating a characteristic inverted hook-shaped deformation profile. The displacement values range between −0.054 mm (maximum) and −0.1 mm (minimum). Similar to the compressive loading scenario, the AF cap demonstrates seven characteristic extremum points in its x-direction displacement pattern under uplift loading, and the positions of each extremum point are the same as those of the CF cap. Notably, while the y-direction displacement distribution at the cap's base presents an inverse pattern compared to compressive loading, the relative displacement magnitudes between the cap's edge and central regions remain comparable. This behavioral consistency confirms that the AF maintains superior mechanical symmetry, demonstrating remarkable adaptability to vertical loading from diverse directional inputs through its coordinated deformation mechanisms.

Figure 20 illustrates the horizontal displacement patterns at the bottom edge of both AF and CF caps under horizontal loading. The analysis reveals distinct behavioral characteristics between the two foundation types. For CF, the cast in situ foundation demonstrates smooth horizontal displacement distribution along the cap bottom edge. A minor displacement reduction (~2.644 mm) is observed near the base pile location. The horizontal displacement values are ~2.644 mm, indicating consistent load transfer through the monolithic structure. For AF behavior in X-direction, significant displacement amplification occurs at splice seams, reaching maximum values of 2.863 mm (C-1) and 2.735 mm (C-2). C-1 exhibits pronounced parabolic deformation near base piles, exceeding CF's displacement by 8%. C-2 shows moderated displacement (3% greater than CF) through prestressed tendon load transfer. For AF behavior in Y-direction, symmetric parabolic displacement forms near base piles with reduced magnitude compared to

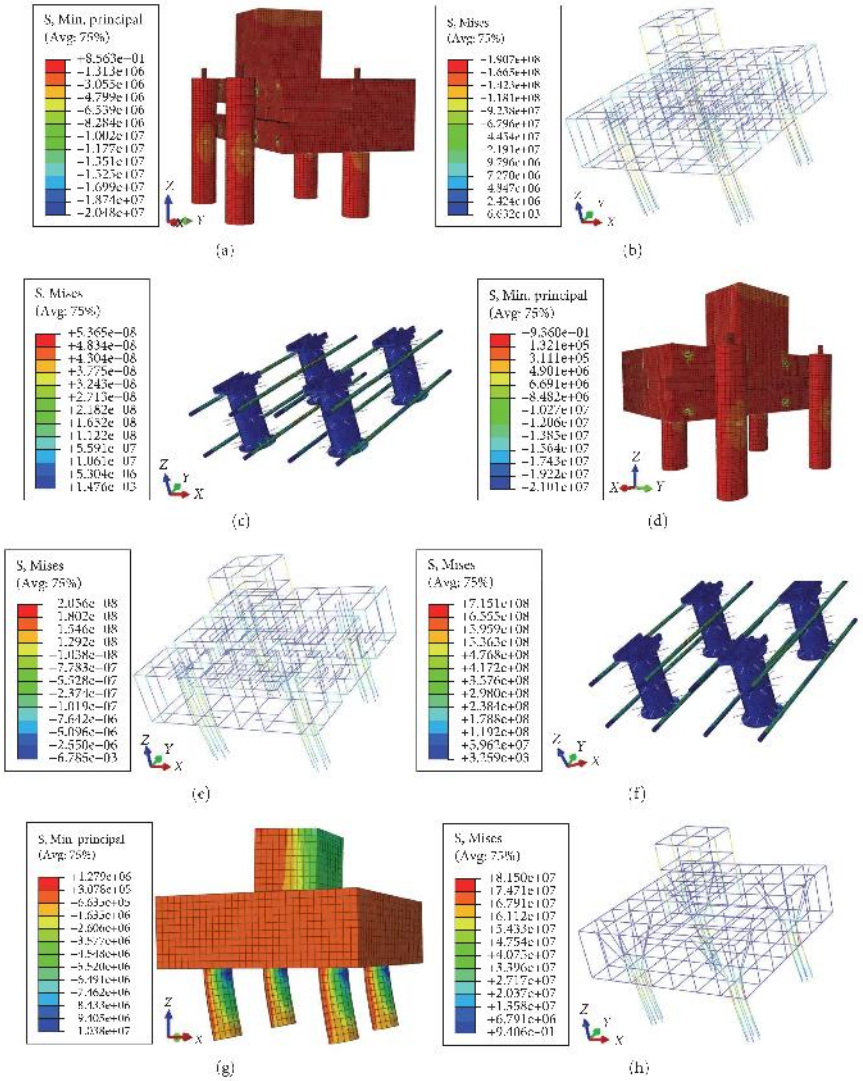

Figure 17: Stress distribution for AF and CF under horizontal load. (a) Pressure distribution of concrete in AF. (b) Stress distribution of bars in AF X-direction. (c) Stress distribution of connection in AF. (d) Pressure distribution of concrete in AF. (e) Stress distribution of bars in AF Y-direction. (f) Stress distribution of connection in AF. (g) Pressure distribution of concrete in CF. (h) Stress distribution of bars in CF. AF, assembled micropile foundation; CF, cast-in-situ pile foundation.

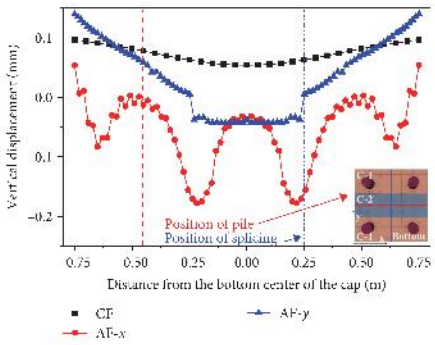

Figure 18: Vertical displacement at the center of the bottom of the cap for AF and CF under compressive load. AF, assembled micropile foundation; CF, cast-in-situ pile foundation.

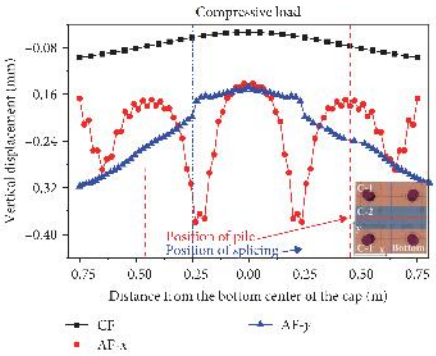

Figure 19: Vertical displacement at the center of the bottom of the cap for AF and CF under uplift load. AF, assembled micropile foundation; CF, cast-in-situ pile foundation.

X-direction. Central cap region demonstrates greater displacement than X-direction counterparts. Maximum displacement remains below X direction peak values. Subsequently, AF's overall horizontal displacement matches CF performance within 3% variation. Effective load transfer mechanism was achieved through prestressed tendon-mediated load distribution from C-2 to C-1 and connector based load transmission from C-1 to base piles.

This comparative study confirms that the AF maintains structural performance parity with traditional cast-in-situ systems while demonstrating unique deformation characteristics attributable to its assembly configuration. Stress concentrations at connector interfaces facilitate post-construction inspection and replacement, demonstrating excellent replaceability. Additionally, the load transfer mechanism of the AF is well-defined, and its structural performance is comparable to that of cast-in-

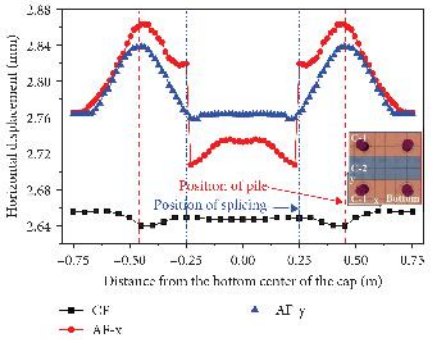

Figure 20: Horizontal displacement at the edge of the bottom of the cap for AF and CF under horizontal load. AF, assembled micropile foundation; CF, cast-in-situ pile foundation.

situ foundations. Therefore, it exhibits high reliability and adaptability in engineering applications.

In summary, under combined vertical and horizontal loading conditions, the novel AF demonstrates optimized stress and displacement distribution characteristics, validating both its mechanical performance and design viability. The advantages of this design are as follows:

4.2.2.1. Stress Localization and Maintenance Advantages. Stress concentrations are intentionally localized at connector interfaces, facilitating targeted inspection and maintenance operations. This design strategy ensures enhanced component replaceability, significantly improving long-term serviceability.

4.2.2.2. Load Transfer Mechanism. The foundation exhibits a well-defined load transfer hierarchy: vertical/horizontal forces → prestressed tendons → bolted connectors → base piles. This systematic force transmission mimics the load path efficiency of cast-in-situ systems.

4.2.2.3. Performance Benchmarking. Structural displacement and stress responses align closely with cast-in-situ foundations, showing deviations within 8% under equivalent loads. Comparable structural performance metrics confirm system reliability while retaining precast advantages (e.g., modular assembly, quality control).

4.2.2.4. Engineering Applicability. Demonstrated stress predictability and component accessibility enable rapid damage diagnosis and localized repairs. The system demonstrates superior structural reliability. This integrated assembled solution successfully balances performance equivalence to conventional methods with the practical benefits of modular construction technology.

4.2.2.5. Economic and Construction Cycle Advantages. Compared to conventional cast-in-situ foundations, the AF enhances construction efficiency by 40%–60% [10, 11, 49] through factory-manufactured standardized components and

dry connection techniques. The lightweight installation equipment significantly reduces transportation and construction challenges in complex terrains (e.g., mountainous areas). Additionally, factory production ensures quality consistency, mitigates defect risks associated with on-site concrete placement, and thereby lowers long term maintenance costs. Although the initial prefabrication costs may be slightly higher, this technology demonstrates notable economic viability and engineering applicability potential.

5. Conclusions

This study proposes a novel AF system designed for OTL applications. Through comprehensive three-dimensional numerical simulations and experimental investigations, the bearing characteristics, stress distribution patterns, and deformation behavior of this innovative foundation system were systematically examined. The principal findings are summarized as follows.

1. The structural configuration demonstrates clear load transfer mechanisms with rational stress distribution characteristics. Vertical loads are primarily transmitted through connecting steel plates, while horizontal loads are effectively transferred via the interface between the connecting steel cylinder and base piles. Stress concentrations are predominantly observed around connector elements and prestressed tendons, creating a maintenance-friendly design that facilitates component inspection and replacement during service life.
2. Under various vertical loading conditions, the foundation exhibits symmetrical stress and displacement distributions. When subjected to horizontal loads from different directions, the lateral displacement patterns of the assembled system show remarkable similarity to those of conventional CFs, and there is only a 3% difference in the displacement in different directions, which indicates excellent directional adaptability and structural stability.
3. Comparative analysis with cast-in-situ piles reveals comparable soil–foundation interaction characteristics for the assembled system. The ultimate bearing capacity under vertical and horizontal loads maintained 95.0% and 92.6% of the performance for cast-in-situ foundations, respectively. While demonstrating slightly higher deformation under equivalent load levels, this reduced stiffness proves advantageous in preventing brittle failure modes.
4. Although current findings are based on finite element simulations and scaled model tests, this research establishes a foundation for future investigations. Full-scale experimental validation and exploration of additional assembled micropile configurations are recommended to further optimize design parameters and advance implementation in power infrastructure projects.

Data Availability Statement

The data presented in this study are available on request from the corresponding author.

Consent

The authors have nothing to report.

Conflicts of Interest

The authors declare no conflicts of interest.

Author Contributions

Linli Bao and Yuesong Zheng: conceptualization. **Zhaoxiang Guo**: methodology. **Yi Zhou**: software. **Zhaoxiang Guo, Dongya Wu**: validation. **Linli Bao**: formal analysis. **Linli Bao**: investigation. **Zhijun Xu**: resources. **Zhaoxiang Guo**: data curation. **Yuesong Zheng, Dongya Wu, Yi Zhou**: writing–original draft preparation. **Zhijun Xu**: supervision. **Bo Xiao, Dongya Wu**: project administration. **Bo Xiao**: funding acquisition. All authors have read and agreed to the published version of the manuscript.

Funding

The research is partially supported by State Grid Henan Electric Power Company Science and Technology Project named Research and Application of Key Technologies for Prefabricated Micro-Pile Foundations in Overhead Transmission Lines, under Grant No. 52171.024000Q.

Acknowledgments

The authors sincerely thank all the respondents for their participation and the organizations for supporting this research.

References

[1] G. L. Kyriakopoulos and G. Arabatzis, "Electrical Energy Storage Systems in Electricity Generation: Energy Policies, Innovative Technologies, and Regulatory Regimes," *Renewable and Sustainable Energy Reviews* 56 (2016): 1044–1067.

[2] G. Arcia-Garibaldi, P. Cruz-Romero, and A. Gómez-Expósito, "Future Power Transmission: Visions, Technologies and Challenges," *Renewable and Sustainable Energy Reviews* 94 (2018): 285–301.

[3] K. Burges, J. Börner, C. Nabe, et al., "Study on the Comparative Merits of Overhead Electricity Transmission Lines versus Underground Cables," *Ecofys Germany GmbH*, 2008.

[4] W. Y. Gu, W. J. Yao, Y. S. Shi, L. Q. Xie, and B. Xue, "Study on Dynamic Stability for the Superlong Pile Foundation of Marine Engineering Structures in Service," *Structures* 41 (2022): 1257–1265.

[5] S. Waldron, J. Smith, K. Taylor, C. McGinnes, N. Roberts, and McCallum, *Repowering Onshore Wind Farms: A Technical and Environmental Exploration of Foundation Reuse* (Centre for Open Science, Construction Scotland Innovation Centre, Glasgow, Scotland, 2018).

[6] Z. Erxian, C. Shuyi, L. Wu, et al., "Bearing Behavior and Mechanism of Variable-Section Anchors in Soil-Rock Composite Foundation," *Rock and Soil Mechanics* 45, no. 7 (2024): 2117–2128.

[7] B. Yuan, J. Liang, B. Zhang, et al., "Optimized Reinforcement of Granite Residual Soil Using a Cement and Alkaline Solution: A Coupling Effect," *Journal of Rock Mechanics and Geotechnical Engineering* 17, no. 1 (2025): 509–523.

[8] B. Yuan, J. Liang, X. Huang, et al., "Eco-Efficient Recycling of Engineering Muck for Manufacturing Low Carbon Geopolymers Assessed Through LCA: Exploring the Impact of Synthesis Conditions on Performance," *Acta Geotechnica* (2024): 1–21.

[9] B. Yuan, W. Chen, Z. Li, et al., "Sustainability of the Polymer SH Reinforced Recycled Granite Residual Soil: Properties, Physicochemical Mechanism, and Applications," *Journal of Soils and Sediments* 23, no. 1 (2023): 246–262.

[10] A.-A. Zekavati, A. Khodaverdian, M.-A. Jafari, and A. Hosseini, "Investigating Performance of Micropiled Raft in Foundation of Power Transmission Line Towers in Cohesive Soil: Experimental and Numerical Study," *Canadian Geotechnical Journal* 55, no. 3 (2018): 312–328.

[11] L. Wen, G. Kong, H. Abuel-Naga, Q. Li, and Z. Zhang, "Rectification of Tilted Transmission Tower Using Micropile Underpinning Method," *Journal of Performance of Constructed Facilities* 34, no. 1 (2020): 04019110.

[12] D. Cheng, Y. P. Zhu, L. P. Wu, G. L. Ran, A. P. Huang, and X. H. Yang, "Buckling Analysis of Micro Steel Pipe Piles in Soil Under Axial Load," *Engineering Mechanics* 42 (2024): 1–15.

[13] A. Misra, C. H. Chen, R. Oberoi, and A. Kleiber, "Simplified Analysis Method for Micropile Pullout Behavior," *Journal of Geotechnical and Geoenvironmental Engineering* 130, no. 10 (2004): 1024–1033.

[14] D. R. Shields, "Buckling of Micropiles," *Journal of Geotechnical and Geoenvironmental Engineering* 133, no. 3 (2007): 334–337.

[15] G. L. You, K. Miura, and M. Ishito, "Behavior of Micropile Foundations Under Inclined Loads in Laboratory Tests," *Lowland Technology International* 5, no. 2 (2003): 16–26.

[16] B. Sharma, "A Model Study of Micropiles Subjected to Lateral Loading and Oblique Pull," *Indian Geotechnical Journal* 41, no. 4 (2011): 196–205.

[17] J. Gong, R. P. Chen, Y. M. Chen, G. M. Cheng, and J. G. Ying, "Prototype Testing Study on Micropiles Under Lateral Loading," *Chinese Journal of Rock Mechanics and Engineering* 23, no. 20 (2004): 3541–3546.

[18] T. D. Richards Jr. and M. J. Rothbauer, "Lateral Loads on Pin Piles (Micropiles)," in *GeoSupport 2004: Drilled Shafts, Micropiling, Deep Mixing, Remedial Methods, and Specialty Foundation Systems*, (American Society of Civil Engineers, 2004): 158–174.

[19] C. Cui, Y. Qi, K. Meng, Y. You, Y. Liang, and C. Xu, "A New Analytical Solution for Horizontal Vibration of Floating Pile in Saturated Soil Based on ESSP Method," *Soil Dynamics and Earthquake Engineering* 187 (2024): 108960.

[20] B. Sharma, S. Sarkar, and Z. Hussain, "A Study of Parameters Influencing Efficiency of Micropile Groups," in *Ground Improvement Techniques and Geosynthetics*, ed. T. Thyagaraj, 14, (Springer, Singapore, 2019): 11–18.

[21] Z. Hussain, B. Sharma, and T. Rahman, "Micropile Group Behaviour Subjected to Lateral Loading," *Innovative Infrastructure Solutions* 4, no. 1 (2019): 1–9.

[22] D. Kyung, D. Kim, G. Kim, and J. Lee, "Vertical Load-Carrying Behavior and Design Models for Micropiles Considering Foundation Configuration Conditions," *Canadian Geotechnical Journal* 54, no. 2 (2017): 234–247.

[23] H. Moradi Moghaddam, M. Keramati, A. Ramesh, and R. Naderi, "Experimental Evaluation of the Effects of Structural Parameters, Installation Methods and Soil Density on the Micropile Bearing Capacity," *International Journal of Civil Engineering* 19, no. 11 (2021): 1313–1325.

[24] L. Hong, X. Wang, W. Zhang, Y. Li, R. Zhang, and C. Chen, "System Reliability Based Robust Design of Deep Foundation Pit considering Multiple Failure Modes," *Geoscience Frontiers* 15, no. 2 (2024): 101761.

[25] W. Zhang, R. Huang, J. Xiang, and N. Zhang, "Recent Advances in Bio-Inspired Geotechnics: From Burrowing Strategy to Underground Structures," *Gondwana Research* 130 (2024): 1–17.

[26] F. Q. Wu, W. Y. Chen, Y. S. Li, R. J. Liu, and Y. Yan, "Mountain Micro Pile Drilling Rig and Micro Pile Foundation Construction Technology," *Advances in Transdisciplinary Engineering* 58 (2024): 59–66.

[27] W. L. Xiong, Z. H. Li, D. Hu, and F. Li, "Performance Analysis of Pile Group Installation in Saturated Clay," *Applied Sciences* 14, no. 18 (2024): 8321.

[28] W. Wang, Y. Gao, Z. Wang, L. Zhang, Z. An, and S. Shao, "An Experimental Study on Plate Splicing of Prefabricated Plate Foundation," *Buildings* 13, no. 8 (2023): 2114.

[29] X. Yunsheng and Z. Kai, "Research on the Application of Wheel Pile Foundation for Transmission Lines," *Journal of Engineering and Technology Science* 3, no. 6 (2020): 7–13.

[30] M. Zhou, X. Zhao, J. Song, Z. Xu, S. Yin, and G. Zhu, "Seismic Performance of Precast UHPC Pipe Pile With Two Pile Cap Beam Connection Types: An Experimental and Numerical Study," *Soil Dynamics and Earthquake Engineering* 186 (2024): 108900.

[31] W. Chen, F. Xiong, Y. Lu, et al., "Experimental Investigation of the Seismic Performance of a Novel Bolt-Assembled Precast Panel Building Structure," *Journal of Earthquake and Tsunami* 13, no. 03n04 (2019): 1940008.

[32] S.-F. Jiang, H.-L. Song, Z.-H. Bian, J. Zhao, and S.-H. Lian, "Experimental and Numerical Study on the Shear Strength of New Bolted Connection Assembled Shear Wall," *Journal of Building Engineering* 69 (2023): 106139.

[33] R. Burak, B. Hall, and K. Parker, "Designing for Adaptability, Disassembly, and Deconstruction," *Pci Journal* 55, no. 3 (2010): 40–43.

[34] P. K. Aninthaneni and R. P. Dhakal, "Demountable Precast RC Frame Building System for Seismic Regions," in *Proceedings of the International Conference on Earthquake Engineering and Seismology (IZIIS 50)*, (Christchurch, New Zealand: Springer Nature, 2016): 12–16.

[35] H. Jiang, Q. Li, W. Jiang, and D. Y. Zhang, "Study on Seismic Performance of Connection Joint Between Prefabricated Prestressed Concrete Beams and High Strength Reinforcement-Confined Concrete Columns," *Steel and Composite Structures* 21, no. 2 (2016): 343–356.

[36] L. Li, Z. Zhang, W. Zu, P. Li, and W. Gong, "Multiphysics Simulation of Frost Heave in Unsaturated Road Systems Under Covering Effect," *Transportation Geotechnics* 51 (2025): 101526.

[37] W. Sun, H. liu, W. Zhang, S. liu, and L. Han, "Determination of Groundwater Buoyancy Reduction Coefficient in Clay: Model Tests, Numerical Simulations and Machine Learning Methods," *Underground Space* 13 (2023): 228–240.

[38] W. Sun, F. Han, Y. Zhang, W. Zhang, R. Zhang, and W. Su, "Experimental Assessment of Structural Responses of Tunnels Under the Groundwater Level Fluctuation," *Tunnelling and Underground Space Technology* 137 (2023): 105138.

[39] W. Sun, H. Liu, W. Zhang, S. Liu, and X. Gao, "Investigation on Overburden Thickness considering Face and Anti-Floating Stability of Shallow Shield Tunnel," *Computers and Geotechnics* 160 (2023): 105562.

[40] Ministry of Housing and Urban-Rural Development of the People's Republic of China, *Code for Design of Concrete Structures (GB50010 2019)* (China Architecture & Building Press, Beijing, 2019).

[41] Ministry of Housing and Urban Rural Development of the People's Republic of China, *Standard for Seismic Design of Prestressed Concrete Structures (JGJ/T140-2019)* (China Architecture & Building Press, Beijing, 2019).

[42] L. Chen and H. G. Poulos, "Analysis of Pile-Soil Interaction Under Lateral Loading Using Infinite and Finite Elements," *Computers and Geotechnics* 15, no. 4 (1993): 189–220.

[43] Y. Hong, B. He, L. Z. Wang, Z. Wang, C. W. W. Ng, and D. Mašín, "Cyclic Lateral Response and Failure Mechanisms of Semi-Rigid Pile in Soft Clay: Centrifuge Tests and Numerical Modelling," *Canadian Geotechnical Journal* 54, no. 6 (2017): 806–824.

[44] Z. Zhuang, F. Zhang, and S. Cong, *ABAQUS Nonlinear Finite Element Analysis and Examples* (Science Press, Beijing, 2005).

[45] China Academy of Building Research, *Technical Code for Building Pile Foundations (JGJ 94-2018)* (China Architecture & Building Press, Beijing, 2018).

[46] S. Iai, "Similitude for Shaking Table Tests on Soil Structure Fluid Model in 1g Gravitational Field," *Soils and Foundations* 29, no. 1 (1989): 105–118.

[47] J. Dong, F. Chen, M. Zhou, and X. Zhou, "Numerical Analysis of the Boundary Effect in Model Tests for Single Pile Under Lateral Load," *Bulletin of Engineering Geology and the Environment* 77, no. 3 (2018): 1057–1068.

[48] Ministry of Housing and Urban-Rural Development of the People's Republic of China, *Code for Design of Building Foundation (GB 50007-2011)* (China Architecture & Building Press, Beijing, 2019).

[49] L. Wen, G. Kong, Q. Li, and Z. Zhang, "Equivalent Diameter of Grouted Micropile Embedded in Marine Soft Clay Under Lateral Load," *Proceedings of the Institution of Civil Engineers-Geotechnical Engineering* 173, no. 1 (2020): 3–12.

检 索 证 明

经 检 索 《 Science Citation Index Expanded 》（SCI-EXPANDED）数据库、《Journal Citation Reports》（JCR）数据库和《中国科学院文献情报中心期刊分区表升级版》，以下 1 篇文献的收录简要信息、期刊的影响因子、分区如下：

标题: Characteristics Investigation on Bearing Performance of a Novel Assembled Micropile Foundation in Overhead Transmission Lines

作者: Zheng, YS (Zheng, Yuesong);Bao, LL (Bao, Linli);Guo, ZX (Guo, Zhaoxiang);Zhou, Y (Zhou, Yi);Wu, DY (Wu, Dongya);Wang, WH (Wang, Wenhao);Xiao, B (Xiao, Bo);Xu, ZJ (Xu, Zhijun)

来源出版物: ADVANCES IN CIVIL ENGINEERING 卷:2025 期:1

DOI:10.1155/adce/39562372025

Web of Science 核心合集中的"被引频次"：0 次

期刊《ADVANCES IN CIVIL ENGINEERING》2023 年影响因子为 1.5

2023 年 JCR 分区如下：

JCR® 类别	类别中的排序	JCR 分区
ENGINEERING, CIVIL	115/182	Q3
CONSTRUCTION & BUILDING TECHNOLOGY	54/92	Q3

经检索《中国科学院文献情报中心期刊分区表升级版》，2025 年分区如下：

刊名	Advances in Civil Engineering
年份	2025
ISSN	1687-8086
Review	否
Open Access	是
Web of Science	SCIE

学科		分区	Top 期刊
大类	工程技术	4	否
小类:	CONSTRUCTION & BUILDING TECHNOLOGY 结构与建筑技术	4	-
小类:	ENGINEERING, CIVIL 工程：土木	4	-

特此证明

（详细内容见附件）

河南工业大学图书馆

检索人：张华静

2025 年 06 月 17 日

地址：河南工业大学图书馆 10 楼 1004 室 电话：037167756359

检索邮箱：hgdcx@hautedu.cn 科技查新邮箱：hgdcxz@haut.edu.cn

河南工业大学图书馆检索证明

第 1 条，共 1 条

标题: Characteristics Investigation on Bearing Performance of a Novel Assembled Micropile Foundation in Overhead Transmission Lines

作者: Zheng, YS (Zheng, Yuesong);Bao, LL (Bao, Linli);Guo, ZX (Guo, Zhaoxiang);Zhou, Y (Zhou, Yi);Wu, DY (Wu, Dongya);Wang, WH (Wang, Wenhao);Xiao, B (Xiao, Bo);Xu, ZJ (Xu, Zhijun)

来源出版物: ADVANCES IN CIVIL ENGINEERING **卷:** 2025 **期:**1 **DOI:** 10.1155/adce/3956237 **出版年:** 2025

Web of Science 核心合集中的 "被引频次": 0

被引频次合计: 0

使用次数（最近 180 天): 0

使用次数（2013 年至今): 0

引用的参考文献数: 49

摘要: It is challenging to develop a widely accepted construction method of micropile foundation (MPF) for transmission line projects in complex terrains. A novel assembled MPF was proposed to address this challenge, and its characteristics of bearing performance were investigated assisted with model experiments and three-dimensional numerical simulations. Results show that the ultimate bearing capacity under vertical and horizontal loads maintained 95.0% and 92.6% of the performance for cast-in-situ foundations, respectively. Pronounced stress concentrations occur near prestressed tendons and connectors, creating visible load path indicators that enable real-time structural health monitoring and targeted component replacement. Vertical loads are effectively transferred from prestressed tendons to shear keys, and then to connecting steel plates. Horizontal load resistance primarily relies on steel cylinder-pile interaction, demonstrating less than 3% directional displacement variation, comparable to cast-in-situ foundation integrity. The assembled connection system achieves consistent quality control through factory-manufactured components. The modular nature and standardized connections significantly advance the industrialization of power infrastructure construction.

入藏号: WOS:001501612900001

语言: English

文献类型: Article

作者关键词: assembled micro-pile;bearing performance;load transfer mechanism;overhead transmission lines;three-dimensional numerical simulation

KeyWords Plus: MODEL TESTS; PILE; TECHNOLOGIES

地址: [Zheng, Yuesong; Xiao, Bo] State Grid Henan Econ Res Inst, Zhengzhou 450052, Peoples R China;[Bao, Linli; Zhou, Yi; Wu, Dongya; Wang, Wenhao] State Grid Henan Elect Power Co, Zhengzhou 450000, Peoples R China;[Guo, Zhaoxiang; Xu, Zhijun] Henan Univ Technol, Sch Civil Engn, Zhengzhou 450001, Peoples R China

通讯作者地址: [Xu, Zhijun] (corresponding author), Henan Univ Technol, Sch Civil Engn, Zhengzhou 450001, Peoples R China

电子邮件地址: xuzhijun@haut.edu.cn

出版商:WILEY

出版商地址: 111 RIVER ST, HOBOKEN 07030-5774, NJ USA

Web of Science Index : 《Science Citation Index Expanded》（SCI-EXPANDED）

Web of Science 类别: Construction & Building Technology;Engineering, Civil

研究方向: Construction & Building Technology;Engineering

IDS 号:3JE1D

ISSN: 1687-8086

eISSN: 1687-8094

来源出版物页码计数: 17

基金资助致谢: The authors sincerely thank all the respondents for their participation and the organizations for supporting this research.

基金资助机构	授权号
State Grid Henan Electric Power Company Science and Technology	

ESI 高被引论文: N

ESI 热点论文: N

输出日期: 2025 年 06 月 17 日

检 索 证 明

经检索《Science Citation Index Expanded》（SCI-EXPANDED）数据库、《Journal Citation Reports》（JCR）数据库和《中国科学院文献情报中心期刊分区表升级版》，以下1篇文献的收录简要信息、期刊的影响因子、分区如下：

标题: Characteristics Investigation on Bearing Performance of a Novel Assembled Micropile Foundation in Overhead Transmission Lines

作者: Zheng, YS (Zheng, Yuesong);Bao, LL (Bao, Linli);Guo, ZX (Guo, Zhaoxiang);Zhou, Y (Zhou, Yi);Wu, DY (Wu, Dongya);Wang, WH (Wang, Wenhao);Xiao, B (Xiao, Bo);Xu, ZJ (Xu, Zhijun)

来源出版物: ADVANCES IN CIVIL ENGINEERING 卷:2025 期:1

DOI:10.1155/adce/39562372025

Web of Science 核心合集中的"被引频次": 0 次

期刊《**ADVANCES IN CIVIL ENGINEERING**》**2023** 年影响因子为 **1.5**

2023 年 **JCR** 分区如下：

JCR® 类别	类别中的排序	**JCR** 分区
ENGINEERING, CIVIL	115/182	Q3
CONSTRUCTION & BUILDING TECHNOLOGY	54/92	Q3

经检索《中国科学院文献情报中心期刊分区表升级版》，**2025** 年分区如下：

刊名	Advances in Civil Engineering
年份	2025
ISSN	1687-8086
Review	否
Open Access	是
Web of Science	SCIE

学科		分区	Top 期刊
大类	工程技术	4	否
小类:	CONSTRUCTION & BUILDING TECHNOLOGY 结构与建筑技术	4	-
小类:	ENGINEERING, CIVIL 工程：土木	4	-

特此证明

（详细内容见附件）

河南工业大学图书馆

检索人：张华静

2025 年 06 月 17 日

地址：河南工业大学图书馆 10 楼 1004 室 电话：037167756359

检索邮箱：hgdcx@hautedu.cn 科技查新邮箱：hgdcxz@haut.edu.cn

河南工业大学图书馆检索证明

第 1 条，共 1 条

标题: Characteristics Investigation on Bearing Performance of a Novel Assembled Micropile Foundation in Overhead Transmission Lines

作者: Zheng, YS (Zheng, Yuesong);Bao, LL (Bao, Linli);Guo, ZX (Guo, Zhaoxiang);Zhou, Y (Zhou, Yi);Wu, DY (Wu, Dongya);Wang, WH (Wang, Wenhao);Xiao, B (Xiao, Bo);Xu, ZJ (Xu, Zhijun)

来源出版物: ADVANCES IN CIVIL ENGINEERING **卷:** 2025 **期:**1 **DOI:** 10.1155/adce/3956237 **出版年:** 2025

Web of Science 核心合集中的 "被引频次": 0

被引频次合计: 0

使用次数 (最近 180 天): 0

使用次数 (2013 年至今): 0

引用的参考文献数: 49

摘要: It is challenging to develop a widely accepted construction method of micropile foundation (MPF) for transmission line projects in complex terrains. A novel assembled MPF was proposed to address this challenge, and its characteristics of bearing performance were investigated assisted with model experiments and three-dimensional numerical simulations. Results show that the ultimate bearing capacity under vertical and horizontal loads maintained 95.0% and 92.6% of the performance for cast-in-situ foundations, respectively. Pronounced stress concentrations occur near prestressed tendons and connectors, creating visible load path indicators that enable real-time structural health monitoring and targeted component replacement. Vertical loads are effectively transferred from prestressed tendons to shear keys, and then to connecting steel plates. Horizontal load resistance primarily relies on steel cylinder-pile interaction, demonstrating less than 3% directional displacement variation, comparable to cast-in-situ foundation integrity. The assembled connection system achieves consistent quality control through factory-manufactured components. The modular nature and standardized connections significantly advance the industrialization of power infrastructure construction.

入藏号: WOS:001501612900001

语言: English

文献类型: Article

作者关键词: assembled micro-pile;bearing performance;load transfer mechanism;overhead transmission lines;three-dimensional numerical simulation

KeyWords Plus: MODEL TESTS; PILE; TECHNOLOGIES

地址: [Zheng, Yuesong; Xiao, Bo] State Grid Henan Econ Res Inst, Zhengzhou 450052, Peoples R China;[Bao, Linli; Zhou, Yi; Wu, Dongya; Wang, Wenhao] State Grid Henan Elect Power Co, Zhengzhou 450000, Peoples R China;[Guo, Zhaoxiang; Xu, Zhijun] Henan Univ Technol, Sch Civil Engn, Zhengzhou 450001, Peoples R China

通讯作者地址: [Xu, Zhijun] (corresponding author), Henan Univ Technol, Sch Civil Engn, Zhengzhou 450001, Peoples R China

电子邮件地址: xuzhijun@haut.edu.cn

出版商:WILEY

出版商地址: 111 RIVER ST, HOBOKEN 07030-5774, NJ USA

Web of Science Index : 《Science Citation Index Expanded》（SCI-EXPANDED）

Web of Science 类别: Construction & Building Technology;Engineering, Civil

研究方向: Construction & Building Technology;Engineering

IDS 号:3JE1D

ISSN: 1687-8086

eISSN: 1687-8094

来源出版物页码计数: 17

基金资助致谢: The authors sincerely thank all the respondents for their participation and the organizations for supporting this research.

基金资助机构	授权号
State Grid Henan Electric Power Company Science and Technology	

ESI 高被引论文: N

ESI 热点论文: N

输出日期: 2025 年 06 月 17 日

.

12.中小容量家用屋顶型光伏发电并网关键技术应用研究

ELECTRICAL EQUIPMENT AND ECONOMY
电气技术与经济
◎国际标准刊号：ISSN 2096-4978 ◎国内统一刊号：CN10-1539/TM ◎邮发代号：80-694 2024年第10期 总第50期

电气技术与经济 ELECTRICAL EQUIPMENT AND ECONOMY 2024年第十期 总第50期 机械工业北京电工技术经济研究所

电气技术与经济 10

2024年第10期 总第50期
（2024年10月20日）

ELECTRICAL EQUIPMENT AND ECONOMY（原《电工文摘》）

主管：中国机械工业联合会
主办：机械工业北京电工技术经济研究所
出版：《电气技术与经济》编辑部
社址：北京市丰台区南四环西路188号12区30号楼
邮编：100070

电话：（010）68218642 68163105
Email：dqjsyjj@vip.126.com
在线投稿：https://publish.cnki.net/dgwz

ISSN 2096-4978
CN10-1539/TM

邮发代号：80-694
定价：88元
广告许可证：京丰工商广登字20170140号

印刷：北京富泰印刷有限责任公司

扫码获取更多《电气技术与经济》最新消息

研究与开发

技术与应用

产品与解决方案

中小容量家用屋顶型光伏发电并网关键技术应用研究

王春红[1]　翁玉娟[2]
（1.郑州电力职业技术学院　2.郑州工商学院基础教学部）

摘　要：当下中小容量家用屋顶型光伏发电并网系统的建设和运行仍面临一系列挑战，如电网接入稳定性、功率调节问题和安全性等方面的技术难题。本文首先简要介绍了光伏发电的构成，然后了解网光伏发电系统的具体结构和设计原则，该系统能够节省了蓄能的成本，是实现电能输出的关键环节。其次选择合适的太阳能电池组件和光伏阵列倾角设计，并对发电量进行准确运算。分析结果表明，随着倾角从0°至30°的增加，平均每日发电量逐渐增加，达到峰值20.1/kWh。然而，当倾角继续增加至40°至90°时，平均每日发电量逐渐下降。PCC电压、电流频率均为50Hz，功率因数保持在0.98。这些结果为选择最佳的光伏板倾角提供了重要参考，有助于优化系统的发电性能，提高能源利用效率。

关键词：家用屋顶型；光伏发电；并网系统；电池组件；功率因数

0　引言

随着全球对清洁能源需求的不断增长以及环境保护意识的提高，光伏发电作为一种可再生、清洁的能源形式备受关注。在家庭屋顶光伏发电领域，其具有资源广泛、可再生性强、分布广泛等诸多优势，逐渐成为了重要的能源供应形式[1]。特别是在家庭屋顶光伏发电领域，其具有资源广泛、可再生性强以及分布广泛等优势，逐渐成为了一种重要的能源供应形式[2]。但由于家庭光伏系统需要接入电网，其技术要求相对较高。电网接入稳定性是一个重要考量因素，需要确保光伏系统的并网操作不会对电网造成不稳定的影响，同时兼顾系统自身的稳定性和安全性。其次，光伏发电系统的功率调节问题也备受关注[3]。光伏发电具有间歇性和波动性，需要有效的调节控制手段来应对不同的工作条件和负载需求，保证系统的可靠运行和发电效率。此外，安全性是光伏发电并网系统设计的关键考虑因素之一，需要防范火灾、电气安全等潜在风险，保障用户和电网的安全。

本文简要介绍了光伏发电的组成，然后分析电网光伏发电系统的具体结构和设计原理。光伏发电系统的并网技术是实现电能输出的关键环节。对光伏发电并网系统的主要设备进行设计与选择，以实现最佳的发电效果。构建出小容量家庭屋顶分布式光伏发电并网结构，能够准确地描述光伏电源出力的随机性。通过输出特性分析，获取输出功率与光强之间存在近似关系。通过计算太阳辐射强度的函数分布，可以准确地描述分布式并网光伏系统中有功功率的概率密度分布，以实现最佳的并网效果。

1　光伏发电及并网技术

1.1　光伏发电

光伏发电系统由光伏电池板、逆变器、电网连接设备等组成，光伏电池板通过光伏效应将阳光转化为直流电，逆变器将直流电转化为交流电，然后与电网连接，将发电的电能输入到电网中供电使用[4]。光伏发电系统结果如图1所示，光伏发电系统包括太阳光、太阳电池方阵、直流配电柜、逆变器、交流配电柜、控制器和蓄电池等组件。太阳光是系统的能源来源，通过太阳电池方阵接收并转化为直流电能。直流配电柜用于集中管理和分配太阳能电池板产生的直流电能，确保安全传输和分配。逆变器是关键设备，将直流电能转换为交流电能，

基金项目：本文系河南省高等学校重点科研项目“中小容量家用屋顶型光伏发电并网关键技术应用研究”（项目编号：23B480007教科技〔2022〕309号文件）阶段性成果之一

以便与电网连接并供电。交流配电柜将逆变器输出的交流电能进行分配和传输，满足家庭或其他用电设备的需求。控制器负责监测系统性能、调节电流和电压等参数，保证系统稳定运行和安全性。蓄电池用于存储多余电能，并在需要时提供备用电力，应对紧急情况如电网断电。这些组件共同构成了光伏发电系统，通过协同作用实现了太阳能转化为电能的过程，为可持续能源供应提供了可靠解决方案[5]。此外，光伏发电系统的安装、调试和维护也是关键的技术环节，需要对家庭屋顶结构、电网接入条件等因素进行充分考虑，确保系统的正常运行和安全性。

图1　光伏发电系统结构

1.2　光伏发电并网技术

光伏发电并网技术是一种关键的清洁能源应用技术，其核心概念是将家庭屋顶上安装的光伏发电系统与电网相连接，实现太阳能发电系统的发电功率与电网进行并网输出，以供应家庭用电并将多余的电力输送到电网中。这项技术在促进清洁能源利用、减少碳排放以及提高能源利用效率等方面具有重要意义[6]。并网发电系统结构如图2所示，在光伏发电并网系统中，典型的结构包括电抗器、MPPT最大功率点跟踪、驱动电路、DC/DC变换器和PWM控制器等关键组件。首先，电抗器作为重要的电力调节器件，用于调节光伏发电系统的电流和电压，确保系统稳定运行并满足电网接入要求。MPPT最大功率点跟踪技术是一种先进的控制算法，能够实时追踪太阳能电池的最大功率点，从而提高光伏系统的发电效率，最大限度地利用太阳能资源。驱动电路负责控制光伏发电系统中各个组件的电路，例如逆变器或者充放电控制器的驱动电路，确保系统稳定运行和高效工作。DC/DC变换器则用于直流到直流的转换，调节光伏发电系统输出的直流电压和电流，以适应电网或充电要求，保障系统运行的稳定性和可靠性[7]。最后，PWM控制器则是一种脉宽调制控制器，用于调节光伏发电系统输出的电压和电流，实现更精确的功率控制，提高系统的稳定性和性能。

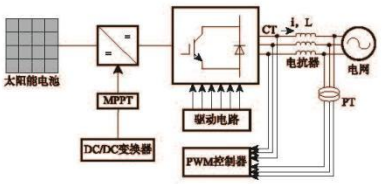

图2　并网光伏发电系统结构

1.3　光伏发电系统的设计原则

光伏发电系统设计以使整个系统具有安全可靠性、先进性和示范性等特性为基本原则，具体如下：

（1）安全可靠性。这涉及到光伏组件的选择和布置、逆变器的质量和效率、系统的安全保护装置等方面，以防止因天气变化或其他外部因素导致系统故障或损坏，确保系统在各种环境条件下能够稳定运行并长期可靠地输出电力[8]。

（2）先进实用性。选用高效的太阳能电池板和逆变器、采用先进的电池管理系统和电网接入技术、优化系统的布局和结构等措施，以提高系统的整体性能并降低系统的投资和运维成本。

（3）扩充性和灵活性。光伏发电系统的设计应具备一定的适应性，能够根据家庭屋顶的空间和条件进行灵活布局和配置。这意味着系统组件应选择灵活多样，能够适应不同的屋顶形状、朝向和倾角，以最大程度地利用太阳能资源。

1.4　主要设备的设计与选择

1.4.1　太阳能电池组件

太阳能电池组件作为将太阳光能转化为电能的核心部件，在光伏发电系统中具有至关重要的作用。其构成通常包括太阳能电池芯片、电池背板、玻璃罩板、防反射膜和边框等要素。其中，太阳能电池芯片是最关键的部分，负责将光能转换为电能。光伏电池的理想转换效率：

$$\eta = \frac{P_{max}}{E_{sun} \times A} \tag{1}$$

式中，η为光伏电池的理想转换效率，表示光伏电池将太阳光能转化为电能的效率，通常以百分比形式表示。P_{max}为光伏电池的最大输出功率，单位为W。E_{sun}为单位面积太阳光照强度，以W/m²表示。A为光伏电池的有效面积m²。

通过计算光伏电池的理想转换效率，可以评估其在特定光照条件下的性能表现。这对于光伏发电系统的设计和优化至关重要。理想情况下，光伏电池的理想转换效率能够达到其最大值，这取决于光伏电池的材料特性和工作环境。因此，准确计算和评估光伏电

池的理想转换效率有助于指导光伏发电系统的性能优化和工程实践，推动太阳能发电技术的发展和应用。

1.4.2 光伏阵列倾角设计

光伏阵列的倾角指的是太阳能电池板与地面的夹角，通常以水平面为基准进行测量，其选择直接影响到光伏系统的发电效率。不同地区的纬度和季节会影响到太阳的入射角度，因此倾角需要根据具体地理位置进行调整。考虑到太阳轨迹的季节变化，倾角的设计需要综合考虑全年的光照情况，以最大化发电效率。根据太阳高度角的变化规律，选择合适的倾角，使得太阳光垂直照射在光伏板上，提高光伏系统的接收效率。在实际应用中，可以根据当地的气候条件和太阳轨迹的具体情况进行调整，以使得光伏阵列的发电效率达到最佳状态。

光伏阵列的倾角设计需要考虑太阳在天空中的高度角，以确保太阳光能最大程度地垂直照射在光伏板上，从而提高发电效率。太阳高度角h的计算公式如下：

$$h = \arcsin(\sin(\phi)\cdot\sin(\delta)+\cos(\delta)\cdot\cos(H\,A)) \quad (2)$$

h为太阳的高度角，表示太阳位于天空中的位置角度。ϕ为地理位置的纬度，δ为太阳的赤纬角，HA为时角，表示太阳时辰与太阳过中天时辰之间的差值。

光伏阵列的倾角应根据最大年发电量原则选择，以最大化光照强度，提高发电效率。倾角β的计算公式如下：

$$\beta = |\phi - \delta| \quad (3)$$

通过式（2）和（3）确定光伏阵列的最佳倾角，从而最大程度地利用太阳能资源，提高光伏发电系统的发电效率。

2 光伏发电并网关键技应用分析

为了验证光伏阵列倾角对光伏发电系统性能的影响，本文进行了一项实验。实验地点选在位于中部地区的一个家庭屋顶，该地区的纬度为40°。本文选择了一块面积较大的屋顶区域进行实验，安装了一套中小容量家用屋顶型光伏发电系统。为了研究不同倾角对系统发电性能的影响，分别设置不同的倾角，并记录了一段时间内系统的发电数据。平均每日发电量如表1所示，当光伏板倾角较小时0°至30°，平均每日发电量逐渐增加，达到峰值20.1/kWh，这是因为在太阳高度角较小时，倾斜面接收到的太阳辐射更多。随着倾角继续增大40°至90°，平均每日发电量逐渐下降，这是因为光伏板的倾角过大时，导致光照入射角度过大，降低了太阳能的利用率。

表1 不同倾角下发电数据

倾角（°）	平均每日发电量（kWh）
0	18.5
30	20.1
60	18.9
90	14.5

接着评估光伏发电系统在不同条件下的性能表现，实验使用了一台三相并网逆变器实验样机，其控制程序基于数字信号处理，模拟了光伏发电系统与电网的实际工作环境。为了观察系统在并网状态下的运行情况，设置了恒定功率输出模式，并监测了点对点通信电压和电流的波形变化。PCC是指电网中的点对点通信接口，用于实现光伏发电系统与电网的数据交换和通信。在本实验中，将PCC作为电网的代表，监测其电压和电流的波形变化，以评估光伏发电系统与电网之间的相互作用。观察到PCC电压u_{pa}幅值由310.94V逐步降至289.58V，逆变器处于恒定功率输出模式时，PCC电流i_{pa}波形随着u_{pa}幅值下降而上升。这表明系统的电压与电流之间存在一定的关系，而频率、相位保持稳定，功率因数保持在0.98。同时，直流电压Udc波形也呈现出稳定的趋势，变化幅度在控制系统允许的误差范围内。这说明在并网状态下，逆变器的运行稳定，未出现明显的负面影响。

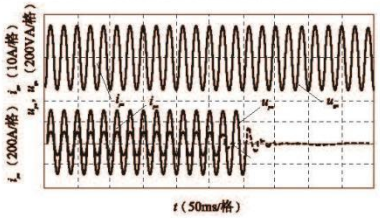

图3 光伏发电系统与电网的稳定运行结果

在中小容量家用屋顶型光伏发电并网中，这些结果进一步验证了光伏发电系统在实际应用中的稳定性和可靠性。太阳能电池组件在光照条件变化时能够稳定地输出电压和电流，而通过对光伏阵列倾角的合理设计，可以最大程度地提高光照的接收效率，从而实现系统的高效发电。

3 结束语

本文旨在评估中小容量家用屋顶型光伏发电并网系统在不同条件下的性能表现，并探讨光伏发电系统与电网之间的相互作用。实验中使用一台三相并网逆变器实验样机，其控制程序基于数字信号处理，模拟了光伏发电系统与电网的实际工作环境。观察了在恒定功率输出模式下，

点对点通信电压和电流的波形变化，以PCC作为电网的代表，监测了其变化情况。实验结果显示，在并网状态下，系统的电压与电流之间存在一定的关系，频率、相位保持稳定，功率因数保持在0.98，表明逆变器的运行稳定，未出现明显的负面影响。此外，通过观察光伏板倾角对平均每日发电量的影响，发现当倾角较小时，发电量逐渐增加，达到峰值20.1kWh，但随着倾角的增大，发电量逐渐下降，说明倾角过大会降低太阳能的利用率。综上，本研究为光伏发电系统的设计和优化提供了重要参考，有助于提高系统的发电效率和运行稳定性。

参考文献

[1] 岳舟，李浩天，廖辰星，等．一种光伏发电用高增益多电平逆变器［J］．电力系统保护与控制，2023，51（16）：136-148.

[2] 李泞吕，赵方凯，陈利顶．城市建筑屋顶光伏发电潜力评估方法和模型［J］．生态学报，2023，43（10）：4284-4293.

[3] 王璐凡．光伏发电并网系统及其关键技术分析［J］．光源与照明，2023（8）：111-113.

[4] 朱涛，常向阳，朱方林，等．江苏县域农村屋顶分布式光伏发电系统建设自然社会影响因素实证分析［J］．太阳能学报，2023，44（5）：217-225.

[5] 赵耀，高少炜，李东东，等．基于天气相似聚类与QRNN的短期光伏功率区间概率预测［J］．电力系统自动化，2023（23）：152-161.

[6] 杨新华，郑越，徐铮，等．光储一体化变流器并网/离网切换控制技术研究［J］．电力电子技术，2022，56（1）：79-82.

[7] 张志敏，彭红义，潘若妍，等．基于MPPT的光伏并网逆变器研究［J］．电源技术，2023，47（1）：108-111.

[8] 李广一，朱涛，杨欢红，等．火电厂区域分布式光伏支架表面锌铝合金镀层的腐蚀行为［J］．电镀与涂饰，2023，42（4）：1-5.

（收稿日期：2024-02-29）

（上接第112页）

5.2 实验结果分析

表2 电气设备故障识别精度实验结果（单位：%）

实验组序号	本文方法	方法1	方法2
yy-01	99.47	95.51	96.44
yy-02	99.38	95.34	96.16
yy-03	99.25	95.26	96.74
yy-04	99.11	95.29	96.44
yy-05	99.02	95.34	96.28
yy-06	99.18	95.28	96.27
yy-07	99.05	95.38	96.88

对实验结果进行分析可以看出，本文方法的故障识别精度相对较高，应用其可得到较为准确的智能变电站设备故障识别结果。与本文方法相比，方法1和方法2相对较差。此实验结果表明，本文方法在优化后进一步提升了故障识别精度，此红外识别优化结果可为智能变电站设备故障的诊断与维护提供有效信息，缩短故障抢修时间。

6 结束语

基于时间序列算法的智能变电站设备故障红外识别优化方法，通过精准捕捉设备运行中的温度变化，实现对设备故障的早期预警和精确诊断。这种方法不仅提高了电力系统的稳定性，减少了非计划停机时间，而且为运维人员提供了更加可靠的故障处理依据。未来，随着技术的不断进步，相信这种优化方法将在智能变电站故障识别领域发挥更加重要的作用，为电力行业的可持续发展提供有力支持。

参考文献

[1] 戴璐平，沈嘉怡，张飞飞．基于时间序列算法的能源电力需求自动预测模型［J］．自动化技术与应用，2024，43（1）：49-51，65.

[2] 杨骏，敬思远，钟勇．面向时间序列有序分类的Shapelet抽取算法［J］．电子科技大学学报，2023，52（6）：887-896.

[3] 于晓，庄光耀．基于轻量化VGG16和BCBAM的电力设备故障红外图像诊断识别［J］．河南科技学院学报（自然科学版），2023，51（6）：60-69.

[4] 张彦迪，陈江宁，老大中．改进激光传感器的电气设备过热故障识别方法［J］．计算机仿真，2023，40（11）：91-95.

[5] 翁东雷，王露民，莫建国，等．基于云计算关联分析的电力设备故障识别模型［J］．电网与清洁能源，2023，39（10）：38-44.

[6] 李明轩，颜培培，杨慧婷，等．基于时间序列算法的变电站设备故障红外识别［J］．无损检测，2022，44（10）：29-34.

[7] 刘云鹏，董王英，许自强，等．基于卷积神经网络的变压器套管故障红外图像识别方法［J］．高压电器，2021，57（10）：134-140.

[8] 别一凡，李波，江军，等．基于改进SSD的变压器套管红外图像油位智能识别方法［J］．电力工程技术，2021，40（5）：158-163.

（收稿日期：2024-02-28）


工业机器人
/引领电气制造业产业变革/
ISSN 2096-4978
（公益广告）


文献知网节
文章目录
0 引言
1 光伏发电及并网技术
1.1 光伏发电
1.2 光伏发电并网技术
1.3 光伏发电系统的设计原则
1.4 主要设备的设计与选择
1.4.1 太阳能电池组件
1.4.2 光伏阵列倾角设计
2 光伏发电并网关键技术应用分析
3 结束语
中小容量家用屋顶型光伏发电并网关键技术应用研究
王春红[1] 金玉婧[2]
1.郑州电力职业技术学院 2.郑州工商学院基础教学部
摘要：当下中小容量家用屋顶型光伏发电并网系统的建设和运行仍面临一系列挑战，如电网接入稳定性、功率调节问题和安全性等方面的技术难题。本文首先简要介绍了光伏发电的构成，然后了解网光伏发电系统的具体结构和设计原则，该系统能够节省了蓄能的成本，是实现电能输出的关键环节。其次选择合适的太阳能电池组件和光伏阵列倾角设计，并对发电量进行准确运算。分析结果表明，随着倾角从0°至30°的增加，平均每日发电量逐渐增加，达到峰值20.1/kWh。然而，当倾角继续增加至40°至90°时，平均每日发电量逐渐下降。PCC电压、电流频率均为50Hz，功率因数保持在0.98。这些结果为选择最佳的光伏板倾角提供了重要参考，有助于优化系统的发电性能，提高能源利用效率。
关键词：家用屋顶型；光伏发电；并网系统；电池组件；功率因数；
基金资助：河南省高等学校重点科研项目“中小容量家用屋顶型光伏发电并网关键技术应用研究”（项目编号：23B480007教科技[2022] 309号文件）阶段性成果之一；
专辑：工程科技Ⅱ辑
专题：电力工业
分类号：TM615
手机阅读
HTML阅读
原版阅读
CAJ下载
PDF下载
AI 辅助阅读
个人成果免费下载
页码：113-116 页数：4 大小：1686K
相关服务推荐


国家新闻出版署
National Press and Publication Administration
首 页
信息发布
办事服务
信息公开
首页 > 查询结果
期刊/期刊社查询
机构名称 电气技术与经济
刊号 10-1539/TM
类别 期刊
主管单位 中国机械工业联合会
主办单位 机械工业北京电工技术经济研究所
语种 中文
出版状态 正常
备注
中华人民共和国国家版权局
国家电影局
中国扫黄打非网
中国文明网
www.wenming.cn

13.基于改进的高斯过程回归的 SOC 估计算法